Pharmacokinetic Evaluation of Triamcinolone Acetonide Nanoparticles Loaded *In Situ* Gel for Non-Invasive Delivery in the Effective Treatment of Posterior Uveitis

THESIS

Submitted in partial fulfilment

of the requirements for the degree of

DOCTOR OF PHILOSOPHY

by

MOHAMMED SHAREEF KHAN

ID. No. 2019PHXF0064H

Under the Supervision of

Prof. PUNNA RAO RAVI

BIRLA INSTITUTE OF TECHNOLOGY AND SCIENCE, PILANI

2023

BIRLA INSTITUTE OF TECHNOLOGY AND SCIENCE, PILANI

Certificate

This is to certify that the thesis titled "**Pharmacokinetic Evaluation of Triamcinolone Acetonide Nanoparticles Loaded *In Situ* Gel for Non-Invasive Delivery in the Effective Treatment of Posterior Uveitis**" submitted by **Mohammed Shareef Khan**, ID No. **2019PHXF0064H**, for an award of a PhD from the Institute, embodies original work done by him under my supervision.

Signature of the Supervisor:

Name in capital letters: PUNNA RAO RAVI

Designation : Professor

Date :

BIRLA INSTITUTE OF TECHNOLOGY AND SCIENCE, PILANI

Declaration

I hereby declare that the work carried out in this thesis titled "**Pharmacokinetic Evaluation of Triamcinolone Acetonide Nanoparticles Loaded *In Situ* Gel for Non-Invasive Delivery in the Effective Treatment of Posterior Uveitis**" is an original piece of research work carried out under the guidance of Prof. Punna Rao Ravi at BITS-Pilani, Hyderabad Campus, Hyderabad. India. This thesis has not been submitted by me for the award of any other degree of any other University/Institute.

Name: MOHAMMED SHAREEF KHAN

Signature:

Date: 27th September 2023

Acknowledgement

For me, "research" has always encompassed more than just animal experiments. It has been, for me, a process of self-education driven by an ongoing cycle of communication with other researchers, self-reflection, asking questions and data collection. These years were trouble-free because of the help, suggestions and timely direction offered by various people along the route.

I wish to sincerely thank Prof. Punna Rao Ravi, who supervised my doctoral research work. I've been associated with him for about nine years. Throughout my master's program, he has instructed me in various courses. He oversaw both my master's and doctoral thesis. He allowed me to freely pursue a number of interdisciplinary areas, which completely altered my perspective on research. I consider myself extremely privileged to have known and worked with him. He is a wise man who conducts comprehensive research. I constantly attempt to model my teaching and learning strategies after him since he serves as a constant source of inspiration. Both his impressive academic ability and his strict moral and ethical code of conduct are excellent and worthy of imitation.

I am obligated to thank Prof. V. Ramgopal Rao, Vice Chancellor; Prof. G. Sundar, Director, BITS Pilani, Hyderabad Campus; Mr. Soumyabrata Chakraborty, Registrar; Prof. Venkata Vamsi Krishna Venuganti, Dean, Academic-Graduate Studies and Research; and Prof. Niranjan Swain, Dean, General Administration, for offering the assistance I needed to complete my research.

I would like to convey my sincere gratitude to Prof. Sajeli Begum, Professor and Head of the Department of Pharmacy, for her assistance and for extending the facilities to work at the Institute. I am incredibly appreciative to Dr. Nirmal Jayabalan and Dr. Akash Chaurasiya for serving as members of the Doctoral Advisory Committee (DAC) and offering their insightful criticism and encouragement throughout this project.

I really appreciate the assistance I received from other faculty members, including Prof. Ahmed Kamal, Prof. D. Sriram, Prof. P. Yogeeswari, Prof. V. V. Vamsi Krishna, Prof. Swati Biswas, Prof. Onkar Kulkarni, Prof. Arti Dhar, Prof. Balaram Ghosh, Dr. Srinivas Prasad K, Dr. Abhijeet Rajendra Joshi and Dr. Yuvraj Singh.

I wish to express my sincere gratitude to my colleagues Ms. Radhika Rajiv Mahajan and Ms. Swagata Sinha, Mr. Pradeep Singh Rawat. Mr. Radha Krishna Mullapudi and many others for their unwavering support during my Ph.D. They helped me gain a lot through the sharing of knowledge and have been incredibly patient and kind to me. My work has benefited greatly from their technical suggestions and critical critique. I also want to thank my seniors, Dr. Shailender Joseph, Dr. Rimy Diwan, Dr. Chandra Teja Uppuluri and Dr. Avantika Dalvi, who provided a lot of support and guidance during their stay at BITS Pilani, Hyderabad Campus.

I would like to thank the Lady Tata Memorial Trust for providing me with SRF so that I could continue my research. A special thank you to Mr. Rohan Dhanrao, the program officer, who has been promptly assisting with the LTMT fellowship paperwork even throughout the epidemic. In addition, I want to thank Prof. Saurabh Srivastav of NIPER-Hyderabad, who served as the LTMT fellowship's external doctorate adviser.

I also appreciate the assistance I received from the non-teaching staff, in particular from the lab technicians, Mrs. Saritha, Mrs. Rekha, Mrs. Sunita and Mr. Rajesh, as well as from other members of the office, store, library, laboratory and security teams. The CAL technicians, Mr. Uppalaiah, Mr. Mallesh, Mr. Narasimha and Mr. Kumar, deserve my gratitude.

The graduate students in the pharmacy departments deserve special attention. Students that have worked with me include Shahid Iqbal Mir and Divya Dhawan.

I would like to express my gratitude to all of my mentors, colleagues and friends, including Dr. Suman, Dr. Vishnu, Dr. Shubhmita, Dr. Nikhila, Dr. Jaspreet, Dr. Shubham, Dr. Preeti, Dr.

Himanshu, Dr. Yamini, Dr. Giridhari, Dr. Lokesh, Dr. Deepanjan, Dr. Sony Priyanka, Dr. Kalyani, Dr. Kavita, Dr. Pravesh, Dr. Suresh, Dr. Kirti, Dr. Pragya, Dr. Soniya, Dr. Sai, Dr. Sivakrishna, Dr. Deepika, Trupti, Sanjay, Milan, Ganesh, Sravani, Asif, Ganesh, Srashti, Ganga, Purbali, Parameswar, Manisha, Priyadarshini, Velmurugan, Shridula, Shreya, Manthan, Suraj, Sumeet, Kanan, Sonali, Avinash, Shivani, Lavanya, Ashutosh, Samrun, Soukya, Suraj, Venkatesh, Asha, Raghuraman, Srivarsha, Vandana, Shreya, Vikash, Rupal, Pramod, Prafful, Aparajita, Tarun, Himaja, Sanjeev, Nikhitha, Goverdhan Darakhshan, Jegadheeswari, Shridula and Shreya.

I want to express my sincere gratitude to my parents, Mr. Mohammed Shalauddin Khan and Mrs. Sayara Banu, for their patience while I pursued my doctorate and for their encouragement of my professional ambitions. For their constant inspiration and assistance, my sisters Saleha Khan and Anjum Khan deserve special acclaim. I wish to thank my wife, Farheen Khan, in particular, for her unwavering support. I want to extend a special thank you to my friend and brother, Benzamin Khatter, who has always provided me with moral support and guided me through challenging situations.

Abstract

Triamcinolone acetonide (TAA), one of the first synthetic glucocorticoids to be approved for the treatment of inflammatory eye diseases. TAA has been used clinically since 1957. The acetonide salt form of triamcinolone is triamcinolone acetonide. TAA's anti-inflammatory and immunosuppressive properties make it the preferred medication for treating ocular inflammations. Due to its lipophilic nature and limited solubility in aqueous solutions, it exerts a potent anti-inflammatory effect and has a prolonged ocular distribution. The use of TAA in the treatment of posterior uveitis (PU) is highly advised. The conventional formulation (aqueous suspensions) of TAA (especially at low dose) applied as ocular drops were shown to be unsuccessful in obtaining effective concentrations in the vitreous humour (target tissue) due to its poor aqueous solubility (17 µg/mL) and dissolving rate in the lachrymal fluids. Therefore, TAA is marketed as a suspension formulation (Triesence, Trivaris and Kenalog) that is suggested for intravitreal injection. The main issues associated with intravitreal injections are secondary ocular hypertension, retinal detachment, cataract formation, postoperative infectious sand non-infectious diseases, pseudoendophthalmitis and endophthalmitis.

Despite all of these complications, TAA is only offered as an intravitreal injection in the market. In the literature, there were surprisingly few attempts to address these issues with drug delivery. This provides a huge gap that requires rapid attention.

There are several formulation techniques that can be used to solve the issues related to intravitreal injection. Conventional ophthalmic drops suffer from various static and dynamic barriers of the eye, specifically in terms of low pre-corneal residence time. To increase the residence time at the corneal surface, researchers have experimented with viscous solutions/suspensions, hydrogels, ointments and gelling systems. *In situ* gelling systems are determined to be the most promising of the various formulations. Compared to hydrogels and

ointments, *in situ* gels are simple to make and can be administered with superior dosage precision. They offer longer residence durations than viscous solutions or suspensions.

As a result, in the current research work, we developed and assessed various TAA formulations with the goal of achieving higher therapeutic concentration in the vitreous humour.

To determine the dose of TAA that can produce effective concentrations in the posterior segment of the eye, a dosa identification study of TAA is first conducted. In order to enable reliable and precise quantification of TAA in various *in vitro* samples and *in vivo* biological matrices, analytical and bioanalytical methods were developed and validated. Form the ocular pharmacokinetic study, it is determined that an aqueous suspension of TAA with 20% HP-β-CD (TAA-HP-β-CD-Susp) at 4 mg/30µL dose strength produced a TAA concentration in the vitreous humour of more than 100 ng/mL and achieved a maximum concentration of 264.9 ng/mL. The concentration of TAA in the vitreous humour was maintained above 100 ng/mL for a period of 3 h (between 1 h to 4 h). Therefore, we can infer that aqueous suspension of TAA with 20% HP-β-CD (TAA-HP-β-CD-Susp) at 4 mg/30µL dose strength is optimal for pre-corneal administration to produce effective TAA concentrations in the vitreous humour. The developed HPLC method offered high sensitivity to determine more than 95% of the entire time course in aqueous humour and vitreous humour with minimal sampling volume, which is critical in ocular pharmacokinetics studies

The quick elimination of medications/formulations after dosing is one of the main difficulties with conventional ocular formulations. A dual responsive *in situ* gel using a combination of thermoresponsive polymer (reacted tamarind seed xyloglucan (RXG)) and ion-sensitive polymer (kappa-Carrageenan (κ-CRG)) was designed and optimized to prevent rapid ocular clearance and to increase longer residence time on the corneal membrane. Using rheological investigations, a number of parameters influencing the formulations sol-to-gel transition were

investigated and adjusted. Finally, TAA was loaded in the optimized blank *in situ* gel (TAA-RXG-κ-CRG). The *in vivo* residence time of TAA-RXG-κ-CRG *in situ* gel, as well as *in vitro* drug release, dose precision, *ex vivo* ocular toxicity and other characteristics, were studied. Pharmacokinetic studies in rabbits were carried out to assess improvement in the TAA concentration achieved in the posterior segment of the eye for the optimized *in situ* gelling formulation of TAA (TAA-RXG-κ-CRG) and compared with suspension formulation of TAA (TAA-HP-β-CD-susp). The TAA loaded RXG-κ-CRG *in situ* gel resulted in significantly higher concentrations (1.64 times increase in C_{max}), drug exposure (4.01 times increase in $AUC_{0\text{-}t}$) and sustained the concentration for longer duration (5.2 times increase in $MRT_{0-\infty}$) in the vitreous humor than the TAAHP-β-CD-Susp.

The bioavailability of drugs administered via the topical ocular route has been found to be enhanced using nanocarrier systems. They enable prolonged drug release, minimizing the need for frequent dosage, increased retention time, reduced toxicity, improved solubility and dissolution rates. In light of this, TAA nano-formulations were prepared and tested for their physicochemical characteristics, *in vitro* release and stability properties and *in vivo* performance.

TAA nanocrystals (NCs) were prepared by anti-solvent precipitation technique using the DoE principle to improve the solubility and dissolution rates of TAA, resulting in a higher concentration of TAA into the vitreous humour via the topical ocular route. The characterization of TAA-NCs included morphology, yield (%) and size. TAA-NCs were loaded in an RXG-κ-CRG based dual responsive *in situ* gel for topical ocular delivery of TAA. The *in situ* gel formulations were evaluated for their rheological properties, stability, *in vitro* drug release and *in vivo* aqueous and vitreous humour pharmacokinetics. Pharmacokinetic parameters were calculated for the aqueous suspension of NCs (TAA-NC-Susp) and the *in situ* gelling formulation of NCs (TAA-NC-ISG) and they were compared to the pharmacokinetic

parameters of the aqueous suspension of plain TAA (TAA-HP-β-CD-Susp). The PS, PDI and yield (%) values for TAA-NCs were 243 ± 5.7 nm, 0.24 ± 0.08 and 88.5 ± 2.4, respectively. In the physiological conditions (STF at 34 ± 0.5°C), the TAA-NC-ISG formulation demonstrated a rapid sol-to-gel transition. The vitreous humour C_{max} values of TAA-NC-ISG (854.9 ng/mL) and TAA-NC-Susp (635.4 ng/mL) were significantly higher than TAA-HP-β-CD-Susp (264.9 ng/mL). Further, the total vitreous humour exposure (AUC_{0-t}) for TAA-NC-ISG (7126.1 ng×h/mL) was 1.9 times and 8.8 times higher than TAA-NC-Susp (3720.2 ng×h/mL) and TAA-HP-β-CD-Susp (810.4 ng×h/mL), respectively. The residence time of TAA ($MRT_{0-\infty}$) in the vitreous humor for TAA-NC-ISG (11.2 h) was 1.9 times higher than that of TAA-NC-Susp (6.0 h) and 3.6 times higher than TAA-HP-β-CD-Susp (3.1 h). This shows that the NCs formulation of TAA improved the drug delivery towards the vitreous humor compared to the aqueous suspension of TAA with 20% HP-β-CD (TAA-HP-β-CD-Susp). This suggests that the drug delivery of TAA to the vitreous humour was further enhanced by the NCs formulation.

To further increase drug concentration and control drug release in the vitreous humour, we formulated TAA-based polymeric lipid hybrid nanoparticles (PLHNPs) utilizing PLGA and phosphatidylcholine (TAA-PLHNPs). The TAA-PLHNPs were evaluated for size, drug loading efficiency, zeta potential, morphology and physical stability. To be delivered topically to the eyes, the TAA-PLHNPs were suspended in a dual responsive *in situ* gelling system composed of RXG-κ-CRG (ISG). The rheological characteristics, stability, *in vitro* drug release and *in vivo* aqueous and vitreous humour pharmacokinetics of the *in situ* gel formulations were assessed. Pharmacokinetic parameters of the *in situ* gelling formulation of PLHNPs (TAA-PLHNP-ISG) and the aqueous suspension of PLHNPs (TAA-PLHNP-Susp) were computed and compared to those for the aqueous suspension of plain TAA (TAA-HP-β-CD-Susp). The PS, PDI and LE (%) values for TAA-PLHZNPs were 163 ± 2.8 nm, 0.27 ± 0.02 and 39 ± 1.9, respectively. The TAA-PLHNP-ISG formulation showed a quick sol-to-gel transition in the

physiological conditions (STF at 34 ± 0.5°C). The vitreous humour concentration (C_{max}) of TAA-PLHNP-ISG (946.53 ng/mL) was significantly higher compared to TAA-PLHNP-Susp (647.50 ng/mL) compared to TAA-HP-β-CD-Susp (264.9 ng/mL). In addition, the vitreous humour exposure (AUC_{0-t}) of TAA-PLHNP-ISG (10093.76 ng×h/mL) was significantly higher than TAA-PLHNP-Susp (6094.92 ng×h/mL) compared to TAA-HP-β-CD-Susp (810.4 ng×h/mL). The residence time of TAA ($MRT_{0-\infty}$) in the vitreous humor for TAA-PLHNP-ISG (16.26 h) was 1.5 times higher than that of TAA-PLHNP-Susp (10.77 h) and 5.2 times higher than TAA-HP-β-CD-Susp (3.1 h). The *in vivo* performance of TAA loaded polymer-lipid hybrid nano-formulations (TAA-PLHNPs as well as TAA-PLHNP-ISG) exhibited higher vitreous humor exposure as well as maintained the concentrations of TAA in the vitreous humor for longer duration than compared to the aqueous suspension of TAA with 20% HP-β-CD (TAA-HP-β-CD-Susp).

Overall, it was concluded that the developed nano-formulations considerably increased the TAA concentrations in the vitreous humour upon topical ocular administration and addressed several shortcomings associated with conventional topical ocular delivery of TAA.

Content/Index page

List of Tables

List of Figures

Abbreviations

Acronym/Symbol	Abbreviation/Meaning
%	Percentage
%bias	Percentage relative error
%RSD	Percentage Relative standard deviation
°	Degree (angle)
°C	Degree Celsius
µg	Micro gram
µL	Microliter
µm	Micrometre
η^*	Complex viscosity
ω	Angular frequency
Å	Angstrom
ACN	Acetonitrile
Amm.Ac	Ammonium acetate
ANOVA	Analysis of Variance
AUC	Area under the curve
$AUC_{0-\infty}$	Area under the curve from t=0 to t=infinity
AUC_{0-t}	Area under the curve from t=0 to t=a specific sampling point
$AUC_{0-tlast}$	Area under the curve from t=0 to t=last sampling point
BA	Bioavailability
BRB	Blood retinal barrier
BAB	Blood-aqueous barrier
BDB	Benzododecinium bromide
BLQ	Below limit of quantification
BBD	Box-Behnken design
Corticosteroids	CSTs
CCD	Central composite design
CI	Confidence Interval
cm	Centimetre
cm^2	Square-Centimetre
C_{max}	Concentration maximum or peak concentration
cP	Centi-Poise
CPCSEA	Committee for the purpose of control and supervision of experiments on animals
Da	Daltons
DMSO	Dimethyl sulfoxide
DCM	Dichloromethane
DMF	Dimethylformamide
DoE	Design of experiments
DSC	Differential scanning calorimetry

EDTA	Ethylenediaminetetraacetic acid (disodium salt)
EE	Entrapment efficiency
f2	Similarity factor
F_{cal}	Calculated F-value for data
FDA	Food and Drugs Association
F_{tab}	Tabulated or critical F-value for assessing statistical significance
G'	Elastic modulus
*G**	total resistance to flow
G''	Viscous modulus
GAA	Glacial acetic acid
GRAS	Generally regarded as safe
h	Hour(s)
HPLC	High performance liquid chromatography
HP-β-CD	Hydroxypropyl-β-cyclodextrin
HQC	High quality control
IVT	Intravitreal
IV	Intravenous
IAEC	Institutional Animal Ethics Committee
cCCD	circumscribed (rotatable) Central Composite Design
ICH	International Conference on Harmonization
IS	Internal standard
ISG	RXG-κ-CRG based dual responsive *in situ* gel
Kg	Kilogram
κ-CRG	kappa carrageenan
kV	Kilo volts
LE	Loading Efficiency of drug
L	Litre
LLOQ	Lower limit of quantification
LOD	Limit of detection
log D	Logarithmic value of Distribution coefficient
Log P	Logarithmic value of Partition coefficient
LOQ	Limit of quantification
LQC	Low quality control
LVER	Linear viscoelastic range
MeOH	Methanol
M	Molarity
m/z	Mass to charge ratio
mg	Milligram
min	Minute
mL	Millilitre
mm	Millimetre
mM	Millimolar

MQC	Medium quality control
MRT	Mean residence time
mV	Milli Volts
n	Number of replicates
NC	Nanocrystals
NCA	Non-compartmental analysis
ng	Nanogram
nm	Nanometre
NPs	Nanoparticles
NMP	N-Methyl-2-pyrrolidone
PCH	Phosphotidylcholine
PLGA	Poly (lactic-co-glycolic acid)
Pa	Pascal
PBD	Piribedil
PDA	Photodiode array
PDI	Polydispersity index
pH	Negative log of H^+ ion concentration
PK	Pharmacokinetics
pKa	Negative log of acid dissociation constant
PRESS	Predicted residual sum of squares
PS	Particle size
pXRD	Powder X-ray diffraction
PVA	Polyvinyl alcohol
QC	Quality control
RPE	Retinal pigment epithelium
RXG	Reacted tamarind seed xyloglucan
R^2	Regression coefficient
R^2_{adjusted}	Regression coefficient of the model adjusted for significant terms
$R^2_{\text{Predicted}}$	Regression coefficient of the predicted model for a response
RH	Relative humidity
RP-HPLC-UV	Reverse Phase HPLC coupled with ultraviolet detector
rpm	Rotations per minute
RSM	response surface methodology/methods
R_t	Retention time
S	Average of the slopes
SD	Standard deviation
SEE	Standard error of estimate
Sec	Seconds
SEM	Scanning electron microscopy
STF	Simulated tear fluid
tan δ	loss tangent
$t_{1/2}$	Elimination half life

T_{max}	Time taken to reach maximum plasma concentration
TSX	Tamarind seed xyloglucan
TAA	Triamcinolone acetonide
TAA-HP-β-CD-Susp	Plain TAA suspended in HP-β-CD solution
TAA-RXG-κ-CRG	Plain TAA loaded in RXG-κ-CRG *in situ* gel
TAA-NCs	TAA Nanocrystals
TAA-NC-ISG	TAA-NCs loaded in RXG-κ-CRG *in situ* gel
TAA-NC-Susp	TAA-NCs dispersed in MilliQ water
TAA-PLHNPs	TAA loaded polymeric lipid hybrid nanoparticles
TAA-PLHNP-ISG	TAA-PLHNP loaded in RXG-κ-CRG *in situ* gel
TAA-PLHNP-Susp	TAA-PLHNPs dispersed in MilliQ water
ULOQ	Upper limit of quantification
USP	United States pharmacopeia
v/v	Volume/volume
VSS	Volume of distribution at steady state
w/v	Weight/volume
WHO	World health organization
ZP	Zeta potential
α	Alpha or axial point in CCD
δ	Phase shift angle
α	Alpha
β	Beta
σ	Standard Deviation of y-intercepts

1

INTRODUCTION

1.1 Basic anatomy of the eye

The eye is a complex and vital sensory organ in the human body as it enables vision [1]. It is a delicate organ that is in direct contact with the environment and is very susceptible to a number of diseases, despite possessing strong protective barriers [2]. The eye is primarily composed of three layers: the sclera, uveal tract and retina, each of which performs complex functions to maintain the eye's normal operation [3,4]. The outer fibrous layer known as the sclera is primarily responsible for providing mechanical stability so that the eye and its delicate optical system may be protected [5]. Collagen and elastic fibre make up the majority of the sclera and the irregularity of these fibres gives the sclera an opaque appearance [1]. The primary role of the sclera is to provide attachment for the extraocular muscle insertions and resistance to both internal and external stresses [6]. The human scleral surface area (≈16–17 cm^2) has a considerable impact on the pharmacokinetics of drug diffusion [7]. The intermediate vascular layer consisting of the iris-ciliary body and choroid is known as the uveal tract, sometimes known as the vascular tunic. Each component of this group serves a distinct purpose [8]. The choroid, which is part of the vascular layer, supplies the retina with blood. The retina is the eye's deepest, most vascular and nerve-rich region. Images and optic nerve signals are made in the retina. Like a choroid, it covers the portion of the eye. It has numerous layers: the inner limiting layer, the nerve fibre layer, the ganglion cell layer, the inner plexiform layer, the inner nuclear layer, the outer plexiform layer, the outer nuclear layer, the photoreceptor layer (rods and cones) and the retinal pigment epithelium (RPE). RPE cells, like the corneal epithelium, have tight connections that prevent positively charged, polar, hydrophilic, small-molecular-weight molecules from moving across cells. RPE and retinal blood vessel endothelium form the blood retinal barrier. Drug distribution to the retina is challenging due to the above anatomical barriers [2,9,10].

The eye is a spherical object having a circumference of 69–85 mm divided into a 22-27 diameter of two segments that are anterior and posterior segments, which accommodate one-third and two-thirds of the ocular architecture, respectively [3,4]. The anterior segment includes tears, cornea, conjunctiva, anterior and posterior chambers, iris, ciliary body, lens, trabecular meshwork and aqueous humour [11]. The posterior segment includes the sclera, choroid, retina, Bruch's membrane, vitreous fluid, optic nerve and retinal blood vessels. The inner limiting membrane seals the vitreous humour, a gel-filled sac that extends to the macula behind the lens in the posterior segment [3].

A number of disease conditions can affect either the anterior or the posterior segment of the eye. The anterior segment is susceptible to dry eye disease, ocular allergic conjunctivitis, keratitis, anterior uveitis, glaucoma and many other diseases [12]. The posterior segment is susceptible to diabetic retinopathy, viral retinitis, choroid neovascularization, proliferative vitreoretinopathy, posterior uveitis, retinal vascular occlusions, age-related macular degeneration and diabetic macular oedema [13].

1.2 Uveitis

A complex group of ailments distinguished by intraocular inflammation are referred to as "uveitis" [14]. Uveitis has a prevalence of 38–714 cases per 100,000 people and an annual incidence of 17–52 cases per 100,000. In certain research, uveitis is slightly more common in women. Uveitis can develop at any age; however, most studies report a mean age of 30–40 years. Uveitis affects approximately 60–80 % of people between the ages of 20 and 50 years old, accounting for 2 million individuals globally every year, with tropical and underdeveloped nations seeing higher rates of infectious uveitis due to the presence of more infectious agents and higher population densities, which contributes to a larger spread of infection [15,16]. If left untreated, it may become a chronic condition needing long-term treatment, which has an impact on the patient’s quality of life as well as placing a strain on the healthcare system [17].

1.2.1 Classification of uveitis

Several ocular inflammatory signs were attributed to uveitis in older studies. In recent years, they have been connected to complex autoimmune diseases such as Bechet's disease and rheumatoid arthritis [15]. Before the mid-20th century, syphilis and tuberculosis were thought to cause eye inflammation. Since then, many inflammatory mechanisms that cause uveitis and other immunological illnesses have been discovered. T cells (adaptive immune system) may produce uveitis in immunologically related illnesses caused by an infectious pathogen or autoantigen [16]. Uveitis can be characterized by its aetiology (infectious or non-infectious) or anatomical location.

1.2.1.1 Anatomical classification

Uveitis is characterized by inflammation of the iris, choroid and ciliary body of the eye [16]. Inflammation can also lead to conditions such as vitritis, papillitis and retinal inflammation (vitreous). Around 5%-10% of those who are visually impaired become totally blind [17].

Uveitis is categorised anatomically by the Standardization of Uveitis Nomenclature working group (Figure 1.1). Acute anterior uveitis affects the iris and ciliary body (the anterior chamber of the eye) and is often (30–40%) linked to Human leukocyte antigen B27-associated inflammatory illnesses, including psoriatic arthritis and spondylitis [19,20]. Systemic diseases, including sarcoidosis and multiple sclerosis, are linked to vitreous humour inflammation [21]. Retina and choroid damage result from posterior uveitis. Posterior uveitis can result from toxoplasmosis and tuberculosis. Retinal oedema, degeneration and detachment can result from posterior uveitis [22].

Inflammation of all uveal layers is referred to as panuveitis. Panuveitis is caused by sarcoidosis. Uveitis may also result from a treatable underlying systemic illness [16]. Local or systemic steroid injections treat intermediate, posterior and panuveitis [23].

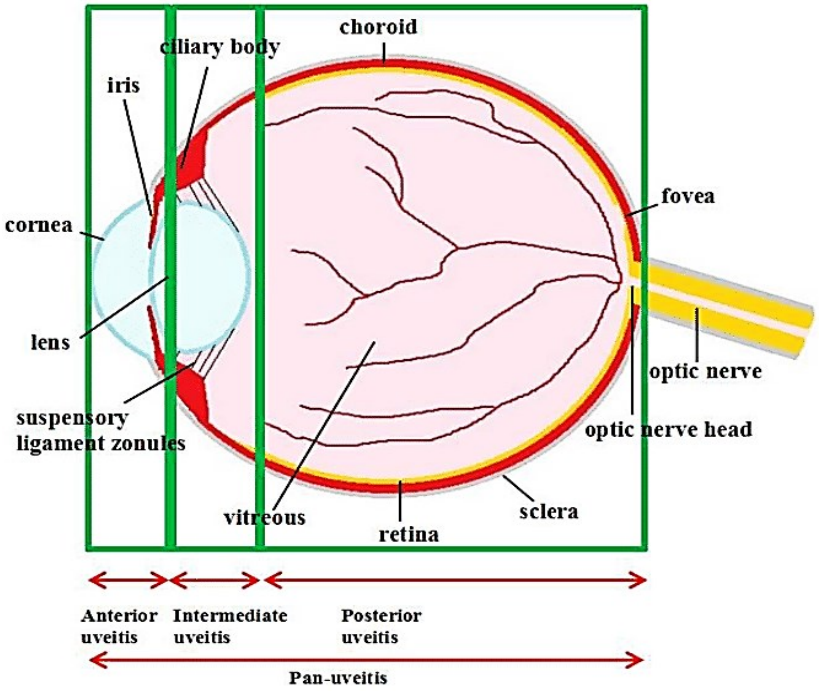

Figure 1.1 Anatomical classification of Uveitis. According to the anatomical site of the inflammatory process, uveitis is divided into four categories: anterior, intermediate, posterior and panuveitis [18].

1.2.1.2 Aetiological classification

Uveitis is often associated with immune system problems, such as ocular infections or systemic inflammation. To aid diagnosis, the International Uveitis Study Group (IUSG) devised a streamlined clinical categorization (Figure 1.2). Uveitis is either infectious (antigen-mediated), non-infectious (autoimmune or autoinflammatory) or masquerade (e.g., cancer-related), according to IUSG [17,24]. Leptospirosis, leprosy, tuberculosis and toxoplasmosis account for half of the infectious uveitis cases in tropical and poor countries [25]. Its prevalence and severity depend on age, gender, location, genetics, environment, socioeconomic variables and type of uveitis [26]. Uveitis treatment is especially difficult for posterior segment inflammation [25].

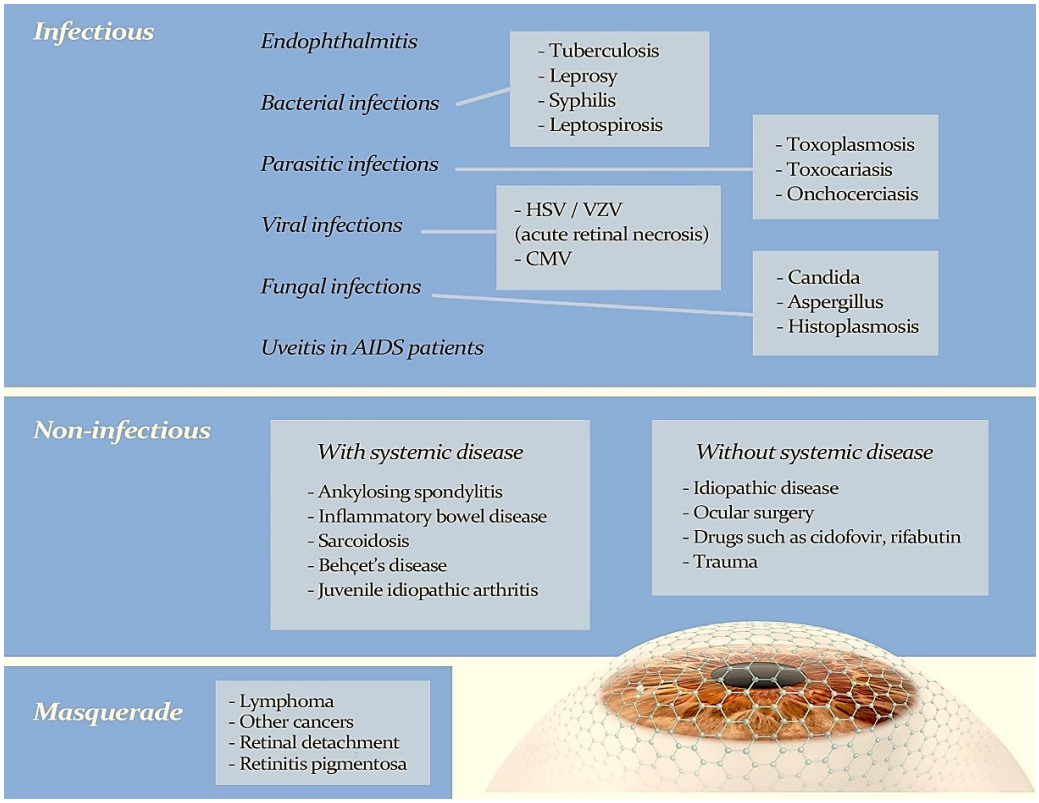

Figure 1.2 Uveitis aetiological classification [19]

1.2.2 Pathophysiology of uveitis

Inflammation of the uveal tract is a common occurrence during any kind of uveitis. An unfavourable condition of inflammation that is harmful to healthy tissues might develop from different regions of the uveal system, acting as vascular/lymphatic conduits for trafficking inflammatory cells into other ocular tissues [20]. Similar to the blood-brain barrier, the blood-retinal barrier (BRB) and blood-aqueous barrier (BAB) normally block the entry of big protein molecules and cells into the eye [21]. These barriers, however, are breached by white blood cells during inflammation, notably neutrophils during an acute start of uveitis or mononuclear cells during chronic uveitis [22]. In light of this, a patient with uveitis may exhibit a wide range of clinical symptoms, such as a painful red eye, photophobia, weeping, as well as visual disruption brought on by floaters in the vitreous or scotomas in the retina [23]. By looking for inflammatory cells in the anterior chamber and protein exudates that cause a "flare" on slit-lamp fundoscopy, anterior uveitis may be quickly identified [24]. A slit-lamp with an extra lens

can be used to readily see the vitreous, retina or choroid, which are the possible sites of inflammation in posterior and intermediate uveitis [23]. Inflammation in these conditions can be acute or chronic. In most cases of posterior uveitis, disease development can be seen as a variety of clinical symptoms, such as inflammatory cells in the vitreous, granulomas in the chorioretinal area, retinal vascular dilation (retinal vasculitis) and oedema in the macula, optic nerve and/or retina [25].

The inflammation of the posterior uveal tract is referred to as posterior uveitis (retina and choroid). The International Uveitis Study Group and Standardization of Uveitis Nomenclature working group classifies posterior uveitis as localised, multifocal or diffuse chorioretinitis, retinochoroiditis, retinitis and neuroretinitis. Posterior uveitis can be infectious (bacterial, viral, fungal and parasitic), autoimmune or part of a masquerade syndrome.

1.3 Barriers for drug delivery to the posterior segment of the eye

Delivery of drugs/therapeutic agents to the posterior segment of the eye is a major challenge. A variety of anatomical and physiological barriers that make up the ocular tissue's defence mechanism prevent the penetration of exogenous substances into the retina [26]. These anatomical and physiological barriers can be classified into three different categories, static barriers, dynamic barriers and metabolic barriers, as shown in Figure 1.3.

1.3.1 Static barriers

Drug molecules are physically prevented from diffusing into the retina and posterior part of the eye by the static barriers in the eye. The Cornea, which covers the anterior sixth of the eye, is the most important static mechanical barrier in the eye. It is a transparent membrane with three main layers: the outermost epithelium, the middle stroma, and the innermost endothelium. Drug permeability is significantly influenced by this transparent, ellipsoid barrier, each of which offers a unique polarity and a potential rate-limiting structure. The lipoidal-shaped corneal epithelium contains 90% of the cells that make up the cornea. These cells are connected by

desmosomes and they are encircled by ribbon-like tight junctional complexes. The zonula occludens slows paracellular drug absorption from the tear film into the epithelium's intracellular regions as well as into the cornea's inner layers [9]. Topically administered hydrophilic drugs are far less likely to penetrate the corneal epithelium. A major barrier to the absorption of lipophilic drugs is the highly hydrated stroma, which makes up 90% of the corneal layer and is composed of an extracellular matrix and collagen fibrils arranged in a lamellar configuration. The innermost layer of the cornea is made up of hexagonal-shaped cells called the endothelium, which provides secretory function and selective carrier-mediated transporter properties. In order to permeate the cornea, a drug should have amphiphilic characteristics [27].

The cornea is continuous with the sclera (white part of the eye) and conjunctiva (translucent tissue). The strong, fibrous outer covering of the eye is made up of the sclera. It preserves the form of the eye and offers a place for the extraocular muscles to enter. At the point where the optic nerve pierces it, it is just around 1 mm thick [28]. The pore width and intracellular gaps of the fibre matrix that makes up the sclera, which is composed of collagen and elastin chains, may affect the flow of drugs [29]. In addition, the variances in the collagen architecture of the posterior sclera, the lateral orientation of fibres and the effects of myopia may all have an impact on how well drugs are transported, with either a lower or higher permeability depending on these modifications [30,31]. The permeability of a drug through the sclera is impacted by a variety of factors/conditions [32]. Scleral permeability is strongly correlated with molecular weight, suggesting that drugs with smaller molecular sizes have higher permeability and drugs with high molecular weight have lower permeability. Further, for a given molecular size, the shape of the molecule can affect the scleral permeability. This is particularly true with globular proteins, which are more permeable than compared to linear dextran’s of the same molecular weight. Therefore, molecular shape/radius is also a key factor affecting scleral permeability

[33,34]. The sclera's anatomy and, thereby, its permeability properties are reported to alter as a result of disease, surgery or trauma [35].

The permeability studies of drugs through choroid and the retinal pigment epithelium (RPE), two components of Bruch's membrane, demonstrate that permeability increases with an increase in the lipophilicity of the drugs. When molecules are passively transported across the RPE, their molecular permeability values in the outward (retina-choroid) and inward (choroid-retina) directions are the same; however, it differs for molecules that are actively transported between the two [9]. The presence of RPE melanin may change how drugs are disposed of in the eye. Through electrostatic, van der Waals and/or straightforward charge-transfer interactions with this pigment, melanin binds to free radicals and drugs, which may change the availability of the free drug at the targeted location [36]. Since melanin binds to all basic and lipophilic drugs, melanin binding may significantly reduce pharmacological action [37]. Due to the presence of melanin, lipophilic substances are more likely to bind to the choroid- Bruch's membrane, which increases the permeability of such drugs through the choroid [38,39].

The permeability of the sclera and its anatomical structure is unaffected by ageing; however, studies have demonstrated that the choroid and Bruch membranes are much more permeable as people age [35]. Due to an increase in thickness with ageing (from 2 μm in the first decade of life to 4.7 μm in the tenth decade), Bruch's membrane may offer increased resistance to the permeability/transport of small molecules. Additionally, the build-up of basal laminar deposits and lipid-rich membranous debris may play an important role in the delivery of drugs [39].

1.3.2 Dynamic barriers

The precorneal barriers, which include blinking, tear film, tear turnover, draining of solution from the cul-de-sac and induced lacrimation, are a part of the dynamic barriers that are particularly effective in removing the drug from the surface of the eye. Dynamic barriers also

include nasolacrimal drainage, the passage through the lymphatic and blood arteries, bulk fluid movement and the active transport processes of RPE transporter proteins [2,10,27].

The reflexive action of blinking shields the eye from dryness, intense light and objects advancing on it. Blinking also regulates the production of tears, which moisten and cleanse the eye's surface. On average, infants blink only twice every minute. In adolescence, this rises to 14–17 times per minute and remains stable throughout maturity. Additionally, blinking may intensify in reaction to discomfort, glaring lights, shifts in temperature and humidity and conversations.

The surface of the cornea is covered by a pre-corneal tear film. In order to eliminate debris and pathogens from the glycocalyx of the ocular surface, mucin forms a hydrophilic layer in the tear film, which covers the ocular surface and serves a protective role [31,40]. The volume of a human tear is typically between 7-10 μL and it can momentarily fit in 30 μL of the cul-de-sac. The secretion rate of tear fluid on the surface of the cornea is 1 to 2 μL/min. Therefore, most of the conventional/low viscous liquid formulations, with an aqueous vehicle, administered in the precorneal area are washed out within a few minutes of instillation. When all the precorneal barriers are taken into consideration, the contact time of any given drug product with the absorptive membranes is shorter. This results in less than 5% of the administered dose reaching the intraocular tissues [41–43].

The nasolacrimal drainage system, via the nasolacrimal duct, clears the majority (between 80 and 90 percent) of the volume of liquid formulation that is instilled into the eye. Due to the nasolacrimal drainage system, the volume of precorneal fluid is continuously maintained at a level of 7–10 μL. The nasolacrimal duct functions as a physiological defence system, expelling any surplus fluid that is present. In addition to the nature of the drug, viscosity, pH, tonicity, injection volume and other additional factors can impact the functioning of the nasolacrimal drainage system. The rate of solution drainage increases with the instilled volume of the drug

product. The pH, tonicity and surface tension should be compatible with the tear fluids. Further, the drug and the excipients used in the drug product should not cause any irritation of the cornea or the conjunctiva [44,45].

The blood and lymphatic circulation present in the conjunctiva are another dynamic barrier which works against the delivery of drugs through the ocular route. The conjunctiva is relatively 30 times more permeable compared to the cornea. Further, due to higher blood and lymphatic circulation in the conjunctival membranes, the drugs are rapidly absorbed through the conjunctiva into the systemic circulation, followed by subsequent distribution and elimination processes of the drug. The conjunctival/episcleral clearance processes play a key role in lowering intraocular drug penetration and therefore it should be considered in designing the drug delivery to the posterior segment of the eye [46–48].

The majority of drug clearance occurs through the choroidal vasculature, conjunctival vascular and/or lymphatic vessels. Drugs can be transported away by bulk fluid flows in ocular tissues. According to reports, uveoscleral drainage occurs between 6% and 50% of the time and causes a bulk outflow of fluid from the suprachoroidal region. The convective current of aqueous humour and the conjunctival vascular and/or lymphatic vessels clears the majority of the drugs [49].

The vitreous fluid of rabbits has an osmotic pressure of around 0-1 mmHg, while the choroid has an osmotic pressure of 12-14 mmHg [50]. A fluid flow is caused by the differential in osmotic pressure between the choroid and the vitreous. The outward bulk fluid flow is also influenced by the hydrostatic pressure differential between the suprachoroid and the episcleral tissue [51]. The suprachoroid and the episcleral tissue have hydrostatic pressure differences of around 12 mmHg, which act as a propulsion mechanism for the bulk fluid flow outward. P-glycoproteins (P-gp) and multidrug resistance-associated proteins (MRPs), two examples of

drug efflux pumps, have been found in RPE with an efflux action directed toward the choroid [52,53]. The extracellular pH, temperature and drug concentration plays a crucial for active drug transport [54].

1.3.3 Metabolic barriers

The active movement of nutrients or xenobiotics is facilitated by membrane-bound proteins known as transporters. The absorption, distribution, metabolism and excretion of drugs depend heavily on such transporters. It has been documented that several ocular tissues have both influx and efflux transporters. It has been discovered that the existence of efflux pumps in specific ocular tissues controls the intracellular drug concentration necessary to achieve therapeutic efficacy. Several ocular tissues, including the ciliary body and RPE, contain drug-metabolizing enzymes [55,56]. The cytochrome P-450 (CYP) family of drug-metabolizing enzymes, which are the most significant ones, are present in the eye as part of a complex metabolising enzyme system that biotransforms drugs as a defensive mechanism [57].

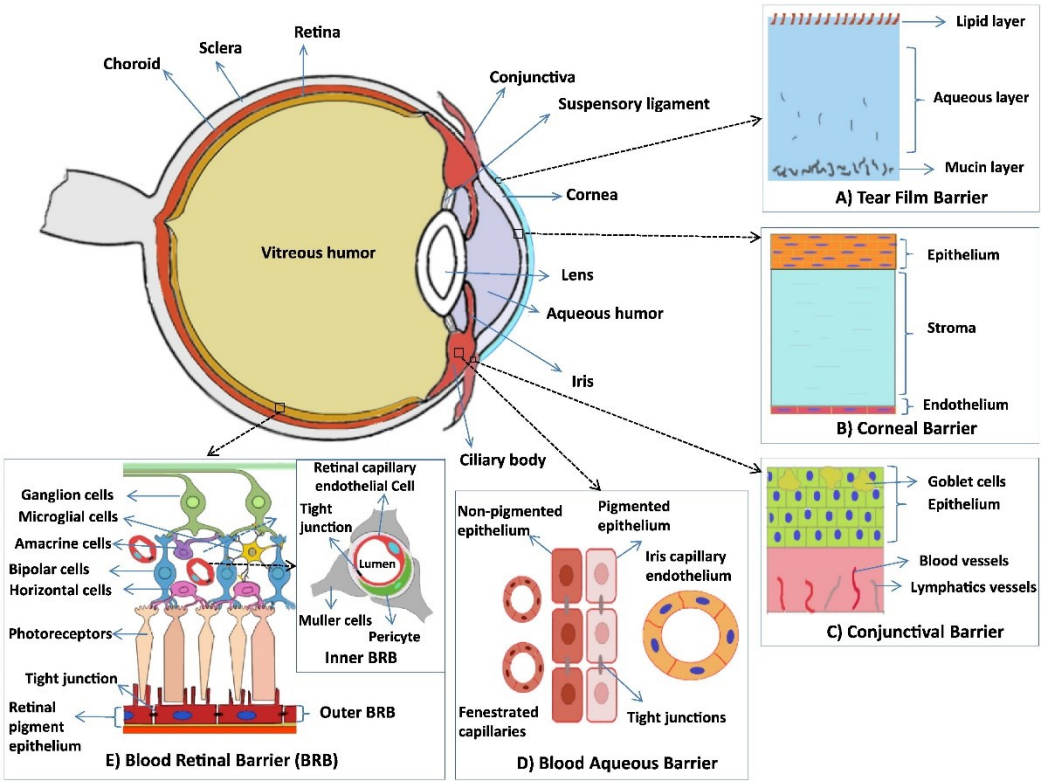

Figure 1.3 Static and dynamic barriers for ocular drug delivery to the posterior segment [58]

1.4 Drug delivery routes to the posterior segment of the eye

Maintaining therapeutic levels for long-term therapy and controlling the drug's availability at the target area are the key goals of any drug delivery system. The ease of formulation administration and safety/tolerance to the ocular tissues must all be taken into account while developing a drug delivery system for the eye. There have traditionally been four ways to deliver drugs to the back of the eye that includes periocular, intravitreal, systemic and topical delivery techniques. Figure 1.5 illustrate the various routes of drug delivery to the posterior segment of the eye.

1.4.1 Topical delivery

Drug administration by topical application is comparatively simple and safe. Nonetheless, delivery to the posterior region via this route is regarded as ineffective. Considering that 5% of the topically applied dosage reaches the anterior segment of the eye and only a small portion of that (0.001%) is anticipated to reach the posterior region [59]. This is explained by a number of factors, as shown in Figure 1.4. The issues involved in the topical delivery of drugs through the ocular route are**:** (i) limited dosing volume (not more than 30 µL/ eye); (ii) quick clearance from the ocular surface by dynamic barriers like lacrimation, blinking and conjunctival hyperaemia; (iii) metabolism of the drug by enzymes present in tear fluid; (iv) non-productive absorption into systemic circulation via highly vascularized conjunctiva, choroid, uveal tract and inner retina; (v) difficulty in permeation through corneal epithelium (vi) aqueous humour outflow [60–62].

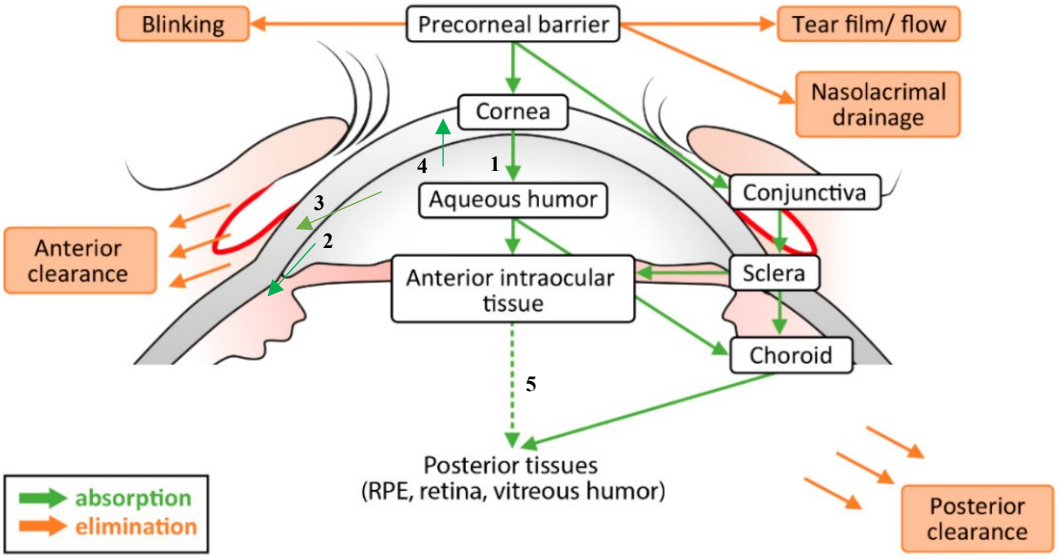

Figure 1.4 Schematic illustration of the pharmacokinetics of the ocular route. (1) drug absorption into the aqueous humour (AH) through the cornea; (2) drug distribution to the iris and ciliary body and absorption into systemic circulation; (3) clearance of the drug by the aqueous humour flow via the trabecular meshwork into Schlemm's canal, reaching the venous and lymphatic systems; (4) drug distribution to the cornea and (5) drug distribution to the posterior tissues [63] .

1.4.2 Intravitreal delivery

To administer a drug through the intravitreal route, a needle with a gauge size of 30G is typically used in conjunction with the pars plana to inject the drug product directly into the vitreous humour [64]. Contrary to topical and systemic delivery approaches, intravitreal injection enables high concentrations of drug to be achieved near the internal eye tissue, such as the choroid and retina. However, intravitreal injections are inevitably linked to side effects, including vitreous haemorrhage, retinal detachment, cataracts and endophthalmitis. With an intravitreal injection, endophthalmitis and retinal detachment are found at rates of 0.2% and 0.05%, respectively. In addition, patient compliance is poorer with such regimens due to the uncomfortable and invasive procedures necessitating hospitalisation and a highly trained physician for administration, both of which contribute to the expense in addition to the expensive nature of the medication itself [65].

1.4.3 Periocular delivery

The term "periocular route" refers to the delivery of medication to the area around the eye. Examples of such delivery systems include subconjunctival, peribulbar, posterior juxta scleral, sub-tenon and retrobulbar injections. The bulk of the medication is transported to the posterior region after subconjunctival injection through the sclera, with systemic recirculation and a small amount of trans-corneal absorption serving as supplementary pathways [66,67]. Periocular treatment is less invasive than intravitreal but less effective. This approach has better retina and vitreous drug bioavailability (0.01-0.1%) than topical administration (0.001% or less) [68,69].

1.4.4 Oral and parenteral delivery

The most common routes for the delivery of drugs are the oral and parenteral routes. Following the administration of a drug through the oral route [in the form of the solid dosage form (e.g., tablets or capsules or powders) or liquid dosage forms (e.g., solutions or suspensions or emulsions)] or parenteral route (liquid dosage forms), the drug reaches the systemic circulation and as a part of drug distribution to the eye, a certain fraction of the drug reaches the tissues of the eye. The drug's availability in the posterior eye segment is constrained by the BAB and BRB, which are selectively permeable to highly lipophilic molecules [9]. Since BRB prohibit drugs from diffusing into the posterior chamber of the eye, drug delivery to the posterior chamber and the retina is exceedingly challenging. The drugs' low bioavailability (1%–2%) at the BRB necessitates frequent administration at large doses, which causes severe systemic adverse effects.

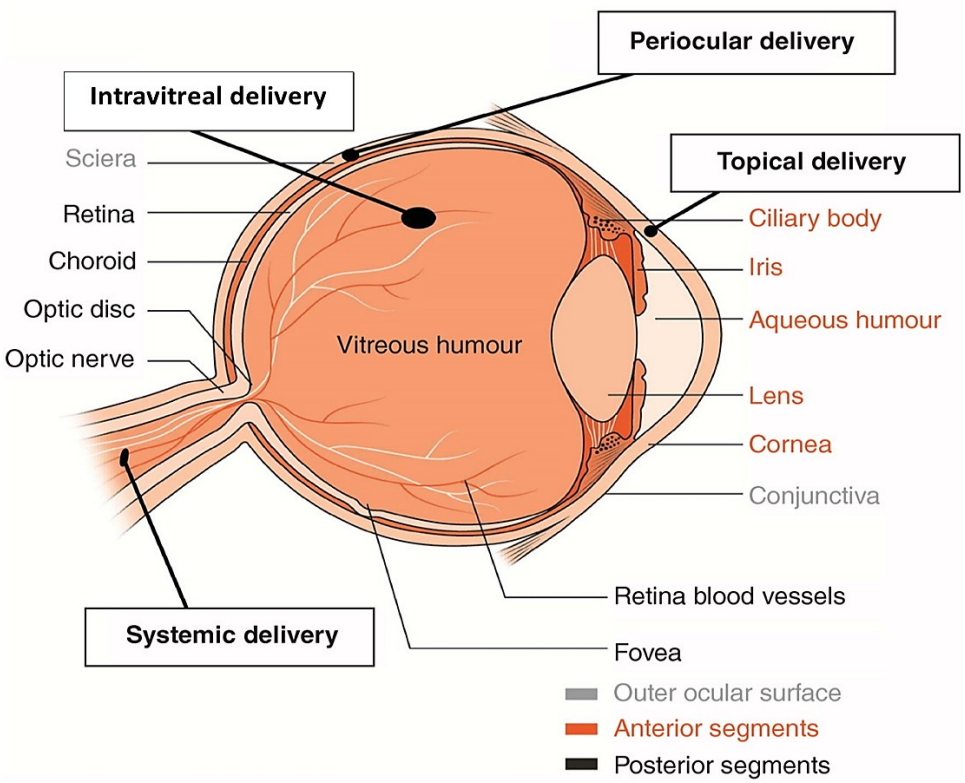

Figure 1.5 Various possible routes of drug administration (topical, intravitreal, periocular and systemic) to the posterior segment of the eye [70].

1.5 Drug therapy for the treatment of posterior segment inflammatory disorders

Corticosteroids (CSTs) have been utilized to treat inflammatory diseases since the 1950s [71]. In the 1970s, intraocular use of CSTs was pioneered and proven to be effective with minor systemic side effects [72]. Corticosteroids can be delivered topically, periocularly or systemically (primarily oral but can also be given as intravenous or intramuscular injections). Because they exclusively penetrate the anterior portion of the eye, topical CSTs treat anterior uveitis and episcleritis. Periocular CSTs help manage intermediate uveitis with decreased vision, macular oedema from panuveitis or posterior uveitis and other conditions [15]. The periocular route delivers high local CSTs to the anterior and posterior eye segments without systemic side effects. However, many patients may require systemically given CSTs, often oral prednisone, due to the nature of the disease or issues with the local (periocular) administration of CSTs (for example, CSTs-induced ocular hypertension). A brief course of oral CSTs may be helpful for the control of inflammation in individuals with acute or episodic illnesses. In

order to manage the inflammation in individuals with chronic illness, long-term suppressive CSTs therapy and early treatment with high-dose oral prednisone may be required [73,74].

Corticosteroids that have been approved by the FDA to treat inflammation in the posterior ocular region include Triesence® (triamcinolone acetonide suspension), Ozurdex® (dexamethasone implant), Retisert® (fluocinolone acetonide implant), Iluvien® (fluocinolone acetonide implant) and Susvimo® (ranibizumab implant). These products are excellent examples of some of the initiatives made to create formulations with the prolonged release [75].

Triamcinolone acetonide (TAA) is a commonly prescribed synthetic CSTs used to treat a variety of inflammatory conditions. The acetonide salt form of triamcinolone is more potent than triamcinolone and eight times more potent than prednisolone [71,76]. It is effective in treating a variety of eye conditions, such as uveitis, diabetic macular oedema, refractory cystoid macular oedema and other ocular disease conditions that require long-term steroid medication. Delivery of TAA to the posterior segment is challenging due to the strong protective anatomical, physiological and biochemical barriers. Therefore, all the current marketed preparations are delivered by injecting directly into the eye through the intravitreal or periocular route [77].

1.6 Triamcinolone acetonide (TAA)-Drug profile

Triamcinolone acetonide (TAA) was one of the first synthetic glucocorticoid corticosteroid approved for the treatment of inflammatory eye disorders [78,79]. The clinical use of TAA dates back to 1957. It has a strong anti-inflammatory effect and high ocular distribution, which is primarily due to the lipophilic nature of the drug [80]. Chemically TAA is 9-fluoro-11β,16α,17,21-tetrahydroxypregna-1,4-diene-3,20-dione-16,17-acetonide (Figure 1.6) [71]. The key physicochemical characteristics of TAA are shown in Table 1.1

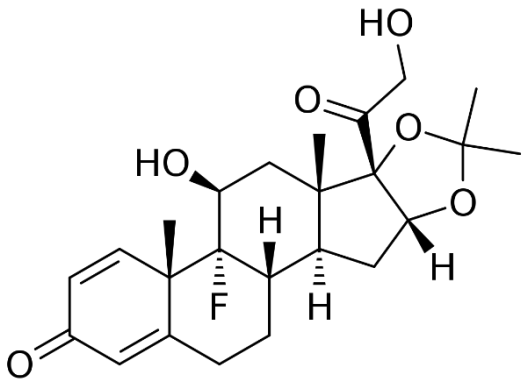

Figure 1.6 Chemical structure of Triamcinolone acetonide (TAA)

Table 1.1 Physicochemical properties of TAA

Parameter[a]	Description/Value
Drug Name	Triamcinolone acetonide (TAA)
Category	Corticosteroid -glucocorticoid
Chemical Name	9-fluoro-11β,16α,17,21-tetrahydroxypregna-1,4-diene-3,20-dione-16,17-acetonide
Chemical Formula	$C_{24}H_{31}FO_6$
Molecular weight	434.50 g/mol
Physical state	white crystalline powder
Melting point	290-294 °C
Aqueous solubility	NMT 17 µg/mL in buffered systems of pH 1.2, 4.5 and 7.4, MilliQ water and STF
Partition coefficient (log P)	2.31
Ionization constant (pKa)	13.4 (Acidic), -3.3 (Basic)
Hygroscopicity	Non-hygroscopic
BCS class	IV

[a] Data collected from available literature [81–84]

1.6.1 Mechanism of action of TAA

Corticosteroids provide an anti-inflammatory effect by preventing leukocyte and macrophage migration to the afflicted area by reversing vascular dilatation and permeability. These procedures result in lessened erythema, pruritus and oedema. Inhibiting nuclear factor kappa-B (NF-kappa-B) causes a reduction in the expressions of the anti-inflammatory protein's interleukin-6 (IL-6), interleukin-8 (IL-8), monocyte chemoattractant protein-1 (MCP-1) and COX-2, which plays a key role in the anti-inflammatory mechanism. Triamcinolone acetonide

inhibits phospholipase A2 on the phospholipid layer of cell membranes, which slows down the lysis of leukocyte lysosomal membranes and stops arachidonic acid from forming (Figure 1.7). This action inhibits inflammation and suppresses the immune system. Ultimately, it inhibits the production of leukotrienes and prostaglandins by reducing the expression of the enzyme's cyclooxygenase and lipoxygenase [85].

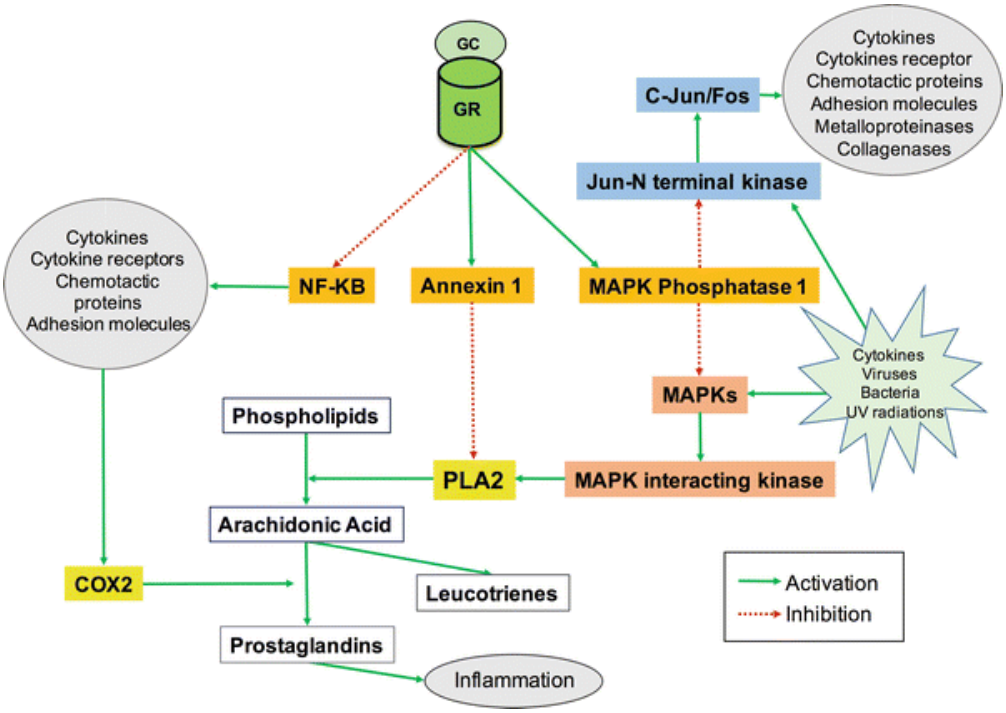

Figure 1.7 Anti-inflammatory pathways of glucocorticosteroids involved in the control of inflammation [86].

1.6.2 Pharmacokinetics of TAA following intravenous, oral and inhalation administration

Derendorf *et al.* investigated the pharmacokinetics of TAA following intravenous (2 mg), oral (5 mg) and inhalation administration (2 mg) of the drug. Following the intravenous bolus administration, the mean residence time was 2.7 ± 0.8 h, the terminal half-life was 2.0 ± 0.7 h and the total body clearance was 37.3 ± 12.8 L/h. The volume of distribution at steady-state was 103 ± 59 L. The terminal half-life determined from the oral administration was 2.6 ± 1.4 h, which was similar to the value obtained from intravenous bolus administration. The absolute oral bioavailability was low at 23 ± 10%, primarily due to its high first-pass metabolism. The

terminal half-life of TAA following the administration of the drug through the pulmonary route (inhalation) was found to be 3.6 ± 1.5 h which is 50% higher than that of intravenous administration. The pulmonary bioavailability of TAA was found to be 22 ± 12% which was similar to that of oral bioavailability. The researches have reported that the systemic levels of all three treatments resulted in a considerable reduction in blood lymphocyte counts [87] at the dose levels administered in the study.

Jermak *et al.* have reported that TAA produces three major metabolites: 21-carboxytriamcinolone acetonide, 6b-hydroxytriamcinolone acetonide and 21-carboxy-6b-hydroxytraimcinolone acetonide [71]. The parent compound is more active than its metabolites because of the increased water solubility of the metabolites, which noticeably increases their rates of elimination. The 6-hydroxylation process decreases metabolite activity and the anti-inflammatory activity of TAA [88].

1.6.3 Pharmacokinetics of intravitreally injected TAA

Ye *et al.* investigated the time course of the TAA concentration in the rabbit's vitreous humor after intravitreal injection of 4 mg and 8 mg of the drug. In the study, the estimated half-lives of intravitreal TAA were 24 days and 34 days for the 4 mg dose and 8 mg dose, respectively. The maximum concentration of TAA in the vitreous humor for 4 mg and 8 mg doses were 2.745 mg/mL and 5.498 mg/mL, respectively. The area under the curve in the vitreous humor time course profile was 95.560 mg/mL/d and 247.789 mg/mL/d for 4 mg and 8 mg doses, respectively. The researchers concluded that an intravitreal injection of TAA at a dose of 8 mg resulted in a longer half-life, higher concentration and more bioavailability than an intravitreal injection of 4 mg TAA [89].

The pharmacokinetics of TAA intravitreal injection have been the subject of numerous investigations. According to Chin *et al*., the half-life of TAA administered through the

intravitreal route at a dose of 0.3 mg was 1.57 days in the vitrectomized rats and 2.89 days in the non-vitrectomized rats [90]. Kim *et al*. came to the same conclusion, observing that vitrectomy could increase drug clearance. In addition, they reported that TAA administered intravitreally at various dosages could result in a range of elimination half-lives [91]. The clearance of TAA was also dependent on the drug release rate from the intravitreal drug delivery system [92].

1.7 Current status of research in drug delivery approaches to the posterior segment of the eye

There are limited options for the treatment of diseases that affect the back of the eye due to the invasive nature of the methods that are currently available for the administration of drugs, as well as the requirement that medication be given on a regular basis in order to effectively treat such diseases. As a result, it is crucial to create formulations that can sustain the required therapeutic drug concentrations at the back of the eye for extended periods of time. Such formulations will reduce the number of repeated systemic, oral, parenteral or local injections. A promising approach would be to develop a topical formulation (in the form of topical eye drops) that can provide sufficient drug transport to the posterior eye segment by overcoming the various barriers present in the eye. Patients choose eye drops over other ocular formulations because they are simple to administer, painless, non-invasive and inexpensive [93,94].

1.7.1 Conventional formulations for drug delivery to the posterior segment of the eye

Ocular drug administration by topical eye drops is the most convenient, safe, immediately active, patient compliant and non-invasive in nature. After topical drop instillation, an eye drop produces a pulse drug permeation and then its concentration rapidly falls. Drug concentration decrease may follow first-order kinetics. Thus, viscosity enhancers, permeation enhancers and cyclodextrins can be added to topical eye drops to improve medication contact time, penetration and ocular bioavailability [95]. Viscosity enhancers improve topical drop

absorption and precorneal residence duration by increasing formulation viscosity. Some examples of viscosity enhancers are hydroxypropyl methyl cellulose, hydroxy methyl cellulose, hydroxyl ethyl cellulose and sodium carboxy methyl cellulose. However, the high viscosity imparted by such polymers to the formulation limits their usage and they are often recommended to be used at night before bed when blurred vision is less of an issue [96].

Permeation enhancers can improve drug transport through mechanical barriers like corneal epithelium. Chelating compounds, preservatives, surface active agents and bile salts were investigated as permeation enhancers. Permeation enhancers for ocular administration include benzalkonium chloride, polyoxyethylene glycol ethers (lauryl, stearyl and oleyl), ethylenediamine tetra acetic acid sodium salt, sodium taurocholate, saponins and cremophor EL. Though permeation enhancers increase ocular drug absorption, some of these permeation enhancers were reported to exhibit local toxicity at higher concentrations. Due to the high sensitivity of ocular tissues, caution should be given when selecting penetration enhancers [96,97]. Drug solubility, precorneal residence duration and ocular bioavailability can be improved by conventional ocular formulations such as emulsions, suspensions and ointments [96].

Johannsdottir *et al.* developed dexamethasone/γ-cyclodextrin complex micro-suspension aqueous eye drop using poloxamer, sodium chloride and ethylenediamine tetra acetic acid sodium salt as the important excipients in an aqueous vehicle. Topical administration into the eye resulted in increased concentrations of dexamethasone in the rabbits' posterior segments. The findings showed that following repeated daily administration of dexamethasone for 7 and 15 days, there was no accumulation in the tissues of the eye. This strategy allows for the replacement of invasive procedures like intravitreal implants or injections with a variety of lipophilic drugs that can be employed to treat posterior segment disorders [98].

Tajika *et al.* found that 0.05% [^{3}H] difluprednate emulsion increased the anti-inflammatory effect of the prednisolone derivative. Their research findings showed that emulsion could deliver the therapeutic agent to anterior ocular tissues and a limited quantity to posterior tissues after single and repetitive topical drop instillation in rabbit eyes [99].

Nayak *et al.* developed a polyethyleneglycolylated (PEGylated) TAA microemulsion for delivery to the posterior portion of the eye. Developed PEGylated microemulsion was able to maintain the circulation of the loaded drug up to 6 h and that too in a higher amount when compared to non-PEGylated ME in the posterior region [100].

Consequently, there are a very limited number of works reported on conventional eye drop formulations that can effectively deliver medications to the posterior portion of the eye for the treatment of posterior uveitis.

1.7.2 *In situ* gel formulations for drug delivery to the posterior segment of the eye

The *in situ* gelling technique is a novel drug delivery system that takes advantage of the stimuli-responsive features of liquids to form semisolid gels in the conjunctival cul-de-sac of the eye in response to changes in pH or ion activation or temperature or a combination of such stimuli. *In situ* gels that undergo a sol-to-gel phase transition as a result of a change in temperature are called thermoresponsive *in situ* gels, while *in situ* gels that undergo a sol-to-gel phase transition as a result of a change in pH are called pH-responsive *in situ* gels and *in situ* gels that undergo an ion activation process are called ion activated *in situ* gels. Following the administration, the liquid formulation (in the form of eye drops) transforms rapidly into a semisolid gel, allowing for controlled drug release, a prolonged therapeutic effect and fewer dosing intervals, all of which lead to increased patient compliance [101,102].

Currently, the majority of the literature reviews show that the *in situ* gelling system-based conventional drug delivery system targets the anterior segment disease (e.g., glaucoma).

However, there are no published reports of *in situ* gelling system-based drug delivery systems administered in the precorneal area/conjunctival cul-de-sac for treating posterior segment diseases.

1.7.3 Nano-formulations for drug delivery to the posterior segment of the eye

Nanoparticles (NPs) (typically 10-1000 nm in size) transport drugs to the posterior portion of the eye through passive or active (ligand-mediated) targeting. Because of their nanosize range, NPs for ocular delivery can target the posterior region of the eye to treat posterior uveitis more successfully than conventional dosage forms such as solutions, suspensions, emulsions, ointments and other routes of administration. In recent years, a variety of drug-loaded NPs formulations have been investigated to treat posterior segment eye disorders. Liposomes, nanomicelles, polymeric NPs and dendrimers have been investigated for targeting the posterior segment of the eye [103,104].

Tahara *et al.* examined the non-invasive delivery of several PLGA-loaded therapeutic agents to target posterior segment diseases [105]. Araujo *et al.* prepared nanostructured lipid carriers (NLCs) of TAA. The developed NLCs were mixed with Nile red. These NLCs were observed in the retina upon topical application, peaking 40 min later. Due to their prolonged retention followed by corneal absorption, NLCs are a potential technique for establishing targeted and persistent drug concentration in the posterior region of the eye [106].

Nirbhavane *et al.* produced TAA loaded cationic NLCs. The cell uptake investigation revealed that dye-loaded nanocarriers may enter cells within 2 h and remain inside the cells for over 24 h, whereas the retention of plain dye inside the cells was very low after 24 h. *Ex vivo* penetration in porcine corneal tissue confirmed that the formulation requires 2 h to deposit into the cornea and remain there for up to 24 h [107].

Formica *et al.* formulated TAA loaded lipid nano-capsules that showed therapeutic efficacy in the endotoxin-induced uveitis rabbit model with a considerable improvement in the clinical indicators of an inflammatory response [108].

Khalil *et al.* developed TAA loaded chitosan-coated liposomes, which demonstrated therapeutic efficacy by delaying the release of TAA in *in vivo* animal experiments. The liposomes demonstrated tremendous promise for the treatment of disorders affecting the posterior eye segment, whose options for treatment are frequently constrained by the presence of ocular barriers [109].

Cholkar *et al.* used 2 FDA-approved polymers (Vitamin-E tocopherol polyethylene-glycol succinate (TPGS) and octoxynol-40) to develop a 0.2% rapamycin-loaded mixed nanomicellar formulation to deliver the payload inside the anterior segment. *In vivo* studies showed an increase in the concentration of rapamycin at the posterior segment of the eye [110].

Davis *et al.* showed that liposomes containing annexin A5 dramatically improved absorption and transcytosis through corneal epithelial barriers following topical treatment. The liposomes were reported to deliver a significant amount of Avastin (bevacizumab) to the posterior portion of the eye, including the retina [111].

Shafie *et al.* studied betamethasone phosphate-loaded mucoadhesive chitosan-sodium alginate NPs, which demonstrated prolonged release and significantly high concentration in the vitreous humour (68% of the drug over 6 h, then decreased to 59.5% and 34.1% at 12 h and 24 h, respectively), as compared to a free drug (14.6% after 1 h and the drug disappeared after 2 h) [112].

Several studies have demonstrated the application of various nano-formulation strategies for topical drug delivery to the posterior chamber of the eye. While these nano-formulations did increase drug concentrations in the vitreous humour, the drug release was not efficiently

controlled; instead, there was often a burst release followed by a drop-in drug concentration. Furthermore, the drug absorption rate was found to be highly dependent on the formulation's residence time after being administered. So, to address the challenges of a limited residence period on the cul-de-sac, the nano-formulations can be loaded into an *in situ* gelling system.

1.7.4 Nano-formulations loaded *in situ* gel for drug delivery to the posterior segment of the eye

The formulation of NPs is one of the strategies now employed to boost the bioavailability of hydrophobic drugs like CSTs. Particularly, the incorporation of the drug into the polymer matrix generates a system that shields the drug from the enzymatic metabolism present in the tear film and permits a regulated and sustained release of the drug. The NPs have the ability to deliver the drug to deeper tissues, where typically conventional formulations are unable to reach. In order to overcome the problem of limited residence time in the precorneal region, formulations that convert into a gel upon contact with the eye as a function of pH or ions or temperature are being developed. The development of NPs incorporated into an *in situ* gelling system would eliminate the drawbacks of the burst release of the drug from the NPs, resulting in an increased drug concentration in the posterior segment of the eye [113].

Esteruelas *et al.* prepared riluzole PLGA NPs, which were loaded in an *in situ* gelling system. The prepared formulations were applied as a topical eye drop and concentration in the posterior segment after 24 h of administration was determined. The results showed an increase in the concentrations of riluzole for the drug-loaded NPs loaded *in situ* gel in comparison to the riluzole NPs suspension, presenting a feasible alternative for posterior segment delivery [114].

Ahmed *et al.* investigated ketoconazole-loaded trans-ethosomes with thermosensitive gel. Fluorescence laser microscopy was used to examine the distribution of formulation in the anterior and posterior segment of New Zealand rabbits at 1 h, 2 h and 4 h following the instillation of the formulation into the conjunctival sac. Fluoresceine isothiocyanate-trans-

ethosomes loaded *in situ* gel revealed a considerably higher distribution of nanovesicles in the posterior segment than fluoresceine isothiocyanate loaded *in situ* gel [115].

Tatke *et al.* investigated *in situ* gel of TAA loaded solid lipid NPs (SLNs) for improved topical ocular delivery. When compared to the control suspension, the transcorneal permeability studies showed increased permeability of the drug-loaded towards TAA loaded SLNs. The drug concentrations in the anterior and posterior segment tissues of the eye, as well as in tears, were higher with *in situ* gel containing TAA loaded SLNs compared to TAA loaded SLNs and the control suspension. The use of SLNs and *in situ* gelling systems created a powerful platform for topical drug administration [116].

Nano-formulations and *in situ* gel-loaded nano-formulations appears to offer the benefit over conventional formulations among the numerous formulation approaches described to treat posterior segment disorders.

1.8 Problem identification and research objectives

In ophthalmology, TAA is frequently used, particularly for disorders involving posterior inflammation. It is used as an adjuvant therapy in the care of age-related macular degeneration, diabetic macular oedema, retinal vein occlusion and other disorders that need long-term ocular steroid administration, such as intermediate and posterior uveitis. It is regarded as being generally safe and very effective. Current marketed preparations of TAA are suspension formulations that are injected intravitreally into the eye. The most recommended doses of TAA are 4 mg and 20 mg [71,117]. Intravitreal injections of TAA into the eye directly delivers the desired dose to the target area while minimising extraocular side effects. Reportedly, TAA administered as an injectable suspension forms a depot at the site of delivery and releases the drug over an extended period of time [118]. Despite the fact that these effects are desirable, such a system provides no further advantages. Such invasive delivery techniques have

apparently been associated with a variety of significant risks and shortcomings, both generally and especially for TAA and other CSTs, in addition to the terrifying idea of getting a needle in the eye.

Patient compliance and convenience are completely eliminated with intraocular injections. Patients must stay at a medical centre for at least a few hours throughout the drug delivery procedure, which needs specialised staff. In order to provide an injection, a complex process is required that calls for aseptic conditions, anaesthesia of the eye, etc. [119]. Additionally, this method of drug delivery is connected to a number of high-risk and potentially blinding side effects, including infections, endophthalmitis, globe perforation, retinal detachment and other common side effects like increased intra ocular pressure (IOP), pain, redness and vision issues [120].

From a thorough review of the literature, it was concluded that the majority of side effects and complications associated with current TAA therapy are largely attributable to the route of administration, specifically direct intraocular injections and can be easily avoided by using a non-invasive delivery technique. A substantial corpus of peer-reviewed articles demonstrates how nanoparticulate drug delivery systems may successfully overcome anatomical and physiological barriers and deliver the drug at various target locations. There have been a few attempts to successfully deliver CSTs and other drugs as nanoparticulate systems that may be applied topically as eye drops and have reported effective delivery to the posterior segment of the eye [121–124].

The inability of topically applied drugs to cross the cornea is significantly hampered by their brief residence time in the eye. These limitations on the formulations are implied by how quickly the formulation leaves the eye via nasolacrimal drainage (into tears). It is possible to successfully resist drug removal and improve penetration by putting the nanoparticulate

formulations in a high viscous vehicle. The prepared TAA nanoparticulate system will therefore be suspended in an *in situ* gelling polymeric matrix that responds to the eye's temperature, pH or ionic composition. This means that the polymer will transform from sol to gel upon delivery. The advantage of *in situ* gelling systems is that they are easy to administer and resistant to removal from the eye, giving the formulation time to be absorbed by the cornea.

The current research work intends to design, optimize and evaluate (*in vitro* and *in vivo*) a novel ocular nanoparticulate drug delivery system for TAA that can be applied topically in a non-invasive way and to achieve therapeutic concentrations in the posterior chamber for effective treatment of posterior uveitis.

Therefore, the following **objectives** were envisioned for the current research work:

1. To perform dose identification studies of TAA that can produce effective concentrations in the posterior segment of the eye employing a validated bioanalytical method.

2. To design and evaluate *in situ* gelling systems loaded with TAA for non-invasive delivery.

3. To design, develop and optimize suitable nanoparticulate systems of TAA for non-invasive delivery and to assess the physicochemical and *in vitro* properties of the optimized TAA nanoparticulate systems loaded into the *in situ* gelling system.

4. To perform *in vivo* pharmacokinetic studies of the *in situ* gels loaded with TAA nanoparticulate systems for non-invasive ocular delivery and to determine the efficacy of the formulations in achieving therapeutic concentration in the posterior segment of the eye.

2

DOSE IDENTIFICATION OF TRIAMCINOLONE ACETONIDE FOR NON-INVASIVE PRE-CORNEAL ADMINISTRATION IN THE TREATMENT OF POSTERIOR UVEITIS USING A RAPID, SENSITIVE HPLC METHOD WITH PHOTODIODE-ARRAY DETECTOR

2.1 Introduction

Triamcinolone acetonide (TAA) is a long-acting synthetic glucocorticoid, more potent than equivalent doses of prednisone [78,79]. TAA is the acetonide salt form of triamcinolone. TAA is the drug of choice in the management of ocular inflammations due to its anti-inflammatory and immuno-suppressant activity [83,125]. TAA is highly recommended for the treatment of posterior uveitis (PU). However, the delivery of CSTs like TAA through the oral route for the treatment of PU is found to be less effective due to their high hepatic first pass and gut-wall metabolism and low distribution of the drug from the systemic circulation to the uveitis tissue [126]. The dissociation constant (pKa) and log P of TAA are 13.4 and 2.31, respectively [83,125]. Due to its poor aqueous solubility (≤12 μg/mL) and dissolution rate in the lachrymal fluids, conventional formulations (aqueous suspensions) of TAA (particularly at low doses) administered as ophthalmic drops were found to be ineffective in achieving effective concentrations in the vitreous humour (target tissue). In the market, TAA is available as a suspension formulation (Triesence, Trivaris, Kenalog) recommended to be administered via intravitreal injection. Major complications associated with intravitreal injections are secondary ocular hypertension, Retinal detachment, cataract formation, postoperative infectious and non-infectious, pseudoendophthalmitis and endophthalmitis [127–129].

Few research groups have reported the development of novel, non-invasive ocular drug delivery systems of TAA to achieve effective concentrations of the drug at vitreous humour for efficient management of the disease condition [130–133]. However, there are no research reports on conventional formulations of TAA for non-invasive ocular administration. In addition, there are no reports on the dose recommended for ocular administration of conventional formulations of TAA to achieve effective concentrations in the vitreous humour. In the present study, we have designed and evaluated conventional formulations of TAA (aqueous suspensions) with different dose strengths to identify the dose strength required to

achieve effective concentrations in vitreous humour following pre-corneal administration the formulations. In all the formulations, Hydroxypropyl-β-cyclodextrin (HP-β-CD) was used at 20% w/v concentration (in the aqueous suspension) to improve the saturation solubility of the drug. HP-β-CD based aqueous formulations are prepared routinely for ocular administrations. The safety profile of HP-β-CD is extensively reported in the literature [134,135]. HP-β-CD is well tolerated in concentrations as high as 45% w/v in ophthalmic drops [136,137]. Being lipophilic in nature, TAA can be entrapped into the non-polar cavity of the HP-β-CD, thereby forming an inclusion complex. Formulations containing three different dose strengths of TAA (1mg/30µL, 2mg/30µL, 4mg/30µL) were prepared. An Ocular pharmacokinetic study was conducted in male New Zealand rabbits to determine the time course of the drug in aqueous humour, vitreous humour and plasma. In the pharmacokinetic evaluation of such ocular drug delivery systems of TAA, we need to have a highly selective, sensitive and rapid bioanalytical method for quantification of TAA in aqueous humour and vitreous humour (to determine the ocular pharmacokinetic parameters of TAA) and in plasma (to determine the systemic exposure of drug upon ocular administration and thereby systemic toxicity).

The majority of the literature showed the use of a sophisticated LC-MS/MS system for the estimation of TAA in different biological matrices [83,138–145]. Although the LC-MS/MS system offers high sensitivity, the components of the biological matrix, which are co-extracted with the analyte of interest during the sample processing, can significantly affect the response of the analyte. In addition, components of the biological matrix which are co-extracted can contaminate the mass analyser due to continuous deposition during the sample analysis. Few HPLC methods using UV/PDA detectors were reported for quantification of TAA in different biological matrices like plasma, aqueous humour and vitreous humour. However, the reported HPLC methods involve a longer analysis time (≥ 20 min).

The volume of aqueous humour, vitreous humour that can be collected at any given time point in pre-clinical animal models like rabbits, is low. The volume of aqueous humour available in the ocular tissues of rabbits is as low as 0.35 mL. Moreover, the reported methods use a relatively large volume of plasma, with a minimum of 100 µL in any of the reported HPLC methods, for the analysis, which is a challenge in the case of pre-clinical pharmacokinetic studies [146–148]. In addition, most of the reported methods involve complex and time-consuming sample processing steps for the extraction of TAA from the biological matrices.

The objective of the present study is to identify the dose strength for pre-corneal administration of aqueous suspension of TAA using a new, rapid, selective, sensitive, precise and economical RP-HPLC-PDA method for the quantitation of TAA in rabbit aqueous humour, vitreous humour and plasma samples obtained in the ocular pharmacokinetic studies.

2.2 Experimental

2.2.1 Materials, reagents and animals

Triamcinolone Acetonide (TAA) and Piribedil (used as internal standard) were obtained as gift samples from Strides Pharma Science Limited, Bengaluru, India and Dr Reddy's Laboratories, Hyderabad, India respectively. 2-Hydroxypropyl-β-cyclodextrin (HP-β-CD - Average Mw≈1,460) was purchased from Sigma Aldrich, Mumbai, India. HPLC grade methanol (MeOH), acetonitrile (ACN), ammonium acetate, glacial acetic acid and disodium EDTA were purchased from SD Fine-Chemical Limited, Mumbai, India. Sample processing and analysis were performed using high-quality HPLC-grade water obtained from a Milli-Q water purification system (Millipore®) MA, USA. Male New Zealand Rabbits (2-2.5 kg) were procured from VAB Biosciences, Hyderabad, India.

2.2.2 Instruments and chromatographic conditions

The chromatographic system used in the analysis is equipped with two LC-20AD pumps system for solvent delivery, a DGU-20A3R degasser, a CTO-20AC column oven, a SIL-

20AC HT auto-injector and an SPD-M20A photodiode array–UV detector (Shimadzu Corporation, Kyoto, Japan). LC solutions software (version 1.25) was employed for data collection and integration. Sartorius Research® micropipettes (Sartorius India Pvt. Ltd., Hyderabad, India) were used for all sample preparations. A single-channel vortex mixer (Model: VORTEX 3S022, IKA, Bengaluru, India), multi-tube vortex shaker (Model: VX-200, Labnet International, NJ, USA), refrigerated centrifuge (Model: C-24 BL, Remi, Mumbai, India) and vacuum concentrator (Model: SCANVAC Scan Speed 32, Labogne ApS, Lynge, Denmark) were used in the process of concentrating the sample by solvent evaporation. A deep freezer (Model: BFS-345-S, Celfrost Innovations Pvt. Ltd., Mumbai, India) was used in storing the plasma samples. Sonicator (Model: SONICA® 2200 MH, Soltec, Milan, Italy) was used for degassing the mobile phase. A pH meter (Model: pH 2700, Eutech Instruments, Mumbai, India) was used for measuring the pH of all buffer systems. The aqueous component of the mobile phase was filtered using a 0.22 µm filter membrane (Millipore®) MA, USA.

The Chromatographic separation was achieved on an end-capped C18 reverse-phase (RP) column (Luna®, 150 mm long and 4.6 mm internal diameter, particle size 5 µm, Phenomenex, CA, USA) equipped with a guard column of the same packing material. The mobile phase consisted of a mixture of 10 mM ammonium acetate (pH 4.45 ± 0.1, adjusted with glacial acetic acid) (solvent A) and acetonitrile (solvent B) in the ratio of 58:42 *v/v*. Sample analysis was performed in isocratic mode at a mobile phase flow rate of 1 mL/min. The chromatographic system was stabilized for 45 min by monitoring the baseline with the mobile phase flow rate at 1 mL/min prior to the analysis of the samples. The column temperature was maintained at 40 ºC. Both TAA and PBD (IS) were monitored at a wavelength of 240 nm. The retention time of TAA and IS were 3.9 ± 0.1 and 5.0 ± 0.1 min, respectively, in all three biological matrices (plasma, aqueous and vitreous humour). The total run time for each sample was set for 7 min and the injection volume was 70 µL.

2.2.3 Solubility studies and characterization studies of the mixture of TAA and HP-β-CD

2.2.3.1 Solubility studies

Solubility of TAA was assessed in various solvent systems like MilliQ water, simulated tear fluid (STF-pH 7.4); pH 1.2 (0.1 N HCl) and buffer systems like pH 4.5 sodium acetate (Na. Ac), pH 7.4 phosphate buffer (USP 35–NF 30). In addition, the solubility of TAA was also determined in various solubilizers (like polyethylene glycol (PEG-400) and propylene glycol (PG)), surfactants (like Poloxamer-188, Poloxamer-407, Tween 80 (T-80), *s*odium lauryl sulfate (SLS) and D-α-Tocopherol polyethylene glycol 1000 succinate (TPGS), hydrophilic polymers (like polyvinylpyrrolidone (PVP-K30), methocel E4M (M-E4M) and sodium hyaluronate (sHA) in the concentration range of 0.2 to 2.5% w/v and complexing agent (HP-β-CD) at concentrations of 15, 20 and 25% w/v in water. In the solubility studies, excess TAA was added in 2 mL of each of the above solvent systems (*n*=3). The samples were equilibrated for 24 h in an orbital shaking incubator (REMI laboratory instruments, Mumbai, India), maintained at 37 ± 1 °C at 100 rpm. The samples were centrifuged at 15000 × *g* (14000 rpm using a 7 cm radius rotor head) for 15 min and the supernatant was appropriately diluted and analyzed using HPLC.

2.2.3.2 Characterization studies of the mixture of TAA and HP-β-CD

To determine the compatibility and/or interaction of TAA with HP-β-CD, physical mixtures of TAA and HP-β-CD were prepared by mixing them at a 1: 1 ratio. The FT-IR analysis of TAA, HP-β-CD and physical mix of TAA + HP-β-CD was performed with potassium bromide as a reference on a JASCO apparatus (FTIR-4200, JASCO, Tokyo, Japan). The samples were mixed with potassium bromide and pressed into pellets. The scans were done at ambient temperature with a resolution of 4 cm^{-1}, in the wavenumber range of 4000 to 400 cm^{-1}. The proportion of the sample in pellets was 2 mg/200 mg KBr in all the FT-IR analysis. The average spectrum obtained from three recordings was taken for each sample.

The thermal behaviour of TAA, HP-β-CD and the physical mixture of TAA + HP-β-CD was studied using Differential Scanning Calorimetry (DSC-60, Shimadzu Corporation, Kyoto, Japan). Briefly, 2-5 mg of each sample was accurately weighed in an aluminium pan and crimp sealed. The samples were analyzed in the temperature range of 40 to 300 °C at a 10 °C/min rate. A blank aluminium pan was used as a reference in the analysis. Nitrogen was used as purged into the sample compartment at a flow rate of 100 mL/min to provide an inert atmosphere. Before the analysis, the instrument was calibrated for constant cell temperature using indium and constant heat capacity using sapphire standards.

2.2.4 Preparation of aqueous suspensions of TAA containing HP-β-CD (TAA-HP-β-CD-Susp)

Various co-solvents (PG, PEG 400), surfactants (Tween 80, TPGS, sHA *etc.,*) and complexing agents (HP-β-CD) both alone and in combination were tried to increase the saturation solubility of TAA in order to formulate aqueous solutions of the drug. In all the formulation trials, TAA powder with an average particle size of 75-90 µm was used. None of the solubility enhancement approaches yielded a stable aqueous solution of TAA at a dose strength of 4 mg/30µL. Therefore, an aqueous suspension of TAA was tried using different cellulose-based hydrophilic polymers like (HPMC and M-E4M). None of the hydrophilic polymers produced stable suspensions in the concentration range of 0.2 to 2.5% w/v. At higher concentrations (beyond 2.5% w/v), the aqueous suspension formed using the hydrophilic polymers exhibited higher viscosity and lacked sufficient flow properties to administer the formulation as an ophthalmic drop. Though HP-β-CD (used as a solubility enhancer in the concentration range of 10 to 40%) did not solubilize TAA in water, it formed a stable aqueous suspension of TAA at 20% w/v concentration (TAA- HP-β-CD-Susp). The dosing volume of the formulations was fixed at 30 µL as it is recommended to use a minimum dosing volume for ophthalmic drops, preferably less than 50 µL/eye in rabbits [149]. Therefore, aqueous suspensions of TAA at

three different dose strengths (1 mg/30µL, 2 mg/30µL and 4 mg/30µL) were prepared using HP-β-CD at 20% w/v concertation in Milli-Q water (TAA-HP-β-CD-Susp).

2.2.5 Collection of rabbit plasma, aqueous humour and vitreous humour

Prior approval was obtained for the protocol from the Institutional Animal Ethics Committee (IAEC) (IAEC no.: BITS-Hyd/ IAEC/2020/10) to conduct all animal experiments in the study. For the collection of blood samples, animals were anaesthetized using xylazine (at 5 mg/kg dose) and ketamine (at 35 mg/kg dose) and administered through intramuscular injection. Blood was collected from the marginal ear vein of male New Zealand rabbits (2-2.5 kg) using a butterfly needle into a microcentrifuge tube containing disodium EDTA solution as the anticoagulant (4.5% w/v disodium EDTA in Milli-Q water). The anticoagulant was added at a level of 10% for each unit volume of blood collected into the centrifuge tube. The collected blood sample was centrifuged at 1000 × g (7 cm rotor head at 3600 rpm) for 15 min at 4 ^{o}C to separate the plasma. Supernatant plasma was carefully transferred into vials using micropipettes and stored at −20 °C until further use.

For the collection of the aqueous and vitreous humour, the animal was euthanized by carbon dioxide inhalation. Then a 30-gauge insulin needle (3 mm dia) was placed behind the limbus superotemporally and directed towards the centre of the globe to draw the aqueous humour. The aqueous humour collected from all the animals was pooled and used for the method development and validation. Following the collection of aqueous humour, the eyeball was removed by a surgical procedure. The eyeball was immediately snap-frozen using dry ice. Vitreous humour was collected from the frozen eyeball and stored at -20 ^{o}C until further use. In the PK studies, eight animals (n=8) were used for each formulation. The Time course of TAA in aqueous humour and vitreous humour for each formulation was determined based on a composite sampling technique. At each sampling time point, one animal was sacrificed. Immediately after sacrificing the animal, aqueous humour was collected using a 30-gauge

insulin needle (3 mm dia) from both eyes and the eyeball was removed surgically from the animal. The eyeball was immediately snap-frozen and vitreous humour was collected from both eyes. In the case of plasma time course, at each sampling point, the plasma sample was collected from the animal being sacrificed and two more animals. The plasma time course was constructed using composite sampling based on the plasma samples collected from three animals at each sampling time point.

2.2.6 Sample preparation and drug extraction from plasma, aqueous humour and vitreous humour

Protein precipitation followed by solvent evaporation was employed to extract the drug from all three biological matrices (plasma/aqueous humour/vitreous humour). To 45 µL of the biological matrix, 5 µL of IS and 5 µL of TAA-appropriate working standard solutions were added and vortexed mixed for 1 min. To the above mixture, acetonitrile (as protein precipitating agent) was added in the ratio of 1:10 v/v ratio (1 part of ACN for 10 parts of the mixture, by volume) and vortexed for 1 min followed by centrifugation at 12500 × g for 20 min at 4 °C. The supernatant obtained was transferred into a fresh micro-centrifuge tube (1.5 mL) and evaporated to dryness under vacuum. The dried sample was reconstituted with 100 µL of mobile phase and vortexed for 1 min, then centrifugated at 12500 × g for 20 min at 4 °C. The supernatant obtained was transferred into vials and injected into the HPLC system using the optimized chromatographic conditions described earlier.

2.2.7 Preparation of calibration curve and quality control standards

TAA and PBD (IS) Primary stock solutions were prepared separately at a 1 mg/mL concentration using DMSO as the solvent. To prepare the calibration curve standards of TAA in plasma and quality control standards in aqueous humour/vitreous humour, one intermediate stock solution of TAA (100 µg/mL) and IS (100 µg/mL) were prepared separately from their respective primary stock solutions. From the intermediate stock solution of TAA, a set of primary working standard solutions containing a concentration of 4.5, 8, 10, 15, 22, 25 and 30

µg/mL of TAA were prepared by appropriate dilution. Further, secondary working standard solutions containing a concentration of 0.5, 1.0 and 1.5 µg/mL of TAA were prepared from the appropriate primary working standard solutions. 10 mM ammonium acetate buffer (pH 4.45) and acetonitrile in the ratio of 58:42 *v/v* were used as the solvent to prepare the intermediate stock solution and various working standard solutions of TAA.

Seven standard solutions in the range of 50-3000 ng/mL (for calibration curve in plasma) and four quality control samples 50 ng/mL (LLOQ), 100 ng/mL (LQC), 1000 ng/mL (MQC), 2500 ng/mL (HQC) of TAA (in all the three matrices) were prepared by spiking 5 µL of an appropriate working standard solution of TAA (either primary or secondary working standard solution) in the 45 µL of the biological matrix. In all the calibration curve standards and quality control standards, 5 µL of suitable dilution of IS (from its intermediate stock solution) was spiked in the 45 µL of the biological matrix to yield a concentration of 400 ng/mL.

2.2.8 Method Validation

The developed method was fully validated in rabbit plasma as per the International Conference on Harmonisation (ICH) guidelines and the United States FDA [150]. The developed method was partially validated for parameters like selectivity, sensitivity, accuracy, precision and recovery in aqueous humour and vitreous humour.

The method selectivity was established by comparing overlaid chromatograms of six different lots of analyte and IS-free plasma, aqueous and vitreous humour samples (without the addition of TAA and IS) with their respective IS spiked samples and samples spiked with both TAA and IS. The linearity of the method was determined using seven-point calibration in the concentration range of 50-3000 ng/mL. Calibration curves were constructed using the peak area analyte (TAA) ratio to the IS versus the analyte concentration data of six replicate (n=6) calibration series. The data obtained were subjected to least-square linear regression analysis. The sensitivity of the method is determined using limit of detection (LOD) and limit of

quantitation (LOQ). LOD and LOQ were calculated based on the standard deviation of the y-intercepts and the average of the slopes of the six calibration curves. The lowest limit of quantification (LLOQ) of the method is established by determining the accuracy (in terms of %bias) and precision (in terms of %RSD) of six replicate injections of plasma samples containing 50 ng/mL of TAA.

The method's accuracy, precision and intermediate precision were determined using six replicates of LLOQ concentration and three QC standards (LQC, MQC and HQC) in all three matrices (plasma, aqueous and vitreous humour). The method's accuracy, expressed in terms of %bias, was computed by calculating the difference between the experimentally determined concentrations and their respective theoretical (nominal) concentrations obtained from the linear regression calibration equation. The method's precision was estimated at LLOQ and at each QC level in all three matrices and reported as %RSD of replicate sample analysis. Intra-day precision was determined by analysing LLOQ and each of the three QC standards in all three matrices, in triplicates, at two different times in a day. Inter-day precision was assessed by triplicate analysis of LLOQ and each QC standard in all three matrices on three different days. Recover of the drug from each of the biological matrices using the protein precipitation technique at LLOQ and all QC levels in all three matrices were assessed by comparing the peak area ratios of the analyte and IS of the biological sample with that of the aqueous analytical standard containing the same nominal concentration.

The stability of TAA in plasma at LLOQ, LQC, MQC and HQC levels in triplicate was determined under three different stress conditions: post-preparation auto-injector storage (up to 24 h, at 15 ºC), freeze-thaw (samples stored at -20 °C) and long-term storage (samples stored at -20 ºC for a period of 30 days). Auto-injector stability of the processed samples was assessed using four sets of samples (LLOQ, LQC, MQC and HQC) in triplicates by analysing the samples at different time points over a period of 24 h. Freeze-thaw stability samples were

subjected to three freeze-thaw cycles using samples (LLOQ, LQC, MQC and HQC) with at least 12 h frozen condition (−20 °C) between the cycles. Frozen samples were thawed at room temperature for at least 1 h prior to analysis. The long-term stability of the samples was determined by analysing the samples on the 0^{th}, 10^{th}, 20^{th} and 30^{th} days during the 30-day storage period. In the stability studies, the percentage deviation from the mean concentrations observed at zero time was calculated at each stress condition.

The robustness of the method was determined by deliberately making changes, one factor at a time, in the optimized chromatographic conditions. The effect of pH of an aqueous phase, mobile phase composition, column oven temperature and the mobile phase flow rate was studied by varying the factors over ±5% of their corresponding optimized value. MQC samples were used to evaluate the robustness of the developed method. System suitability and mean percentage recovery of the MQC samples were determined by changing the method conditions as described above. RSD (%) values obtained from system suitability should be ≤ 10% and the mean percentage recovery should be within 100 ± 20% for TAA.

2.2.9 Ocular pharmacokinetic study of aqueous suspensions of TAA containing different dose strengths in Male New Zealand rabbits

Male New Zealand rabbits weighing 2-2.5 kgs were used in the study. For one week before the pharmacokinetics studies, the animals were acclimatized in our institute animal facility conditions (22 ± 1 °C room temperature; 55 ± 10% relative humidity; 12 h light/dark cycle). Animals were provided free access to food and water during the acclimatization. Rabbits being coprophages, the cages are designed with a platform inside to prevent coprophagy.

Aqueous suspensions of TAA with 20% HP-β-CD (TAA-HP-β-CD-Susp) containing different dose strengths (1 mg/30µL, 2 mg/30µL, 4 mg/30µL) administered at a dose volume of 30 µL/eye in both eyes using a micropipette (10-100 µL) and tips into the inferior cul-de-sac of the rabbit eye. Ocular pharmacokinetic studies were also performed for aqueous suspension

of TAA (TAA-Susp) without the addition of HP-β-CD containing a dose strength of 4 mg at a dose volume of 30 µL/eye. All the formulations were vortexed for 5 min to form a homogenous dispersion prior to their pre-corneal administration. Post-instillation of the formulations, the eyes of the animals were closed for a minute. Blood samples were collected from the marginal vein of the right ear using a butterfly needle. Aqueous and vitreous humour were collected from both eyes of a single animal at each time point. Blood samples were collected into the centrifuge tubes, pre-treated with disodium EDTA (4.5% w/v) as an anticoagulant at 0^{th} (before administration of the formulation) and at 30^{th}, 60^{th}, 90^{th}, 120^{th}, 240^{th} and 360^{th} min following the ocular administration of formulations. Aqueous humour and vitreous humour were collected as per the procedure described in section 2.4.

2.3 Results and discussions

2.3.1 Method development

In the preliminary method development trials, different aqueous phase components (like Milli-Q water, 0.05% v/v formic acid in Milli-Q water, 0.05% v/v trifluoroacetic acid in Milli-Q water and 10 mM ammonium acetate buffer) and different organic phase components (MeOH and ACN) in various proportions were tested. The mobile phase system with MeOH as the organic phase resulted in poor peak properties (broader/split peaks), while ACN as the organic phase produced good peak properties for the analyte (TAA). Out of the various aqueous phase components tried 10 mM ammonium acetate resulted in reproducible retention times of TAA with better peak properties than other aqueous phase components.

In developing any bio-analytical method, internal standard (IS) plays a critical role in determining the efficiency and reproducibility of the sample processing method followed in the extraction of analyte from the biological sample. Various compounds like Rufinamide, Telmisartan, Piribedil and Tadalafil were tried as IS in the method development of TAA. However, Piribedil was ideal as the IS as it was well resolved from the TAA (analyte) peak and had good peak properties. The run time for each sample was 7 min. Other compounds that

tried as IS either interfered with the analyte peak and showed poor peak properties or had a longer run time for each sample analysis.

In the final method, Piribedil was selected as IS for TAA with a mobile phase consisting of a mixture of 10 mM ammonium acetate buffer (pH 4.5) (aqueous phase/solvent A) and ACN (non-aqueous phase/solvent B) in the ratio of 58:42 v/v. In the optimized method, the retention times for PBD and TAA were 3.9±0.1 and 5.1±0.1 min, respectively. The developed method's sample run time (7 min) was less than any of the HPLC methods reported to date. The obtained peaks were checked for various chromatographic parameters like retention factor ($k \geq 2$), injection precision (RSD<1% for n=6 injections), resolution (>2), tailing factor (≤ 2) and theoretical plate number (>2000).

2.3.2 Sample preparation and drug extraction from plasma, aqueous humour and vitreous humour

The developed bioanalytical method for TAA was fully validated in plasma, while partial validation was performed in the aqueous and vitreous humour, considering the limitation of the low volume of the two matrices. TAA and IS were extracted from the biological matrices using the protein precipitation technique with different precipitating agents like MeOH and ACN alone and in various combinations. Preliminary extraction trials were carried out with 1:1, 1:3, 1:5, 1:7 and 1:10 v/v ratios of plasma to the precipitating agent. As the volume ratio of the precipitating agent increased, the protein load decreased and the chromatogram was found to be clean with good baseline stabilization. However, the peak responses were affected due to the dilution effect at a higher volume ratio of precipitating agent. Therefore, following the protein precipitation of the sample (at 1:10 v/v ratio), the sample was centrifuged and the supernatant was collected. The collected supernatant evaporated to dryness under vacuum and then reconstituted with mobile phase before injecting into the HPLC. The protein precipitation method was simple, rapid and reproducible, with higher recovery for both TAA (>88.41%) and IS (>90.01%).

2.3.3 Method validation

2.3.3.1 Selectivity

The method was found to be selective for reliable quantification of TAA in all three biological matrices (plasma, aqueous humour and vitreous humour). No interference was observed from endogenous matrix components at TAA or IS retention times in the processed blank biological samples, zero biological samples (biological sample spiked only with IS), QC standards and *in vivo* pharmacokinetic samples shown in Figure 2.1.

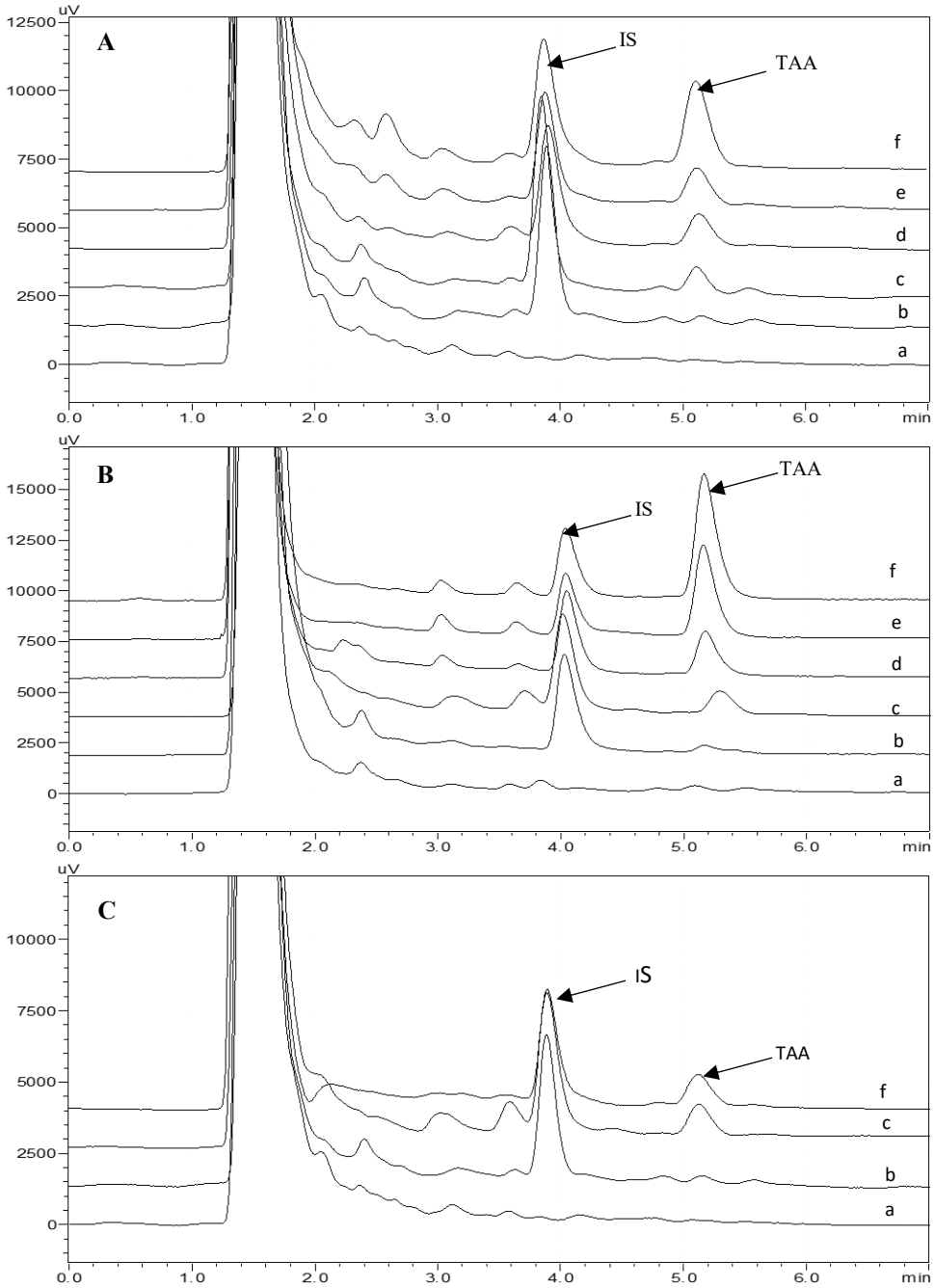

Figure 2.1 Overlaid Chromatograms of TAA in A) Plasma samples, B) Aqueous humour

samples and C) Vitreous humour samples. Chromatograms (a), (b), (c) in all the sections are the corresponding blank matrix sample (without spiking TAA and IS), zero sample (spiked only with IS) and lower limit of quantitation (LLOQ) standard, respectively. (d), (e) and (f) are the chromatograms of pharmacokinetic samples collected following ocular administration of aqueous suspension of TAA containing 1 mg/30µL, 2 mg/30µL and 4 mg/30µL dose strength, respectively.

2.3.3.2 Linearity and sensitivity

The calibration curves were linear in the selected concentration range of 50–3000 ng/mL for plasma, with IS at 400 ng/mL (mean regression coefficient, R^2=0.998). Calibration curves were constructed with peak area ratios of TAA/IS versus nominal concentration of TAA. The linear regression analysis determined slope, intercept, R^2 and R^2adj values and the results are summarised in Table 2.1. Lower values of the standard error of estimate (SEE) indicate the high precision of the developed method. Further, the F_{cal} value (6898.2) for the regression analysis of the calibration curve data is significantly higher than the F_{crit} value (6.62) at a 5% level of significance, indicating that the ability of the linear regression equation in predicting the concentration within the calibration range which is further supported by higher R^2 (0.9993) and R^2_{adj} (0.9991) values. The difference between R^2 and R^2_{adj} values is less than 0.2, indicating that the number of calibration points had no significant impact on the regression coefficient.

The method sensitivity was estimated in terms of LOD and LOQ based on the standard deviation values of y-intercept values and mean slope obtained from the six replicate (n=6) calibration curves. The LOD and LOQ for TAA in plasma were found to be 8.3 ng/mL and 25 ng/mL, respectively (Table 2.1). Based on the LOQ value obtained, the lower limit of quantification LLOQ was set at 50 ng/mL. Six replicate injections at LLOQ concentration (in all three matrices) revealed that the method was reliable, reproducible with %RSD < 11.63 and accurate with %bias < 4.47.

Table 2.1 Linear regression parameters for plasma calibration standards, LOD, LOQ for TAA

Calibration Curve Series*	Slope	Intercept	Statistical parameters obtained from the Mean calibration curve	LOD and LOQ (ng/mL)
1	1.0486	0.0163	R^2 = 0.9993 R^2_{adj} = 0.9991 SEE = 0.0342 F_{cal} = 6898.2 95% CI of Intercept: -0.056 to 0.044	8.3 and 25
2	1.0646	0.0178		
3	1.0359	0.0129		
4	1.0166	0.0137		
5	1.0218	0.0176		
6	1.0492	0.0198		
Mean	1.0395	0.0164		
SD	0.0182	0.0026		
%RSD	**1.752**	**16.065**		

Note: Standard deviation (SD), Percentage relative standard deviation (RSD), Regression coefficient (R^2) and Adjusted R^2 (R^2_{adj}), Standard error of estimate (SEE), Confidence interval (CI); n=6 in all cases. At α = 0.05, the F_{crit} value is 6.61 and the F_{cal} value (6898.2) is significantly higher than the F_{crit}. LOD = 3.3 × (SD of calibration curve intercepts/mean of calibration curve slopes) and LOQ = 10 × (SD of calibration curve intercepts/mean of calibration curve slopes)
*Each Calibration curve series corresponds to one full calibration curve; the slope and intercept values represent the same.

2.3.3.3 Accuracy and precision

The data obtained for accuracy and precision studies performed using LLOQ concentration and all QC standards are presented in Table 2.2. The mean accuracy values expressed in terms of %bias, in all the three matrices, in both intra-day and inter-day repeatability studies for LLOQ samples were between -6.93% to 2.03% (much less than the acceptable limit of ±20%) while that of all the three QC standards were found to be between -3.89% to +7.27% (which are well within the acceptable limits of ±15%). The intra-day and inter-day precision measured in terms of %RSD for LLOQ samples in all three matrices were less than 7.87% (which is well within the maximum limit of 20%) while that of all the three QC standards were less than 7.72% (which are well within the maximum limit of 15%). The results obtained from intra-day and inter-day repeatability studies indicate that the developed method is accurate and precise in the quantification of TAA in all three biological matrices.

2.3.3.4 Recovery

The mean %recovery values of TAA from the spiked rabbit plasma, aqueous humour and vitreous humour samples, when compared with aqueous analytical standards containing similar concentration, were between 88.41% to 103.84% with %RSD less than 9.37% for LLOQ as well as the three QC standards (Table 2.2). The mean %recovery of IS was between 90.04 to 94.29%, with %RSD not more than 6.78% across all the samples. The high mean %recovery values with low %RSD values indicate that the protein precipitation method followed in TAA extraction from all three biological matrices is an efficient and reliable extraction method.

Table 2.2 Accuracy, precision and recovery of the method for determination of TAA in various Matrices.

Biological Matrix	Sample	Intra-day		Inter-day		%Recovery	
		%RSD	%Bias	%RSD	%Bias	Mean ± SD	%RSD
Plasma	LLOQ	5.65	1.92	7.87	2.03	89.35±3.49	3.91
	LQC	2.33	3.14	3.23	3.99	93.81±6.64	7.08
	MQC	3.07	3.02	4.87	3.9	96.95±2.77	2.86
	HQC	2.54	2.8	4.47	3.9	98.712±3.68	3.73
Aqueous humour	LLOQ	2.12	-0.47	6.82	-3.09	103.84±7.46	7.18
	LQC	6.11	-1.9	7.72	0.5	95.41±6.09	6.38
	MQC	5.95	2.57	3.36	3.65	88.75±3.86	4.35
	HQC	2.65	2.33	3.79	2.65	97.17±3.20	3.29
Vitreous humour	LLOQ	3.17	-6.24	5.3	-6.93	101.44±9.51	9.38
	LQC	4.62	-2.34	4.63	-3.89	95.64±6.13	6.41
	MQC	5.25	1.59	4.26	2.17	88.41±1.91	2.16
	HQC	4.11	2.25	4.34	7.27	96.65±3.54	3.66

Note: Standard deviation (SD), %relative standard deviation (%RSD), *n*=6 samples in all cases. *LLOQ = 50 ng/mL, LQC = 100 ng/mL, MQC = 100 ng/mL, HQC = 2500 ng/mL and IS = 400 ng/mL Accuracy is given as %Bias = [100 × (predicted concentration – nominal concentration)/nominal concentration]. %Recovery = [(Peak area of quality control standard in biological matrix/peak area of aqueous analytical standard of same concentration) × 100].

2.3.3.5 Stability

TAA stability in plasma was evaluated using LLOQ and three QC standards under different stress conditions to ensure the samples were stable during handling, storage and processing.

The results obtained from stability studies in different stress conditions are depicted in Figure 2.2. No significant degradation of TAA in plasma samples was observed under all three stress conditions, i.e., auto-injector stability (at 15 °C) study of the processed plasma samples over 24 h post-preparation, freeze-thaw stability (-20 ºC) study up to three cycles for three consecutive days and long-term stability (−20 °C) for 30 days. In any stress conditions, the %deviation from the zero-time sample was observed to be in the range of -5 to 5%.

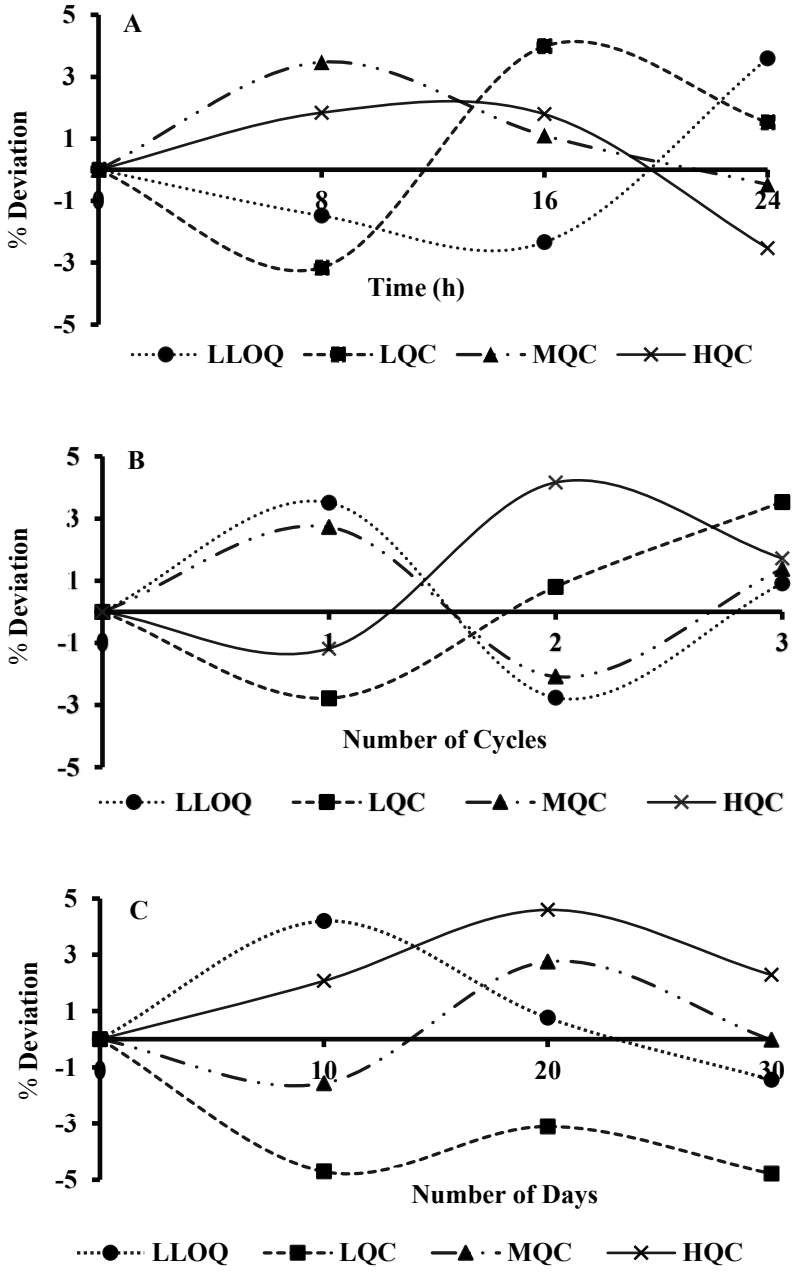

Figure 2.2 Stability study of TAA in plasma samples subjected to different stress conditions: (A) Auto-sampler stability; (B) Freeze-thaw stability; and (C) Long-term stability. Each data

point represents the mean of three independent determinations with %RSD less than 5%. LLOQ = 50 ng/mL, LQC = 100 ng/mL, MQC=1000 ng/mL and HQC = 2500 ng/mL.

2.3.3.6 Robustness

Robustness of the method evaluated for change in the mobile phase flow rate (0.95 and 1.05 mL/min), mobile phase composition (ACN: Buffer (40:60) 1mL/min and ACN: Buffer (44:56) 1mL/min), pH of the aqueous phase (pH 4.3 and pH 4.7) and temperature of column oven (38 ºC and 42 ºC). RSD (%) from six replicate injections of MQC for the changes made in each of the factors described above was found to be less than 6.3%. The resolution of the peaks was >2 and the tailing factor for the TAA peak was <1.5 for changes made in each element. The %RSD of the retention times of the TAA and IS were 3.6 to 7.6, respectively. Mean percentage recovery values for six replicate samples of MQC for the changes made in each factor were found to be between 92.6% to 99.3%. The results obtained for robustness studies were well within the acceptance criteria of not more than 10% (RSD) and within 100 ± 20% for percentage recovery.

2.3.4 Solubility Studies and Characterization studies of the mixture of TAA and HP-β-CD

2.3.4.1 Solubility studies

TAA Solubility studies were carried out in different solvent systems to determine the suitable composition of the solvent system for the preparation of a stable ophthalmic solution of TAA with a dosing volume of NMT 30µL. The results from the solubility studies of TAA are given in Table 2.3.

TAA was found to have low solubility (NMT 17 µg/mL) in buffered systems of pH 1.2, 4.5 and 7.4, MilliQ water and STF. However, TAA showed a significant difference in its solubility properties in different co-solvents, surfactants and solubilizers. TAA was found to have the highest solubility in HP-β-CD among the various excipients tried in the solubility studies. Solubility of TAA increased with an increase in the concentration of HP-β-CD from 15% w/v to 25% w/v. But the increase in solubility of TAA was not very significant at 20% w/v and

25% w/v concentration. Based on the solubility data and the safety profile of HP-β-CD, we have used HP-β-CD at 20% w/v in the final formulation.

Table 2.3 Saturation solubility studies of TAA in different Vehicles/Excipients

Vehicles/Excipients	Concentration[a] (µg/mL)	Vehicles/Excipients	Concentration[a] (µg/mL)
MilliQ water	16.07 ± 1.49	PVPK30	23.26 ± 1.59
STF[c]	13.72 ± 2.95	Soluplus	38.75 ± 2.14
pH 1.2 buffer (0.1 N HCl)	8.46 ± 1.98	PVA	21.77 ± 3.28
pH 4.5 Na. Ac buffer (USP[b])	15.57± 1.59	M-E4M	20.06 ± 2.45
pH 7.4 phosphate buffer (USP[b])	13.82 ± 2.51	HPMC	22.04 ± 2.91
PEG-400	14.67 ± 2.54	TPGS	76.94 ± 5.07
PG	14.19 ± 2.14	sHA	17.19 ± 1.22
T-80	47.74 ± 1.49	HP-β-CD -15%	1453.94 ± 19.98
Poloxomer-188	20.09 ± 3.08	HP-β-CD -20%	2636.6 ± 14.10
Poloxomer-407	25.09 ± 2.13	HP-β-CD -25%	3065.73 ± 15.37

Note: [a]All the data is represented as Mean ± SD of replicate analysis (*n = 3*), [b]Vehicle (buffers) of the specific pH were prepared as per the compositions given in USP-2016, [c]Composition of simulated Tear Fluid (STF) [151].

2.3.4.2 Characterization studies of the mixture of TAA and HP-β-CD

The FTIR spectra of TAA, HP-β-CD and the physical mixture of TAA + HP-β-CD are given in Figure 2.3. TAA showed characteristic peaks at 3395 cm^{-1} (due to O-H stretching vibration), 2945 cm^{-1} (due to C-H stretching vibration) and 1710 cm^{-1} (due to stretching vibration of the carbonyl group at aliphatic ester bonds). In addition, peaks were observed at 1662 cm^{-1} (due to C=C stretching vibration), 1122 cm^{-1} (due to asymmetric axial stretching vibration of C–O–C bond in aliphatic esters) and 1050 cm^{-1} (due to C-F stretching vibration). The FT-IR spectra of HP-β-CD showed a broad band between 3600 and 3200 cm^{-1} (with a peak at 3392 cm^{-1}) corresponding to the O-H stretching vibration by the hydroxyl groups present in its structure. The same broad band was observed in the spectrum of the TAA+ HP-β-CD physical mixture. The bands from 2970 and 2931 cm^{-1} corresponding to the C−H stretching vibration are present both in the HP-β-CD spectrum and TAA+ HP-β-CD physical mixture. The absorption band at 1645 cm^{-1} is related to H−O−H bending. The bands in the

range of 500–1500 cm^{-1} arise from a single type of molecular vibration due to strong coupling caused by neighbouring bonds vibrating with similar frequencies, specific to the α-1,4 glycosidic bonds present in the cyclodextrin. All these bands were also seen in the spectrum of the TAA+ HP-β-CD physical mixture.

The spectra of the TAA+ HP-β-CD physical mixture and that of HP-β-CD are indistinguishable due to a combination of the following factors: (a) each HP-βCD molecule has a relatively large number of polar groups (O–H, C–O, etc.), giving rise to intense absorption bands; (b) both the host and guest molecules absorb coincidentally in most of the spectral regions; (c) there is an excess of free HP-β-CD in the inclusion complex sample. However, the presence of TAA in the physical mixture is undoubtedly confirmed by the peaks observed at 2945,1706, 1641 and 1526 cm^{-1}. In the TAA+ HP-β-CD physical mixture spectrum, the peak at 1050 cm^{-1} due to the C-F stretching vibration in TAA was not observed. This could be the entrapment of the C-F bond of TAA into the cavities of HP-β-CD, suggesting the possibility of inclusion complexation between TAA and HP-β-CD.

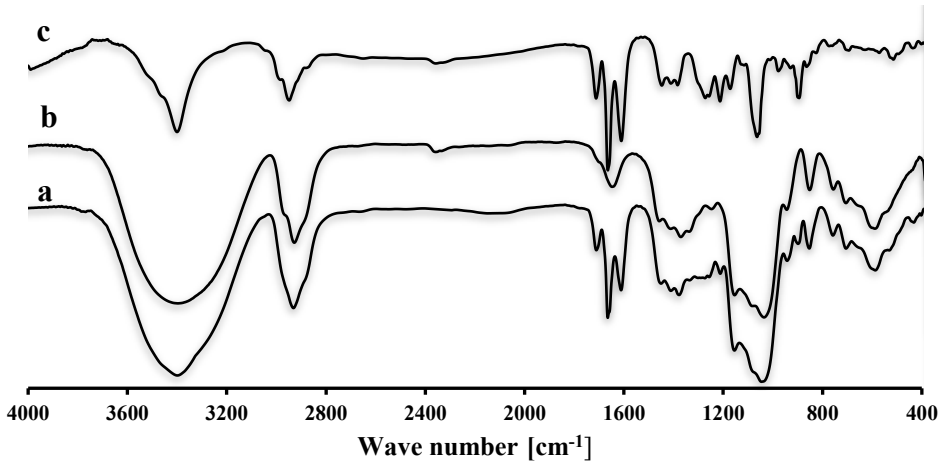

Figure 2.3 FT-IR spectra of (a)TAA (b) HP-β-CD (c)TAA+ HP-β-CD Physical Mixture

The DSC thermograms of TAA, HP-β-CD and the physical mixture of TAA + HP-β-CD are given in Figure 2.4. TAA showed an endothermic peak at 292°C, which corresponds to its melting point. A broad peak was observed for HP-β-CD in the range of 60 ºC to 100 ºC. The

thermogram of the physical mixture of TAA+HP-β-CD revealed a slight shift in the melting endothermic peak of TAA. However, the normalized energy (enthalpy per gram of TAA) was found to be the same for the endothermic peak in the TAA sample and physical mixture of TAA + HP-β-CD, indicating that there is no degradation of TAA in the presence of HP-β-CD. The results obtained from the FT-IR and DSC studies reveal that TAA is compatible with HP-β-CD.

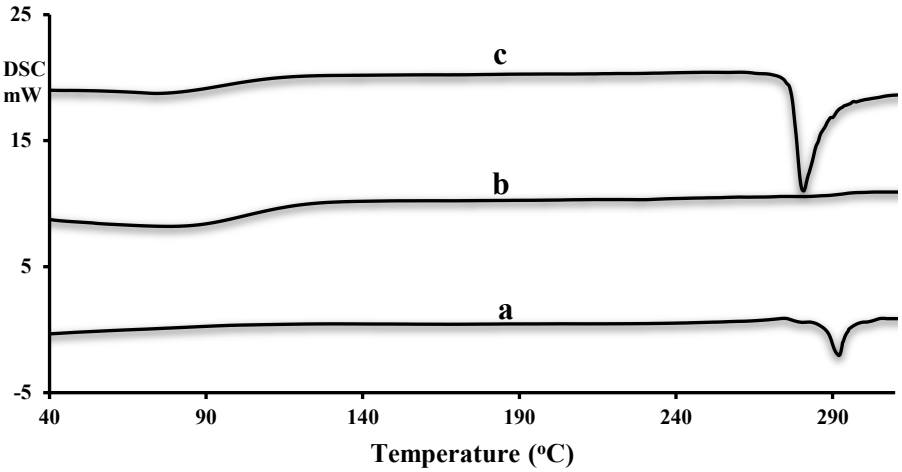

Figure 2.4 DSC Thermogram of (a)TAA (b) HP-β-CD (c)TAA+ HP-β-CD Physical Mixture

2.3.5 Ocular pharmacokinetic study of aqueous suspensions of TAA containing different dose strengths in Male New Zealand rabbits

Researchers have studied the effect of administering TAA through buccal and intravenous routes in the dose range of 1 mg/kg to 2 mg/kg dose in rabbits and through oral, intravenous and pulmonary routes using dose strengths of 2mg/kg to 5mg/kg in humans [87,152]. In addition, reports were found on intravitreal injections of TAA at dose strengths of 4 mg and 16 mg [91,153]. However, there are no published reports on the minimum dose required for the pre-corneal administration of conventional formulations of TAA to achieve effective concentrations in the vitreous humour.

Ocular pharmacokinetic studies of an aqueous suspension of TAA without the addition of HP-β-CD (TAA-Susp) containing a dose strength of 1 mg/30µL, 2 mg/30µL and 4 mg/30µL did not result in measurable concentrations neither in aqueous humour nor in vitreous humour at

any of the sampling points post the administration of the formulation. This could be due to the drug's poor solubility and dissolution rate resulting in poor permeation of the drug through the corneal epithelium, which is the major barrier in the absorption of drugs into the aqueous humour. Aqueous suspension of TAA (containing dose strength of 1 mg/30µL) with 20% HP-β-CD (TAA-HP-β-CD-Susp) showed measurable concentration in aqueous humour up to 6 h post the administration of the formulation. This clearly indicates that HP-β-CD played a critical role in improving the absorption of the drug into the aqueous humour. However, the concentration of TAA in the vitreous humour was less than the LLOQ levels for the aqueous suspension of TAA (containing a dose strength of 1 mg/30µL) with 20% HP-β-CD. Therefore, we have performed ocular pharmacokinetic studies of an aqueous suspension of TAA containing 20% HP-β-CD (TAA-HP-β-CD-Susp) starting with a dose of 2 mg/30µL and 4 mg/30µL, with the objective of achieving measurable and effective concentrations (with those reported in the literature) in the vitreous humour.

The time course of TAA in plasma, aqueous humour and vitreous humour obtained following the pre-corneal administration of aqueous suspensions of TAA with 20% HP-β-CD (TAA-HP-β-CD-Susp) at different dose strengths are given in Figure 2.5. The time-course data of TAA obtained in aqueous humour, vitreous humour and plasma were subjected to non-compartmental analysis using Phoenix WinNonlin software (version 7.0, Pharsight Corporation, NC, USA) to determine various pharmacokinetic parameters reported in Table 2.4.

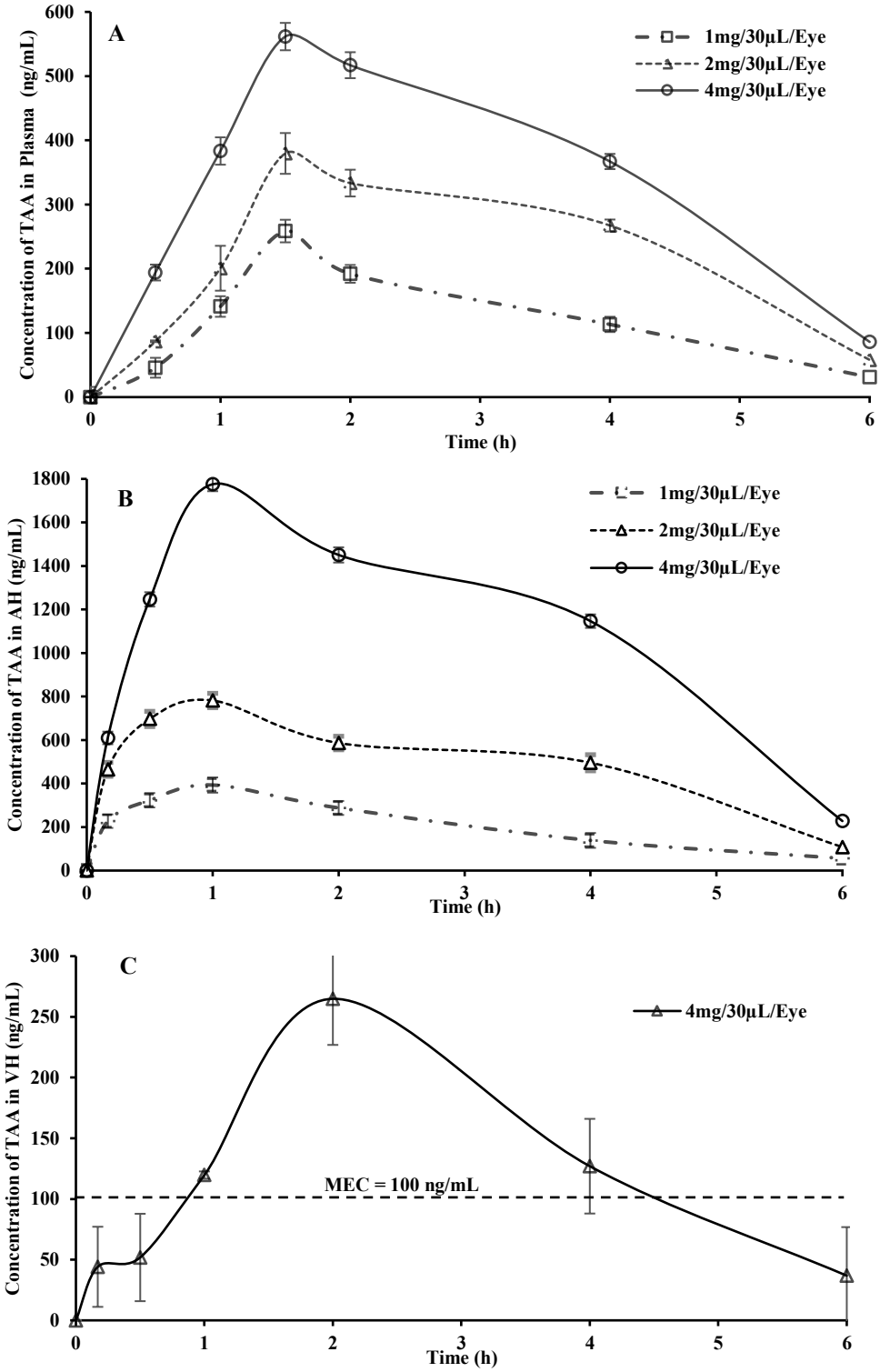

Figure 2.5 Mean concentration versus time profiles of TAA in (A) Plasma; (B) Aqueous humour (AH); and (C) Vitreous humour (VH), following ocular administration of aqueous suspension of TAA with 20% HP-β-CD (TAA-HP-β-CD-Susp) containing 1 mg/30µL, 2 mg/30µL and 4 mg/30µL dose strength. Each data point represents the mean of three independent determinations in the case of the plasma time course (*n*=3), while each data point represents the mean of two independent determinations in the case of aqueous humour and vitreous humour (*n*=2).

Note: Aqueous suspension of TAA with 20% HP-β-CD (TAA-HP-β-CD-Susp) containing 1 mg/30µL and 2 mg/30µL did not yield quantifiable concentrations in vitreous humour at any of the sampling points.

PK parameters in aqueous and vitreous humour were calculated using pooled concentration data obtained from the individual eyes of a single animal sacrificed at each sampling time point. It was assumed that pooling the concentration data from individual eyes of the same animal accounts for the residual variability rather than the intrinsic differences in the pharmacokinetic process of different formulations administered to the animals. As we could only construct the mean concentration versus time profiles in aqueous humour and vitreous humour from the pooled concentration data, the ocular pharmacokinetics parameters like C_{max}, AUC and MRT were calculated as single values without standard deviation. Therefore, unlike the plasma profile, statistical analysis was not done for aqueous and vitreous humour data.

Based on the observed data, the maximum concentration (C_{max}) and the time taken to reach the maximum concentration (T_{max}) in aqueous humour, vitreous humour and plasma were reported. Based on the results obtained, we can infer that the C_{max} values in aqueous humour increased proportionately with an increase in the dose strength of the formulation. A similar trend was observed in the C_{max} values in plasma with an increase in the dose strength of the formulation. However, the concentrations of TAA in vitreous humour were found to be below LLOQ values at all sampling time points following the administration of aqueous suspension containing 1 mg/30µL and 2 mg/30µL dose strengths. The time course of TAA in vitreous humour was achieved only with an aqueous suspension of TAA containing 4 mg/30µL dose strength. At 4 mg/30µL dose strength, pre-corneal administration of aqueous suspension of TAA produced an effective concentration of >100 ng/mL.

The T_{max} was 1 h in the case of aqueous humour and 1.5 h in the case of plasma for all the dose strengths. In the case of the vitreous humour, the T_{max} was observed at 2 h for a formulation containing 4 mg/30µL dose strength.

The total area under the curve from zero time to the last measurable concentration ($AUC_{0\text{-}tlast}$) and the total area under the curve from zero time to infinity ($AUC_{0\text{-}\infty}$) were determined for the time course of the drug in aqueous humour and plasma for all the dose strengths while $AUC_{0\text{-}tlast}$ and $AUC_{0\text{-}\infty}$ were determined for the time course of drug in vitreous humour only for 4 mg/30µL dose strength. The $AUC_{0\text{-}tlast}$ values in aqueous humour and plasma were more than 90% of their corresponding $AUC_{0\text{-}\infty}$ values at all the dose strengths. The $AUC_{0\text{-}tlast}$ value in vitreous humour was more than 90% of its corresponding $AUC_{0\text{-}\infty}$ value for 4 mg/30µL dose strength. This clearly indicates that the developed method is very sensitive to analyse the samples till more than 90% of the drug is cleared from the aqueous humour and plasma at all dose strengths and from vitreous humour at 4 mg/30µL dose strength.

Table 2.4 Pharmacokinetic parameters of TAA in plasma, aqueous humour and vitreous humour following ocular administration of 30 µL of an aqueous suspension of TAA with 20% HP-β-CD (TAA-HP-β-CD-Susp) containing different dose strengths in male New Zealand white rabbits.

Biological Matrix	Dose	Pharmacokinetic Parameters					
		C_{max} (ng/mL)	T_{max} (h)	$t_{1/2}$ (h)	$AUC_{0\text{-}t}$ (ng×h/mL)	$AUC_{0\text{-}\infty}$ (ng×h/mL)	$MRT_{0\text{-}\infty}$ (h)
[a]Plasma	1mg/Eye	258.78±7.6	1.5	1.5±0.1	720.3±18.4	789.6±18.4	3.1±0.1
	2mg/Eye	379.6±21.3	1.5	1.8±0.1	1342.9±29.5	1490.9±31.6	3.3±0.1
	4mg/Eye	561.6±20.8	1.5	1.7±0.2	2035.7±68.0	2250.6±93.3	3.2±0.0
Aqueous humour	1mg/Eye	393.1	1	1.8	1250.6	1387.3	2.8
	2mg/Eye	781.5	1	1.9	2970.1	3263.0	3.0
	4mg/Eye	1775.4	1	1.7	6697.3	7283.6	3.0
Vitreous humour	4mg/Eye	264.9	2	1.4	810.4	885.0	3.1

Note: [a]For plasma, the parameters are expressed as Mean ± SD (*n*=3 observations) of the data obtained in the pharmacokinetic study except for T_{max}. The values of T_{max} are expressed in terms of the median of *n*=3 observations. For aqueous humour and vitreous humour, the $AUC_{0\text{-}t}$, $AUC_{0\text{-}\infty}$ and $MRT_{0\text{-}\infty}$ values were obtained from the composite sampling of both the eyes of an animal sacrificed at each time point.

Oliveira *et al.* reported that TAA was effective at a concentration of more than 100 ng/mL in vitreous humour [133]. In the current research work, an aqueous suspension of TAA with 20%

HP-β-CD (TAA-HP-β-CD-Susp) at 4 mg/30µL dose strength produced a TAA concentration in the vitreous humour of more than 100 ng/mL and achieved a maximum concentration of 264.9 ng/mL. The concentration of TAA in the vitreous humour was maintained above 100 ng/mL for a period of 3 h (between 1 h to 4 h). Therefore, we can infer that aqueous suspension of TAA with 20% HP-β-CD (TAA-HP-β-CD-Susp) at 4 mg/30µL dose strength is optimal for pre-corneal administration to produce effective TAA concentrations in the vitreous humour.

2.4 Conclusion

In this chapter, conventional formulations of TAA with 20% HP-β-CD (TAA-HP-β-CD-Susp) containing different dose strengths were formulated and evaluated to identify the dose strength required to produce effective concentrations in the vitreous humour. A rapid, selective, sensitive and highly reproducible HPLC-PDA method utilizing a small sampling volume (≤45µL) of aqueous humour, vitreous humour and plasma was developed and validated for TAA quantitation. Ocular pharmacokinetic studies in male New Zealand rabbits revealed that aqueous suspensions of TAA with 20% HP-β-CD (TAA-HP-β-CD-Susp) with dose strengths of 4 mg/30µL produce effective concentrations of more than 100 ng/mL for a period of more than 3 h in the vitreous humour. Comparison of the pharmacokinetic time course of TAA in aqueous humour and vitreous humour for aqueous suspensions of TAA (at 4 mg/30µL dose strength) with (TAA-HP-β-CD-Susp) and without HP-β-CD (TAA-Susp) clearly indicates that HP-β-CD had a significant effect on increasing the ocular absorption of the drug into aqueous humour and vitreous humour. This is primarily due to the increase in saturation solubility and dissolution rate of TAA in lachrymal fluids. The developed HPLC method offered high sensitivity to determine more than 95% of the entire time course in plasma, aqueous humour and vitreous humour with minimal sampling volume, which is critical in ocular pharmacokinetics studies.

3

OPTIMIZATION AND *IN VIVO* EVALUATION OF TRIAMCINOLONE ACETONIDE LOADED *IN SITU* GEL PREPARED USING REACTED TAMARIND SEED XYLOGLUCAN AND KAPPA-CARRAGEENAN FOR OCULAR DELIVERY

3.1 Introduction

Uveitis is an inflammatory disease condition of the eye affecting the uvea or neuro-retina [107,154]. A significant contribution to uveitis has an autoimmune origin that can be treated effectively with immunosuppressants and CSTs [155]. The essential part of the treatment strategy in noninfectious uveitis is to control the inflammation by administering CSTs either alone or in combination with other immunosuppressants [107]. The majority of the CSTs used in the treatment of uveitis are administered as intravitreal injections, which can cause complications like secondary ocular hypertension, retinal detachment and cataract formation [154,156]. Triamcinolone acetonide (TAA), a water-insoluble CSTs, is often prescribed to manage noninfectious intermediate and PU [108]. The currently marketed drug product of TAA is a suspension administered as an intravitreal injection. Due to the nature of drug administration (intravitreal), the currently marketed drug product is reported to have severe side effects like endophthalmitis, pseudoendophthalmitis, retinal detachment and secondary ocular infection. Moreover, the distribution of TAA particles in the vitreous humour can impair vision, hasten cataract formation and raise intraocular pressure [107,129,157]. Therefore, it is vital to develop drug products of TAA that are patient-compliant and effective in treating the disease condition.

Ophthalmic drops are the most convenient and popular drug product, preferred by doctors and patients for treating ocular disease conditions. However, administering drug products in the precorneal area to treat disease conditions affecting the tissues at the back of the eye involves many challenges. It is challenging to achieve therapeutic drug concentrations at the inner-most tissues of the eye, like the uvea/retina, by administering conventional ophthalmic drug products [158]. Factors such as dilution of the administered formulation by lacrimal secretions, rapid clearance of the administered formulation by nasolacrimal drainage and systemic absorption through the conjunctiva result in low availability (5–10%) of the drug in the aqueous humour

and higher systemic absorption (50–90%) [159,160]. Several barriers, including the corneal epithelial layer, which is a protective barrier, limit the entry of drugs into the vitreous humour following the topical administration of ophthalmic drug products [161]. To overcome the problems stated above, ophthalmic drug products are administered at high frequency to maintain therapeutic concentrations in target tissues. This inadvertently causes an increase in systemic exposure to the drug, leading to systemic side effects [162].

The problems associated with conventional ophthalmic drops, specifically in terms of low pre-corneal residence time, can be overcome by various formulation approaches [159]. Researchers have tried using viscous solutions/suspensions, hydrogels, ointments and gelling systems to improve the residence time at the corneal surface. Among the various formulations, *in situ* gelling systems are found to be more promising. *In situ* gels are easy to manufacture and administer with good dosing accuracy compared to hydrogels and ointments. They provide longer residence times compared to viscous solutions/suspensions [159]. Various natural and synthetic polymers have been reported in the literature for their *in situ* gelling properties, which work on stimuli like temperature, ions and pH [163]. The main drawback of synthetic polymers is that they provide gelling properties only at very high concentrations. Natural polymers are biocompatible and can gel even at lower concentrations. In addition, some of the natural polymers exhibit strong mucoadhesive characteristics [164,165].

The physiological conditions (like pH, ion concentration and temperature) in the pre-corneal area of the eye are very dynamic and are impacted by disease conditions like uveitis. Therefore, it is very prudent to design *in situ* gelling systems that can be triggered by more than one stimulus for delivering drugs to treat uveitis [166]. In the current study, we designed an *in situ* dual-responsive gel for TAA delivery as an eye drop to attain therapeutic concentrations in the vitreous humour.

The tamarind seed xyloglucan (TSX) is a polysaccharide consisting of glucan as the backbone and galactose and xylose as the side chains. TSX does not form a gel unless treated with alcohol, sugar or polyphenol such as epigallocatechin gallate or enzymatically reacted with β-galactosidase. Reacted tamarind seed xyloglucan (RXG), obtained from chemical and enzymatic modification of TSX, exhibits mucoadhesive and thermoresponsive *in situ* gelling properties. Due to these properties, RXG is an attractive polymer for numerous drug delivery applications [167–169].

Carrageenan (CRG) is a natural polysaccharide that exhibits ion-responsive *in situ* gelling properties. It is a linear chain anionic polymer consisting of sulfated and non-sulfated D-galactose and D-anhydrogalactose repeating units. The cations (like Na^+, K^+ and Ca^{2+}) present in the physiological fluids at the administered site can neutralize the sulfate groups in CRG and cause the polymer to exhibit ion-responsive *in situ* gelling properties. Three different grades of CRG are mostly used in pharmaceutical industries, namely, kappa-carrageenan (*κ*-CRG*)*, iota-carrageenan and lambda-carrageenan. Each of these grades of CRG has different degrees of sulfonic acid group substitutions in the polymer chain. CRG containing higher sulfate substitution makes it brittle and less responsive to ions, while lower sulfate substitution makes it more responsive to ions, particularly K^+ ions. Each disaccharide repeating unit has only one sulfate group in the case of *κ*-CRG, while Iota-Carrageenan and Lambda-Carrageenan have two and three sulfate groups, respectively. Due to this, *κ*- CRG undergoes gelation in the presence of K^+ ions and, therefore, is more suitable for preparing *in situ* gelling formulations [170–172].

In the current chapter, we have designed and optimized a dual responsive TAA loaded *in situ* gels using a combination of RXG and κ-CRG to address the shortcomings of aqueous suspension of TAA with 20% HP-β-CD (TAA-HP-β-CD-Susp) for ocular delivery. *Ex vivo* studies were conducted to determine the safety of the optimized *in situ* gels. The efficacy of

the optimized *in situ* gels was determined by performing ocular pharmacokinetic studies in New Zealand white rabbits.

3.2 Materials and methods

3.2.1 Material and analytical method

3.2.1.1 Material

Dr. Reddy's Laboratories, Hyderabad, India and Strides Pharma Science Limited, Bengaluru, India, provided free samples of TAA and piribedil (used as an internal standard in the bioanalytical method), respectively. Encore Natural Polymers Private Limited, Ahmedabad, India, provided a gift sample of tamarind seed xyloglucan (TSX; the viscosity of a 3% w/v solution in water at 25 °C is 2800 mPa.s). κ-CRG (Molecular weight (g/mol): 788.65, the viscosity of a 0.3% w/v solution in water at 25 °C is 10 to 25 mPa.s) and β-Galactosidase enzyme (≥ 8.0 units/mg solid; Source: Aspergillus oryzae species) and benzododecinium bromide were purchased for Sigma-Aldrich Private Limited, Mumbai, India. HPLC grades reagents (glacial acetic acid, ammonium acetate and disodium EDTA) and solvents (acetonitrile and methanol) were purchased from SRL Chemicals Private Limited, Mumbai, India. The buffer salts, including NaCl, $NaHCO_3$, KCl, $MgCl_2$, $CaCl_2$, Mannitol and others, were provided by SD Fine Chemicals Private Limited, Mumbai, India. High-quality purified water collected from the Milli-Q water purification system (Millipore®) MA; USA was used in the HPLC analysis. Male New Zealand white rabbits, weighing between 2 to 2.5 kg, were supplied by VAB Biosciences Limited, Hyderabad, India.

3.2.1.2 Analytical method

Analysis of TAA concentration in various *in vitro* and *in vivo* (vitreous and aqueous humour obtained from ocular pharmacokinetic studies) samples was performed using a validated HPLC method (Section 2.3.1 and 2.3.3, Chapter 2).

3.2.2 Preparation of the *in situ* gels

3.2.2.1 Purification of the TSX

The TSX sample received from the industry sample was purified to remove the fat and protein impurities present in it. Fat impurities were removed by treating 5 g of TSX with 15 g of isopropyl alcohol in a 50 mL tube [169]. This mixture was vortexed for 15 min, followed by centrifugation at 2000 × g for 10 min at 25 °C. The supernatant was decanted to carefully collect the sediment. This procedure, as mentioned above, was repeated one more time. The sediment collected after the second cycle was heated at 60 °C to remove the solvent.

The protein impurities were removed from the dried powder obtained in the previous step by the procedure reported in the literature [173]. The dried powder was added in small quantities to a sufficient quantity of deionized water under continuous agitation to form a homogenous dispersion (3% w/v dispersion). The dispersion was stored in a refrigerator for 12 h for the powder particles to undergo hydration. The hydrated dispersion was then heated for 2 h at 60 °C under mild stirring and cooled to room temperature. The dispersion was centrifuged for 10 min at 2000 × *g* at 25 °C. The clear supernatant was separated from the pellet. The pellet was subjected to one more cycle of hydration, heating and centrifugation, as described above. The supernatants collected from both cycles were pooled together. Ethanol (95% v/v) was added to the pooled supernatant in the ratio of 3:1 (v/v), under constant agitation, to precipitate the purified TSX polymer. The above dispersion was centrifuged for 10 min at 2000 × *g* at 25 ºC to remove the supernatant. The pellet was collected and heated in a Petri plate at 50 °C to obtain a dried powder of purified TSX.

3.2.2.2 Enzymatic modification of TSX

The enzymatic modification of the purified TSX was carried out as per the procedure reported by Brun-Graeppi *et al*. and Han *et al***.** [174,175]. A 3% w/v solution of TSX was prepared using a 10 mM sodium acetate buffer (glacial acetic acid was used to adjust the pH to 5.0) as the

solvent. The solution was then refrigerated for 12 h for the polymer molecules to undergo hydration. Following the hydration of the polymer, the β-galactosidase enzyme was added to the polymer solution to yield a concentration of 7.4 U/mL in the mixture. The enzyme reduces the galactoside content present in the polymer to make it thermo-responsive [176]. The mixture was agitated for 18 h on a magnetic stirrer while maintaining a temperature of 34 ± 0.5 °C. After 18 h of agitation, the mixture was heated at 90 °C for 30 min to inactivate the enzyme. Reacted tamarind seed xyloglucan (RXG), which has undergone an enzyme reaction, was precipitated with 95% v/v ethanol and then dried at 50 ± 0.5 °C. The RXG obtained from the above step was stored at room temperature (25 ± 0.5 °C) until it was used.

3.2.2.3 Characterization of the RXG by FTIR, SEC and H-NMR

3.2.2.3.1 Fourier transform infrared spectroscopy (FT-IR) of the RXG

FT-IR analysis of the RXG was performed on a JASCO apparatus (FTIR4200, JASCO, Tokyo, Japan), using potassium bromide as a reference. RXG was mixed thoroughly with potassium bromide and compressed to form a pellet (2 mg of RXG in 200 mg of potassium bromide). The pellet was characterized in the range of 4000 to 400 cm^{-1} by performing 64 scans at room temperature with a resolution of 4 cm^{-1}. An average of three recordings was used to get the average spectrum of the sample.

3.2.2.3.2 Determination of the molar mass of RXG by size-exclusion chromatography (SEC)

The molar masses of TSX and RXG were determined using a size exclusion chromatography instrument (Waters Corporation, MA, USA). Ultrahydrogel™ linear column (dimensions: 300mm×7.8mm, 10 µm, Waters Corporation, MA, USA) was used for chromatographic separation. The analytes were detected using a refractive index detector. An aqueous solution containing a mixture of sodium nitrate and sodium azide at concentrations of 50 mM and 0.02% w/v was used as the mobile phase. The mobile phase was pumped in an isocratic mode at 0.8 mL/min through the column, maintained at 30 °C in a column oven. The injection volume was fixed at 10 µL. The run time for each sample was set to 15 min. Individual samples of TSX

(1% w/v) and RXG (1% w/v) were prepared by dissolving the polymers in a sufficient volume of highly purified water. The average molar masses of TSX and RXG were determined based on the calibration curve (6,300-739,000 Da) constructed using the Shodex- P-82 (Pullan) analytical standard (Show Denko America Inc., NY, USA).

3.2.2.3.3 Nuclear magnetic resonance spectroscopy (NMR) of RXG

Nuclear magnetic resonance spectroscopy of RXG was performed using a 400 MHz ^{1}H-NMR spectrometer (Bruker, Billerica, MA, USA) operated at an ambient temperature of 25 °C. RXG (10 mg) was dissolved in deuterated water (1 mL) and stored in the refrigerator for 12 h for hydration of the polymer. Following the hydration of the polymer, a small volume of the sample was taken in a 5 mm NMR tube and analyzed. The nuclear magnetic resonance of RXG was analyzed in the frequency range of 0 to 10 ppm.

3.2.2.4 Preparation of RXG in situ gels

RXG *in situ* gels were prepared by adding RXG powder to deionized water under continuous agitation to form a homogenous dispersion. This dispersion was refrigerated for 24 h to hydrate the polymer. Following the hydration of the polymer, the dispersion was mixed at 500 rpm for 6 h to form a homogenous solution. Mannitol (5.2% w/v) was added as an isotonicity adjusting agent to the above solution. Further, benzododecinium bromide, a bacteriostatic and fungistatic preservative, was added (0.01% w/v) to the polymer solution to form a blank RXG *in situ* gel.

3.2.2.5 Preparation of κ-CRG in situ gels

κ-CRG *in situ* gels were prepared by adding κ-CRG powder to deionized water under continuous agitation at 500 rpm for 2 h to get a clear solution. Mannitol (5.2% w/v) was added to the above solution to adjust the isotonicity. Since κ-CRG is an ion-sensitive polymer, mannitol (a non-electrolyte) was selected for adjusting the isotonicity. Finally, benzododecinium bromide (0.01% w/v) was added and stirred for 30 min to form a blank κ-CRG *in situ* gel.

3.2.2.6 Preparation of in situ gels containing a combination of RXG and κ-CRG

To prepare *in situ* gels containing a combination of RXG and κ-CRG, first, a weighed quantity of RXG was added to a defined volume of deionized water under agitation to form a homogenous dispersion. This dispersion was refrigerated for 24 h to hydrate the polymer and form a clear solution. A defined quantity of κ-CRG was added to the above solution and stirred at 500 rpm for 2 h to form a homogenous solution. To this solution containing the mixture of RXG and κ-CRG polymers, mannitol (5.2% w/v) and benzododecinium bromide (0.01% w/v) were added and stirred for 30 min to form blank RXG-κ-CRG *in situ* gel.

3.2.2.7 Loading of TAA in the optimized in situ gels

TAA powder with particle sizes in the range of 5-10 μm was added to the optimized blank *in situ* gels of RXG **(**Table 3.1: F4), κ-CRG (Table 3.1: F14) and RXG-κ-CRG (Table 3.1: F15) under magnetic stirring at 500 rpm to produce 100 mg/mL (10% w/v) dose strength in each of the formulations [177]. The dose strength of the *in situ* gels was fixed at 100 mg/mL in order to achieve 4 mg of TAA in 40 μL of the *in situ* gel for performing the ocular pharmacokinetic studies in male New Zealand rabbits. Until further use, TAA loaded *in situ* gels were kept in the refrigerator (2–8 °C).

3.2.3 Optimization of the *in situ* gels using the vial tilt method

3.2.3.1 Optimization of RXG proportion based on thermoresponsive gelation properties

In the preliminary studies, blank formulations containing different concentrations of RXG alone were prepared (Table 3.1 F1 to F3) and their solution state viscosity at 25 ± 0.5 °C was determined. RXG being a thermoresponsive polymer, the formulations were characterized for their gelation temperature, gelling time and gelling capacity using the 'vial tilting method' [178]. Briefly, 1 mL of the test formulations were taken in a glass vial (2.5 mL) and placed in a water bath with a temperature controller set at 25 °C. The temperature of the water bath was increased from 25 °C to 40 °C at a rate of 1 °C/min. The vial containing the sample was equilibrated for 1 min at every 1 °C increase in temperature and inverted by 90°. The

temperature at which the sample (in the vial) did not exhibit any flow was considered the gelation temperature of the sample. The time needed for the conversion from sol to gel at that particular temperature was considered the gelling time. Further, the gelling capacity of the representative formulation was assessed based on the flow properties and stiffness of the gel over a period of time. RXG formulations, which were free-flowing in the solution state at 25 ± 0.5 °C and showed gelation below 34 ± 0.5 °C, were selected for further studies. TAA powder was loaded into the optimized RXG *in situ* gel (Table 3.1: F4).

3.2.3.2 Optimization of κ-CRG proportion based on ion-responsive gelation properties in the presence of simulated tear fluid

Blank formulations containing different proportions of κ-CRG alone (Table 3.1: F5 to F8) were prepared and evaluated for their gelation properties in the presence of simulated tear fluid (STF, prepared by dissolving 0.68 g of NaCl, 0.22 g of $NaHCO_3$, 0.008 g of $CaCl_2 \cdot 2H_2O$, 0.14 g of KCl in 100 mL of deionized water) using the vial tilting method [179]. Briefly, STF was added to the blank κ–CRG formulations in a 1:4 ratio (the average volume of lachrymal fluids present in the cul-de-sac is around 7-15 µL) in a vial and left to equilibrate for 1 min at 34 ± 0.5 °C [180]. After the equilibration time, the vial was inverted at 90°. The time (from the time of addition of STF) at which there was a cessation of flow was considered as the gelling time and the duration it remained in the gel form was taken as gelling capacity. The concentrations of κ-CRG, which were free flowing at 25 ± 0.5 °C and showed no flow upon tilting the vial in the presence of STF, were taken up for designing dual responsive *in situ* gels. TAA was loaded in the optimized κ-CRG *in situ* gel (Table 3.1: F14).

3.2.3.3 Optimization of the in situ gels containing a combination of RXG and κ-CRG in the presence of STF at 34 °C

Two important factors were considered for designing dual-responsive *in situ* gelling systems. First, the concentrations of RXG and κ-CRG that yield low solution state viscosity at 25 ± 0.5 °C (critical for easy dispensation of the formulation) and second, the ability of the prepared

dual responsive system to respond quickly to the stimuli resulting in the gel formation. The gelling properties were evaluated for the prepared formulations in the presence of STF maintained at 34 ± 0.5 °C by measuring the gelation time and gelling capacity (Table 3.1: F9, F10). Based on the results obtained from these combination systems of RXG and κ-CRG, the *in situ* gels were further optimized by the addition of KCl (Table 3.1: F11 to F13) to control the viscosity at 25 ± 0.5 °C and produce a strong gel in the presence of STF maintained at 34 ± 0.5 °C. Finally, TAA was loaded in the optimized *in situ* gel containing a combination of RXG and κ-CRG (Table 3.1: F15).

3.2.4 Physical appearance and pH of the *in situ* gels

The pH of blank *in situ* gels (Table 3.1: F1 to F3 and F5 to F13) and TAA loaded i*n situ* gels (Table 3.1: F4, F14 and F15) was determined with the help of a calibrated pH meter (Eutech Instruments, Pune, India). Further, the *in situ* gels were observed visually for their physical appearance and clarity.

3.2.5 Determination of sol-to-gel transition of the *in situ* gels using a rheometer

The rheological properties, including the sol-to-gel transition, of optimized *in situ* gels (blank RXG-κ-CRG (F13) and TAA loaded RXG-κ-CRG (F15)) developed in the study were assessed with a rheometer (Anton Paar MCR 302, Graz, Austria). Parallel plate geometry was used in the analysis. First, the linear viscoelastic region (LVER) was determined for each sample by performing amplitude and frequency sweep experiments. Then in the LVER, the rheological properties of the samples were analyzed using a temperature sweep between 25 °C to 40 °C in oscillatory mode. The gelation of the samples was evaluated at three different experimental setups: 1) a temperature ramp, 2) a temperature ramp in the presence of STF and 3) a temperature ramp in the presence of deionized water. The loss tangent (*tan δ*) vs temperature and complex viscosity (*η**) vs temperature plots were constructed from the data obtained in the

rheological studies. The gel strength of the optimized *in situ* gels was determined from the plots [181,182].

The loss tangent (*tan δ*), which represents the relative amount of energy dissipation, is determined by dividing the loss modulus (G ") by the storage modulus (G "). Depending on the value of *tan δ*, the sample is considered to be in a viscoelastic solid state ($0 < tan\ \delta < 1$) or in a gel state ($tan\ \delta = 1$) or in a viscoelastic liquid state ($tan\ \delta \geq 1$). For an ideal *in situ* gelling system under storage, the formulation's *tan δ* value should be ≥ 1. Once it is exposed to stimuli for gelation, it should gradually decrease to 1 and approach 0, reflecting the gelling nature of the system and ultimately forming a strong gel. Further, the strength of the gelling system was determined by the complex viscosity (*η*),* which was determined from the ratio of total resistance to flow (*G**) and the angular frequency (*ω*) [183].

3.2.6 Measurement of contact angle of the *in situ* gels

A quantitative measure of wetting properties between a solid and liquid is given by the contact angle or theta (θ). Contact angle measurements were performed on an Optical Tensiometer **(**Theta Flex, Biolin Scientific**,** Hamburg, Germany) at 25 ± 0.5 °C and 60% relative humidity using the sessile drop method. A sample volume of 4 µL of each formulation (blank RXG (F3), blank κ-CRG (F5), blank RXG-κ-CRG (F13) and TAA loaded RXG-κ-CRG (F15)) was dropped onto a goat cornea at a rate of 1 mL/min using a 300 µL syringe and a microtube of 200 µL. During the analysis of every sample, five images were captured over 1 min and analyzed using the circle fit method [184]. Triplicate samples were measured in the study.

3.2.7 Determination of mucoadhesive strength of the *in situ* gels by rheological synergism

The mucoadhesive strength of the *in situ* gels was evaluated by the rheological synergism method reported in the literature [185]. The rheological synergism existing between a formulation (due to the mucoadhesive polymer used in the formulation) and mucin was determined using a rheometer in parallel plate assembly with a gap of 0.5 mm. Mucin (Type

III) was dispersed in STF (pH 7.4 ± 0.05) to yield a concentration of 10% w/v and stored at 4 ^{o}C for 12 h to hydrate. The hydrated mucin dispersion was agitated at 350 rpm for 30 min to get a clear solution. To determine the mucoadhesive strength, 150 µL of the *in situ* gel sample was added to 150 µL of mucin solution and analyzed using the rheometer.

The storage modulus values of the mucin solution, TAA loaded RXG-κ-CRG (F15) and the TAA loaded RXG-κ-CRG (F15) with mucin mixture were measured at 34 ± 0.5 °C by frequency sweep to evaluate the mucoadhesive interactions between the polymers and mucin. The mucoadhesive strength between mucin and polymers used in a formulation was determined using the following Equation 3.1:

Equation 3.1 $$\Delta G' = G'_{F+m} - (G'_F + G'_m)$$

Where, G'_{F+m} is the storage modulus of the mixture of *in situ* gel and mucin, G'_F and G'_m are the storage modulus values of the *in situ* gel and mucin, respectively. $\Delta G'$ is the measure of mucoadhesive interaction between the *in situ* gel and mucin.

3.2.8 *In vitro,* drug release studies of the TAA loaded *in situ* gels

The *in vitro* drug release studies of pure TAA, TAA loaded RXG (F4), TAA loaded κ-CRG (F14) and TAA loaded RXG-κ-CRG (F15) *in situ* gels were investigated using a membrane-less method in a dissolution apparatus (USP Type II) (Model TDT-08L, Electro lab, Mumbai, India) [186]. Briefly, 40 µL of the *in situ* gelling formulation (containing 4 mg of TAA) was carefully dispensed into a stainless-steel circular container (with a 1.4 cm internal diameter and 0.5 cm depth) and glued at the bottom of a 1000 mL dissolution jar. The dissolution jars were maintained at 34 ± 0.5 °C. The jars were filled with 300 mL of STF containing 0.5% w/v of Tween 80, which was previously equilibrated at 34 ± 0.5 °C and the paddle rotation was set at 75 rpm.

Dissolution samples (2 mL) were drawn using 0.45 µm syringe filters at specific time points (0.25, 0.5, 1, 2, 4,6, 8, 12, 24 and 48 h) during the dissolution study. Following the withdrawal

of the sample at each time point, a fresh medium (2 mL) was added to the dissolution jar. A validated RP-HPLC analytical method was used to analyze the dissolution samples (Section 2.3.1, Chapter 2). *In vitro* dissolution data were fit into different mathematical models to understand release kinetics (*viz.,* zero-order, first-order and Higuchi square root kinetics) and release mechanism (Korsmeyer-Peppas model) [187].

3.2.9 *Ex vivo* ocular toxicity studies of the *in situ* gels by the HET-CAM method

The *ex vivo* ocular irritation studies were carried out using the Hen's Egg Test-Chorion Allantoic Membrane (HET-CAM) method [188]. Fresh eggs (of approximately 50-60 g) were purchased from a local chicken farm and incubated at temperature of 37 ± 0.5 °C and relative humidity of 55 ± 5% RH for five days. On the 5th day, the eggs were candled to separate fertile eggs from the non-fertile ones. The fertile eggs were placed in the incubator for 10 more days for proper growth of CAM. The eggs were rotated manually every 12 h during the incubation period. The eggshell was broken carefully to open the air cell using a rotating dentist blade without disturbing the inner membrane. The exposed CAM was moistened with NaCl solution (0.9% w/v) and the opened eggs were placed in an incubator for 30 min. The inner layer was removed carefully using forceps from each of the opened eggs to expose the CAM for applying the test samples. In the study, four treatment groups were studied. Group 1: positive control (treated with 0.1 N NaOH); Group 2: negative control (treated with NaCl solution, 0.9% w/v); Group 3: treated with the blank RXG-κ-CRG *in situ* gel (F13) and Group 4: treated with TAA loaded RXG-κ-CRG *in situ* gel (F15). In each treatment group, 3 eggs (with properly formed or exposed CAM) were used. In the study, the treatment sample (200 µL) was placed on the surface of the CAM of the egg. Following the application of each treatment sample, the extent of damage to the blood vessels was observed for 300 Sec and scores were assigned. Based on the data obtained from vascular lysis, an irritation score (IS) was determined for each treatment using Equation 3.2.

Equation 3.2 $$IS = \frac{(301-H)}{300} \times 5 + \frac{(301-L)}{300} \times 7 + \frac{(301-C)}{300} \times 9$$

Where, 'H' is the time (in Sec) taken to the start of haemorrhage reactions on CAM, 'L' is the time (in Sec) taken to the start of vessel lysis on CAM and 'C' is the time (in Sec) taken to the start of coagulation formation on CAM.

The ocular irritation properties of the *in situ* gels were judged based on there IS values. The formulation was considered 'non-irritant' if the IS value was in the range of 0–0.9; 'slightly irritant' if the IS value was in the range of 1–4.9; 'moderately irritant' if the IS value was in the range of 5–9.9; and 'strongly irritant' if the IS value was in the range of 10–21.

3.2.10 Hemolysis study of the *in situ* gels

The hemolytic activity of the *in situ* gelling systems was determined to check if the formulations are isotonic and are well tolerated by the ocular tissues [189]. A butterfly needle was used to draw blood from the marginal ear vein of rabbits into a microcentrifuge tube containing disodium EDTA solution as the anticoagulant (4.5% w/v). The collected blood was centrifuged at 1000 × g for 15 min to separate the red blood cells (RBC). The separated RBCs were washed thrice using a physiological saline solution. The RBCs were then suspended in a sufficient volume of saline solution to yield a hematocrit of 2% (v/v). To determine the hemolysis properties, 1.5 mL of the test sample (NaCl solution (0.9%w/v) (negative control), Triton X-100 (positive control), Blank RXG-κ-CRG (F13) and TAA loaded RXG-κ-CRG (F15)) was mixed with 1.5 mL of the RBC suspension. The resultant mixture was incubated at temperature of 37 ± 0.5 °C for 1 h. Following 1 h of incubation, the mixture was centrifuged at 1000 × g for 15 min and the supernatant was collected. The pellet obtained was observed for morphological changes in the RBCs under a digital microscope (ZEISS, Axiocam 705 colour, Oberkochen, Germany). The absorbance value of the supernatant was measured at 540 nm. The hemolysis (%) of each test sample was determined by substituting the absorbance value of

the supernatant of the corresponding sample in Equation 3.3. The study was performed in triplicates.

Equation 3.3 $$\text{Hemolysis (\%)} = \frac{(A_s - A_b)}{(A_c - A_b)} \times 100$$

Where, A_c is the absorbance value of the supernatant obtained by treating RBC suspension with Triton X-100, A_s is the absorbance value of the supernatant obtained by treating RBC suspension with an in *situ* gelling formulation and A_b is the absorbance value of supernatant obtained by treating RBC suspension with 0.9% w/v NaCl solution.

3.2.11 Histopathological studies of the *in situ* gels

Histopathology was carried out to determine the irritation potential of the formulation on the structure and integrity of the corneal epithelium. Fresh goat eyeballs procured from a local slaughterhouse centre were used in the study. The cornea was excised from the goat eyeball by making an incision of 2 mm while keeping the scleral ring intact. The cornea was immediately washed with NaCl solution (0.9% w/v) for 1 min. The cornea was then incubated with each of the treatments separately for 6 h. The treatments used in the study were STF (pH 7.4 ± 0.05) (negative control), isopropyl alcohol (75% v/v) (positive control) and *in situ* gels (blank RXG-κ-CRG (F13), TAA loaded RXG-κ-CRG (F15)). After the incubation period, the cornea was washed with NaCl solution (0.9% w/v) and fixed immediately using tissue freezing media. The frozen cornea was stored at -80 °C. Cross-sections (< 5µm) were excised from the frozen cornea using a cryotome (Leica Biosystems, CM1520 cryostat, Wetzlar, Germany) and mounted on a glass slide. Ethyl alcohol (at a gradient of 30-50-70-90-100%) and xylene were used to dehydrate the tissue. The dehydrated tissue was washed with NaCl solution (0.9% w/v) and stained with hematoxylin and eosin. Excess hematoxylin and eosin were removed by washing the tissue with NaCl solution (0.9% w/v) and observed for histological changes under a digital microscope (ZEISS, Axiocam 705 colour, Oberkochen, Germany) at 10× magnification [190].

3.2.12 Ocular pharmacokinetic studies of the optimized TAA loaded *in situ* gel

An ocular pharmacokinetic study of the final optimized *in situ* gel (RXG-κ-CRG-TAA (F15)) was performed in eight (*n*=8) male New Zealand rabbits (weight: 2-2.5 kg) with normal eyes (with no signs of inflammation). Institutional Animal Ethics Committee had reviewed and approved the study protocol prior to the study (Protocol No.: BITS-Hyd/IAEC/2020/10). The study was conducted in our institute's animal house facility, where the animals were acclimatized (conditions: temperature of 22 ± 1 °C; relative humidity of 55 ± 10% and 12 h light-dark cycle) for 1 week prior to the study.

In the study, a micropipette was used to instil 40 µL of TAA loaded RXG-κ-CRG (F15) in both the eyes (at the lower cul-de-sac) of all the rabbits. Immediately following the dosing, the eyelids were closed for 10 s to maximize the contact between the cornea and the administered formulation. One rabbit at 0.5, 1, 2, 4, 6, 8, 12 and 24 h post formulation instillation was euthanized by carbon dioxide inhalation. In each euthanized rabbit, aqueous humour was collected using an insulin needle (30-gauge, 3 mm diameter) by placing the needle behind the limbus superotemporally and directing it towards the centre of the eye. The left and right eyeballs were removed from the rabbit following the collection of aqueous humour. Dry ice was used to immediately freeze the eyeballs. From the frozen eyeball, vitreous humour was collected and stored at -20 °C.

The samples (vitreous and aqueous humour) obtained from ocular pharmacokinetics were analyzed using a validated HPLC method (Section 2.3.3, Chapter 2). The time course data of TAA in aqueous humour and vitreous humour was analyzed using non-compartmental analysis. Pharmacokinetic parameters like C_{max} (the maximum concentration of TAA produced in the matrices), T_{max} (the time to reach C_{max}), $MRT_{(0–t)}$ (the mean residence time from t = 0 to t = t_{last}) and $MRT_{(0–\infty)}$ (the mean residence time from t = 0 to t = ∞) were determined were calculated. The $AUC_{(0-t)}$ (area under the TAA time course curve from t = 0 to t = t_{last}) values

were determined using the trapezoidal method from the TAA time course profiles obtained in the study.

In chapter 2 (Section 2.3.5), we determined that the TAA-HP-β-CD-Susp at 4 mg/30 μL dose strength was effective in achieving therapeutic concentrations of TAA in the vitreous humour. Therefore, in this chapter, we have compared the ocular pharmacokinetic performance of the current optimized *in situ* gel (TAA loaded RXG-κ-CRG (F15) with that of TAA-HP-β-CD-Susp.

3.3 Results and discussion

3.3.1 Preparation of the *in situ* gels

3.3.1.1 Purification of TSX

The protein and fat impurities present in the TSX powder were removed to produce gels with good elastic properties. Isopropyl alcohol was used to remove fat impurities. The protein impurities were denatured and precipitated by the application of heat. The precipitated proteins were separated by centrifugation. The resultant TSX powder showed a negative result when subjected to the ninhydrin test for the presence of proteins. The pure TSX (which was free from protein and fat impurities) was subjected to enzymatic modification.

3.3.1.2 Enzymatic modification of TSX

The enzyme β-galactosidase was used to treat TSX in order to make it thermoresponsive by reducing the galactose residues present in TSX by at least 40%. Brun-Graeppi *et al*. have reported that the reduction in galactoside residues in TSX by the galactosidase enzyme is dependent on time. The enzymatic modification of TSX was conducted under specific conditions for a period of 18 h, which reduced ≥40% of the galactose residues in the polymer to produce RXG [174]. The RXG obtained from the enzyme modification was analyzed using SEC to determine its molar mass. Further, RXG was also characterized using FT-IR spectroscopy and ^{1}H-NMR spectroscopy. The data obtained was similar to the earlier published reports.

To check the consistency in the properties of RXG obtained by the enzymatic modification of TSX, three independent lots of RXG were prepared from TSX. Rheological analysis (loss tangent (*tan δ*), complex viscosity (*η**)) for three samples of RXG from every lot was performed to ensure consistency within and across the lots. For all samples, within and across lots, the %RSD values of loss tangent (*tan δ*) and complex viscosity (*η**) were found to be ≤5%.

3.3.1.3 Characterization of the RXG by FTIR, SEC and ^{1}H-NMR

3.3.1.3.1 Fourier transform infrared spectroscopy (FT-IR) of RXG

Figure 3.1 shows the FT-IR spectrum of RXG. The hydroxyl (O-H) groups of the glucan backbone are represented by a distinctive wide peak in the xyloglucan's IR spectra at 3439.08 cm^{-1}. The peak for the C-H stretching vibration of the alkanes in the xyloglucan structure was observed at 2927.94 cm^{-1}. The peaks for the (C-O-C) stretching vibration of the cyclic ether were observed at 1074.35 cm^{-1} and 943.19 cm^{-1}. These peaks observed for RXG in the FTIR spectra are consistent with those reported by Madgulkar *et al*. and Kawasaki *et al*. [191,192].

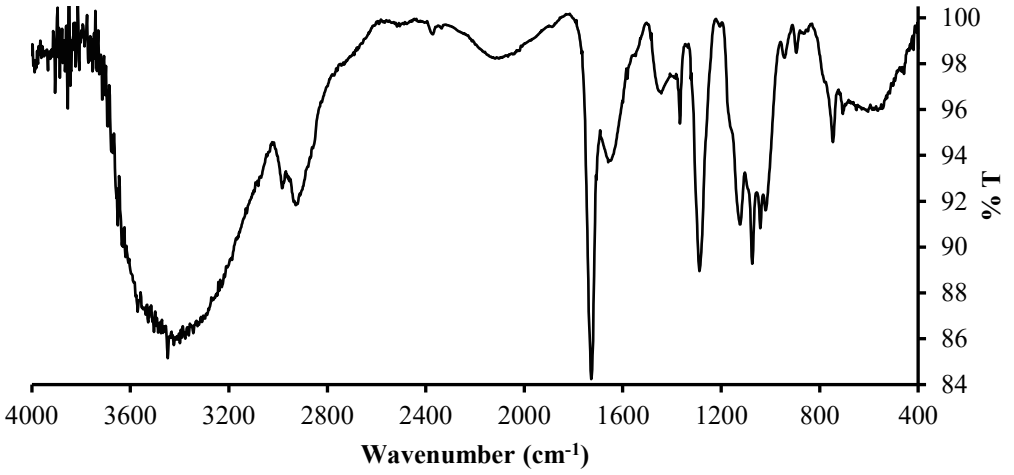

Figure 3.1 FTIR spectrum of RXG

3.3.1.3.2 Determination of the molar mass of RXG by Size-exclusion chromatography (SEC)

The SEC chromatograms of TSX and RXG are presented in Figure 3.2. In the chromatograms, TSX had an elution volume of 7.72 mL, while RXG had a relatively higher elution volume of 8.26 mL. This clearly indicates that there is a reduction in the molar mass of RXG compared

to TSX, which is due to the reduction in the galactose residues in TSX. The molar mass of both polymers was determined from the calibration curve constructed using the standard (Shodex standard). The molar masses of RXG and TSX were found to be 3.9×10^3 g/mol and 6.3×10^3 g/mol, respectively. The molecular mass values obtained for RXG in the current study were consistent with the molar mass reported by Brun-Graeppi *et al*. [174].

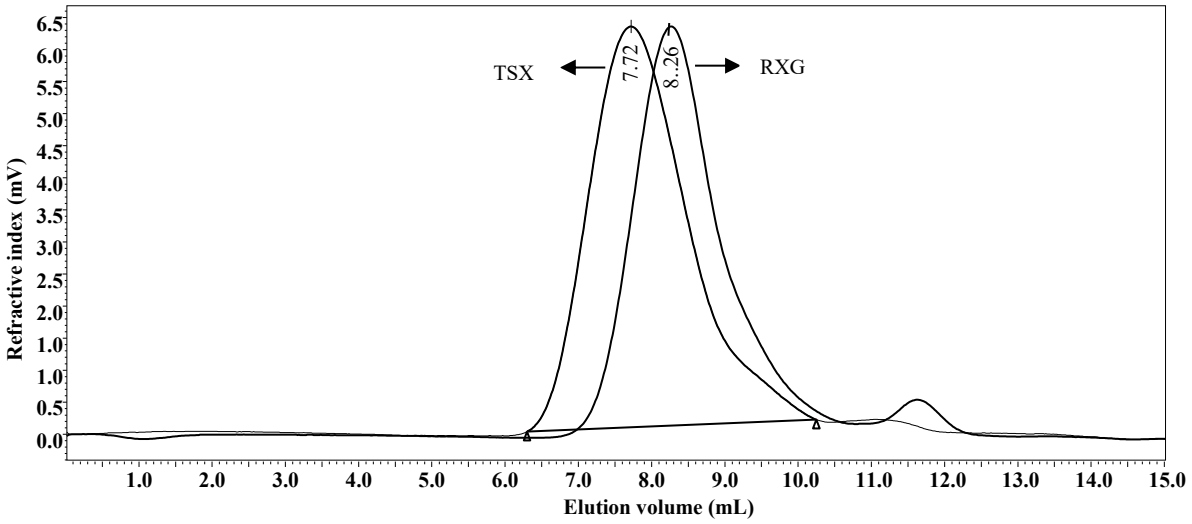

Figure 3.2 SEC chromatograms of RXG and TSX

3.3.1.3.3 Nuclear magnetic resonance (NMR) spectroscopy of RXG

Figure 3.3 displays the ^{1}H-NMR spectrum of the RXG. In the spectrum, signals for RXG were observed in the range between 3 and 5.2, which is typical for polysaccharides. The data obtained for RXG was coherent with that reported in the literature [193]. The signals observed between 4.0 and 5.4 ppm are due to the anomeric hydrogens associated with polysaccharides, as described by Jonsson *et al*. [194]. Although the anomeric α and β hydrogens can be seen in this region, the signals from carbohydrate polymers in NMR spectra are localized in a narrow region, especially for complex carbohydrates like xyloglucan. The signals observed in the regions between 0.8 and 1.4 ppm are due to the methyl and methylene groups of residual solvent impurities like ethanol and isopropyl alcohol used in the process to obtain RXG from TSX. Similar signals were observed for RXG in work reported by Chawananorasest *et al*. [195].

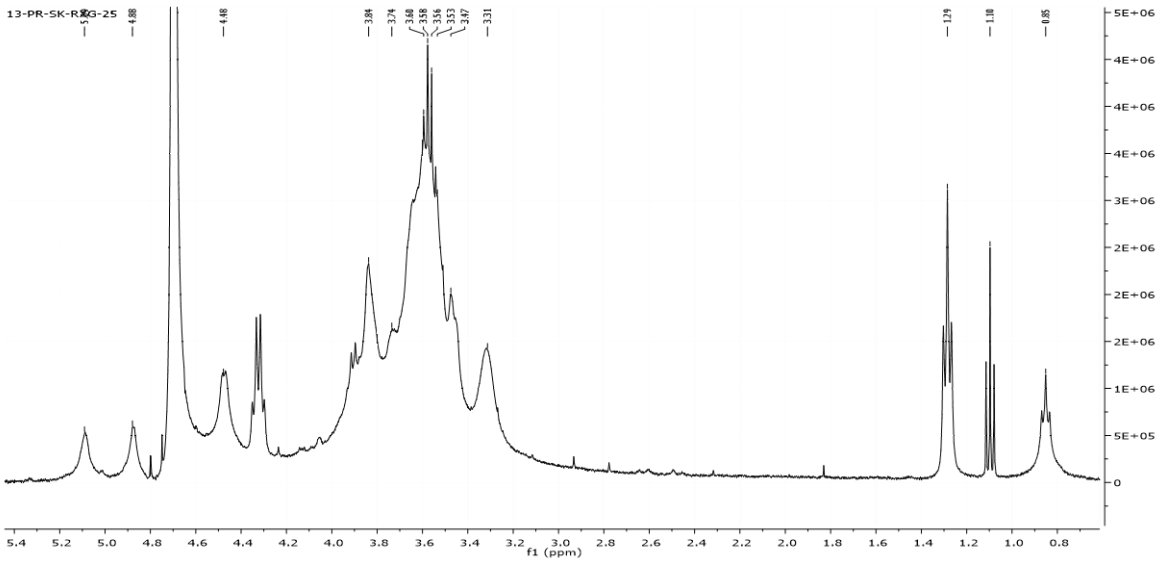

Figure 3.3 ^{1}H-NMR Spectrum of RXG

3.3.2 Optimization of RXG and κ-CRG in the design of dual responsive *in situ* gels

The concentration of RXG was optimized by evaluating the thermoresponsive behaviour and gelling properties of blank *in situ* gels prepared using different proportions of only RXG. Formulations were screened to identify the proportion of RXG with a favourable sol-to-gel transition temperature below 34 ± 0.5 °C and a low solution state viscosity (free-flowing nature) on storage below 25 ± 0.5 °C for easy and accurate dispensation of the formulation. Formulations containing RXG at 2%, 2.5% and 3% w/v were evaluated individually to determine gelling temperature, time and capacity. The gelation time of the formulations increased with the increased concentration of RXG (Table 3.1 F1 to F3) due to the higher equilibration time required for higher concentrations of RXG at a given temperature. The gel strength also increased with an increase in the concentration of RXG. The formulation containing RXG at 3% w/v formed a stronger gel, while the formulation containing RXG at 2% w/v formed a weaker gel.

Similarly, the concentration of κ-CRG was optimized by evaluating the gelling properties of blank *in situ* gels containing different concentrations (0.25%, 0.5%, 0.75% and 1.0% w/v) of only κ-CRG. The gelling properties of the formulations were evaluated in the presence of STF

maintained at 34 ± 0.5 °C (Table 3.1 F5 to F8). A formulation containing 1.0% w/v of κ-CRG formed a strong gel, while the formulation containing 0.75% w/v of κ-CRG formed a weak gel. Formulations containing 0.25% w/v and 0.5% w/v of κ-CRG did not undergo sol-to-gel transformation. Although the gel strength increased with an increase in the concentration of κ-CRG, the gelling time decreased. Based on the results obtained from the standalone *in situ* gelling systems (blank RXG and blank κ-CRG formulations), dual responsive *in situ* gelling systems were prepared by combining RXG and κ-CRG (Table 3.1 F9, F10). Formulations prepared by combining the optimized concentrations of RXG (2% w/v) and κ-CRG (1% and 0.75% w/v) from their standalone formulations formed highly viscous solutions in the solution state (25 ± 0.5 °C) itself and were difficult to dispense from the container. In the subsequent studies, RXG (2% w/v) was combined with different concentrations of CRG (0.25% and 0.5% w/v) (Table 3.1 F11, F12). However, the formulations containing CRG at 0.25% and 0.5% w/v did not undergo a sol-to-gel transition in the presence of STF at 34 ± 0.5 °C. The inclusion of electrolytes such as potassium chloride (KCl) in the formulation was reported to improve the sol-to-gel transition properties of CRG-based *in situ* gelling systems. KCl acts as an initiator for the κ-CRG to undergo gelation in the presence of STF. *In situ* gels containing RXG (2% w/v), κ-CRG (0.25% w/v) and KCl (0.1% w/v) formed a free-flowing solution at room temperature (25 ± 0.5 °C), but in the presence of STF at 34 ± 0.5 °C it formed a weak gel. The formulation containing RXG (2% w/v), κ-CRG (0.5% w/v) and KCl (0.1% w/v) was viscous even at room temperature (25 ± 0.5 °C) and difficult to dispense. Finally, the formulation containing RXG (2% w/v), κ-CRG (0.3% w/v) and KCl (0.1% w/v) (Table 3.1; F13) exhibited desirable flow properties in the solution state (25 ± 0.5 °C) while undergoing rapid sol-to-gel transition and forming a stronger gel in the presence of STF maintained at 34 ± 0.5 °C.

3.3.3 Physical appearance and pH of the *in situ* gels

The blank *in situ* gels of RXG (Table 3.1: F1 to F3) appeared to be translucent, while those of the blank κ-CRG *in situ* gels were transparent (Table 3.1: F5 to F8). TAA loaded RXG, TAA loaded κ-CRG and TAA loaded RXG-κ-CRG *in situ* gels formed turbid suspensions due to the insoluble TAA particles (Table 3.1: F4, F14, F15). All formulations at their optimized concentrations were free-flowing liquids at room temperature (25 ± 0.5 °C) and transformed into gels in the presence of STF at 34 ± 0.5 °C. The pH of all formulations was within the acceptable range of lachrymal fluids (pH range of 6.5 to 7.6), as shown in Table 3.1 [185].

Table 3.1 Composition and physical properties of blank and TAA loaded *in situ* gels

Formulation	RXG	κ-CRG	KCl	Mannitol	BKB	TAA	pH*	Gelling capacity		Gelation time (s)*,@	Physical appearance
	(% w/v)							STF at 25 ºC	STF at 35 ºC		
F1	3	-	-	5.2	0.01	-	6.8 ± 0.2	-	+++	117 ± 4	Translucent
F2	2.5	-	-	5.2	0.01	-	6.8 ± 0.2	-	++	143 ± 2.5	Translucent
F3	2	-	-	5.2	0.01	-	6.8 ± 0.2	-	+	157 ± 1.9	Slight Translucent
F4	2	-	-	5.2	0.01	100 mg/mL	6.8 ± 0.2	-	++	150 ± 3.0	Turbid Suspension
F5	-	1	-	5.2	0.01	-	6.5 ± 0.2	+++	+++	48 ± 2.1	Transparent
F6	-	0.75	-	5.2	0.01	-	6.5 ± 0.2	+	+	57 ± 5	Transparent
F7	-	0.5	-	5.2	0.01	-	6.5 ± 0.2	-	-	-	Transparent
F8	-	0.25	-	5.2	0.01	-	6.5 ± 0.2	-	-	-	Transparent
F9	2	1	-	5.2	0.01	-	6.6 ± 0.2	++	+++	27 ± 2.3	Slight Translucent
F10	2	0.75	-	5.2	0.01	-	6.6 ± 0.2	+	++	35 ± 3.3	Slight Translucent
F11	2	0.5	0.1	5.2	0.01	-	6.6 ± 0.2	+++	++++	29 ± 3.8	Slight Translucent
F12	2	0.25	0.1	5.2	0.01	-	6.6 ± 0.2	+	++	41 ± 1.7	Slight Translucent
F13	2	0.3	0.1	5.2	0.01	-	6.6 ± 0.2	++	+++	28 ± 3.1	Slight Translucent
F14	-	0.3	0.1	5.2	0.01	100 mg/mL	6.5 ± 0.2	++	++	32 ± 1.5	Turbid Suspension
F15	2	0.3	0.1	5.2	0.01	100 mg/mL	6.6 ± 0.2	+++	++++	27 ± 2.5	Turbid Suspension

*pH, Gelation time values are presented as mean ± SD (n=3).
Gelling capacity: (-) No gelation; +, weak gels, dissolved rapidly after a few min; ++, immediate gelation, remains for a few h; +++, immediate gelation, remains for a longer period up to 10 h; + + + +, Immediate gelation, remains for an extended period for more than 12 h.
@Gelation time in the presence of simulated tear fluid (STF) at 34 ± 0.5 ºC

3.3.4 Determination of sol-to-gel transition of the *in situ* gels using a rheometer

The results obtained from the rheological evaluation of formulations (blank RXG-κ-CRG (F13) and TAA loaded RXG-κ-CRG (F15)) are shown in Figure 3.4a and Figure 3.4b. Figure 3.4a depicts the loss tangent vs temperature behaviour of the formulations, while Figure 3.4b shows the complex viscosity (η^*) properties of the formulations as a function of time. The shift in loss tangent (*tan δ*) values for the optimized blank RXG-κ-CRG (F13) in the temperature range of 34-37 °C shows a clear sol-to-gel transition; additionally, at 25 °C, the *tan δ* value was greater than one, indicating the ease of dispensing the formulation as an eye drop. The *tan δ* value in the presence of STF was less than one from the beginning (starting from 25 °C), indicating gel formation. This suggests the ion sensitivity of the κ-CRG, which was not seen when the same system was exposed to deionized water due to the absence of ions. Further, a gradual shift in the loss tangent and complex viscosity values with an increase in temperature to 34 ± 0.5 °C indicates the thermoresponsive nature of the RXG. The optimized TAA loaded RXG-κ-CRG (F15) showed a relatively higher loss tangent and complex viscosity value in the presence of STF, which was contributed by the loaded drug (TAA). These results were in agreement with rheological studies conducted by Brun-Graeppi *et al*. [174].

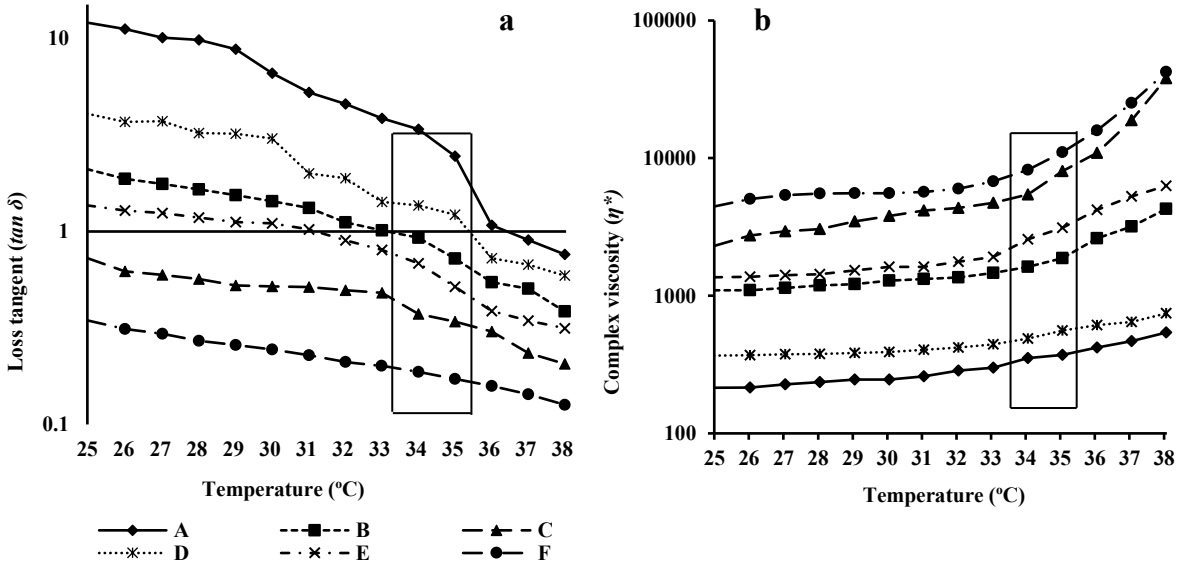

Figure 3.4 Semi logarithmic plots of loss tangent (*tan δ*) and complex viscosity (η^*) of optimized blank RXG-κ-CRG (F13) and TAA loaded RXG-κ-CRG (F15) *in situ* gels as a

function of temperature in the presence of STF and deionized (DI) water.

Note: A- blank RXG-κ-CRG (F13) in the presence of DI water; B- blank RXG-κ-CRG (F13); C- blank RXG-κ-CRG (F13) in the presence of STF; D- TAA loaded RXG-κ-CRG (F15) in the presence of DI water; E- TAA loaded RXG-κ-CRG (F15); F- TAA loaded RXG-κ-CRG (F15) in the presence of STF.

3.3.5 Measurement of contact angle of the *in situ* gels

The contact angle of the *in situ* gels was measured to determine the spreadability and wettability of the applied area. As reported by Ruppenthal *et al*., a lower contact angle indicates the ease of application and spreadability of *in situ* gel on the ocular surface [184]. A comparison of the contact angle values of the formulations is shown in Figure 3.5. The contact angle of blank RXG-κ-CRG (F13: θ = 45.2°) was found to be lower than that of blank RXG (F3: θ = 56.2°) as well as blank κ-CRG (F5: θ = 49.6°) *in situ* gels. TAA loaded RXG-κ-CRG (F15: θ = 42.8°) had a relatively lesser contact angle compared to blank RXG-κ-CRG (F13: θ = 45.2°). Loading the drug in the *in situ* gel decreased the contact angle. This may be ascribed to the increased viscosity of RXG-κ-CRG (F15) *in situ* gel due to the presence of TAA particles in a suspended state in the formulation.

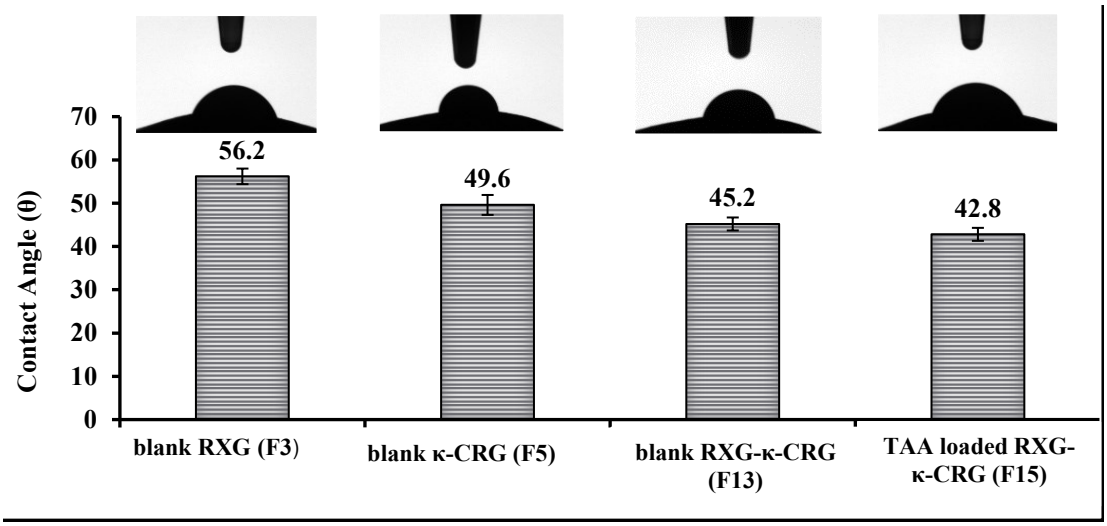

Figure 3.5 Contact angle measurements of blank and TAA loaded *in situ* gels (Data is presented as mean ± SD of determinations, n=3).

3.3.6 Determination of mucoadhesive strength of the *in situ* gels by rheological synergism

By using a frequency sweep, the linear viscoelastic region of the polymeric system was identified. It was observed that all polymeric systems have zero or no effect at frequencies below 1.5 Hz. Further, keeping the frequency constant at 1.5 Hz, the amplitude was determined. An amplitude of 0.5% was found to be ideal for all formulations. The rheological studies of all the *in situ* gels were performed at 1.5 Hz frequency and 0.5% amplitude while keeping the temperature constant at 34 ± 0.5 °C.

The storage modulus value of mucin (G'_m = 1.9) was discovered to be the lowest due to the absence of an interacting polymeric system. The gelling system (G'_F = 12.4) showed a higher storage modulus compared to the mucin due to the viscosity of the polymeric system. The mixture of mucin and polymeric gelling system (G'_{F+m} = 62.2) showed significantly higher storage modulus due to the interaction between the mucin and the polymeric network of the gel. These findings are comparable to the research work published by Destruel *et al*. [185]. The storage modulus values (G'_m, G'_F and G'_{F+m}) were used to determine the interaction between the mucin and polymeric gelling system ($\Delta G'$) using Equation (3.1), mentioned in section 3.2.7. The results obtained are shown in Figure 3.6 Higher $\Delta G'$ (47.9) values indicate a strong interaction between the mucin and the optimized TAA loaded RXG-κ-CRG (F15) *in situ* gel.

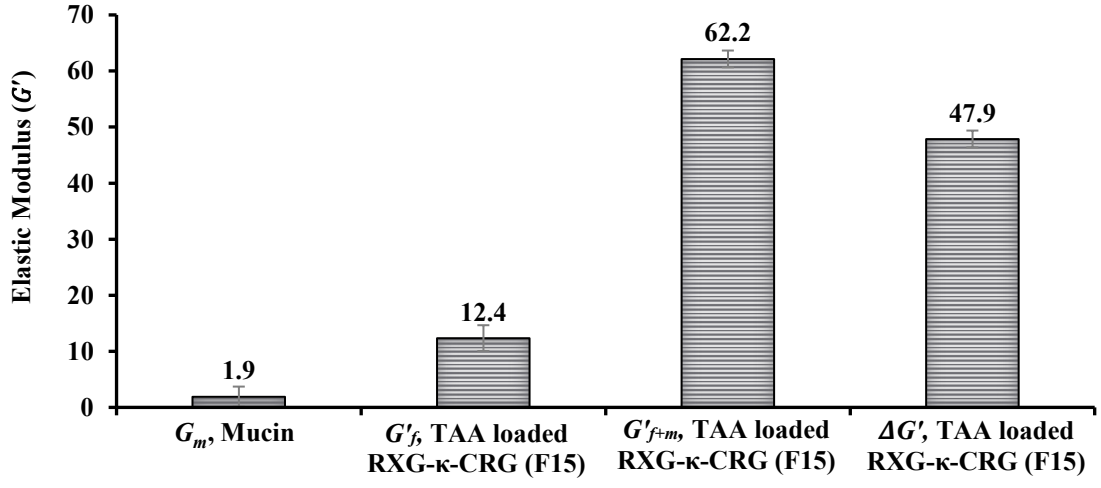

Figure 3.6 Elastic Modulus and rheological synergism for *in situ* gel formulation; G'_m

corresponds to mucin, G'_Fcorresponds to TAA loaded RXG- κ-CRG (F15) *in situ* gel formulation, G'_{F+m} corresponds to TAA loaded RXG- κ-CRG (F15) *in situ* gel plus Mucin, $\Delta G'$ corresponds to the interaction between the mucin and polymeric gelling system.

3.3.7 *In vitro* drug release studies of TAA loaded *in situ* gels

The drug release studies were performed in STF (pH 7.4 ± 0.05) containing Tween 80 (0.5% w/v). The solubility of TAA in STF was 13.7 µg/mL. Therefore, to maintain the sink condition, 300 mL of STF containing 0.5% w/v Tween 80 was used in the study. The solubility of TAA in STF containing 0.5% w/v Tween 80 was 48 µg/mL. The mean cumulative percentage of drug released vs time plots were constructed from the *in vitro* dissolution data (Figure 3.7). Plain TAA was dissolved completely within 15 min. However, the drug release was slow and sustained from each of the RXG-TAA (F4), κ-CRG-TAA (F14) and RXG-κ-CRG-TAA (F15) *in situ* gels. The TAA loaded RXG-κ-CRG (F15) gel showed the slowest release among all the *in situ* gels, with 95% drug release over a period of 24 h. TAA loaded RXG (F4) and TAA loaded κ-CRG (F14) *in situ* gels showed 90% drug release within 8 h and 12 h, respectively. κ-CRG sustained the drug release more compared to RXG polymer. The dual-responsive *in situ* gel, containing the combination of RXG and κ-CRG, slowed and prolonged the drug release compared to the *in situ* gels containing individual polymers. The formation of a strong polymeric network between RXG and κ-CRG in response to the ions present in the dissolution media and the temperature of the media resulted in increased viscosity, which slowed the drug diffusion through the gel matrix. These findings were consistent with the loss tangent (*tan δ*) and complex viscosity (η^*) values obtained for the TAA loaded RXG-κ-CRG (F15) *in situ* gel, which exhibited a significant increase in complex viscosity (η^*) and loss tangent (*tan δ*) value of ≤1 when exposed to STF in 34 to 37 °C temperature range. Similar observations were reported by Dalvi *et al*., where they found a good agreement between the rheological and the *in vitro* drug release properties of the *in situ* gels [173].

The summary of the results obtained by fitting the dissolution data into various kinetic models is presented in Table 3.2. The 'n' value (the release exponent) of TAA loaded RXG-κ-CRG (F15) from the Korsmeyer-Peppas model was 0.996. The regression coefficient (R^2) for the model was 0.995. Case II mechanism of drug release was observed from TAA loaded RXG-κ-CRG (F15) *in situ* gel as the value of 'n' was found to be between 0.89 and 1. Case II release mechanism indicates that, after the sol-to-gel transition of the *in situ* gel, the drug release was primarily controlled by polymer relaxation (polymer erosion) compared to drug diffusion through the polymer gel network. The kinetics of drug release followed a near zero order as the value of 'n' was closer to 1. The 'n' values for TAA loaded RXG (F4) and TAA loaded κ-CRG (F14) were 0.46 and 0.72, respectively. The drug release from TAA loaded RXG (F4) followed Fickian diffusion, while that of TAA loaded κ-CRG (F14) followed the non-Fickian or anomalous release.

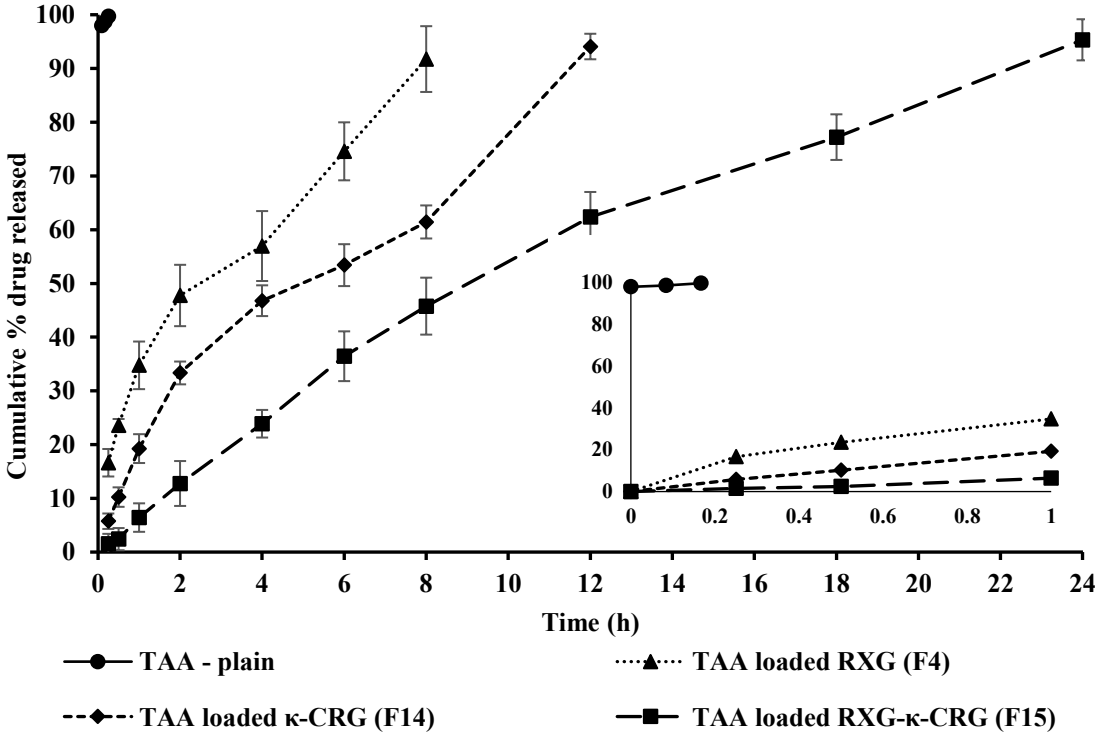

Figure 3.7: *In vitro* release profiles of plain TAA and optimized TAA loaded *in situ* gels (TAA loaded RXG, TAA loaded κ-CRG and TAA loaded RXG- κ-CRG *in situ* gels). Each data point is the mean cumulative% TAA released ± SD of n = 3 independent formulations

Table 3.2: *In vitro* drug release kinetics data of TAA loaded *in situ gels*

Formulation	Kinetic Parameters			
	Zero Order (R^2)	First Order (R^2)	Korsmeyer-Peppas	
			n	(R^2)
TAA loaded RXG (F4)	0.967	0.930	0.46	0.985
TAA loaded κ-CRG (F14)	0.963	0.869	0.72	0.981
TAA loaded RXG-κ-CRG (F15)	0.971	0.933	1.00	0.995

'R^2'is the regression coefficient; '*n*' is the release exponent indicative of the release mechanism in the Korsmeyer-Peppas model.

3.3.8 *Ex vivo* ocular toxicity studies of the *in situ* gels by the HET-CAM method

A sensitive, quick and inexpensive substitute for the Draize eye test is the ocular irritation test using the HET-CAM method. This method provides evaluation parameters representing the inflammatory process that are similar to the inflammatory changes in the conjunctival tissues of the rabbit eye. Figure 3.8 presents a comparison of the images obtained from the HET-CAM test of the treatments used in the study. The positive control (treated with 0.1 N NaOH) significantly damaged the CAM after 0.5 min, causing rosette-like coagulation. In addition, blood arteries in CAM were also found to undergo lysis when exposed to positive control. The negative control (treated with 0.9% w/v NaCl), blank RXG-κ-CRG (F13) and TAA loaded RXG-κ-CRG (F15) *in situ* gels did not show any distinct change in the CAM (neither haemorrhage nor coagulation). The positive control received an IS value of 20, while the negative control, blank RXG-κ-CRG (F13) and TAA loaded RXG-κ-CRG (F15) *in situ* gels received an IS value of 0. Based on the IS scores and the visual changes observed in CAM, it can be inferred that the optimized *in situ* gels (blank RXG-κ-CRG (F13) and TAA loaded RXG-κ-CRG (F15)) were non-irritant and well tolerated by the eye.

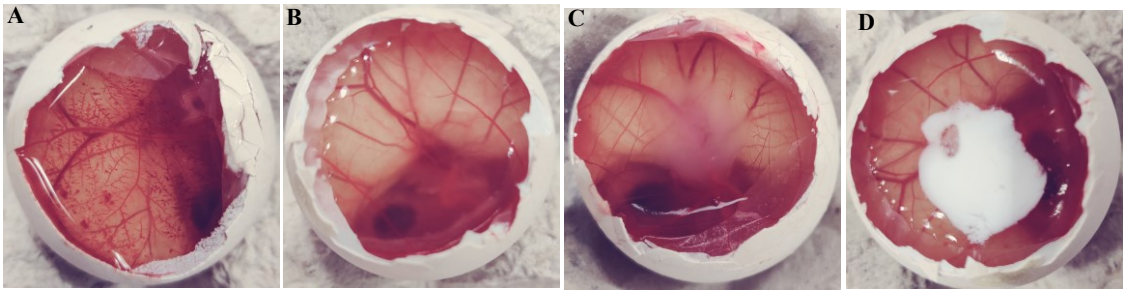

Figure 3.8: Comparative visual differences in the membrane obtained from *ex vivo* ocular

irritation study by HET-CAM test of (A) positive control (0.1 M NaOH); (B) negative control (0.9% w/v NaCl); (C) blank RXG-κ-CRG *in situ* gel (F13); and (D) TAA loaded RXG-κ-CRG *in situ gel* (F15).

3.3.9 Hemolysis study of the *in situ* gels

The RBCs treated with the optimized *in situ* gel formulations (blank RXG-κ-CRG (F13) and TAA loaded RXG-κ-CRG (F15)) were checked for their shape and size (at 40× magnification). The morphology of the RBCs was found to be intact when treated with negative control (0.9% w/v NaCl solution), blank (F13) and TAA loaded (F15) *in situ* gels. However, the RBCs incubated with Triton X-100 were completely lysed, as shown in Figure 3.9. Further, the hemolysis (%) values of the RBCs incubated with blank (F13) and TAA loaded (F15) *in situ* gel formulations were found to be 1.18% and 1.72%, respectively. These results suggest that optimized *in situ* gelling formulations are isotonic and biocompatible with no/minimal detectable disruption of RBCs.

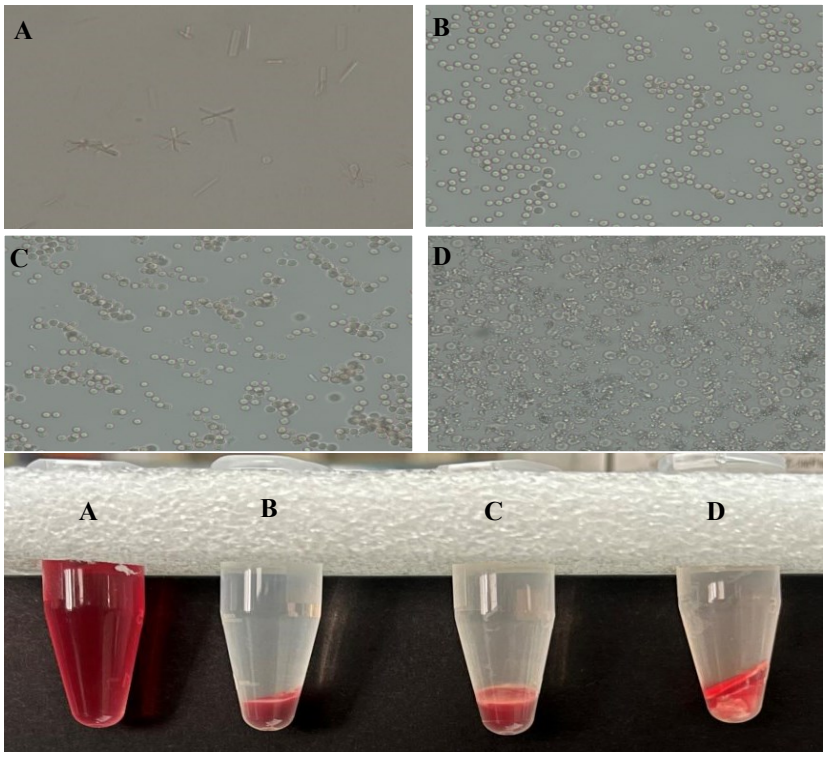

Figure 3.9: Results obtained from hemolysis studies of RBCs treated with **(A)** Positive control (Triton X-100); (B) Negative control (0.9% NaCl); (C) blank RXG-κ-CRG *in situ* gel (F13); (D) TAA loaded RXG-κ-CRG *in situ gel* (F15).

3.3.10 Histopathological studies of the *in situ* gels

The microscopic examinations of the corneal structure incubated with STF (negative control) showed intact epithelium and stroma without any sign of tissue damage. There was a visible distortion of the epithelial cell layer with widened intercellular spaces in the presence of 75% v/v isopropyl alcohol (positive control). The cornea incubated with the optimized *in situ* gels (blank RXG-κ-CRG (F13) and TAA loaded RXG-κ-CRG (F15)) exhibited no discernible difference from the STF-treated cornea (Figure 3.10). We can infer that the optimized formulations are safe and do not alter the membrane structure and cellular arrangement of the cornea.

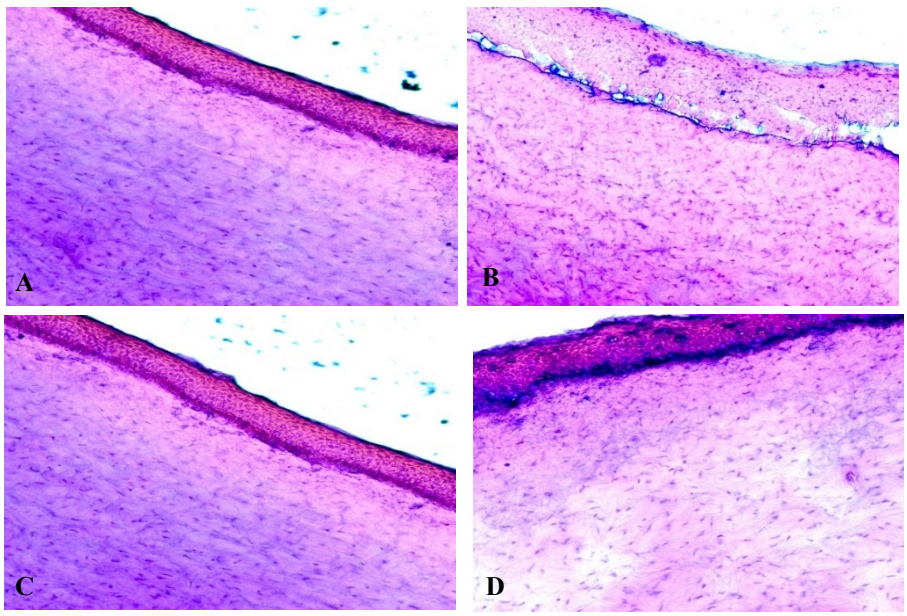

Figure 3.10: Photomicrographic representations of corneal histopathology evaluation. (A) negative control (STF); (B) Positive control (75% IPA); (C) blank RXG-κ-CRG *in situ* gel solution (F13); (D) TAA loaded RXG-κ-CRG *in situ gel* suspension (F15).

3.3.11 Ocular pharmacokinetic studies of the optimized TAA loaded *in situ* gel

The comparative mean concentration-time profiles of TAA in the vitreous and aqueous humour of TAA loaded RXG-κ-CRG (F15) and TAA-HP-β-CD-Susp are shown in Figure 3.11. Phoenix WinNonlin software (version 8.3.3.33, Pharsight Corporation, NC, USA) was used to perform non-compartmental analysis on the time course data of TAA in both the matrices to compute parameters like C_{max}, T_{max}, AUC_{0-t} and $MRT_{0-\infty}$. In a given matrix, pooled

concentration data from both eyes (n = 2) of a single animal killed at each sampling time point was used to compute the pharmacokinetic parameters.

The vitreous humour is the most important site for the localization of the drug in the treatment of PU. Any formulation that can produce higher concentrations in the vitreous humour and sustain them for a longer duration would be ideal for treating conditions like PU. Figure 3.11b shows that the concentrations of TAA in the vitreous humour for TAA loaded RXG-κ-CRG *in situ* gel compared to TAA-HP-β-CD-Susp were significantly higher (1.64 ties) (C_{max} of TAA loaded RXG-κ-CRG (434.7 ng/mL) > TAA-HP-β-CD-Susp (264.9 ng/mL)) and sustained ($MRT_{0-\infty}$ of TAA loaded RXG-κ-CRG (16.1 h) > TAA-HP-β-CD-Susp (3.1 h)) for a longer duration. In addition, the total vitreous humour exposure of TAA, expressed in AUC_{0-t}, for TAA loaded RXG-κ-CRG (3271.1 ng×h/mL) was much higher (4.04 times) than that of TAA-HP-β-CD-Susp (810.4 ng×h/mL) as shown in Table 3.3. We can infer that TAA loaded RXG-κ-CRG *in situ* gel has better therapeutic potential as compared to TAA-HP-β-CD-Susp.

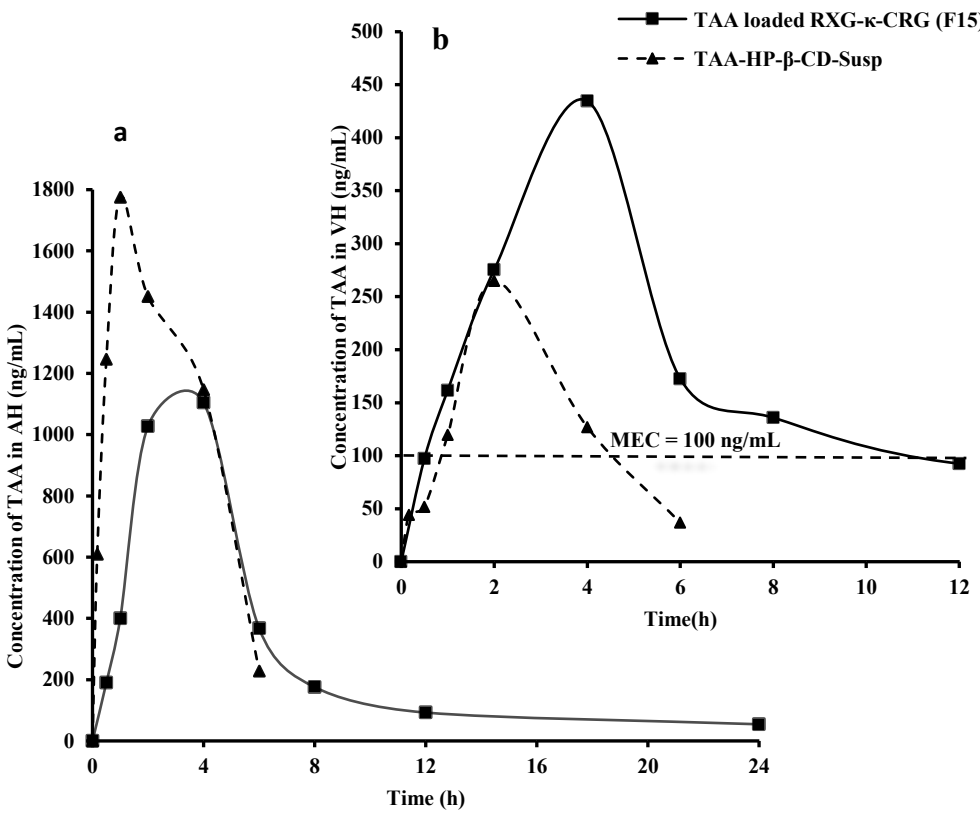

Figure 3.11: Mean concentration-time profiles obtained following ocular administration of

optimized TAA loaded RXG-κ-CRG (F15) *in situ* gel and an aqueous suspension of TAA-HP-β-CD-Susp in male New Zealand white rabbits, a: in aqueous humour (AH) and, b: in the vitreous humour (VH). Each data point represents the mean of two independent determinations (*n*=2).

Note: The concentration of TAA in AH and VH was found to be below the quantitation limit in the samples collected after 6 h in the case of TAA-HP-β-CD-Susp, while TAA loaded RXG-κ-CRG (F15) could produce measurable concentrations of TAA till 12 h in VT and till 24 h in AH.

Table 3.3: Pharmacokinetic parameters of TAA in the vitreous humour and aqueous humour following ocular administration of optimized TAA loaded RXG-κ-CRG (F15) *in situ* gel in male New Zealand white rabbits.

Biological matrix	PK parameters	Units	Treatments	
			TAA-HP-β-CD-Susp	TAA loaded RXG-κ-CRG (F15)
Vitreous humour	C_{max}	ng/mL	264.9	434.7
	T_{max}	h	2.0	4.0
	AUC_{0-t}	ng×h/mL	810.4	3271.1
	$MRT_{0-\infty}$	h	3.1	16.1
Aqueous humour	C_{max}	ng/mL	1775.4	1105.0
	T_{max}	h	1.0	4.0
	AUC_{0-t}	ng×h/mL	6697.3	6476.9
	$MRT_{0-\infty}$	h	3.0	9.5

*Data of TAA-HP-β-CD-Susp is reproduced from Table 2.4, Chapter 2.

Note: Composite sampling from both the eyes of an animal killed at each time point was done to determine the values of C_{max}, AUC_{0-t} and $MRT_{0-\infty}$.

A comparative time course profile of TAA in aqueous humour for TAA loaded RXG-κ-CRG *in situ* gel and TAA-HP-β-CD-Susp is presented in Figure 3.11a. The concentrations of TAA in aqueous humour were less for TAA loaded RXG-κ-CRG (C_{max} of 1105.0 ng/mL) compared to TAA-HP-β-CD-Susp (C_{max} of 1775.4 ng/mL). This could be due to the slow release of TAA from the gel matrix formed by RXG-κ-CRG, resulting in lower permeation rates of TAA through the cornea into the aqueous humour. In the case of TAA-HP-β-CD-Susp, the suspended particles of TAA undergo dissolution in the lachrymal fluids at the precorneal area and permeate rapidly through the cornea into the aqueous humour, resulting in higher C_{max} values (Table 3.3). Aqueous humour concentrations of TAA were sustained for more time in the case of TAA loaded RXG-κ-CRG ($MRT_{0-\infty}$ of 9.5 h) compared to TAA-HP-β-CD-Susp ($MRT_{0-\infty}$

of 3.0 h). TAA-HP-β-CD-Susp, being a conventional formulation, was readily cleared from the precorneal area due to the tear turnover, tear fluid dilution and nasolacrimal drainage. TAA loaded RXG-κ-CRG *in situ* gel formed a viscous gel layer which increased the residence time of the formulation in the precorneal area and also reduced the effects of dilution by tear fluids and nasolacrimal drainage. Further, the gel formed an intimate contact with the corneal epithelium for the drug to diffuse across the cornea. The overall aqueous humour exposure (AUC_{0-t}) was similar for both formulations.

Overall, TAA loaded RXG-κ-CRG (F15) *in situ* gel improved the availability of TAA in the vitreous humour and also sustained the concentration of TAA for longer duration compared to TAA-HP-β-CD-Susp. This can help in reducing the dosing frequency and dose of the TAA in the treatment of PU.

3.4 Conclusion

In this chapter, TAA loaded dual responsive *in situ* gel, using a combination of thermoresponsive polymer (RXG) and ion-sensitive polymer (κ-CRG), was successfully designed and optimized based on the thorough rheological evaluation. The formulation had sufficient solution state viscosity at room temperature for easy and accurate administration in the form of drops. The formulation could undergo a quick sol-to-gel transition in the presence of simulated tear fluid at 34 ± 0.5 °C. The optimized dual-responsive *in situ* gel was found to be safe and well tolerated by the corneal membrane. The formulation had strong mucoadhesive characteristics and good spreadability on the surface of the cornea. The optimized TAA loaded dual responsive *in situ* gel improved the overall exposure of TAA in the vitreous humour and prolonged the concentration of TAA for extended period compared to TAA-HP-β-CD-Susp. This study shows that TAA can be administered even in the precorneal area for the treatment of PU instead of administering it through the intravitreal route.

4

DESIGN, OPTIMIZATION, *IN VITRO* AND *IN VIVO* EVALUATION OF TRIAMCINOLONE ACETONIDE NANOCRYSTALS LOADED *IN SITU* GEL FOR TOPICAL OCULAR DELIVERY

4.1 Introduction

One of the most challenging yet exciting research areas in the field of pharmaceutical drug development is the ocular drug delivery [94,196]. Despite being a readily accessible organ, the eye has effective static, dynamic and efflux pump barriers that limit the delivery of drugs to achieve therapeutic concentrations at the targeted intraocular tissues. These barriers include corneal layers, sclera, retina, blood aqueous barrier, blood retinal barrier, tear dilution, conjunctival blood flow, choroidal blood flow and lymphatic clearance [4,197]. The conventional dosage forms and traditional modes of administration are found to be ineffective in delivering drugs to the posterior segment of the eye [198]. Though topical administration (by instilling the drug product as eye drops in the pre-corneal area) is the most convenient way of delivering the drugs, the availability of drugs at the posterior portion of the eye is very low [8,199].

Researchers have been working on designing novel formulations for improving the delivery of drugs to the posterior segment of the eye. Currently, nanotechnology-based drug delivery technologies, such as nanocrystal suspension, solid-lipid nanoparticles, nanostructured lipid carriers, liposomes, polymeric nanoparticles, dendrimers and niosomes, are being explored by researchers to improve the intraocular availability of the drugs and also to minimise systemic side effects and reduce the frequency of dosing of the drugs [186,200,201]. Nanocrystal formulations are very effective in addressing the issues related to solubility and dissolution rate of drugs that are insoluble or weakly soluble [202,203]. The increase in solubility and dissolution rate of the drug in nanocrystal form is due to the increase in the number of molecules at the surface of the nanocrystal particle [204]. In addition, the sub-micron particle size (100–1000 nm) of nanocrystals, enables efficient drug transport into or across cells, improving ocular drug absorption and extending the potency and duration of the therapeutic action [205]. Typically, nanocrystals are composed of a drug plus stabilizers (polymers or

surfactants) [206]. Therefore, compared to other nano-formulations, nanocrystal formulations have the benefit of carrying higher drug load [202]. Two methods, top-down and bottom-up, can be used to generate nanocrystal formulations of a drug. Top-down techniques make use of high-energy procedures like pearl milling and high-pressure homogenization that reduce pure drug particles into smaller-sized particles [207]. The bottom-up strategy (microprecipitation) involves drug precipitation, in the forms of nanocrystals, after being dissolved in a non-solvent (solvent-antisolvent) under controlled crystallization conditions [208,209].

Uveitis is an inflammatory disease. It refers to a wide range of disorders defined by intraocular inflammation, including the uvea and other ocular structures (retina, orbit, sclera) [154,155,210]. Uveitis frequently has an autoimmune cause and responds well to corticosteroids and immune-suppressants as a therapy [155,211]. Typically, corticosteroids are employed to treat PU [135]. The long-acting synthetic glucocorticoid, TAA is the drug of choice for treating ocular inflammations and is highly recommended for the treatment of PU due to its anti-inflammatory and immunosuppressive activity [109,155,211].

To address the shortcomings of aqueous suspension of TAA with 20% HP-β-CD (TAA-HP-β-CD-Susp), in the current chapter, we developed and assessed the efficacy of TAA nanocrystals (TAA-NCs) for ocular delivery. TAA-NCs was prepared using a bottom-up strategy (solvent-antisolvent precipitation method) and optimized the characteristics of TAA-NCs by employing the principles of design of experiments (DoE). In addition, TAA-NCs were loaded in the optimized dual responsive blank *in situ* gel (ISG) (discussed in Section 3.3.2, Chapter 3) to extend the residence time of the TAA-NCs and/or drug on the ocular surface following topical application of the formulation. The ocular pharmacokinetics of the optimized TAA-NCs and TAA-NCs loaded dual responsive *in situ* gel (TAA-NC-ISG) were compared with TAA-HP-β-CD-Susp in male New Zealand rabbits.

4.2 Materials and methods

4.2.1 Materials

Free samples of TAA and piribedil (used as an internal standard in the bioanalytical technique) were obtained from Dr. Reddy's Laboratories, Hyderabad, India and Strides Pharma Science Limited, Bangalore, India, respectively. D-α-Tocopherol polyethylene glycol 1000 succinate (TPGS), Poloxamer 407, sodium deoxycholate and polyvinyl alcohol (PVA, average molecular weight: 1,60,000 Daltons) were bought from Sigma-Aldrich Private Limited, Mumbai, India. Polyvinylpyrrolidone (PVP K30, average molecular weight: 40,000 Daltons) was procured from TCI chemicals, Chennai, India. Hydroxy propyl methyl cellulose (HPMC E5 LV, apparent viscosity of 2% w/v in water is 4-6 cps) was purchased from Molychem, Mumbai, India. Soluplus ((polyvinyl caprolactam-polyvinyl acetate-polyethylene glycol graft copolymer (PCL-PVAc-PEG)) was received as a gift sample from BASF (Mannheim, Germany). Methanol, acetonitrile, glacial acetic acid, ammonium acetate and disodium EDTA were bought from Harihara Scientific Pvt. Ltd. in Hyderabad, India. The buffer salts, which included potassium chloride (KCl), magnesium chloride ($MgCl_2$), calcium chloride ($CaCl_2$), mannitol and others, were supplied by SD Fine Private Limited, Mumbai, India. The Milli-Q water purification system (Millipore®, MA, USA) provided high-quality filtered water that was used in the HPLC analysis. New Zealand white male rabbits weighing 2 to 2.5 kg were supplied VAB Biosciences Limited, Hyderabad, India.

4.2.2 Preliminary trials for preparation of TAA-NCs

Nanoprecipitation technique, involving solvent-antisolvent method, was used to prepare TAA-NCs. The effect of various stabilizers (PVA, PVP K30, TPGS, Poloxamer 407, sodium deoxycholate, HPMC E5 LV and soluplus) and manufacturing process parameters (ultrasonication amplitude, ultrasonication time, homogenization speed, homogenization time and stirring time used in magnetic stirrer) on the physico-chemical characteristics like particle

size (PS), polydispersity index (PDI), zeta potential (ZP) and percent yield (yield (%)) of TAA-NCs were evaluated in the preliminary trials.

4.2.2.1 Formulation of TAA-NCs

Briefly, 40 mg of TAA along with sodium deoxycholate were dissolved in ethanol. Aqueous solution of soluplus was prepared in a separate beaker. Ethanolic solution containing TAA and sodium deoxycholate was added dropwise into the soluplus solution using a syringe under ultrasonication (Vibra cell, Sonics, Connecticut, USA) to produce a nanosuspension. The nanosuspension was further subjected to high-speed homogenization (Polytron PT 3100D, Kinemetica, Lucerne, Switzerland) to achieve smaller and uniform PS (Figure 4.1). The entire manufacturing process was done under controlled temperature condition by maintaining the temperature at 12 °C. The final nanosuspension was transferred to 50 mL centrifuge tubes followed by centrifugation for 45 min at 12,000 rpm at 10 °C to generate a pellet. The pellet was redispersed in MilliQ water containing mannitol (aqueous solution of mannitol at 3% w/v concentration, used as cryoprotectant) and freeze-dried. The freeze-dried TAA-NCs were stored at 2-8 ºC. The freeze-dried TAA-NCs were dispersed in deionized water to form aqueous suspension of TAA-NCs (TAA-NC-Susp) which was used in various physical characterization, *in vitro* and *in vivo* studies.

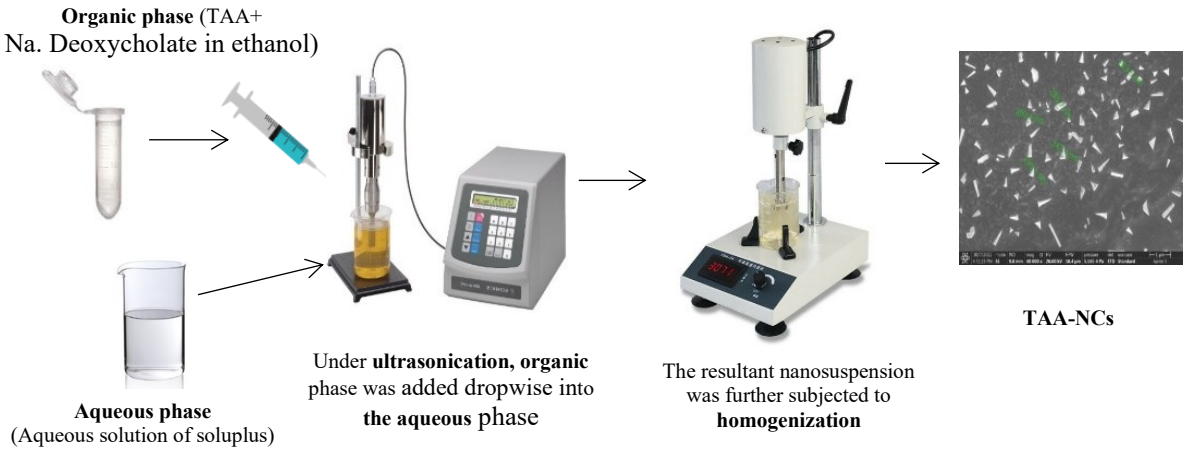

Figure 4.1 Schematic representation showing the step-wise procedure for the preparation of TAA-NCs.

4.2.3 Screening and optimization design for the preparation of TAA-NCs

A hybrid design approach, involving a screening design followed by an optimization design, was used in preparation of optimized TAA-NCs. Design Expert software (version 13, Stat-Ease Inc., Minneapolis, USA) was used in the screening and optimization studies.

4.2.3.1 Screening of factors by fractional factorial design

A two-level fractional factorial design with resolution IV involving three centre point runs (2^{6-2}_{IV} design with a total of 19 runs) was used to screen and identify the critical factors. A total of 6 factors (that includes material attributes and manufacturing process parameters) affecting the critical physico-chemical characteristics of TAA-NCs were identified based on the preliminary trials. The independent factors, along with the levels for each factor, taken up for the screening design are listed in Table 4.1.

The following physico-chemical characteristics of TAA-NCs were taken as critical responses for the screening design: yield (%), PS, ZP and PDI. The PS and PDI of nanocrystals can influence not only the dissolution rate but also the uptake of nanocrystals by the ocular epithelial membranes. The ZP of nanocrystals can affect the physical stability as well as uptake process. The yield (%) of TAA-NCs determines the total amount of the formulation to be administered at one dosing point.

Regression analysis was performed independently for each of the critical responses as a function of the dependent factors, and based on the results obtained, only the statistically significant factors were considered to be critical and taken up for further optimization using response surface methodology (RSM). Further, in the optimization design, only those critical responses which showed a variation in their values across the 16 non-centre experimental runs in the screening design were chosen for the regression analysis.

Table 4.1 Factors with their levels in the screening design for the formulation of TAA-NCs.

Factor Code	Actual factors	Levels		
		-1	**0**	**1**
$\mathbf{X_1}$	Homogenization time (min)	5	10	15
$\mathbf{X_2}$	Ultrasonication amplitude (%)	25	35	45
$\mathbf{X_3}$	Soluplus concentration (% w/v)	0.8	1.4	2
$\mathbf{X_4}$	Homogenization speed (rpm)	8000	12000	16000
$\mathbf{X_5}$	Ultrasonication time (min)	5	10	15
$\mathbf{X_6}$	Amount of sodium deoxycholate (mg)	15	30	45

4.2.3.2 Optimization by circumscribed central composite design

Three critical factors, namely soluplus concentration (% w/v), homogenization time (min) and ultrasonication amplitude (%), had a statistically significant effect on the critical responses of TAA-NCs based on the results obtained from the screening design. Out of the four critical responses, PS and yield (%) were found to vary significantly over the 16 non-centre experimental runs in the screening design. Therefore, only PS and yield (%) were taken as the final critical responses in the optimization design. To determine the mathematical relation between the three critical factors and the critical responses and to optimize the preparation of TAA-NCs, a circumscribed rotatable central composite design (cCCD) was employed. A second-order polynomial equation was constructed using cCCD involving 20 experimental runs with 6 centre points runs, separately, for PS and yield (%). In the cCCD, each factor was evaluated at 5 levels (-1.682, -1, 0, +1, +1.682; levels given in the transformed scale/coded scale). Analysis of variance (ANOVA), R^2 adjusted, R^2 predicted, predicted residual sum of squares (PRESS) of the regression models as well as other statistical parameters were used to identify the best-fit model (i.e., linear, 2-FI or quadratic) for each response. Response surface methodology (RSM) graphs or 3-D graphs were plotted to understand the effect of any two critical factors on a given critical response. The quadratic or the second-order polynomial equation generated by the cCCD is as follows:

Equation 4.1

$$Y = \beta_0 + \beta_1 X_1 + \beta_2 X_2 + \beta_3 X_3 + \beta_{12} X_1 X_2 + \beta_{13} X_1 X_3 + \beta_{23} X_2 X_3 + \beta_{11} X_1^2 + \beta_{22} X_2^2 + \beta_{33} X_3^2$$

Where, 'Y' is the dependent variable, 'β_0' is the arithmetic mean response of the 20 experimental runs and 'β_i's' and 'β_{ii}'s' (i = 1–3) are the coefficients of individual linear and quadratic effects of the variables, respectively, and 'β_{ij}'s' (i,j = 1–3; $i < j$) are the coefficients of the effect of interaction between the i^{th} and j^{th} variable.

4.2.3.3 Desirability value and validation of the model

The objective of implementing DoE in this work was to design TAA-NCs with desirable critical physico-chemical properties. Since two physico-chemical properties (PS and yield (%)) were found to be critical, a simultaneous optimization technique using desirability function, was adapted to determine the optimum levels of the critical factors to prepare TAA-NCs with desired PS as well as yield (%). Out of the various solutions given by the DoE software, the solution (with specific values of the critical factors, X_1, X_2 and X_3) with the highest desirability value was chosen as the optimized conditions for the preparation of TAA-NCs. To validate the optimized conditions obtained from the desirability function, six independent replicate formulations of the TAA-NCs were prepared based on the optimized conditions and characterized for their PS and yield (%). The predicted values for PS and yield (%) were determined from their corresponding regression models by fixing the levels of the critical factors as per the solution provided by the desirability function. The observed PS and yield (%) of the six independent replicate formulations were statistically compared to the predicted values using Wilcoxon signed rank test at 5% level of significance. No statistical difference between the observed and predicted values indicates the validity of the regression models for PS and yield (%) in predicting the critical responses of the TAA-NCs.

4.2.4 Physical Characterization of TAA-NCs

4.2.4.1 Measurement of PS, PDI and ZP of TAA-NCs

The physical properties like PS, PDI and ZP of TAA-NCs were assessed based on the principle of dynamic light scattering using Zetasizer Nano ZS (Malvern Instruments, Worcestershire, UK). All measurements were made using laser of 633 nm at a fixed scatter angle of 173° (backscatter). Prior to analysis, the freshly prepared samples of TAA-NCs (nanoprecipitation) method were diluted 10 times with MilliQ water and equilibrated for 2 min at 25 °C. The results of three independent (n=3) measurements were used to calculate the mean PS, PDI and ZP values.

In case of the lyophilized TAA-NCs and TAA-NC-ISG, the formulations (10 mg) were first dispersed in MilliQ water (2 mL) and then further diluted 10 times with MilliQ water. The diluted samples were allowed to be equilibrate for 2 min at 25 °C before the analysis. The mean PS, PDI and ZP values were calculated from three independent (n=3) measurements.

4.2.4.2 Determination of yield (%) of TAA-NCs

A direct method was employed to determine the yield (%) of TAA-NCs. The TAA-NCs suspension (either freshly prepared TAA-NCs suspension or freeze dried TAA-NCs reconstituted in MillQ water) was centrifuged at 12,000 rpm for 30 min at 10 °C to create a pellet, which was then vacuum dried using a vacuum concentrator (SCANVAC Scan Speed 32, Labogne ApS, Lynge, Denmark). The dry pellet was dissolved in NMP and analyzed using a validated HPLC method (Section 2.3.1, Chapter 2). The yield (%) was estimated using the equation (Eq. 4.2) given below.

Equation 4.2 $$\textbf{Yield}\ (\%) = \frac{W_{TAA\ in\ Pellet}}{W_{Total\ TAA\ added}} \times 100$$

Where, $W_{Total\ TAA\ added}$ represents the total amount of TAA added in the preparation of TAA-NCs and $W_{TAA\ in\ Pellet}$ represents the total quantity of TAA present in the pellet formed following centrifugation of the TAA-NCs suspension.

4.2.4.3 Scanning electron microscopy (SEM) imaging of TAA-NCs

The optimized TAA-NCs surface morphology was investigated using a SEM (FE-SEM, FEI, Apreo LoVac, TermoFisher Scientific, MA, USA). For analyzing the sample, 40 µL of the optimized TAA-NCs dispersion was deposited on an aluminium stub and vacuum-dried overnight. The dried sample was sputter-coated with gold under vacuum using a sputter coater (Leica EM ACE200, Wetzlar, Germany) in an inert (argon gas) environment. The SEM images were recorded by scanning the gold coated samples at 5 kV acceleration voltage.

4.2.4.4 Differential scanning calorimetry (DSC) of TAA-NCs

Thermal analysis was performed using DSC-60 (TA-60 WS, Shimadzu, Kyoto, Japan) for pure TAA, lyophilized TAA-NCs and powder mixture of TAA with the various excipients used in the preparation of TAA-NCs. The samples (5 mg) were taken in aluminium pans and crimp-sealed. Empty sealed aluminium pan was used as reference for the analysis. The reference and sample pans were put in the DSC sample chamber and allowed to equilibrate at 30 °C in the presence of nitrogen gas purged at a flow rate of 50 mL/min. Following the equilibration, the samples were analyzed in the temperature range of 30–300 °C at a heating rate of 10 °C/min in nitrogen environment.

4.2.4.5 Powder X-ray diffractometry (pXRD) of TAA-NCs

The physical state of TAA in the optimized TAA-NCs was determined by performing pXRD using a Rigaku Ultima IV diffractometer (Texas, USA) for pure TAA, freeze-dried TAA-NCs and physical mixture of TAA and various excipients used in the preparation of TAA-NCs. The samples were scanned at a rate of 4 degrees/min in the 2θ range of 5-40° in the study. The samples were irradiated using nickel filtered Cu-Kα radiation (λ = 1.54 Å) at a voltage of 40 kV and a current of 30 mA.

4.2.5 Preparation of TAA-NCs loaded RXG-κ-CRG *in situ* gelling formulation

In chapter 3 (Section 3.3.2), we discussed the optimization of blank RXG-κ-CRG *in situ* gel (ISG) using a combination of reacted tamarind seed xyloglucan (RXG) and kappa-Carrageenan (κ-CRG) at 2% w/v and 0.3% w/v, respectively. In the current work, we loaded the lyophilized powder of the optimized TAA-NCs in the optimized blank *in situ* gel to form TAA-NC loaded *in situ* gel (TAA-NC-ISG). The rheological characteristics of the TAA-NC-ISG and ISG were studied in parallel plate geometry using a rheometer (Anton Paar MCR 302, Graz, Austria). In the study, first the amplitude and frequency sweep tests were done to identify the linear viscoelastic region (LVER) for each sample. The samples' rheological characteristics were next examined in the LVER using a temperature sweep in oscillatory mode between 25 °C and 40 °C. The sample's gelation was assessed in two experimental setups: 1) temperature ramp and 2) temperature ramp with STF. The data obtained from the rheological investigations was used to build the loss tangent (*tan δ*) vs temperature and complex viscosity (*η**) vs temperature plots to evaluate the gelation behaviour of the TAA-NC-ISG.

4.2.6 *In vitro* drug release study from TAA-NC-Susp and TAA-NC-ISG formulations

A membrane-free technique, with a slight modification of the dissolution apparatus (USP Type II) (Model TDT-08L, Electro lab, Mumbai, India), was employed to study the *in vitro* drug release of TAA-NC-Susp and TAA-NC-ISG formulations [12]. A round stainless-steel container with a 1.4 cm internal diameter and 0.5 cm depth was adhered to the bottom of a 1000 mL dissolution jar. The study formulation (40 µL of TAA-NC-Susp or TAA-NC-ISG, equivalent to 4 mg of TAA) was carefully taken in the stainless-steel container. The dissolution jars were filled with 300 mL of STF containing 0.5% w/v of Tween 80, which was previously equilibrated at 34 ± 0.5 °C. The temperature in the dissolution jars was maintained at 34 ± 0.5 °C. The paddle was rotated at 75 rpm. Dissolution samples (2 mL) were taken during the dissolution study at predefined intervals (0.25, 0.5, 1, 2, 4, 6, 8, 12, 24 and 48 h) using a syringe.

The obtained samples were centrifuged for 30 min at 10 °C at 12,000 rpm. After centrifugation, 1 mL of the supernatant was collected and analyzed using a validated RP-HPLC analytical method (Section 2.3.1, Chapter 2). The pellet, obtained after centrifugation, was dispersed with 1 mL of fresh dissolution media (maintained at 34 ± 0.5 °C) and transferred back to the respective dissolution jars. A similar procedure was followed at all sampling time points. Data from *in vitro* dissolution was fitted into different mathematical models to determine the release kinetics (including zero-order, first-order and Higuchi square root kinetics) and release mechanism (Korsmeyer-Peppas model) [187,212].

4.2.7 Stability of TAA-NCs and TAA-NC-ISG formulations

The optimized TAA-NCs (lyophilized powder) and TAA-NC-ISG (TAA-NCs loaded *in situ* gel) formulations were packed in airtight vials and stored at ambient conditions (25 ± 2 °C and relative humidity of 60 ± 5%) and refrigerated conditions (2-8 °C), respectively, for assessing their stability. Generally, *in situ* gels are recommended to be stored in refrigerated conditions to avoid undesirable thickening/transition from sol-to-gel at room temperature. Therefore, TAA-NC-ISG was stored in refrigerated conditions (2-8 °C) [212]. The stability studies were conducted for a period of 60 days, during which the samples (n=3) from both formulation vials were collected after every 15 days and evaluated for their PS, PDI, ZP and yield (%). Data collected at different sampling points was compared with that of the zero-time data of the respective formulation.

4.2.8 *Ex vivo* ocular toxicity tests of TAA-NCs and TAA-NC-ISG formulations using the HET-CAM technique

The Hen's Egg Test-Chorion Allantoic Membrane (HET-CAM) technique was employed in the *ex vivo* ocular irritation study [213]. Fresh eggs (weighing around 50-60 g) were bought from a nearby chicken farm and incubated for five days at a temperature of 37 ± 0.5 °C and a relative humidity of 55 ± 5%. After five days, the eggs were candled to distinguish the fertile ones from the infertile ones. To ensure that the CAM grew properly, the fertilized eggs were

kept in the incubator for further 10 days. During the incubation stage, the eggs were manually rotated every 12 h. A revolving dental blade was used to gently crack the egg shell in order to access the air cell without damaging the inner membrane. Following the opening of the eggs, the exposed CAM was moistened with a NaCl (0.9% w/v) solution and incubated for 30 min. The inner layer of each egg was delicately peeled with forceps to reveal the CAM for applying the test sample on its surface. The study comprised of four treatment groups: Positive control (treated with 0.1 N NaOH) - Group 1, Negative control (treated with 0.9% w/v NaCl solution) - Group 2, TAA-NC-Susp - Group 3 and TAA-NC-ISG - Group 4. Three eggs (n=3) (with a CAM that was correctly developed and exposed) per treatment group were utilized in the study. The treatment sample (200 µL) was applied to the egg's CAM surface and the level of blood vessel damage was observed for a period of 300 sec. Based on the extent of blood vessel damage, an irritation score (IS) was calculated for each sample using the following equation.

Equation 4.3 $$IS = \frac{(301-H)}{300} \times 5 + \frac{(301-L)}{300} \times 7 + \frac{(301-C)}{300} \times 9$$

Where, 'H' denotes the start of the haemorrhage responses on the CAM, 'L' denotes the start of the vascular lysis on the CAM and 'C' denotes the start of the coagulation formation on the CAM.

Based on their IS values, the formulations' ocular irritancy potential was evaluated. The formulation with IS values between 0 and 0.9 was classified as 'non-irritating'; between 1 and 4.9 was classified as 'slightly irritant'; between 5 and 9.9 as 'moderately irritant' and between 10 and 21 as 'strongly irritant'.

4.2.9 Histopathological studies of the TAA-NCs and TAA-NC-ISG formulations

Histopathology studies were conducted to determine the effect of formulations on the cellular structure and integrity of the corneal epithelium. Fresh goat eyeballs were obtained from a nearby slaughter house. A 2 mm incision was made on the eye, leaving the scleral ring intact, and the cornea was removed. The cornea was promptly rinsed for 1 min with 0.9% w/v NaCl

solution. The cornea was then exposed to each of the treatments, separately, for 6 h. The effect of four treatment groups on the corneal epithelium was assessed in the study. Group 1 served as the positive control (75% v/v isopropyl alcohol), Group 2 served as the negative control (STF, pH 7.4 ± 0.05) while the corneal epithelium was exposed to TAA-NC-Susp and TAA-NC-ISG in Group 3 and Group 4, respectively. After 6 h of exposure, the cornea was cleaned with 0.9% w/v NaCl solution and immediately frozen using a tissue freezing medium and preserved at -80 °C. Cross-sections of the frozen cornea that were less than 5 mm in diameter were cut using a cryotome (Leica Biosystems, CM1520 cryostat, Wetzlar, Germany) and placed on a glass slide. Using a gradient of 30-50-70-90-100% ethanol and xylene, the tissue was dehydrated. The dehydrated tissue was cleaned with NaCl solution (0.9% w/v) and stained with hematoxylin and eosin. The tissue was washed with NaCl solution (0.9% w/v) to remove the excess hematoxylin and eosin and examined for histological alterations using a digital microscope (ZEISS, Axiocam 705 colour, Oberkochen, Germany) at 10× magnification [190].

4.2.10 Ocular pharmacokinetic studies of the optimized TAA-NCs and TAA-NC-ISG formulations

Male New Zealand rabbits (n=8 for each treatment, weighing 2-2.5 kg) with normal eyes (without any inflammatory indications) were used to compare the ocular pharmacokinetics of the optimized TAA-NC-Susp and TAA-NC-ISG. The institutional animal ethics committee had examined and approved the study protocol (Protocol No.: BITS-Hyd/IAEC/2022/14), before the study was conducted.

The experiment was carried out at the animal house facility of our institute, where the animals were acclimated (temperature of 22 ± 1 °C; relative humidity of 55 ± 10% and 12 h light-dark cycle) for a week prior to the study. A micropipette was used in the experiment to instil 40 µL of the formulations into each of the two rabbit's eyes (at the lower cul-de-sac). To increase the contact time between the cornea and the administered formulation, the eyelids were kept closed for 10 sec immediately after dosing. At intervals of 0.5, 1, 2, 4, 6, 8, 12 and 24 h after the

formulation was instilled, one rabbit was euthanized by inhalation of carbon dioxide. Using an insulin needle (30-gauge, 3 mm diameter), aqueous humour was drawn from the euthanized rabbit by inserting the needle behind the limbus superotemporally and aiming it at the centre of the eye. The rabbit's left and right eyes were removed after the collection of the aqueous humour. The eyes were quickly frozen using dry ice. The vitreous humour was taken out from the frozen eyeball and stored at a temperature of –20 °C.

The samples (plasma, aqueous humour and vitreous humour) obtained from ocular pharmacokinetics were analyzed using a validated HPLC method (Section 2.3.3, Chapter 2). Non-compartmental analysis was used to examine the time course data of TAA in plasma, aqueous humour and vitreous humour. The pharmacokinetic parameters, including C_{max} (the maximum concentration of TAA), T_{max} (the time to reach C_{max}) and $MRT_{0-\infty}$ (the mean residence time from t = 0 to t = ∞) were determined from the time course data of TAA in each of the matrices. The AUC_{0-t} (area under the TAA time course curve from t = 0 to t = t_{last}) was calculated using the trapezoidal rule method.

4.2.11 Quantification of TAA and Statistical analysis of data

Validated aqueous HPLC-PDA method (Section 2.3.1, Chapter 2) was used to quantify TAA in the formulations, *in vitro* drug release study samples and stability studies samples. The plasma, aqueous and vitreous humor samples collected from ocular pharmacokinetic study of TAA-NC-Susp and TAA-NC-ISG were extracted using a two-step procedure that included protein precipitation and solvent evaporation. The processed samples were quantified using a validated HPLC-PDA bioanalytical method (Section 2.3.3, Chapter 2) with a calibration range of 50-3000 ng/mL for the drug.

The results from physical characterisation studies and *in vivo* experiments were statistically compared between various groups/treatments using unpaired t-test (for comparing two treatments) or ANOVA (for comparing more than two treatments). An appropriate post-hoc

test was then performed at the 5% level of significance (α = 0.05), wherever necessary. The data obtained in various studies is expressed as mean ± standard deviation, based on the number of replicates considered for the study.

4.3 Results and discussion

4.3.1 Preliminary trials for preparation of TAA-NCs

TAA-NCs were pared by nanoprecipitation technique using solvent-antisolvent method. In this method, the addition of drug solution (obtained by dissolving the drug in the solvent selected) into the antisolvent creates super-saturation (of the drug concentration in the solvent mixture) followed by nucleation and particle growth through coagulation and agglomeration. To produce NCs and control their PS using this method, the degree of super-saturation and the efficiency of the stabilizers (added in the antisolvent) are very critical. The measure of super-saturation can be expressed as follows (Eq. 4.4):

Equation 4.4

$$S = \frac{C}{C^*}$$

Where, 'C' represents the actual concentration of the drug in the solvent and 'C^*' represents the concentration of the drug in a solution made up of solvent and the antisolvent. It is well known that a high level of super-saturation causes a wider extent of nucleation, which results in the production of numerous particles with controlled growth [214,215].

Solubility studies were conducted in various organic solvents, including ethanol, N-methyl pyrrolidone (NMP), dichloro methane (DCM), dimethyl sulfoxide (DMSO) and dimethyl formamide (DMF). TAA was found to have good solubility (>15 mg/mL) in all the solvents, except for DCM. Ethanol was selected as the suitable solvent due to its low toxicity profile and less environmental impact compared to the other solvents [216].

The selection of stabilizer is another crucial factor in regulating particle growth. Literature search revealed that there is no relation between the physicochemical characteristics of the drug, the characteristics of the crystal surface, and the stabilizer selected in the preparation of

NCs by solvent-antisolvent method [214]. Additionally, according to Toumela A *et al*., the parameters governing the stabilizing effect of stabilizers are poorly known, and the choice of stabilizer for drug NCs is mostly based on empirical data [217]. Therefore, a few trials were conducted to study the effect of various stabilizers [like steric stabilizers (polyvinyl pyrrolidone K-30, hydroxypropyl methylcellulose E5 LV, polyvinyl alcohol, and D-α-tocopherol polyethylene glycol succinate), amphiphilic surfactants (soluplus and different grades of pluronics) and anionic surfactants (sodium deoxycholate and sodium lauryl sulphate)] on the PS, PDI and stability of the NCs. Based on the results obtained, a combination of soluplus and sodium deoxycholate was used as a stabilizer system in the preparation of TAA-NCs. Soluplus offers higher wettability and steric stabilization than other stabilizers due to its bi-functional nature and large molecular size [218–220]. The PS and PDI of the TAA-NCs were better when soluplus was combined with sodium deoxycholate than compared to using soluplus alone in the preparation.

4.3.2 Screening and optimization design for preparation of TAA-NCs

Six independent factors with their upper and lower levels to be used in the preparation of TAA-NCs were identified based on the results obtained from the preliminary formulation trials. A two-level fractional factorial design with resolution IV was used to screen the critical factors out the six factors. The critical factors in the screening design were identified based on their effect on critical responses, namely, PS, PDI, ZP and yield (%) of the TAA-NCs. Three factors were found to have statistically significant effect on the responses based on the data obtained from the screening design. The data obtained from the experimental runs in the screening design showed no or little variation in the ZP and PDI values of the TAA-NCs. Therefore, for the optimization design, only PS and yield (%) responses were considered. The three critical factors affecting the PS and yield (%) (Table 4.1) were, X_1: homogenization time (min), X_2: ultrasonication amplitude (%) and X_3: soluplus concentration (% w/v). These factors were

further optimized using a circumscribed central composite design (cCCD). Each factor was studied at five different levels. Table 4.2 presents the levels of each factor (in their original scale) in each of the experimental runs and the observed responses obtained for TAA-NCs prepared in each of the runs. The regression equations were constructed for PS and yield (%) based on the results obtained from the cCCD. The regression models for both PS and yield (%) were subjected to ANOVA and the statistical output is presented in Table 4.3. The statistical significance of any of the factorial terms was judged based on the '*P*' value. If the '*P*' value is less than 0.05 (as the significance level was set at 0.05), the factorial term was considered to have statistically significant impact on the response variable or else the effect of the factorial term was considered insignificant.

4.3.2.1 Effect of critical factors on PS

The effect of the three critical factors on the PS is given by the least square second-order polynomial equation (in the coded form) given below:

Equation 4.5

$$\boldsymbol{Sqrt(PS, Y_1)} = 17.03 - 2.24\,X_1 - 0.65\,X_2 - 0.47\,X_3 - 0.93\,X_1X_2 + 0.03\,X_1X_3 - 0.20\,X_2X_3 + 0.85\,X_1^2 + 0.34\,X_2^2 + 0.51\,X_3^2$$

The 'F_{cal}' value for the model (8.86) was significantly higher than the 'F_{crit}' value with $P<0.001$. The lack of fit was insignificant ($P>0.05$) for the regression model of PS. Square root transformation was applied to the response variable Y_1 (PS) to reduce the variability in the residuals data, improve the value of predicted R^2 and reduce the difference between predicted R^2 and adjusted R^2 values to less than 0.2. In the residuals versus the run number plot, the distribution of residuals was random and centred around zero, indicating that run sequence in the optimization design does not affect the residuals. All the above statistical results suggest the validity and predictability of the regression equation obtained for PS. The PS values in the experimental runs ranged from 218 nm in the 3rd run to 588 nm in the 15th run (Table 4.2).

According to the results of the ANOVA, homogenization time had the highest impact on the PS of TAA-NCs. The PS of the TAA-NCs decreased as the homogenization time increased, as shown in the 3D response plot (Figure 4.2a). Ultrasonication amplitude had a marginal impact on the PS of TAA-NCs. As the homogenization time increased, the amount of energy transferred by the homogenizer (shear forces) increased, resulting in the PS reduction of the TAA-NCs.

Table 4.2 The CCD design matrix for TAA-NCs in a randomised run order

Run No.	X_1 Homogenization time (min)	X_2 Ultrasonication amplitude (%)	X_3 Soluplus concentration (% w/v)	Y_1 PS (nm)	Y_2 Yield (%)
1	15	25	0.8	360	85
2	10	35	1.4	263	77
3	15	45	2.0	218	72
4	10	35	1.4	283	78
5	10	35	1.4	288	73
6	15	45	0.8	250	90
7	15	25	2.0	315	68
8	10	35	2.4	328	65
9	10	18.2	1.4	373	76
10	10	35	1.4	298	74
11	5	45	2.0	390	66
12	10	35	1.4	243	75
13	5	25	2.0	400	71
14	18.4	35	1.4	220	75
15	1.6	35	1.4	588	74
16	10	35	0.4	363	94
17	10	35	1.4	375	74
18	10	51.8	1.4	285	77
19	5	45	0.8	480	90
20	5	25	0.8	415	89

Note: The response data are shown as the average of three independent measurements. The %RSD of repeat measurements was less than 5% in every instance.

4.3.2.2 Effect of critical factors on Yield (%)

The following least square second-order polynomial equation, in the coded form, presents the effect of the three critical factors on the yield (%).

Equation 4.6

$$\boldsymbol{Yield}\ \%(\boldsymbol{Y_2}) = 75.17 + 0.059\,X_1 + 0.42\,X_2 - 9.15\,X_3 + 1.57\,X_1X_2 + 0.75\,X_1X_3 - 0.78\,X_2X_3 + 0.14\,X_1^2 + 0.92\,X_2^2 + 1.92\,X_3^2$$

The 'F_{cal}' value for the model (39.73) was significantly higher than the 'F_{crit}' value with P<0.001. The lack of fit was insignificant (P>0.05) for the regression model of yield (%). The difference between the predicted R^2 and adjusted R^2 values was less than 0.2. The sequence of experimental run orders in cCCD had no impact on the residuals, as the distribution of residuals in the residuals versus the run number plot was found to be random and centred around zero. The validity and predictability of the regression equation for yield (%) was established based on the statistical analysis of the data obtained in the study. The yield (%) values in the experimental runs ranged from 64% (8th run) to 94% (16th run) in the optimization design (Table 4.2).

Table 4.3 Statistical results (ANOVA) displaying terms with significant coefficients for the chosen critical responses of TAA-NCs.

Source	Particle Size (Y_1)				Yield (Y_2)			
	Sum of Squares	df	F_{cal}	P_{cal}	Sum of Squares	df	F_{cal}	P_{cal}
Model	39.33	9	8.86	0.0010*	1237.17	9	39.73	<0.0001*
X_1	27.37	1	55.50	<0.0001*	0.047	1	0.014	0.9092#
X_2	2.34	1	4.75	0.0543#	2.40	1	0.69	0.4240#
X_3	1.20	1	2.44	0.1495#	1144.4	1	330.73	<0.0001*
X_1X_2	2.77	1	5.63	0.0392*	19.68	1	5.69	0.0383#
X_1X_3	2.95E-03	1	5.99E-03	0.9398#	4.48	1	1.30	0.2815#
X_2X_3	0.13	1	0.27	0.6157#	4.88	1	1.41	0.2625#
X_1^2	4.18	1	8.47	0.0155*	0.27	1	0.078	0.7862#
X_2^2	0.67	1	1.36	0.2711#	12.27	1	3.55	0.0891#
X_3^2	1.50	1	3.03	0.1122#	53.25	1	15.39	0.0029*
Residual	4.93	10			34.60	10		
Lack of Fit	1.59	5	0.47	0.7841#	18.70	5	1.18	0.4314#
Pure Error	3.35	5			15.90	5		
Total	44.26	19			1271.77	19		

Note: *Statistically significant with P<0.05; #Statistically not significant with P≥0.05

The soluplus concentration was found to have the highest impact on the yield (%) of the TAA-NCs out of the three critical factors. Increasing the soluplus concentration decreased the yield (%) (Figure 4.2b). The solubility of TAA in water increases with increasing concentration of

soluplus in the aqueous vehicle. This causes less amount of TAA to undergo precipitation during the preparation of TAA-NCs in the solvent-antisolvent addition method.

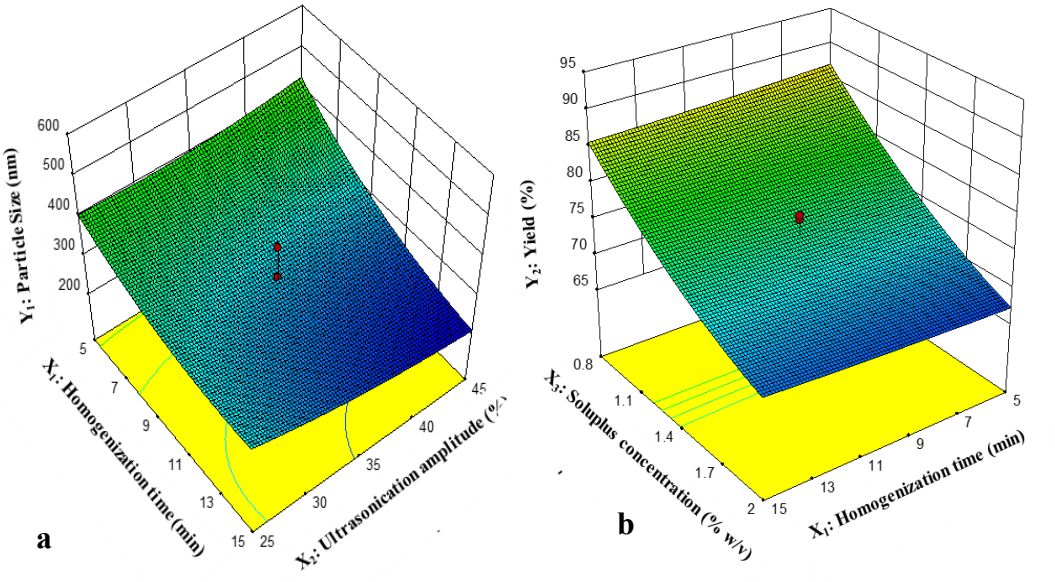

Figure 4.2 3D response surface plots demonstrating the impact of critical factors on TAA-NCs critical responses: (a) PS and (b) Yield (%) for optimized TAA-NCs.

4.3.2.3 Desirability value and validation of the model

In optimization methods involving multiple response variables, simultaneous optimization techniques using desirability function is very effective [221]. Design expert software provides several solutions (in terms of the conditions to be set for the critical factors) with different desirability values. The solution with the highest desirability value is considered to optimal conditions at which the critical factors are to be fixed to achieve the desired values for the critical responses. In the current study, the Design Expert software predicted the following conditions: homogenization time – 15 mins, ultrasonication amplitude - 45% and soluplus concentration - 0.8% w/v; as optimum for the simultaneous optimization of PS and yield (%), with a desirability of 0.886. Verification runs (n=6) was performed to examine the validity of the desirability function to predict the response variables. Six independent replicate formulations of TAA-NCs were prepared using the conditions predicted by the software and characterized for their PS and yield (%). The Wilcoxon signed rank test with an $\alpha = 0.05$

significance level was used to evaluate the statistical difference between the observed and predicted values of both the responses. No significant (P>0.05) difference was found between the observed and predicted values of both PS and yield (%), proving the accuracy of the model in predicting the responses. The optimized TAA-NCs were found to have PS of 243 ± 5.7 nm and yield (%) of 88.5 ± 2.4%.

4.3.3 Formulations characterization using DSC, powder XRD and SEM imaging

The DSC thermograms of TAA, the physical combination of TAA and the various excipients used in the formulation of TAA-NCs and freeze-dried TAA-NCs are given in Figure 4.3a. A sharp endothermic peak corresponding to the melting of pure TAA was observed at 292 °C. In the mixture of TAA and the various excipients, two melting endothermic peaks were observed at 292 °C and 70°C. The endothermic peak at 292 °C was sharp and it corresponds to TAA while the peak at 70 °C was small and broad, which corresponds to the melting endotherm of soluplus. The thermogram for the freeze-dried TAA-NCs showed the peaks for TAA and soluplus at 292 °C and 70 °C, respectively, in addition to the sharp endothermic peak at 160 °C due to the melting of the cryoprotectant mannitol utilized to freeze-dry TAA-NCs.

The pXRD investigations confirmed that the crystalline form of TAA did not change with the formulation of the TAA-NCs, which is in line with the DSC observations. The crystalline peaks of pure TAA between 2θ range of 9-21° and 24-28°, notably at 2θ values of 9°, 14°, 17° and 24°, were present in pure TAA, physical mixture and TAA-NCs as shown in Figure 4.3b**.**

Figure 4.3c displays the SEM image of the pure TAA powder and optimized TAA-NCs. The SEM images of both pure TAA powder and the TAA-NCs showed the crystallised particles that resemble the bulk TAA. Additionally, the PS of TAA-NCs found in SEM was almost same as the PS observed in zetasizer.

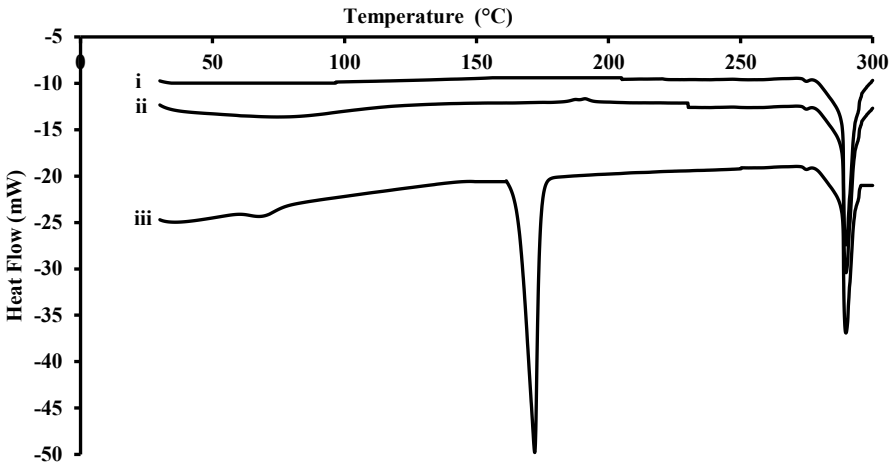

Figure 4.3a The DSC thermograms of (i) pure TAA, (ii) the physical combination of TAA with various ingredients used in the formulation of TAA-NCs and (iii) freeze-dried TAA-NCs.

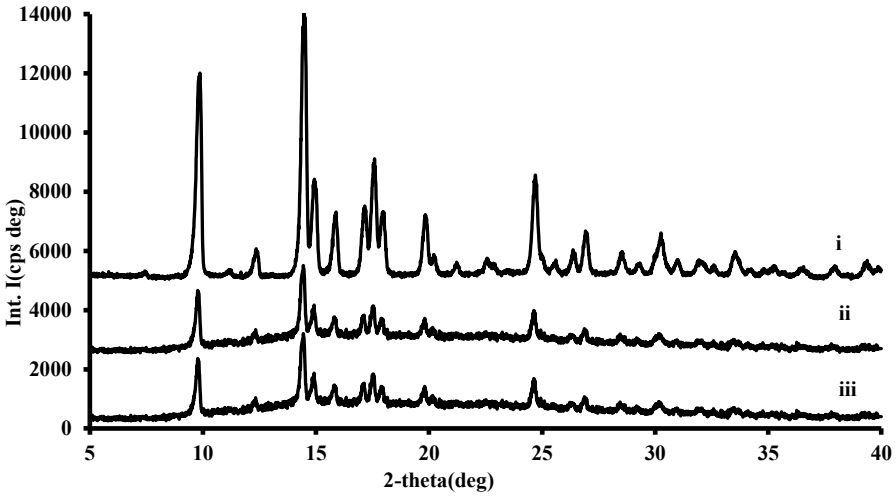

Figure 4.3b The pXRD graphs of (i) pure TAA, (ii) the physical combination of TAA with various ingredients used in the formulation of TAA-NCs and (iii) freeze-dried TAA-NCs.

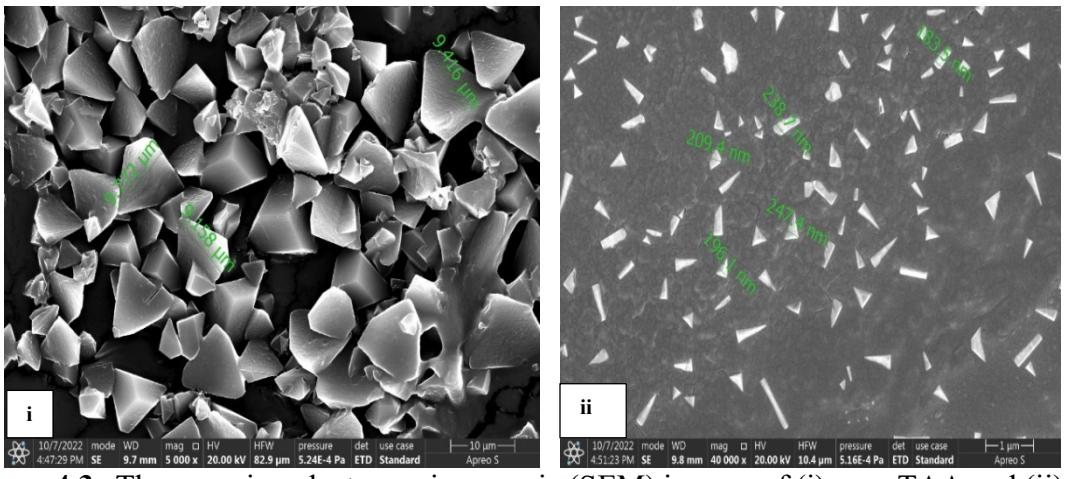

Figure 4.3c The scanning electron microscopic (SEM) images of (i) pure TAA and (ii) freeze-dried TAA-NCs.

4.3.4 Rheological evaluation of TAA-NC-ISG formulation

In chapter 3 (Section 3.3.2), we have optimized different concentrations of RXG and κ-CRG for the preparation of dual responsive blank RXG-κ-CRG *in situ* gel (ISG). The final *in situ* gel was composed of 2% w/v of RXG, 0.3% w/v of κ-CRG and 0.1% w/v of KCl. Considering the fact that the levels of K^+ ions is very low levels in the STF, the KCl salt was added in the optimized *in situ* gel to increase the sensitivity of κ-CRG towards the K^+ ions following the administration of the formulation in the precorneal area. Addition of K^+ ions in the *in situ* gel resulted in significant reduction of κ-CRG concentration in the formulation of dual responsive *in situ* gel. This also helped in controlling the solution state viscosity (at 25 °C) of blank ISG**,** which is very critical for easy dispensation of the formulation in the form of drops. In the current chapter, TAA-NC-ISG was prepared by dispersing the optimized TAA-NCs in the optimized blank *in situ* gel (ISG). The prepared *in situ* gel system showed quick sol-to-gel transition in presence of both temperature and simulated tear fluid (STF). The linear viscoelastic region (LVER) of the TAA-NC-ISG was determined using a frequency and amplitude sweep. The sol-to-gel transformation studies of the TAA-NC-ISG were performed in the LVER of the *in situ* gel. The results obtained from the rheological evaluation of blank ISG and TAA-NC-ISG are shown in Figure 4.4a and 4.4b. Figure 4.4a shows the loss tangent (*tan δ*), while Figure 4.4b shows the complex viscosity (η^*) characteristics of the formulations as a function of temperature. The loss tangent (*tan δ*) values decreased while the complex viscosity (η^*) values increased as the temperature gradually increased from 25 to 40 °C. Both the formulations, in the temperature between 32 to 35 °C, showed a clear sol-to-gel transition, which is evident from the sudden shift in the *tan δ* and η^* values. This shows the thermoresponsive nature of the RXG present in the ISG. Moreover, when TAA-NC-ISG was exposed to STF, the *tan δ* value were less than 1 (also reflected in higher η^* values) even at the starting temperature of 25 °C, indicating a rapid transition from solution form to a gel. This is

due to the ion sensitivity of the κ-CRG of the developed ISGs, which was not observed when TAA-NC-ISG was subjected to only temperature ramp without the STF.

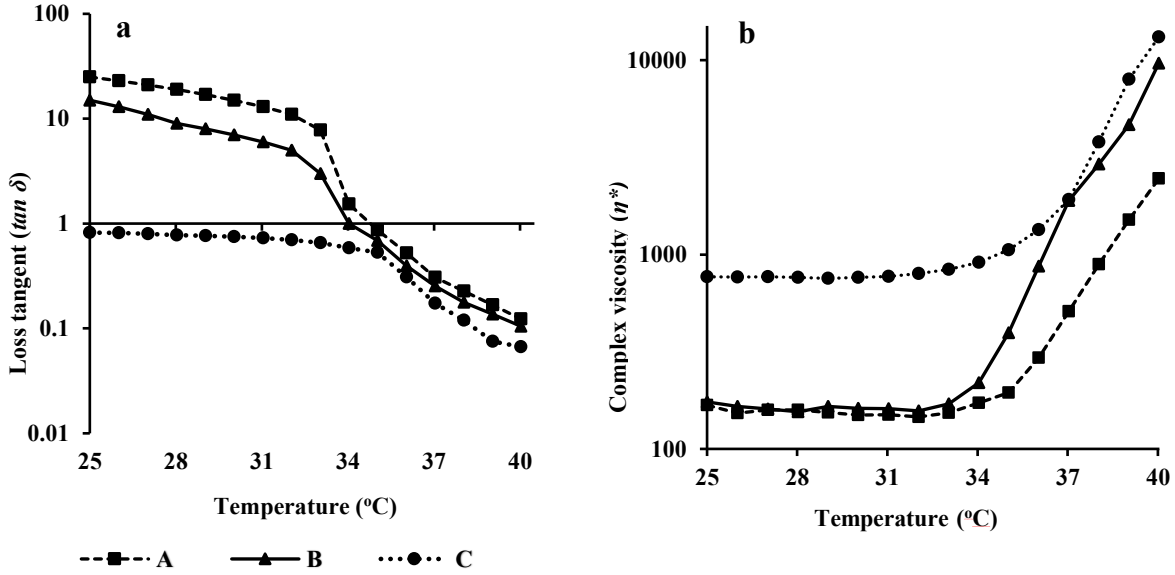

Figure 4.4 Semi-logarithmic plots of (a) loss tangent (*tan δ*) and (b) complex viscosity (*η**) of blank ISG and TAA-NC-ISG as a function of temperature.

***Note:** A- blank ISG and B- TAA-NC-ISG subjected to temperature ramp; C- TAA-NC-ISG subjected to temperature ramp in the presence of STF.

4.3.5 *In vitro* drug release study from TAA-NC-Susp and TAA-NC-ISG formulations

The drug release studies were carried out in STF containing 0.5% w/v of Tween 80 and a pH of 7.4 ± 0.05. The solubility of TAA in STF is 13.7 µg/mL and STF containing Tween 80 (0.5% w/v) is 48 µg/mL. Therefore, 300 mL of STF with 0.5% w/v Tween 80 was used as dissolution media in the study to maintain the sink condition. The *in vitro* dissolution data was used to construct the mean cumulative percentage of drug released vs time graphs (Figure 4.5). TAA was found to be completely dissolved within 15 min, in the case of TAA-NC-Susp. However, the drug release from TAA-NC-ISG was slow and sustained. The gel network formed by the TAA-NC-ISG impeded the drug's diffusion and prolonged the drug release for more than 12 h from the formulation. Different release kinetics models were used to fit the TAA release profile data obtained from the TAA-NC-ISG formulation. Higuchi square-root

kinetics model (R^2=0.977) provided the best fit for the drug release data of TAA-NC-ISG when compared to the zero-order kinetics model (R^2=0.8893) and the first-order kinetics model (R^2=0.8996). The analysis of data using Korsmeyer-Peppas model revealed that the diffusional exponent value was 0.62, indicating that drug release mechanism was non-Fickian or anomalous transport. In anomalous transport mechanism, both polymeric relaxation and drug diffusion play a role in the overall drug release.

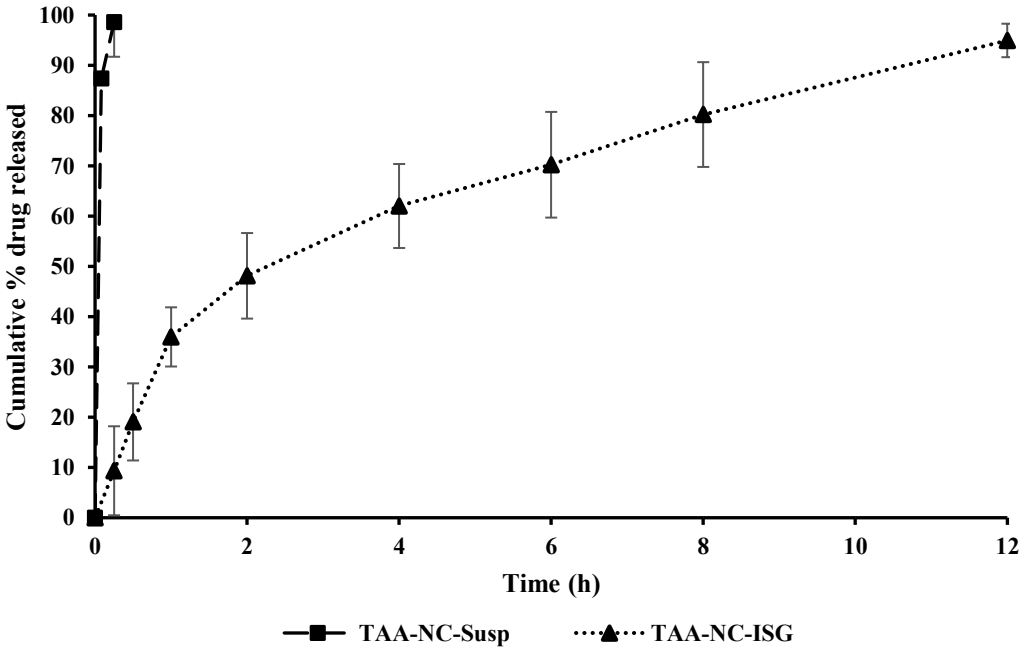

Figure 4.5 *In vitro* drug release profiles of TAA-NC-Susp and TAA-NC-ISG. Each data point represents the mean cumulative percent TAA released ± SD of n = 3 independent formulations.

4.3.6 Stability of TAA-NCs and TAA-NC-ISG formulations

The stability of TAA-NCs and TAA-NC-ISG was observed at room temperature conditions (at 25±2 °C and 60±5% RH) and under refrigeration condition (at 2-8 °C), respectively, for a period of 60 days. There was no discernible difference in the PS and yield (%), over 60-day period, between fresh prepared formulation samples and the formulation samples held under the aforementioned conditions as shown in Figures 4.6a and 4.6b. At each sampling time point for both formulations, the %bias computed for PS and yield (%) was found to be not more than

5%. This demonstrates that both the formulations were stable for 60 days when stored at the respective storage conditions.

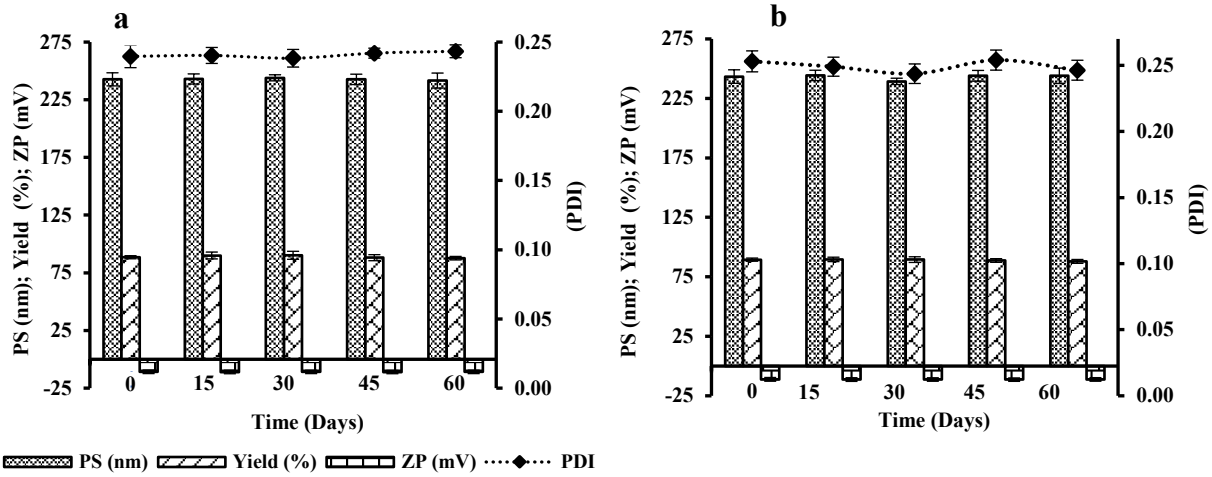

Figure 4.6 Stability data of (a) lyophilized TAA-NCs powder (25±2 °C and 60±5% RH); (b) TAA-NC-ISG (2-8 °C).

4.3.7 *Ex vivo* ocular toxicity tests of TAA-NCs and TAA-NC-ISG formulations using the HET-CAM technique

A comparison of the images captured from the HET-CAM test of the various treatments used in the study is shown in Figure 4.7. After 0.5 min of exposure to the positive control (0.1 N NaOH), the CAM was substantially injured, leading to rosette-like coagulation. Additionally, it was observed that exposure to the positive control caused lysis of blood vessels in the CAM. Negative control (0.9% w/v NaCl) and optimized formulations (TAA-NC-Susp and TAA-NC-ISG) did not show any appreciable change in the CAM (neither haemorrhage nor coagulation). The negative control and optimized formulations (TAA-NC-Susp and TAA-NC-ISG) obtained an IS value of 0, whereas the positive control received a value of 20. It may be concluded from the CAM images and the IS values that the optimized formulations (TAA-NC-Susp, TAA-NC-ISG) were 'non-irritant' and well tolerated by the eye.

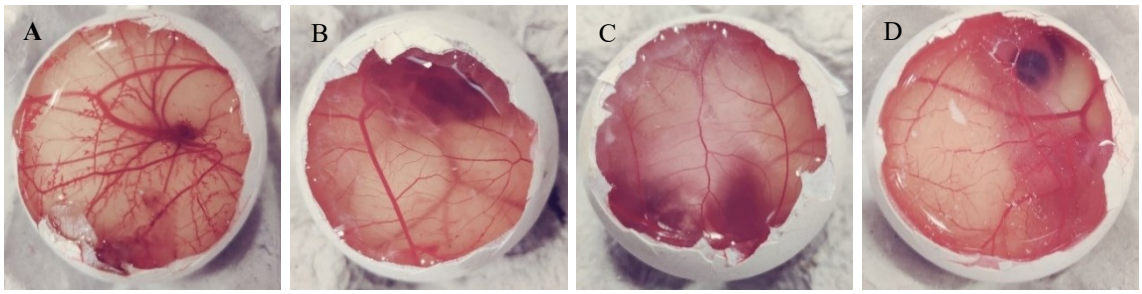

Figure 4.7 Comparative changes observed in the HET-CAM test following *ex vivo* ocular irritation studies: (A) positive control (0.1 M NaOH); (B) negative control (0.9% w/v NaCl); (C) TAA-NC-Susp; and (D) TAA-NC-ISG.

4.3.8 Histopathological studies of the TAA-NCs and TAA-NC-ISG formulations

Microscopic examination of the cornea treated with STF (negative control) revealed intact epithelium and stroma without any indication of tissue damage. In the presence of 75% v/v isopropyl alcohol (positive control), there was a significant deformation of the epithelial cell layer with expanded intercellular gaps. There was no noticeable difference between the cornea treated with the optimized formulations (TAA-NC-Susp and TAA-NC-ISG) and the cornea treated with STF (Figure 4.8). We can conclude that the optimized nanoformulations are safe.

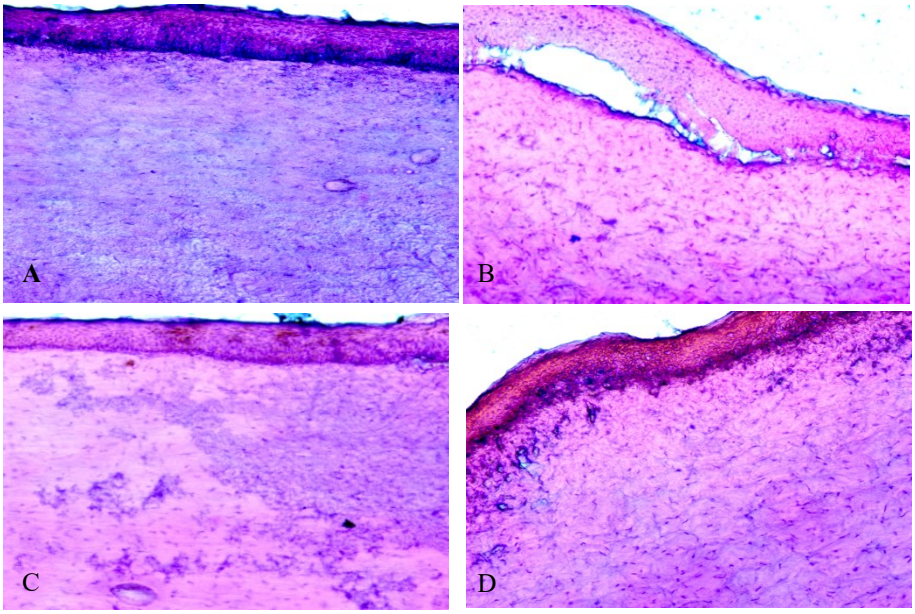

Figure 4.8 Photo micrographic evaluation of cornea exposed to various treatments: (A) negative control (STF); (B) Positive control (75% v/v Isopropyl alcohol); (C) TAA-NC-Susp; and (D) TAA-NC-ISG.

4.3.9 Ocular pharmacokinetic studies of the optimized TAA-NCs and TAA-NC-ISG formulations

In chapter 2 (Section 2.3.5), we have shown that TAA-HP-β-CD-Susp can produce therapeutic concentration of more than 100 ng/mL in the vitreous humor following the topic administration of the formulation at a dose of 4mg/30µL/eye [84,133]. In this chapter, the mean concentration-time profiles of TAA following the topical ocular administration of TAA-NC-Susp and TAA-NC-ISG were compared with each other as well as with TAA-HP-β-CD-Susp, in the vitreous and aqueous humour (Figure 4.9**)**. The time course data of TAA in both the matrices was subjected to non-compartmental analysis using Phoenix WinNonlin software (version 8.3.5.340, Pharsight Corporation, NC, USA) to determine parameters such as C_{max}, T_{max}, AUC_{0-t} and $MRT_{0-\infty}$. The pharmacokinetic parameters were calculated using the pooled concentration data from two eyes of one animal sacrificed at individual sampling point.

The most crucial site for drug localization in the treatment of PU therapy is the vitreous humour. Any formulation that can achieve as much higher concentrations than 100 ng/mL in the vitreous humour and maintain them for a longer period would be ideal for treating the disease condition. Figure 4.9b shows that TAA concentrations (C_{max}) in the vitreous humour for TAA-NC-ISG (854.9 ng/mL) were 1.3 times higher than for TAA-NC-Susp (635.4 ng/mL) and 3.2 times higher than TAA-HP-β-CD-Susp (264.9 ng/mL). In addition, the concentrations of TAA were more sustained for TAA-NC-ISG ($MRT_{0-\infty}$ = 11.2 h) compared to TAA-NC-Susp ($MRT_{0-\infty}$ =6.0 h) compared to TAA-HP-β-CD-Susp ($MRT_{0-\infty}$ = 3.1 h). Additionally, Table 4.4 data suggests that the vitreous humour exposure (AUC_{0-t}) of TAA for TAA-NC-ISG (7126.1 ng×h/mL) was 1.9 times higher than TAA-NC-Susp (3720.2 ng×h/mL) and 8.8 times higher than TAA-HP-β-CD-Susp (810.4 ng×h/mL). The above results indicate that TAA-NC-ISG produced higher and sustained concentrations of TAA in vitreous humor compared to TAA-NC-Susp compared to TAA-HP-β-CD-Susp.

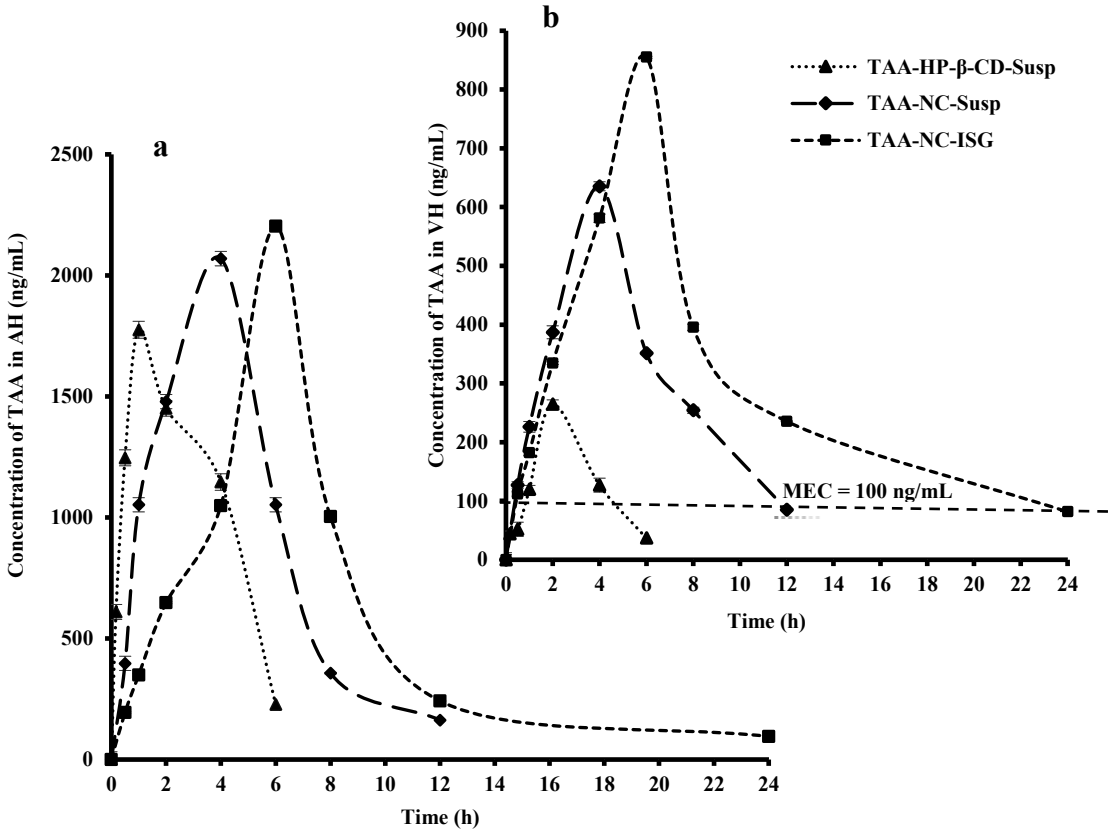

Figure 4.9 Mean aqueous humour (AH) (a) and vitreous humour (VH) (b) concentration-time profiles obtained following ocular administration of TAA-HP-β-CD-Susp, TAA-NC-Susp and TAA-NC-ISG. Every data point is the average of two different assessments (*n*=2).

Figure 4.9a compares the time course profiles of TAA in aqueous humour for TAA-NC-ISG, TAA-NC-Susp and TAA-HP-β-CD-Susp. TAA levels in aqueous humour were higher in TAA-NC-ISG (C_{max} of 2202.9 ng/mL) than TAA-NC-Susp (C_{max} of 2069.2 ng/mL) and TAA-HP-β-CD-Susp (C_{max} of 1775.4 ng/mL). This could be due to the slow release of TAA-NCs from the gel matrix formed by ISG on the corneal epithelium, resulting slow and sustained penetration of TAA at molecular level through the cornea as well as slow and sustained uptake of TAA-NCs through the cornea into the aqueous humour. Compared to TAA-NC-Susp ($MRT_{0-\infty}$ of 4.9 h) and TAA-HP-β-CD-Susp ($MRT_{0-\infty}$ of 3.0 h), aqueous humour TAA concentrations were maintained over a longer period of time in the case of TAA-NC-ISG ($MRT_{0-\infty}$ of 8.6 h). As a conventional formulation, TAA-NC-Susp and TAA-HP-β-CD-Susp were easily removed from the precorneal region due to tear turnover, tear fluid dilution and nasolacrimal drainage. A

viscous gel layer created by ISG increased the formulation's residence times in the precorneal region and reduced the effects of dilution by tear fluids and nasolacrimal drainage. Additionally, the gel provided intimate contact with the corneal epithelium, allowing the drug to spread throughout the surface of the cornea.

Table 4.4 Ocular pharmacokinetic parameters of TAA in the vitreous humour and aqueous humour following topical administration of TAA-NC-Susp, TAA-NC-ISG in male New Zealand rabbits.

Biological matrix	PK parameters	Units	Treatments		
			TAA-HP-β-CD-Susp*	TAA-NC-Susp	TAA-NC-ISG
Vitreous humour	C_{max}	ng/mL	264.9	635.4	854.9
	T_{max}	h	2.0	4.0	6.0
	AUC_{0-t}	ng×h/mL	810.4	3720.2	7126.1
	$MRT_{0-\infty}$	h	3.1	6.0	11.2
Aqueous humour	C_{max}	ng/mL	1775.4	2069.2	2202.9
	T_{max}	h	1.0	4.0	6.0
	AUC_{0-t}	ng×h/mL	6697.3	10846.2	13355.0
	$MRT_{0-\infty}$	h	3.0	4.9	8.6

*Data of TAA-HP-β-CD-Susp is reproduced from Table 2.4, Chapter 2.
Note: The values of C_{max}, T_{max}, AUC_{0-t} and $MRT_{0-\infty}$ were obtained by composite sampling from the two eyes (n=2) of an animal sacrificed at each time point.

Overall, the concentration of TAA in the vitreous humour was gradually increased by TAA-NC-ISG, and maintained the drug's concentration for longer duration compared to TAA-NC-Susp and TAA-HP-β-CD-Susp. Based on the results obtained in the study, we can infer that TAA-NC-ISG can help in reducing the dose and dosing frequency of TAA for non-invasive delivery of the drug in the treatment of PU.

4.4 Conclusion

In this chapter, TAA-NCs were prepared by employing a bottom-up approach using the solvent-antisolvent precipitation method. DoE was used in the screening and optimization of factors affecting the critical responses of the TAA-NCs. The optimized TAA-NCs were then loaded into a dual responsive *in situ* gel containing an ion-sensitive polymer (κ-CRG) and a

thermoresponsive polymer (RXG). The aqueous suspension of TAA-NCs (TAA-NS-Susp) and TAA loaded *in situ* gel (TAA-NC-ISG) were subjected to i*n vivo* ocular pharmacokinetic studies. TAA-NC-ISG showed significantly higher vitreous humour concentrations than TAA-NC-Susp and aqueous suspension of TAA (TAA-HP-β-CD-Susp). The TAA concentrations were sustained for more time in the vitreous humor in the case of TAA-NC-ISG than compared to TAA-NC-Susp and TAA-HP-β-CD-Susp. The findings demonstrate that non-invasive precorneal ocular application of nanocrystal formulations of TAA would be advantageous in achieving therapeutic concentrations in the vitreous humour. TAA-NC-ISG can be an excellent alternative for intravitreal administration of TAA and improve patient compliance and convenience. Finally, we can conclude that TAA can be administered as eye drops by designing novel delivery systems in the management of PU.

5

DESIGN, OPTIMIZATION AND PHARMACOKINETIC EVALUATION OF PLGA PHOSPHATIDYLCHOLINE HYBRID NANOPARTICLES OF TRIAMCINOLONE ACETONIDE LOADED *IN SITU* GEL FOR TOPICAL OCULAR DELIVERY

5.1 Introduction

The complex anatomical and physiological distinctions of the eye and its sensitivity to exogenous substances, including drugs, set it apart from other organs [222]. The anterior and posterior eye segments can either function alone or together when an ocular preparation is applied, despite the fact that they are physically adjacent to one another [158]. A major part (50-60%) of the topically administered drug, following the loss due to spill over of the excess, is commonly absorbed into the systemic circulation via the conjunctiva and nasolacrimal duct, whereas less than 5% typically penetrates the cornea and reaches the intraocular tissues, because of which subtenon, subconjunctival or intravitreal injection must be used to treat fulminating illnesses of the posterior segment such as macular oedema, age-related macular degeneration, uveitic cystoid macular oedema and uveitis [223,224]. The downsides of each of these injection-based drug delivery techniques vary. For instance, intravitreal injections can hasten the formation of a cataract and result in haemorrhage, retinal detachment, endophthalmitis and increased intraocular pressure [225]. Uveitis is complex group of ailments distinguished by the intraocular inflammation, particularly the uveal tract [75]. It results in uveal and neuro-retinal inflammation, which can seriously impair vision and cause morbidity [226].

Clearly, there is an urgent need to develop topical ocular delivery systems that focus on enhancing intraocular availability as well as and residence time of the drug, particularly in the posterior segment of the eye [227]. Researchers have designed viscosity liquids (solutions and suspensions) and gels to improve the drug availability in the intraocular tissues by prolonging the residence time of the formulations on the surface of the cornea before being flushed out of the eye [228]. Such formulation designs yielded limited results for drugs which have low solubility and poor dissolution rate in the tear fluids.

Recent investigations suggest that colloidal systems (microparticles, liposomes, nanoparticles (NPs)), particularly colloidal systems at the nanoscale, can play a significant role in ocular drug delivery [109]. NPs are tiny particles with sizes ranging from 10 to 1000 nm that may or may not contain a therapeutic molecule, depending on their intended purpose [158]. Due to the nanometric size, NPs provide large surface area which results in higher dissolution rates and higher rates of absorption for drugs with solubility issues [229].

Liposomes and biodegradable polymeric nanoparticulate systems have emerged as the two most important drug nanocarriers out of the various nanoparticulate drug delivery systems [230]. In an effort to address various drawbacks related to polymeric nanoparticulate systems and liposomes, novel, integrated systems known as polymeric lipid hybrid nanoparticles (PLHNPs) have been developed by combining the architectural advantage of polymer core with the biomimetic properties of lipids [231]. The lipoidal layer surrounds the central polymer matrix, which has therapeutic drug material (mostly low water soluble/hydrophobic drugs) with high loading efficiency. This outer layer provides biocompatibility and promotes drug retention inside the polymer core [230,232].

A range of synthetic and natural polymers are used to create biodegradable NPs for therapeutic applications. Most commonly used are synthetic polymers like polyacrylates, polycaprolactones and polylactides, as well as their copolymers with polyglycolides [233]. Poly (lactic-co-glycolic acid) (PLGA) is one of the most commonly used polymers in the preparation of NPs due to its biocompatible and biodegradable qualities as well as its versatile degradation kinetics [158]. Most of the lipid-based NPs are prepared using phospholipids like diolein phosphatidylcholine, 1, 2-dipalmitoyl-sn-glycerol-3-phosphocholine, dioleoyl trimethylammonium propane, soya lecithin and phosphatidylcholine etc., as one of the key ingredients [233]. Combining the benefits of a polymer like PLGA and a phospholipid like

phosphatidylcholine (PC) to form PLHNPs can improve the corneal uptake and intraocular penetration of the drug to eventually achieve higher drug concertation in the vitreous humor.

In this chapter, we designed and evaluated TAA loaded PLHNPs (TAA-PLHNPs) in an effort to overcome the shortcomings of TAA-HP-β-CD-Susp for ocular delivery. TAA-PLHNPs were prepared using a bottom-up technique (nanoprecipitation technique), and the concepts of design of experiments (DoE) were employed to optimize the critical physico-chemical properties of TAA-PLHNPs. To further improve the therapeutic concentrations of TAA in the vitreous humor, TAA-PLHNPs were loaded in the optimized dual responsive *in situ* gel (ISG) (discussed in Section 3.3.2, Chapter 3) to prolong the residence time on the corneal epithelium following the topical administration of the NPs. The *in vivo* ocular pharmacokinetics of the optimized TAA-PLHNPs and TAA-PLHNPs loaded dual responsive *in situ* gel (TAA-PLHNP-ISG) were compared with TAA-HP-β-CD-Susp in male New Zealand rabbits.

5.2 Materials and methods

5.2.1 Materials

Free samples of TAA and piribedil (the internal standard used in the bioanalytical method) were obtained from Strides Pharma Science Limited, Bengaluru, India and Dr. Reddy's Laboratories, Hyderabad, India. Poly (lactic-co-glycolic acid) (PLGA 75:25, molecular weight range: 66,000-107,000 Da), D-α-Tocopherol polyethylene glycol 1000 succinate (TPGS), Poloxamer 407 and polyvinyl alcohol (PVA, average molecular weight: 1,60,000) were bought from Sigma-Aldrich Private Limited, Mumbai, India. Polyvinylpyrrolidone (PVP-K30, average molecular weight: 30,000 Da) and Polysorbate 80 (Tween 80) were procured from TCI chemicals, Chennai, India. Phosphatidylcholine (Phospholipon® 90G) was obtained from Lipoid AG (Steinhausen, Switzerland). Methanol, acetonitrile, glacial acetic acid, ammonium acetate and disodium EDTA of HPLC grade were purchased from Harihara Scientific Private Limited, Hyderabad, India. SD Fine Chemicals Private Limited, Mumbai, India, supplied the

sodium chloride (NaCl), sodium bicarbonate ($NaHCO_3$), potassium chloride (KCl), magnesium chloride ($MgCl_2$), calcium chloride ($CaCl_2$), mannitol and other buffer salts used in the study. High-quality filtered water was made available for the HPLC analysis using the Milli-Q water purification system (Millipore®) MA, USA. VAB Biosciences Limited, Hyderabad, India, provided male New Zealand white rabbits weighing between 2 and 2.5 kg.

5.2.2 Preparation of TAA-PLHNPs

TAA-PLHNPs were prepared using the previously reported nanoprecipitation technique involving solvent-antisolvent method, with some modifications [234]. N-methyl-2-pyrrolidone (NMP) was chosen as the solvent while water was selected as the anti-solvent in the preparation of TAA-PLHNPs, based on the solubility of TAA in the two solvents (solubility of TAA in water is 16.1 μg/mL and in NMP it is ≥20 mg/mL). To select a suitable stabilizer for the preparation of TAA-PLHNPs, solubility studies were conducted for TAA in various stabilizers, including, PVA, PVP-K30, TPGS, Poloxamer 407, Tween 80. Further, preliminary studies were conducted to study the effect of various material attributes (including PLGA amount, phosphatidylcholine amount and PVA concentration) and manufacturing process parameters (including ultrasonication amplitude, ultrasonication time, homogenization speed and homogenization time) on the physico-chemical properties such as particle size (PS), polydispersity index (PDI), zeta potential (ZP), and percent loading efficiency (LE %) of TAA-PLHNPs to identify the lower and upper levels of the various factors to be used in the optimization of TAA-PLHNPs.

TAA and PLGA were dissolved in the NMP. Aqueous solution of PVA was prepared in a separate beaker. In a 1.5 mL centrifuge tube, phosphatidylcholine solution was prepared using NMP as the solvent and added to the aqueous solution of PVA. Under high-speed homogenization (Polytron PT 3100D, Kinemetica, Lucerne, Switzerland) using a polypropylene syringe (with a needle having 0.72 mm internal diameter), the NMP solution

containing the mixture of TAA and PLGA was introduced dropwise to aqueous solution containing the mixture of PVA and phosphatidylcholine to form a nanosuspension. The nanosuspension was subjected to an ultrasonication process (Vibra cell, Sonics, Connecticut, USA) to achieve smaller and uniform PS (Figure 5.1). The ultrasonication process was carried out in a temperature-controlled (12 °C) environment. The resultant nanosuspension was centrifuged for 30 min at 12,000 rpm and 10 °C to separate the TAA-PLHNPs (obtained as pellet) from the dispersion medium. The pellet was washed three times with MilliQ water to remove the free drug adhering on the surface of the NPs. The pellet containing TAA-PLHNPs was then redispersed in 10 mL of Milli-Q water containing 3.5% w/v mannitol as cryoprotectant and freeze-dried. The freeze-dried TAA-PLHNPs were stored at 2-8 °C.

The quantity/proportion of each excipient used in the preparation of TAA-PLHNPs was varied as per the experimental run conditions provided by the design matrix selected in the screening and optimization studies. However, the amount of TAA used in each experimental run was fixed at 40 mg.

To perform physical characterisation, *in vitro* drug release and *in vivo* evaluation, the freeze-dried TAA-PLHNPs (625 mg) were dispersed in deionized water (2 mL) to form an aqueous suspension of TAA-PLHNPs (TAA-PLHNP-Susp).

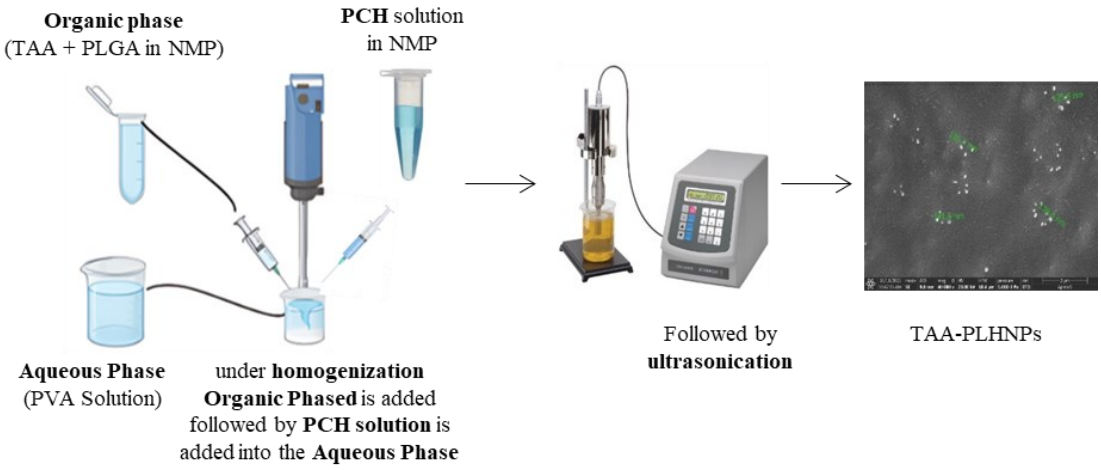

Figure 5.1 Schematic representation showing the step-wise procedure for the preparation of TAA-PLHNPs.

5.2.3 Experimental design for the formulation of TAA-PLHNPs

A hybrid design approach was used to optimize TAA-PLHNPs. First a screening design was performed to identify the critical factors effecting the critical physico-chemical properties of the TAA-PLHNPs and then the critical factors were optimized using a response surface methodology. Design Expert software (version 13, Stat-Ease Inc., Minneapolis, USA) was used to create the design matrices for screening and optimization of the factors as well as for regression and other statistical analysis of the data obtained in the DoE experiments.

5.2.3.1 Screening design for identifying the critical factors

A minimal resolution (Minires) screening design was used to identify the critical factors effecting the critical physico-chemical properties of TAA-PLHNPs. A total of 7 factors (which included both material attributes and process parameters) effecting the critical physico-chemical properties were identified from the preliminary trials conducted in the preparation of TAA-PLHNPs. The 7 independent factors, along with the levels [low (-1) and high (+1)] of each factor, considered in the screening design are shown in Table 5.1. Minires screening design generated 19 runs including 3 centre points runs.

The critical physico-chemical properties of TAA-PLHNPs considered in the screening design were particle size (PS), polydispersity index (PDI), zeta potential (ZP), EE (%) and LE (%). The PS and PDI are the two important properties which effects the drug release from NPs. The physical stability of the NPs is influenced by the ZP. The total amount of the NPs formulation to be administered at one dosage point is determined by the LE (%) while EE (%) indicate the efficiency of the manufacturing method to entrap the drug in the NPs.

Statistical analysis was performed independently for each of the critical physico-chemical properties based on the data obtained from the experimental runs in the screening design. The critical physico-chemical properties that demonstrated a significant variation in their responses

in the experimental runs performed in the screening design were taken up for further analysis in the optimization design.

Table 5.1 Factors with their levels used in the screening design for the preparation of TAA-PLHNPs.

Factor Code	Actual factors	Levels		
		-1	0	1
X_1	PLGA amount (mg)	60	120	180
X_2	Ultrasonication amplitude (%)	20	35	50
X_3	Phosphatidylcholine amount (mg)	40	80	120
X_4	Homogenization speed (rpm)	7000	11000	15000
X_5	Homogenization time (min)	5	10	15
X_6	Ultrasonication time (min)	5	10	15
X_7	PVA concentration (% w/v)	1	1.75	2.5

5.2.3.2 Optimization of critical factors using Box-Behnken design

Three critical factors, namely PLGA amount (mg), phosphatidylcholine amount (mg) and the ultrasonication amplitude (%), had a statistically significant impact on the critical physico-chemical properties of TAA-PLHNPs based on the results obtained from the Minires screening design. Out of the four critical physico-chemical properties, PS and LE (%) were found to vary significantly over the 16 non-centre experimental runs in the screening design. Therefore, only PS and LE (%) were taken as the final critical physico-chemical properties in the optimization design. A Box Behnken design (BBD) was employed to determine the mathematical relationship between the three critical factors and critical responses and to optimise the preparation of TAA-PLHNPs. A second-order polynomial equation was constructed using BBD involving 17 experimental runs, including 5 centre points for each factor assessed at 3 levels (-1, 0, +1). To determine the best-fit model (i.e., linear or 2-FI or quadratic etc.) for each response, a variety of model-based investigations, including analysis of variance (ANOVA), R^2 adjusted, R^2 predicted, predicted residual sum of squares (PRESS) and other statistical parameters were analysed. The polynomial equations obtained for PS and LE (%) were used to explore the design space of the three critical factors. To determine the relationship between any two critical factors and a given critical response, response surface methodology (RSM) graphs

or 3-D graphs were plotted. The general form of the quadratic or second-order polynomial equation generated for each critical response by the BBD is given below.

Equation 5.1

$$Y = \beta_0 + \beta_1 X_1 + \beta_2 X_2 + \beta_3 X_3 + \beta_{12} X_1 X_2 + \beta_{13} X_1 X_3 + \beta_{23} X_2 X_3 + \beta_{11} X_1^2 + \beta_{22} X_2^2 + \beta_{33} X_3^2$$

Where, Y is the dependent variable, β_0 is the arithmetic mean response of the 17 runs and β_i's and β_{ii}'s (i = 1–3) are the coefficients of individual linear and quadratic effects of the variables, respectively, and β_{ij}'s (i, j = 1–3; $i < j$) are the coefficients of the effect of interaction between the i^{th} and j^{th} variable.

5.2.3.3 Desirability function and model validation

In this study, DoE was used to design TAA-PLHNPs with desirable physicochemical properties. To determine the optimal levels of the critical factors (X_1, X_2, and X_3) for preparing TAA-PLHNPs with the desired PS and LE (%), a simultaneous optimisation technique using the desirability function was adapted as there were two critical responses with different objective functions (minimize PS and maximize LE (%)). The solution (with specific values of the critical factors, X_1, X_2, and X_3) with the highest value of desirability was selected as the optimal conditions for the preparation of TAA-PLHNPs out of the various solutions generated by the DoE software. Six independent formulations of the optimized TAA-PLHNPs were prepared with three critical factors set at the levels given by the solution with the highest desirability. The observed responses (PS and LE (%)) for all the six replicates were determined. The predicted responses for PS and LE (%) were obtained by setting the three critical factors at the levels given by the solution in their respective regression equations. A statistical comparison was made between the observed and predicted response values using the Wilcoxon signed-rank test at 5% level of significance to validate the solution provided by the DoE. No statistically significant difference between observed and predicted values indicates that the regression models for PS and LE (%) are valid for predicting the critical responses of the TAA-PLHNPs.

5.2.4 Physical characterization of TAA-PLHNPs

5.2.4.1 *Measurement of PS, PDI and ZP of TAA-PLHNPs*

Based on the principle of dynamic light scattering, the physical properties like PS, PDI, and ZP of TAA-PLHNPs were evaluated using Zetasizer Nano ZS (Malvern Instruments, Worcestershire, UK). All measurements were performed using a 633 nm laser with a fixed scatter angle of 173° (backscatter). Following the preparation of TAA-PLHNPs by the nanoprecipitation method, the formulation (TAA-PLHNPs nanosuspension obtained immediately after the ultrasonication) was diluted 10 times with MilliQ water and allowed to equilibrate for 2 min at 25 °C before the analysis. In case of the lyophilized TAA-PLHNPs and TAA-PLHNP-ISG, the formulations (10mg) were first dispersed in MilliQ water (2mL) and then further diluted 10 times with MilliQ water. The diluted samples were allowed to equilibrate for 2 min at 25 °C before the analysis. The mean PS, PDI, and ZP values were calculated from three independent (n = 3) measurements based on intensity graphs obtained from zeta sizer.

5.2.4.2 Determination of EE (%) and LE (%) of TAA-PLHNPs

The evaluation of EE (%) and LE (%) of TAA-PLHNPs was performed by both direct and indirect methods. In the indirect method, TAA-PLHNP-Susp was centrifuged at 12,000 rpm for 45 min at 4 °C to produce a pellet of the NPs. The supernatant was collected and analysed using a previously developed and validated HPLC method (Section 2.3.1, Chapter 2) to determine the free drug. Further, the pellet was washed three times with MilliQ water to recover any free drug adhered on the surface of NPs. All the three washing were combined and analysed using the same analytical method. The total quantity of free (or unentrapped) TAA was determined from the analysis of the supernatant (after centrifugation) and the washings of the pellet. The EE (%) of the TAA-PLHNPs was determined using the equation given below.

Equation 5.2

$$\text{EE (\%)} = \frac{W_{total\ TAA} - W_{free\ TAA}}{W_{total\ TAA}} \times 100$$

Where, "$W_{total\ TAA}$" refers to the total amount of TAA used to prepare the TAA-PLHNPs and "$W_{free\ TAA}$" refers to the amount of TAA recovered in the supernatant and the washings of pellet.

To determine the LE (%) of TAA-PLHNPs by the direct method, TAA-PLHNP pellet obtained after the three washings was thoroughly dried under vacuum and weighed. The pellet was then dissolved in a predetermined volume of DMSO to extract TAA. Following the extraction of TAA from the pellet by DMSO, a sample was taken from it and diluted appropriately before analysing the same using the validated HPLC method (Section 2.3.1, Chapter 2). The LE (%) of TAA-PLHNPs was calculated using the following equation:

Equation 5.3

$$\text{LE (\%)} = \frac{W_{TAA}}{W_{Pellet}} \times 100$$

Where, "W_{TAA}" refers to the amount of TAA present in the pellet and "W_{Pellet}" refers to the weight of the dried pellet of TAA-PLHNPs.

5.2.4.3 Scanning electron microscopy (SEM) imaging of TAA-PLHNPs

A filed emission scanning electron microscope (FEI, Apreo LoVac, TermoFisher Scientific, MA, USA) was used to examine the surface morphology of the optimized TAA-PLHNPs. 40 µL of the optimized TAA-PLHNPs dispersion was applied on a fixed piece of double-sided conducive tape on an aluminium stub and was vacuum-dried overnight. Then, using a sputter coater (Leica EM ACE200, Wetzlar, Germany) in an argon atmosphere, gold was coated on the surface of the dried sample under vacuum. Following the gold coating process, the samples were scanned to capture their SEM images at a 5 kV acceleration voltage.

5.2.4.4 Differential scanning calorimetry (DSC) of TAA-PLHNPs

The DSC-60 (TA-60 WS, Shimadzu, Kyoto, Japan) was used to perform thermal analysis of pure TAA, lyophilized TAA-PLHNPs and a physical combination of TAA with all the excipients used in the preparation of TAA-PLHNPs. Each sample was weighed (≈5 mg) and

crimp-sealed, separately, in aluminium pans. An empty crimp-sealed aluminium pan was employed as reference. The reference and sample pans were placed in the DSC sample chamber before the run and allowed to equilibrate at 30 °C for 2 mins. Thermal analysis of the samples was performed, in an inert environment, in the temperature range of 30 to 300 °C at a constant heating rate of 10 °C/min. Nitrogen gas was purged into the sample chamber at a flow rate of 50 mL/min to maintain an inert environment.

5.2.4.5 Powder X-ray diffractometry (pXRD) of TAA-PLHNPs

Using a Rigaku Ultima IV diffractometer (Texas, USA), the powder X-ray diffraction (pXRD) examination of freeze-dried TAA-PLHNPs, a physical mixture of TAA-PLHNPs components and pure TAA was conducted to determine the physical state of the drug and as well as the excipients present in the samples. The analysis was performed by illuminating the samples with Cu-Kα radiation (λ = 1.54 Å) that had been Ni-filtered at a voltage of 40 kV and a current of 30 mA. A scanning rate of 2 degrees/min, which covered a 2θ range of 10-80° was used in the analysis of the samples.

5.2.5 Rheological evaluation of TAA-PLHNP-ISG formulation

In chapter 3 (Section 3.3.2), we discussed the optimization of blank RXG-κ-CRG *in situ* gel (ISG) using a mixture of reacted tamarind seed xyloglucan (RXG) and kappa-Carrageenan (κ-CRG) at 2% w/v and 0.3% w/v, respectively. In this chapter, we loaded the freeze-dried powder of the optimized TAA-PLHNPs (discussed in section 2.2) into the optimized blank *in situ* gel under magnetic stirring at 500 rpm maintained at 25 °C for 30 min to form TAA-PLHNPs loaded *in situ* gel (TAA-PLHNP-ISG). A rheometer (Anton Paar MCR 302, Graz, Austria) was used to evaluate the rheological properties of the TAA-PLHNP-ISG and blank ISG in parallel plate geometry. The linear viscoelastic region (LVER) for each sample was first determined using amplitude and frequency sweep tests. The rheological properties of the samples were then evaluated in the LVER using a temperature sweep in oscillatory mode between 25 °C and

40 °C. Two different experimental setups were used to evaluate the gelation properties of the samples: 1) temperature ramp and 2) temperature ramp with STF. The loss tangent (*tan δ*) vs temperature and complex viscosity (*η**) vs temperature plots were constructed using the data obtained from the rheological studies. The TAA-PLHNP-ISG gelation behaviour was assessed based on the plots obtained in the study.

5.2.6 *In vitro* drug release study from TAA-PLHNP-Susp and TAA-PLHNP-ISG formulations

The *in vitro* drug release of TAA-PLHNP-Susp and TAA-PLHNP-ISG formulations was investigated using a membrane-less approach in a dissolution apparatus (USP Type II, Model TDT-08L, Electro lab, Mumbai, India) [186]. In a 1000 mL dissolution jar, a circular stainless-steel container with an internal diameter of 1.4 cm and a depth of 0.5 cm was glued to the bottom. The study formulation (40 µL of TAA-PLHNP-Susp or TAA-PLHNP-ISG, equivalent to 4 mg of TAA) were carefully taken in the stainless-steel container. The dissolution jars were kept at a constant temperature of 34 ± 0.5 °C. STF containing 0.5% w/v of Tween 80 was used as the dissolution media in the study. The dissolution media (300 mL) was pre-equilibrated at 34 ± 0.5 °C before adding into the dissolution jars. The paddle was rotated at a speed of 75 rpm. At pre-determined time intervals (0.25, 0.5, 1, 2, 4, 6, 8, 12, 24 and 48 h), samples (2 mL) were drawn using a syringe during the dissolution study. The samples were centrifuged for 30 min at 10 °C at 12,000 rpm. Following the centrifugation, the clear supernatant was collected and analyzed using a validated RP-HPLC analytical method (Section 2.3.1, Chapter 2). The pellet obtained after centrifugation was reconstituted with 1 mL of fresh dissolution media (pre-equilibrated at 34 ± 0.5 °C) and transferred back to the respective dissolution jars. A similar procedure was followed at all sampling time points. To understand release kinetics (including zero-order, first-order and Higuchi square root kinetics) and release mechanisms, data from *in vitro* dissolution was fitted into various mathematical models [187]. The dissolving profiles of

TAA-PLHNP-Susp and TAA-PLHNP-ISG formulations were compared using similarity factor (f2) [212].

5.2.7 Stability of TAA-PLHNPs and TAA-PLHNP-ISG formulations

In order to evaluate the stability of the optimized TAA-PLHNPs (lyophilized powder) and TAA-PLHNP-ISG, the formulations were packaged in hermetically sealed vials and kept at room temperature (25 ± 2 °C and relative humidity of 60 ± 5%) and refrigerated (2-8 °C) conditions, respectively. TAA-PLHNP-ISG was stored separately in a refrigerator (2-8 °C) based on the storage condition recommended for ISG (Section 4.3.6, Chapter 4). The samples (n=3) from both the formulations were analysed after every 15 days during the 60-day stability study. The physico-chemical properties like PS, PDI, ZP, and LE (%) were determined. Data obtained for the formulations at each sampling point was compared with that of the zero-time data of the respective formulation to determine the %deviation in the physico-chemical properties to assess the stability of the formulations.

5.2.8 *Ex vivo* ocular toxicity tests of TAA-PLHNPs and TAA-PLHNP-ISG formulations using the HET-CAM technique

The *ex vivo* ocular irritation investigations were conducted using Hen's Egg Test-Chorion Allantoic Membrane (HET-CAM) technique [213]. Fresh eggs were acquired from a nearby chicken farm and incubated for five days at temperature of 37 ± 0.5 °C and 55 ± 5% RH. The eggs weighed between 50 and 60 g. The eggs were candled on the 5th day to distinguish viable eggs from the non-fertile ones. To develop CAM, the viable eggs were kept in the incubator for 10 more days. Throughout the incubation stage, the eggs were manually rotated every 12 h. Using a revolving dental blade, the egg shell was delicately cracked to access the air cell without damaging the inner membrane. After applying NaCl (0.9% w/v) solution to the exposed CAM, the opened eggs were placed in an incubator for 30 min. The inner layer of each opened egg was carefully removed using forceps to make the surface of the CAM

accessible for easy application of the formulation samples. Four treatment groups were examined in the study. Group 1 served as the positive control (treated with 0.1 N NaOH), Group 2 served as the negative control (treated with 0.9% w/v NaCl solution), Group 3 was given the TAA-PLHNPs-Susp treatment and Group 4 was given the TAA-PLHNP-ISG treatment. Three eggs, with correctly formed/exposed CAM, were used to apply the treatments in the study. To the surface of egg CAM, treatment samples (200 µL) were applied and the degree of damage to the blood vessel was evaluated for 300 sec and irritation severity scores were recorded. Irritation severity (IS) score for each treatment was calculated using Eq. 5.4 based on the extent of vascular lysis in the CAM.

Equation 5.4 $$IS = \frac{(301-H)}{300} \times 5 + \frac{(301-L)}{300} \times 7 + \frac{(301-C)}{300} \times 9$$

Where, 'H' denotes the time taken for the start of the haemorrhage responses on the CAM, 'L' denotes the time taken for the start of the vascular lysis on the CAM and 'C' denotes the time taken for the start of the coagulation formation on the CAM.

The ocular irritation potential of the *in situ* gels was evaluated based on their IS scores. The treatment/formulation with IS score between 0 and 0.9 was identified as 'non-irritating'; between 1 and 4.9 was identified as 'slightly irritating'; between 5 and 9.9 as 'moderately irritating' and between 10 and 21 as 'strongly irritating'.

5.2.9 Histopathological studies of the TAA-PLHNPs and TAA-PLHNP-ISG formulations

To assess the impact of formulations on the structure and integrity of corneal epithelium, histopathology studies were conducted using fresh goat eyeballs sourced from a nearby slaughtering site. A 2 mm incision was made around the scleral ring to remove the cornea from the eye. The cornea was cleaned immediately using 0.9% w/v NaCl solution for 1 min. The cleaned cornea was incubated with each treatment, separately, for 6 h. In the study, four different treatment groups were investigated. The treatment in Group 1 consisted of positive control (75% v/v isopropyl alcohol), Group 2 consisted of negative control (STF, pH 7.4 ±

0.05), Group 3 was of TAA-PLHNP-Susp and Group 4 was of TAA-PLHNP-ISG. After 6 h of incubation, the cornea was cleaned with 0.9% w/v NaCl solution and frozen immediately using a tissue freezing medium. The cornea was maintained frozen at -80 °C until further use. Before the microscopic evaluation, cross-sections of the frozen cornea were cut into fine sections of less than 5 mm thickness in a cryotome (Leica Biosystems, CM1520 cryostat, Wetzlar, Germany) and placed on a glass slide. The tissue was dehydrated using a gradient of 30-50-70-90-100% v/v of ethanol and xylene. The dehydrated tissue was rinsed with 0.9% w/v NaCl solution before being stained with hematoxylin and eosin. The tissue was washed with NaCl solution (0.9% w/v) to remove excess hematoxylin and eosin before being examined for any histological changes using a digital microscope (ZEISS, Axiocam 705 colour, Oberkochen, Germany) at 10× magnification [190].

5.2.10 Ocular pharmacokinetic studies of the optimized TAA-PLHNPs and TAA-PLHNP-ISG formulations

To evaluate the ocular pharmacokinetics of the optimized TAA-PLHNPs and TAA-PLHNP-ISG formulations, eight (n=8) male New Zealand rabbits (weighing 2-2.5 kg) with normal eyes (without any symptoms of inflammation) were used in the study. Prior to the study, the institutional animal ethics committee had reviewed and approved the study protocol (Protocol No.: BITS-Hyd/IAEC/2022/14).

The animals were acclimated for a week before the study in the animal house facility of our institute (temperature of 22 ± 1 °C; relative humidity of 55 ± 10% and 12 h light-dark cycle). In the pharmacokinetic study, 40 µL of the formulation (TAA-PLHNP-Susp and TAA-PLHNP-ISG) was instilled into each of the rabbit's two eyes (at the lower cul-de-sac) using a micropipette. The eyelids were kept closed for 10 sec after dosing to increase contact between the cornea and the formulation. Following the instillation of the formulation, one animal each at 0.5, 1, 2, 4, 6, 8, 12 and 24 h was euthanized by inhaling carbon dioxide. An insulin needle (30-gauge, 3 mm diameter) was used to draw aqueous humour from the euthanized rabbit. The

insulin needle was positioned behind the limbus superotemporally and aiming it at the centre of the eye to draw aqueous humor from the rabbit eye. After collecting the aqueous humour, the left and right eyes of the rabbit were removed. The eyes were promptly frozen using dry ice. Vitreous humour was collected from the frozen eyeball and stored at -20 °C.

A validated HPLC method (discussed in Section 2.3.3, Chapter 2) was employed to analyze the concentration of TAA in the vitreous humor and aqueous humour samples collected from ocular pharmacokinetic study. Non-compartmental analysis was used to analyse the time course data of TAA in aqueous humour and vitreous humour. Pharmacokinetic parameters like C_{max} (the maximum concentration of TAA), T_{max} (the time to reach C_{max}), AUC $_{(0\text{-}t)}$ (area under the TAA time course curve from t = 0 to t = t_{last}) and MRT $_{(0–\infty)}$ (the mean residence time t = 0 to t = ∞) were determined. Trapezoidal rule (linear up - linear down) method was used to calculate the value of AUC $_{(0\text{-}t)}$.

5.2.11 Quantification of TAA and Statistical analysis of data

A validated HPLC-PDA analytical method (Section 2.3.1, Chapter 2) was used to quantify TAA in the formulations, *in vitro* drug release samples and stability studies samples. For analysing the concentration of TAA in the aqueous and vitreous humour samples, a validated HPLC-PDA bioanalytical method (Section 2.3.3, Chapter 2) with a calibration range of 50–3000 ng/mL was used. The drug was extracted from the biological samples using a two-step process that involved protein precipitation followed by solvent evaporation. The complete steps involved in the extraction of TAA from both the matrices (aqueous humor and vitreous humor) are described in Section 2.3.3, Chapter 2.

Data obtained from physical characterisation studies and *in vivo* investigations of various groups/treatments was statistically compared either using unpaired t-test (for comparing two treatments) or ANOVA (for comparing more than two treatments). A suitable post-hoc test was then carried out, if necessary, at the 5% level of significance ($\alpha = 0.05$). Data obtained in

various studies is expressed as mean ± standard deviation, depending on the number of replicates used in the study.

5.3 Results and discussion

5.3.1 Experimental designs used in the preparation of TAA-PLHNPs

5.3.1.1 Screening design for identifying the critical factors

The saturation solubility of TAA in different stabilizers is presented in Table 5.2. Based on the results obtained, TAA was found to have similar saturation solubility in Poloxamer 407 (25.09 ± 2.13 µg/mL), PVP-K30 (23.26 ± 1.59 µg/mL) and PVA (21.77 ± 3.28 µg/mL) while Tween 80 and TPGS were found to have higher solubility for the drug. The stabilizer in which the drug has the least solubility is considered the most ideal for preparing the NPs as it improves the LE (%), provided the stabilizer can result in forming NPs with desired PS and stability. In the preliminary formulation trails involving Poloxamer 407, PVP-K30, and PVA as the stabilizer, the TAA-PLHNPs prepared using PVA had higher stability, low PDI and higher LE (%) compared to the other stabilizers. Therefore, based on the saturation solubility data and the initial formulation trials, PVA was selected as the most suitable stabilizer for the preparation of TAA-PLHNPs.

MiniRes screening design with resolution IV is very useful screening design where the main effects are not confounded by other main effects as well as two-way interactions. Due to this property, the effect of the main factorial terms can be studied in this design using a fewer number of runs for a given set of factors at two levels.

Out of the seven factors studied in the screening design, three factors, namely, PLGA amount (mg), phosphatidylcholine amount (mg) and the ultrasonication amplitude (%) were found to have statistically significant effect on the critical physico-chemical factors like PS and LE (%) of TAA-PLHNPs. In addition, the data obtained from the screening design indicated that there was no significant variation in the physico-chemical properties like PDI, ZP and EE (%) of the

TAA-PLHNPs across the 16 non-centre point runs. Therefore, only PS and LE (%) were taken as the critical responses in the optimization design using BBD.

Table 5.2 Saturation solubility studies of TAA in different vehicles/excipients.

Stabilizer concentration (1% w/v)	TAA concentration[a] (µg/mL)
Poloxomer 407	25.09 ± 2.13
Polysorbate 80 (Tween 80)	47.74 ± 1.49
Polyvinylpyrrolidone (PVP-K30)	23.26 ± 1.59
Poly vinyl alcohol (PVA)	21.77 ± 3.28
D-α-tocopherol polyethylene glycol succinate (TPGS)	76.94 ± 5.07

Note: [a]All the data is represented as Mean ± SD of replicate analysis ($n = 3$)

5.3.1.2 Optimization of critical factors using Box-Behnken design (BBD)

BBD is one of the most commonly employed quadratic response surface methods for optimization of response variable(s) as a function of three or more critical factors. Table 5.3 provides the design matrix with the levels of each critical factor used in the experimental runs for the preparation of TAA-PLHNPs and the data obtained for PS and LE (%) of the NPs in the corresponding experimental runs. The regression equations for PS and LE (%) were determined based on the observed responses of the experimental runs in BBD. The regression equations were subjected to ANOVA to identify the various statistically significant factorial terms effecting the PS and LE (%) and the results are presented in Table 5.4. The details of sum of squares (SS), degree of freedom (df), 'F_{cal}' value and 'P' value for the factorial terms are presented. The factorial terms with 'P<0.05' are considered to have statistically significant effect on the response variable while those with 'P>0.05' are considered to have insignificant effect. If the 'F_{cal}' of the model is greater than the corresponding 'F_{cal}' then we can conclude that the regression model is statistically valid.

5.3.1.3 Effect of critical factors on PS

The influence of critical factors on PS is described by the following least square second-order polynomial equation (in coded form, with 95% confidence level):

Equation 5.5

$$\boldsymbol{PS\ (Y_1)} = 314.0 + 177.25\ X_1 - 2\ X_2 - 49.50\ X_3 + 6.75\ X_1X_2 - 21.25\ X_1X_3 - 37.25\ X_2X_3 + 22.87\ X_1^2 - 5.13\ X_2^2 + 17.38\ X_3^2$$

The regression model 'F_{cal}' value (7.72) for PS was statistically significant (P_{cal} <0.0001). The lack-of-fit for the regression equation of PS was not significant (P_{cal}>0.05). The values of predicted R^2 and adjusted R^2 were 0.7463 and 0.7908, which were in reasonable agreement with each other and their difference well within 0.2. The residual versus the run number plot was scattered randomly around and closer to '0', suggesting that there was no obvious impact of the run order on the variability of the PS across the different runs. All the above statistical findings demonstrate that the regression equation obtained for PS is reliable and accurate. In the experimental runs, the highest PS was seen in the 8th run with an average PS of 633 nm and the smallest PS was seen in the 12th run with an average PS of 168 nm (Table 5.3).

Table 5.3 BBD design matrix for the preparation of TAA-PLHNPs with the levels of critical factors for each experimental run and the values of the responses obtained for PS and LE (%).

Run No.	X_1 PLGA amount (mg)	X_2 Ultrasonication amplitude (%)	X_3 Phosphatidylcholine amount (mg)	Y_1 PS (nm)	Y_2 LE (%)
1	180	35	120	502	18
2	120	35	80	284	25
3	120	20	40	359	25
4	120	35	80	286	25
5	120	20	120	324	25
6	180	20	80	536	18
7	60	35	120	172	39
8	180	35	40	633	18
9	60	35	40	218	39
10	120	50	120	273	24
11	60	20	80	213	39
12	60	50	80	168	39
13	180	50	80	518	18
14	120	35	80	279	25
15	120	35	80	448	25
16	120	50	40	457	25
17	120	35	80	408	25

Note: The values of PS and LE (%) shown are the mean of three independent formulations. The %RSD of the three independent measurements was less than 5%.

The RSM graph in Figure 5.2a clearly indicate that the PS increased linearly as the PLGA amount increased for any given ultrasonication amplitude (%). This could be due to the increase in the viscosity of the organic solvent with increase in the PLGA amount which negated the effect of ultrasonication and lead to increase on PS of the NPs.

Figure 5.2b depict that increase in the phosphatidylcholine amount decreased the PS of the NPs at any given PLGA amount. Phosphatidylcholine is a surfactant which reduces the interfacial tension between two phases (organic and aqueous phases), resulting in a reduction in the globule size and consequently a drop in PS of the NPs.

A marginal increase in the PS of NPs was observed with increase in the ultrasonication amplitude, particularly when the phosphatidylcholine amount was low (40 to 60 mg) (Figure 5.2c). However, no significant difference was observed in the PS of NPs due to increase in ultrasonication amplitude at higher levels of phosphatidylcholine (80 to 120 mg). Higher ultrasonication amplitude can result in particles collisions which can sometimes lead to aggregation, particularly when the surfactant levels are low.

Table 5.4 Statistical data obtained from ANOVA of the regression models of PS and LE (%) of TAA-PLHNPs.

Source	Particle Size (Y_1)				Loading Efficiency (Y_2)			
	Sum of Squares	**df**	F_{cal}	P_{cal}	**Sum of Squares**	**df**	F_{cal}	P_{cal}
Model	2.82E+05	9	7.72	0.0067*	983.90	9	3.71E+05	<0.0001*
X_1	2.51E+05	1	61.87	0.0001*	915.91	1	3.11E+06	<0.0001*
X_2	32.00	1	7.88E-03	0.9318#	8.76E-03	1	29.74	0.0010*
X_3	19602.00	1	4.83	0.0640#	3.38E-03	1	11.45	0.0117*
X_1X_2	182.25	1	0.045	0.8383#	3.27E-03	1	11.11	0.0125*
X_1X_3	1806.25	1	0.44	0.5263#	3.75E-03	1	12.74	0.0091*
X_2X_3	5550.25	1	1.37	0.2807#	1.76E-03	1	5.96	0.0447*
X_1^2	2203.22	1	0.54	0.4854#	67.55	1	2.29E+05	<0.0001*
X_2^2	110.59	1	0.027	0.8736#	1.20E-05	1	0.041	0.8461#
X_3^2	1271.12	1	0.31	0.5933#	4.00E-04	1	1.36	0.2820#
Residual	28437.00	7			2.06E-03	7		
Lack-of-Fit	2381.00	3	0.12#	0.9425#	5.94E-04	3	0.54#	0.6802#
Pure Error	26056.00	4			1.47E-03	4		
Total	3.11E+05	16			983.90	16		

Note: *Statistically significant with $P<0.05$; #Statistically not significant with $P\geq0.05$

5.3.1.4 Effect of critical factors on LE (%)

The least square second-order polynomial equation (Eq. 5.6) for describing the relationship between the three critical factors and LE (%), in the coded form at 95% confidence level, is as

Equation 5.6

$$\boldsymbol{LE}\ (\%)(\boldsymbol{Y_2}) = 24.55 - 10.70\,X_1 - 0.033\,X_2 - 0.021\,X_3 + 0.029\,X_1X_2 + 0.031\,X_1X_3 - 0.021\,X_2X_3 + 4.01\,X_1^2 - 1.685\text{E} - 03\,X_2^2 + 9.750\text{E} - 03X_3^2$$

Table 5.4 shows that the quadratic model for the LE% was statistically significant with 'F_{cal}' value (3.710E+5) and P_{cal} <0.0001. The predicted R^2 and adjusted R^2 values were found to be 1.0. In addition, the F_{cal} value (0.54) for the lack-of-fit was insignificant with P_{cal} = 0.68. There was no discernible impact of the sequence of experimental runs on the distribution of residuals, which were distributed randomly around zero. The statistical results suggest that the regression model obtained for LE (%) is valid and accurate.

The LE (%) of TAA-PLHNPs ranged between 18% to 39%. The highest LE (%) was observed in run numbers 7, 9, 11 and 12, while the lowest LE (%) was observed in run numbers 1, 6, 8 and 13 (Table 5.3).

The results obtained from ANOVA indicate that the polymer amount was the only variable that had a significant impact on the LE (%). The primary reason for the decrease in LE (%) from 39% to 18% in the various experimental runs was due to the increase in the amount of polymer from 60 to 180 mg (Figure 2d) that is used in the calculation of LE (%), rather than due to the decrease in drug entrapment. Whereas, the EE (%) of the TAA-PLHNPs didn't change significantly (remained in the range of 96.7 to 97.3%). The other factors had little impact or no significant effect on the LE (%) of TAA-PLHNPs.

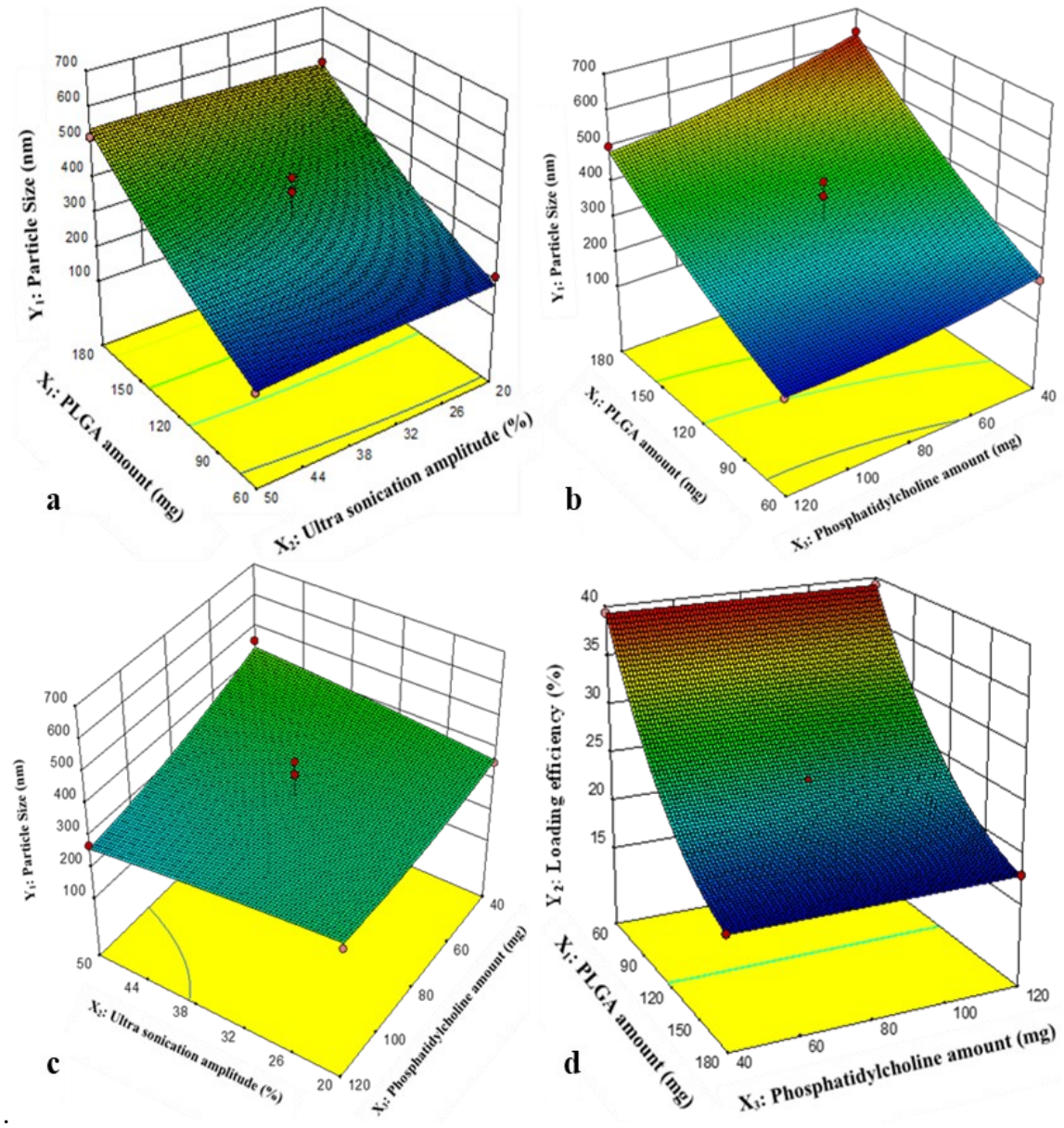

Figure 5.2 3D response surface plots demonstrating the impact of critical factors on the critical physico-chemical properties of TAA-PLHNP: (a, b, c) PS and (d) LE (%).

5.3.1.5 Desirability value and validation of the regression models

Desirability function-based simultaneous optimization technique is extremely effective for optimization studies involving multiple response variables [235]. Design expert software offers a number of solutions (in terms of conditions to be set for the critical factors) with varying desirability values. The solution with highest desirability value (closer to 1) offers the best optimal conditions for the critical factors to achieve the desired responses. For the simultaneous optimization of PS and LE (%) to prepare TAA-PLHNPs, Design Expert software yielded a

solution with a desirability value of 0.997. The software projected the following experimental conditions: polymer amount – 60 mg; ultrasonication amplitude − 39.2%; phosphatidylcholine amount − 102.2 mg to prepare the optimized TAA-PLHNPs. Verification runs (n = 6) were performed in order to examine the validity and reliability of the regression models for PS and LE (%) in predicting the corresponding response variables. Six independent replicate formulations of TAA-PLHNPs were prepared and characterized for their PS and LE (%). The statistical difference between the observed and predicted values (obtained by substituting the optimum levels of the critical factors in the regression equations), for both PS and LE (%), was assessed using the Wilcoxon signed rank test at α=0.05. No significant difference (P>0.05) was observed in the observed and predicted values of PS and LE (%), demonstrating the predictability of the regression models. The PS, ZP and LE (%) of the optimized TAA-PLHNPs were 163 ± 2.8 nm, -22.7 ± 2.4 mv and 39 ± 1.9%, respectively.

5.3.2 Characterization of TAA-PLHNPs formulations using DSC, powder XRD and SEM imaging

The DSC thermograms of TAA, a physical combination of all the excipients used in the formulation of TAA-PLHNPs and freeze-dried TAA-PLHNPs are shown in Figure 5.3a. The DSC thermogram for pure TAA showed a sharp endothermic peak at 292 °C, corresponding to the melting of crystalline TAA powder. The physical combination of TAA, PVA, PLGA and phosphatidylcholine displayed the characteristic TAA melting peak at 292 °C, which is indicative of the absence of incompatibility between TAA and other excipients used in the preparation of TAA-PLHNPs. Finally, the thermogram of freeze-dried TAA-PLHNPs revealed sharp endothermic peak only at 160 ^{o}C which corresponds mannitol, which was used as cryoprotectant in the lyophilisation of TAA-PLHNPs. The absence of melting endothermic peak for TAA at 292 ^{o}C in the freeze-dried TAA-PLHNPs may be due to the presence of TAA in either molecular form or amorphous form in the PLHNPs matrix.

Figure 5.3b presents the SEM image of optimized TAA-PLHNPs. The image shows that the PLHNPs are distinct with no aggregation. Figure 5.3c shows the pXRD graphs of pure TAA, physical mixture of TAA and the excipients used in preparation of TAA-PLHNPs and freeze-dried TAA-PLHNPs. In the physical mixture, sharp peaks of pure TAA can be observed at 2θ range of 9-21° and 24-28°, particularly at 2θ = 9°, 14°, 17° and 24°. However, no peaks were observed in the pXRD graph of freeze-dried TAA-PLHNPs suggesting that TAA may entrapped in the amorphous or molecular state in the PLHNPs, which supports the data obtained in DSC studies.

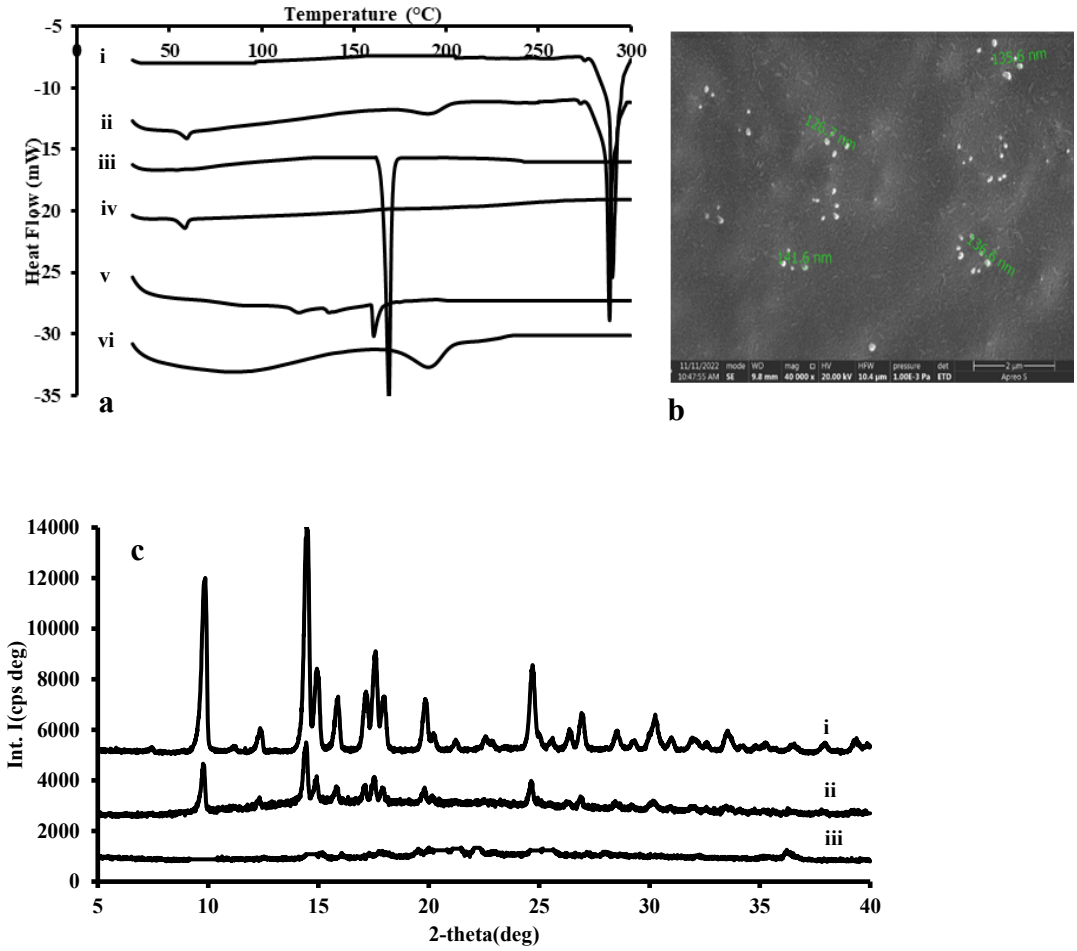

Figure 5.3 (a) DSC thermograms of (i) TAA, (ii) physical mixture of TAA, PLGA, phosphatidylcholine and PVA, (iii) lyophilized TAA-PLHNPs (iv) PLGA (v) phosphatidylcholine (vi) PVA; (b) optimized TAA-PLHNPs surface morphology by SEM; (c) pXRD graphs of (i) pure TAA, (ii) the physical combination of TAA-PLHNPs components and (iii) freeze-dried TAA-PLHNPs.

5.3.3 Rheological evaluation of TAA-PLHNP-ISG formulation

The results obtained from the rheological evaluation of blank ISG and TAA-PLHNP-ISG are shown in Figure 5.4a and 5.4b. Figure 5.4a presents the loss tangent (*tan δ*) whereas Figure 5.4b displays the complex viscosity (*η**) properties of the formulations as a function of temperature. As the temperature increased gradually from 25 to 40 °C, the loss tangent (*tan δ*) values decreased and complex viscosity (*η**) values increased. The *tan δ* and *η** values of both formulations showed a quick shift at temperature between 32–35 °C, indicating a clear sol-to-gel transition. This demonstrate the thermoresponsive nature of the RXG present in the ISG. When TAA-PLHNP-ISG was subjected to temperature ramp in the presence of STF, the *tan δ* value was found to be less than 1 even from the starting temperature of 25 °C, indicating a rapid transition from sol-to-gel. This is due to the ion sensitivity of κ-CRG present in TAA-PLHNP-ISG. This can be confirmed from *tan δ* (more than 1 between 25 to 33 °C) and *η** (with a slight increase in the values between 25 to 33 °C) values of the formulations which suggest that the formulations did not convert rapidly from sol-to-gel in the temperatures between 25 to 33 °C, when subjected to temperature ramp without STF.

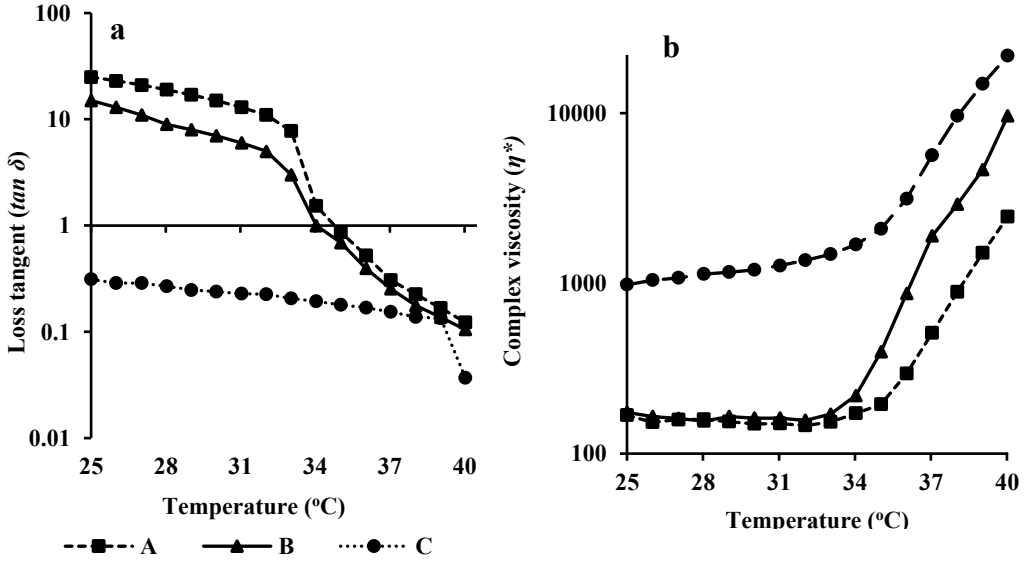

Figure 5.4 Semi-logarithmic plots of (a) loss tangent (*tan δ*) and (b) complex viscosity (*η**) of blank ISG and TAA-PLHNP-ISG as a function of temperature.

*__Note__: A- blank ISG and B- TAA-PLHNP-ISG subjected to temperature ramp; C- TAA-PLHNP-ISG subjected to temperature ramp in the presence of STF.

5.3.4 *In vitro* drug release study from TAA-PLHNP-Susp and TAA-PLHNP-ISG formulations

The *in vitro* drug release studies were conducted in STF with a pH of 7.4 ± 0.05, containing Tween 80 (0.5% w/v). The saturation solubility values of TAA in STF and STF with Tween 80 (0.5% w/v) are 13.7 µg/mL and 48 µg/mL, respectively. In order to maintain the sink condition during the *in vitro* dissolution studies, 300 mL of STF with Tween 80 (0.5% w/v) was used as the dissolution medium. The mean cumulative percentage of drug released vs time plots were constructed using the *in vitro* dissolution data (Figure 5.5). The release of TAA from the TAA-PLHNP-ISG happens in a two-step process. First, TAA is released from the polymer network of PLGA and then diffuse across the lipid layer on the surface of the NPs into the gel network formed by the *in situ* gel. TAA is then release into the dissolution media from the gel network by either drug diffusion or erosion of polymer gel. Therefore, the dissolution data from the TAA-PLHNP-ISG was not modelled using the kinetic models due to their limitations. However, the dissolution data of TAA-PLHNP-Susp was modelled to identify the release kinetics of the TAA from the formulation. The Higuchi kinetics model (R^2=0.965) was determined to be the best fit when compared to the zero-order kinetics model (R^2=0.836) and the first-order kinetics model (R^2=0.927). The drug release was slightly faster in the initial period with more than 28% drug release in the first 1 h followed by a slow and sustained release for more than 24 h (with 95% drug release at the end of 24 h). The dissolution data was also analysed using Korsmeyer-Peppas model to understand the mechanism of drug release form TAA-PLHNP-Susp. The release exponent ‘n’ in Korsmeyer-Peppas model determined from the dissolution data was found to be 0.66, suggesting a non-Fickian or anomalous transport (for ‘n’ between 0.5 to 0.89) of the drug from the TAA-PLHNPs. The release of TAA from TAA-PLHNPs is governed by drug diffusion as well as polymer relaxation. Since the value of ‘n’ is

closer to 0.5, out of the two mechanisms, drug diffusion is considered to play a dominant role in the overall drug release from TAA-PLHNPs.

The drug release from TAA-PLHNP-ISG was slower and more sustained than compared to TAA-PLHNPs. The drug release from TAA-PLHNP-ISG was around 15% at 1 h and around 85% at the end of 24 h. This is due to the presence of viscous gel network formed by the ISG around the TAA-PLHNPs in the case of TAA-PLHNP-ISG. The drug molecules after releasing from the TAA-PLHNPs, should further diffuse through the gel network of the ISG, which further delayed the drug release. The similarity factor (f2=41) value indicated that the drug release from TAA-PLHNPs and TAA-PLHNP-ISG were significantly different from each other.

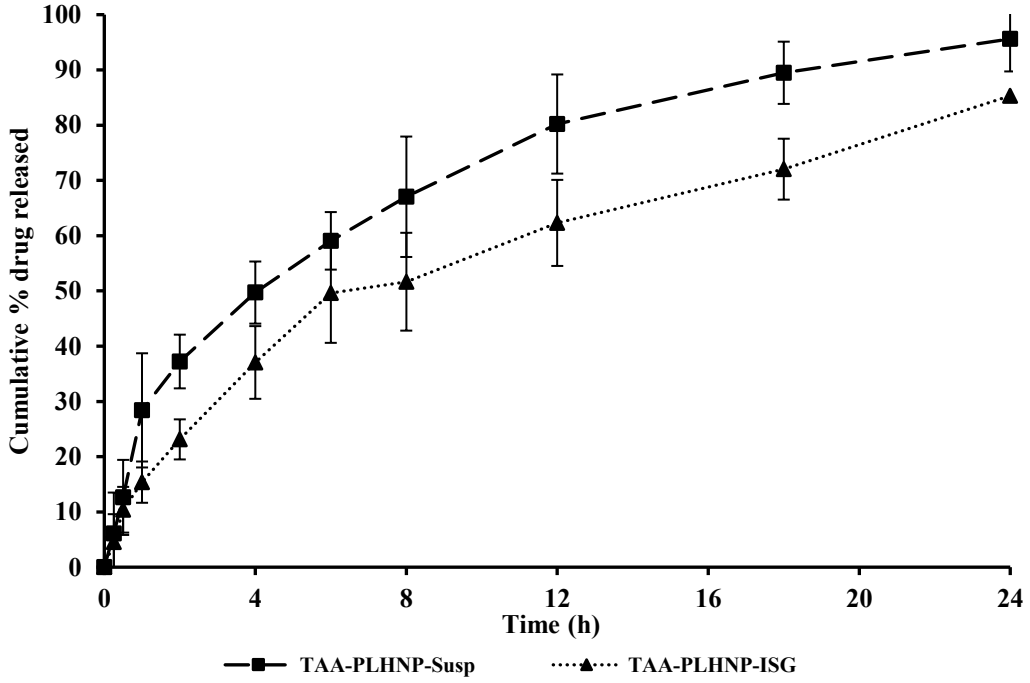

Figure 5.5 *In vitro* drug release profiles of TAA-PLHNP-Susp and TAA-PLHNP-ISG. Each data point represents the average cumulative% TAA released ± SD of n = 3 different formulations.

5.3.5 Stability of TAA-PLHNPs and TAA-PLHNP-ISG formulations

The stability studies of TAA-PLHNPs and TAA-PLHNP-ISG were conducted at room temperature (at 25 ± 2 °C and 60 ± 5% RH) and under refrigeration condition (at 2-8 °C),

respectively, for a period of 60 days. The PS, PDI, ZP and LE (%) of freshly prepared formulations and formulations stored under the aforementioned conditions for more than 60 days did not differ significantly as shown in Figures 5.6a and 5.6b. The %bias estimated for PS, PDI, ZP and LE (%) was found to be less than 5.0% at each sample time point for both formulations. This shows that both formulations were stable for 60 days when stored at their respective storage conditions.

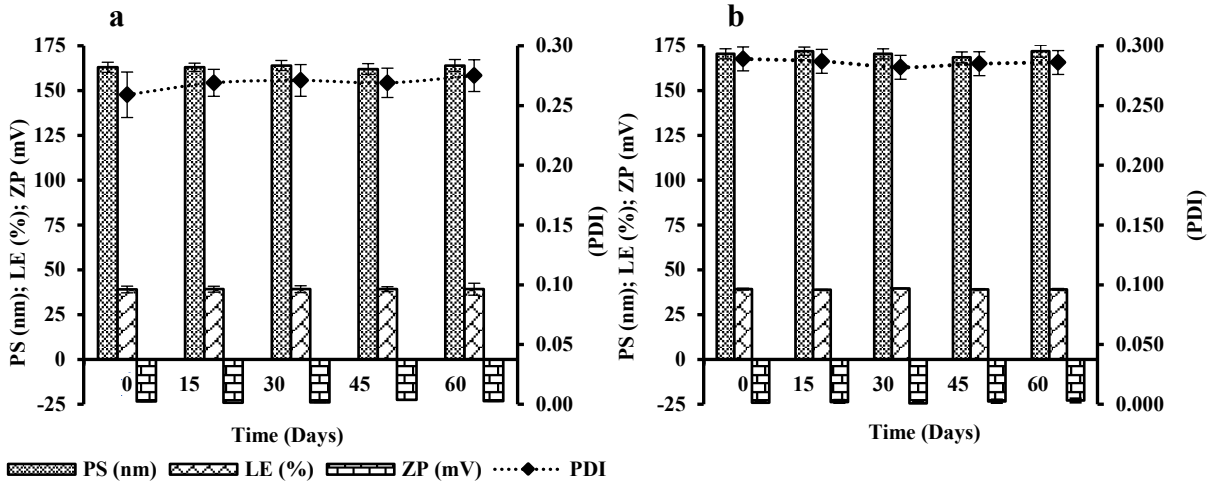

Figure 5.6 Stability data of (a) lyophilized TAA-PLHNPs stored at 25 ± 2 °C and 60 ± 5% RH and (b) TAA-PLHNP-ISG stored at 2-8 °C.

5.3.6 *Ex vivo* ocular toxicity tests of TAA-PLHNPs and TAA-PLHNP-ISG formulations using the HET-CAM technique

Figure 5.7 illustrates a comparison of the images acquired by the HET-CAM test of the various treatments used in the study. The CAM was severely injured by the positive control (0.1 N NaOH treatment) after 0.5 min, resulting in rosette-like coagulation. In addition, lysing of the blood vessels was observed in CAM after exposure to positive control. Negative control (0.9% w/v NaCl) and optimized formulations (TAA-PLHNP-Susp and TAA-PLHNP-ISG) did not show any discernible change in the CAM (neither haemorrhage nor coagulation) during the study. The positive control secured IS value of 20, while the negative control and optimized formulations (TAA-PLHNP-Susp and TAA-PLHNP-ISG) received IS value of 0. From the IS

values and the visual changes seen in CAM, it can be inferred that TAA-PLHNP-Susp and TAA-PLHNP-ISG were "non-irritant" and well-tolerated by the eye.

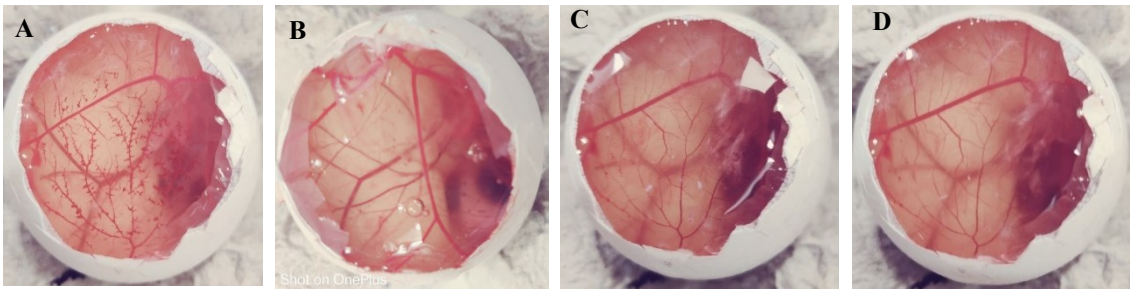

Figure 5.7 Images obtained from *ex vivo* ocular irritation study performed using HET-CAM test: (A) positive control (0.1 M NaOH); (B) negative control (0.9% w/v NaCl); (C) TAA-PLHNP-Susp; and (D) TAA-PLHNP-ISG.

5.3.7 Histopathological studies of the TAA-PLHNPs and TAA-PLHNP-ISG formulations

A microscopic examination of the cornea treated with STF (negative control) revealed intact epithelium and stroma, with no evidence of any changes in the cornea and stroma. There was a noticeable deformation of the epithelial cell layer with increased intercellular spaces in the presence of 75% v/v isopropyl alcohol (positive control). The STF-treated cornea and the cornea incubated with optimized formulations (TAA-PLHNP-Susp and TAA-PLHNP-ISG) did not show any significant difference from one another (Figure 5.8). It can be inferred that the optimized formulations do not affect the cellular structure of cornea and therefore are safe for ocular administration.

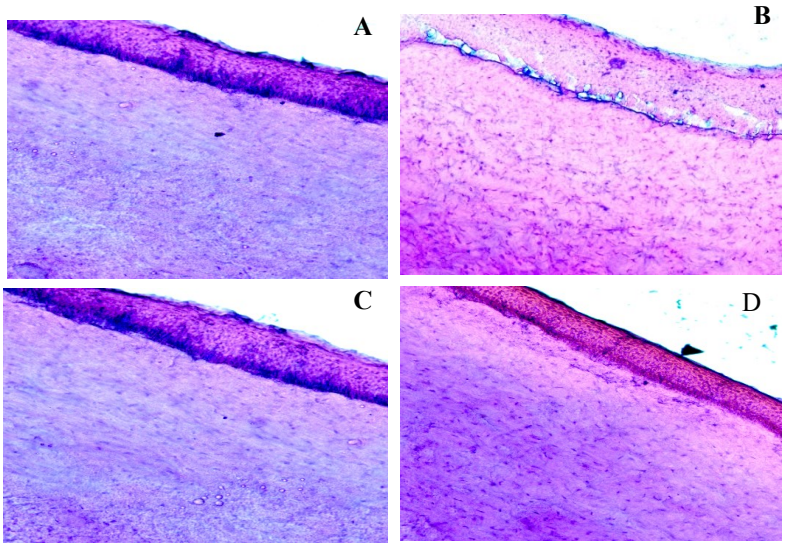

Figure 5.8 Photo-micrographic comparison of histological changes in the cornea following

its exposure to various treatments: (A) negative control (STF); (B) Positive control (75% v/v IPA); (C) TAA-PLHNP-Susp; and (D) TAA-PLHNP-ISG.

5.3.8 Ocular pharmacokinetic studies of the optimized TAA-PLHNPs and TAA-PLHNP-ISG formulations

The mean concentration-time profiles of TAA in the vitreous and aqueous humour (Figure 5.9) obtained following topical ocular administration of TAA-PLHNP-Susp and TAA-PLHNP-ISG were compared with each other as well as with that of TAA-HP-β-CD-Susp (Section 2.3.5, Chapter 2). To estimate pharmacokinetic parameters like C_{max}, T_{max}, AUC_{0-t} and $MRT_{0-\infty}$, the time course data of TAA in both the matrices was subjected to non-compartmental analysis using Phoenix WinNonlin software (version 8.3.5.340, Pharsight Corporation, NC, USA). The time course profiles of TAA in both the matrices were constructed by pooling the concentration data from two eyes of a single animal sacrificed at individual sampling time points in the study. The most important site for drug localization in the treatment of PU is the vitreous humour. An ideal topical ocular formulation of TAA for treatment of PU would be the one that can produce concentrations of TAA higher than 100 ng/mL in the vitreous humour and sustain them for longer duration of time. Such formulation can reduce the dose as well as the dosing frequency of TAA.

Figure 5.9b shows that TAA concentrations (C_{max}) in the vitreous humour for TAA-PLHNP-ISG (946.53 ng/mL) were 1.5 times higher than TAA-PLHNP-Susp (647.50 ng/mL) and 3.6 times higher than TAA-HP-β-CD-Susp (264.9 ng/mL). In addition, the concentrations of TAA were more sustained for TAA-PLHNP-ISG ($MRT_{0-\infty}$ = 16.26 h) compared to TAA-PLHNP-Susp ($MRT_{0-\infty}$ = 10.77 h) compared to TAA-HP-β-CD-Susp ($MRT_{0-\infty}$ = 3.10 h). The results in Table 5.5 further show that the total vitreous humour exposure (AUC_{0-t}) of TAA for TAA-PLHNP-ISG (10093.76 ng×h/mL) was 1.7 times higher than that of TAA-PLHNP-Susp (6094.92 ng×h/mL) and 12.5 times higher than that of TAA-HP-β-CD-Susp (810.4 ng×h/mL). The above results indicate that TAA-PLHNP-ISG produced higher and sustained

concentrations of TAA in vitreous humor compared to TAA-PLHNP-Susp compared to TAA-HP-β-CD-Susp.

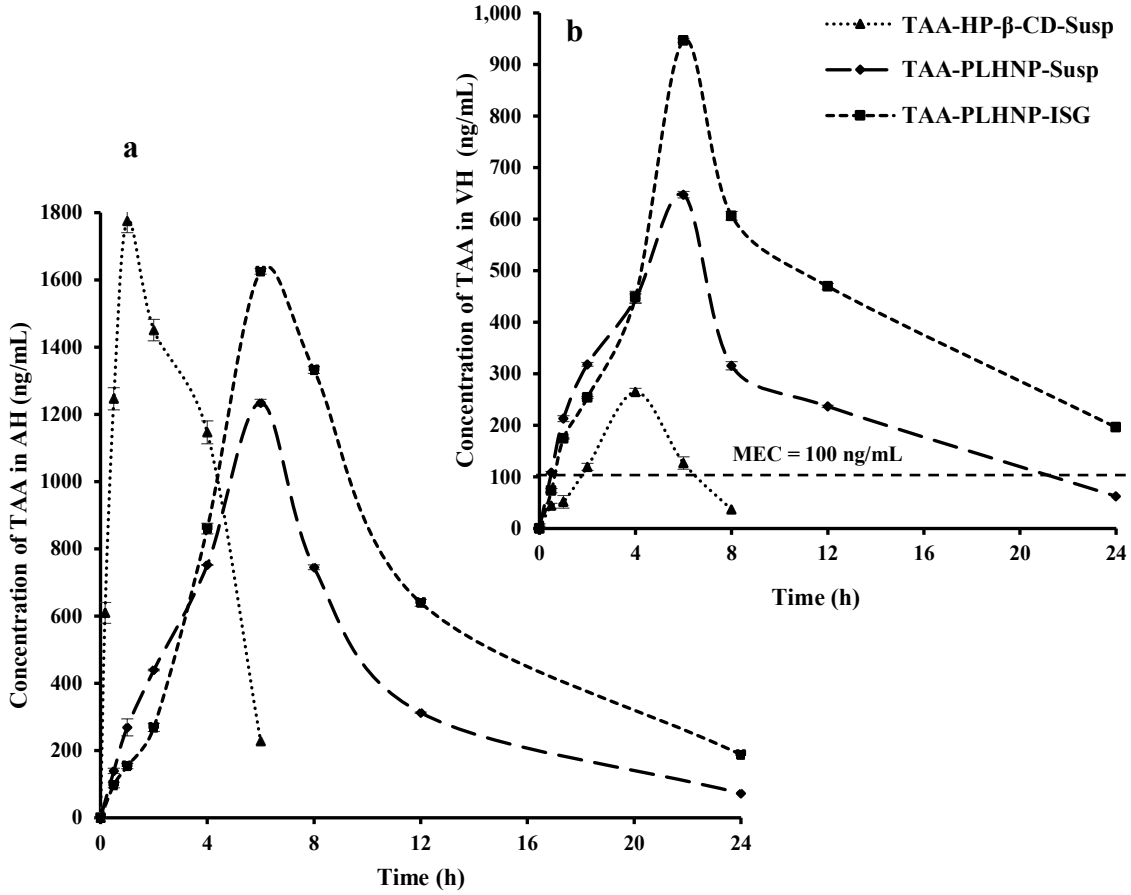

Figure 5.9 Mean aqueous humour (AH) (a) and vitreous humour (VH) (b) concentration-time profiles obtained following ocular administration of TAA-HP-β-CD-Susp; TAA-PLHNP-Susp; and TAA-PLHNP-ISG. Each data point is the mean of two independent assessments (*n*=2).

A comparison of the time courses profiles for TAA-PLHNP-ISG, TAA-PLHNP-Susp and TAA-HP-β-CD-Susp in the aqueous humour is represented in Figure 5.9a. TAA concentrations in aqueous humour were slightly higher in TAA-HP-β-CD-Susp (C_{max} of 1775.40 ng/mL) compared to TAA-PLHNP-Susp (C_{max} of 1234.60 ng/mL) but no significant difference was observed with TAA-PLHNP-ISG (C_{max} of 1625.32 ng/mL). The T_{max} of TAA-HP-β-CD-Susp (1 h) was much lesser than both TAA-PLHNP-Susp (6 h) and TAA-PLHNP-ISG (6 h). This could be due to the higher and faster dissolution of TAA in the lachrymal fluids from TAA-

HP-β-CD-Susp compared to TAA-PLHNP-Susp and TAA-PLHNP-ISG. However, the overall aqueous humor exposure (represented by the AUC_{0-t} in the aqueous humor) and residence time of TAA in the aqueous humor (represented by the $MRT_{0-\infty}$ in the aqueous humor) of the two nano-formulation were significantly higher than TAA-HP-β-CD-Susp. Due to tear turnover, tear fluid dilution and nasolacrimal drainage, TAA-HP-β-CD-Susp was cleared rapidly from the precorneal area. Among the two nano-formulations, TAA-PLHNP-ISG had higher AUC_{0-t} and $MRT_{0-\infty}$ in the aqueous humor due to the viscous gel formed by the formulation in the precorneal area immediately after its administration. The viscous gel formed by TAA-PLHNP-ISG prolonged the residence time of the formulation in the precorneal area and lessened the effects of dilution by tear fluids and nasolacrimal drainage. Moreover, the gel provided an intimate contact with the corneal epithelium, which enabled the drug to be spread across the whole corneal surface and thereby enhancing the extent of intra-ocular permeation.

Table 5.5 Ocular pharmacokinetic parameters of TAA in the vitreous humour and aqueous humour following topical administration of TAA-PLHNP-Susp, TAA-PLHNP-ISG in male New Zealand rabbits.

Biological matrix	PK parameters	Units	Treatments		
			TAA-HP-β-CD-Susp*	TAA-PLHNP-Susp	TAA-PLHNP-ISG
Vitreous humour	C_{max}	ng/mL	264.9	647.5	946.53
	T_{max}	h	2.0	6.0	6.0
	AUC_{0-t}	ng×h/mL	810.4	6094.92	10093.76
	$MRT_{0-\infty}$	h	3.1	10.77	16.26
Aqueous humour	C_{max}	ng/mL	1775.4	1234.60	1625.32
	T_{max}	h	1.0	6.0	6.0
	AUC_{0-t}	ng×h/mL	6697.3	10074.28	15779.39
	$MRT_{0-\infty}$	h	3.0	9.14	11.49

*Data of TAA-HP-β-CD-Susp is reproduced from Table 2.4, Chapter 2.

Note: The values of C_{max}, T_{max}, AUC_{0-t} and $MRT_{0-\infty}$ were obtained by composite sampling from the two eyes (n=2) of animal sacrificed at each time point.

Overall, TAA-PLHNP-ISG not only increased the concentrations of TAA in the vitreous humour but also sustained the concentrations of the drug for a longer period than TAA-PLHNP-Susp and TAA-HP-β-CD-Susp. Based on the results obtained in the study, we can

conclude that TAA-PLHNP-ISG can help in decreasing the dose and dosing frequency of TAA for non-invasive drug delivery in the treatment of PU.

5.4 Conclusion

In this chapter, TAA-PLHNPs were prepared by employing a bottom-up approach using the nanoprecipitation method. The principles of the DoE were used in the screening and optimization of critical factors affecting the critical physico-chemical properties (responses) of the TAA-PLHNPs. The physico-chemical, *in vitro* and *in vivo* properties of the optimized TAA-PLHNPs were determined. The optimized TAA-PLHNPs were loaded into the optimized dual responsive blank *in situ* gel made of a thermoresponsive polymer (RXG) and an ion-sensitive polymer (κ-CRG). *In vivo* ocular pharmacokinetic studies were performed to compare the performance of aqueous suspension of TAA-PLHNPs (TAA-PLHNP-Susp) and TAA-PLHNPs loaded *in situ* gel (TAA-PLHNP-ISG) with TAA-HP-β-CD-Susp. TAA-PLHNP-ISG produced 1.5 and 3.6 times higher vitreous humor concentrations (C_{max}) of TAA than TAA-PLHNP-Susp and TAA-HP-β-CD-Susp, respectively. Further, TAA-PLHNP-ISG sustained the TAA concentrations for a longer duration (16.26 h) compared to TAA-PLHNP-Susp (10.77 h) and TAA-HP-β-CD-Susp (3.10 h). Both the nano-formulations were found to be stable for 6 months during their storage. The results show that non-invasive precorneal ocular administration of PLHNPs formulations of TAA would be beneficial in achieving therapeutic concentrations in the vitreous humour. TAA-PLHNP-ISG can be an excellent alternative for intravitreal administration of TAA and improve patient compliance and convenience.

6

COMPARISON OF THE DEVELOPED TRIAMCINOLONE ACETONIDE NANO-FORMULATIONS

6.1 Introduction

In the current research investigation, we have developed and optimized various formulations of TAA that were intended to be applied topically into the eyes in order to increase the drug concentration in the posterior segment of the eye (vitreous humour) for the treatment of PU. To increase the availability of TAA at therapeutic concentrations, two alternative strategies, *viz., in situ* gelling systems and nanoparticulate formulations and their combination, were investigated. Formulations were evaluated for their physicochemical characteristics, *in vitro* properties and *in vivo* performance. To ascertain the *in vivo* effectiveness of all the formulations, ocular pharmacokinetic studies were conducted by administering the formulations in the precorneal area of the eye (topically) in male New Zealand white rabbits and the time course of TAA in the aqueous humor and vitreous humor were determined.

In this chapter, we compared the properties (physico-chemical, *in vitro* and *in vivo*) of the various TAA nano-formulations optimized in the study, namely, aqueous suspension of TAA-NCs (TAA-NC-Susp) and TAA-NCs loaded RXG-κ-CRG *in situ* gel (TAA-NC-ISG), aqueous suspension of TAA-PLHNPs (TAA-PLHNP-Susp) and TAA-PLHNPs loaded RXG-κ-CRG *in situ* gel (TAA-PLHNP-ISG).

6.2 Comparison of the manufacturing process of TAA nano-formulations

TAA-NCs were prepared employing solvent-antisolvent precipitation technique using a bottom-up approach. The processing parameters and stabilizer selection were critical in achieving the desired PS. The stabilizer system consisted of a mixture of soluplus and sodium deoxycholate. The data obtained from the DoE suggest that the concentration of soluplus had a significant impact on yield (%), whereas homogenization time and ultrasonication amplitude were shown to be the most important factors affecting the PS of TAA-NCs.

TAA-PLHNPs were prepared using the nanoprecipitation technique. In this procedure, TAA and PLGA were dissolved in an organic solvent (NMP) in a beaker. PC was dissolved in NMP

and added to aqueous solution containing PVA to form a homogenous mixture of PVA-PC solution. Finally, the polymeric solution of TAA and PLGA was added drop-wise into the PVA-PC solution under homogenization followed by ultrasonication. During the addition of polymeric solution of TAA and PLGA in to the aqueous solution of PVA-PC, TAA gets entrapped in the network of PLGA which aggregates and forms NPs due to the diffusion of NMP into the aqueous phase. The homogenization and ultrasonication energies provided during the process controlled the PS of the TAA loaded PLGA particles formed. Further, the mixture of PVA-PC -PLGA in the aqueous phase formed a deposition on the surface of the TAA loaded PLGA particles leading to the formation of TAA-PLHNPs. DoE was used in the optimization of TAA-PLHNPs, where, PLGA amount, phosphatidylcholine amount and ultrasonication amplitude were found to significantly affect the PS and LE (%) of the NPs.

Both TAA-NCs and TAA-PLHNPs were prepared by nanoprecipitation techniques. The precipitation method of TAA-NCs was comparatively easy and simple as it involved few number of ingredients and fewer steps. However, the methods of precipitation of both the nano-formulations were reproducible and straightforward to use, which can be easily adapted to pharmaceutical industries.

6.3 Comparison of physico-chemical, *in vitro* drug release and physical stability of TAA nano-formulations

The physico-chemical properties like PS, PDI, ZP, LE (%) and yield (%) (in the case of TAA-NCs) of the optimized TAA-NCs and TAA-PLHNPs are presented in Table 6.1. The TAA-PLHNPs have relatively smaller PS than TAA-NCs. The ZP of TAA-PLHNPs was higher than that of TAA-NCs. The differences in the PS of the NPs is due to the differences in the type and concentration of the stabilizers used in the preparation of NPs as well the type and quantum of energy provided in the preparation of the respective NPs. Both the nano-formulations exhibited a negative charge on their surface. Sodium deoxycholate (an anionic surfactant) was used as

stabilizer in the preparation of TAA-NCs and therefore responsible for the negative charge on the surface of the particles. Phosphatidylcholine (though a zwitter ion molecule but exhibits negative charge in the pH conditions of 6.5 to 9) was used in the preparation of TAA-PLHNPs. The molecules of PC which gets deposited on the surface of the NPs are responsible for the negative charge on the surface. The ZP of TAA-PLHNPs (-23.4 ± 1.4 mV) was slightly higher compared to TAA-NCs (-11 ± 1.5 mV) due to the differences in the concertation and extent adsorption of phosphatidylcholine and sodium deoxycholate used in the preparation of TAA-PLHNPs and TAA-NCs, respectively. The PDI of both the optimized TAA-NCs and TAA-PLHNPs was well within the usually accepted range of 0.4 for monodisperse nano-formulations, suggesting that their methods of preparation are reproducible and reliable.

The *in vitro* drug release studies revealed that TAA-PLHNP-Susp extended the release of TAA for more than 24 (with around 95% drug release at the end of 24 h) due to the combination of rate controlling polymer (PLGA) as well the lipophilic excipient (phosphatidylcholine) playing a significant role in the drug release. However, in the case of TAA-NC-Sups, the drug dissolved instantly in the simulated tear fluid (7.4 ± 0.05), suggesting that the nanocrystal formulation increased the saturation solubility of the drug. Loading the nano-formulations into the RXG-κ-CRG *in situ* gel (TAA-NC-ISG and TAA-PLHNP-ISG) resulted in a slower release of TAA when compared to the aqueous suspension of the respective nano-formulations (i.e., TAA-NC-Susp and TAA-PLHNP-Susp). The viscous gel network formed by the *in situ* gel contributed to the decrease in drug release from the nano-formulations loaded *in situ* gels.

The lyophilized powder of TAA-NCs and TAA-PLHNPs were found to be stable over a period of 60 days when stored at 25 ± 2 °C and 60 ± 5% RH. The nano-formulations loaded *in situ* gels (TAA-NC-ISG and TAA-PLHNP-ISG) were stable for 60 days when stored under refrigeration conditions (2-8 °C). There was no significant difference observed in the physical

properties for the nano-formulations like PS, PDI, ZP, yield (%) and LE (%) during the stability studies over the period of 60 days.

Table 6.1 Physical characteristics of TAA loaded nano-formulations

Physical characteristics	TAA-NCs	TAA-NC-ISG	TAA-PLHNPs	TAA-PLHNP-ISG
PS (nm)	243 ± 5.7	239 ± 4.0	163 ± 2.8	168 ± 3.6
PDI	0.24 ± 0.08	0.25 ± 0.07	0.27 ± 0.02	0.29 ± 0.01
ZP (mV)	-11 ± 1.3	-10.9 ± 1.5	-23.4 ± 1.4	-23.9 ± 1.1
LE (%)	NA	N A	39 ± 1.9	38 ± 1.7
Yield (%)	88.5 ± 2.4	87.9 ± 2.1	NA	NA

Note: The values given for the physical characteristics of nano-formulations are represented as mean ± SD of n=3 independent measurements

6.4 Comparison of the rheological characteristics of TAA loaded and TAA nano-formulations loaded *in situ* gels

The rheological characteristics of the *in situ* gels were assessed in two different experimental configurations: 1) a temperature ramp in the presence of STF (for Blank RXG-κ-CRG, TAA-RXG-κ-CRG, TAA-NC-ISG and TAA-PLHNP-ISG) and 2) a temperature ramp in the presence of deionized water (only for Blank RXG-κ-CRG). The graphs of complex viscosity (η*) vs temperature and loss tangent (tan δ) vs temperature are used to compare the sol-to-gel transition and the gel strength of the formulations. It can be seen from Figures 6.1a and 6.1b that all formulations showed faster gelation and higher gel strength than compared to blank RXG-κ-CRG, both in the presence of DI water as well as STF. This can be attributed to the presence of suspended solids in the formulation compared to the blank *in situ* gel. TAA-RXG-κ-CRG had the highest gel strength compared to TAA-PLHNP-ISG compared to TAA-NC-ISG though the proportion of the *in situ* gelling polymers and KCl, is exactly same in all the formulations. In the case of TAA-RXG-κ-CRG, TAA powder with an average PS of around 5-10 μm was loaded into the *in situ* gel while the PS of TAA-NCs and TAA-PLHNPs loaded in the *in situ* gel were 243 ± 5.7 nm and 163 ± 2.8, respectively. Therefore, the differences in the

viscosity of the gel formed could be due to the PS of TAA loaded into the *in situ* gel. The larger PS of TAA can be attributed to the higher gel strength for TAA-RXG-κ-CRG.

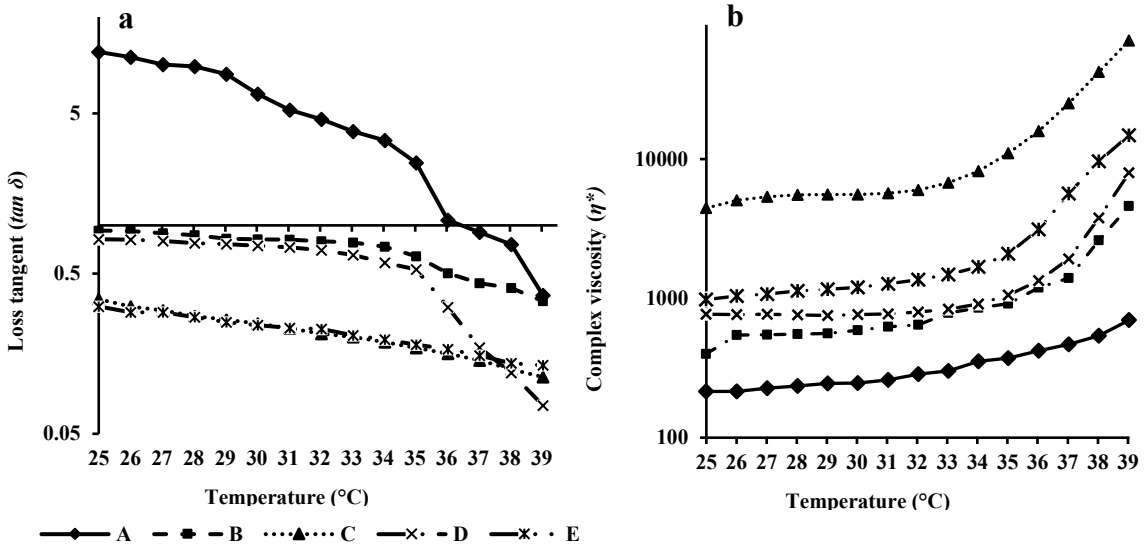

Figure 6.1 Semi-logarithmic plots of (a) loss tangent (*tan δ*) and (b) complex viscosity (*η**) of Blank RXG-κ-CRG, TAA-RXG-κ-CRG, TAA-NC-ISG and TAA-PLHNP-ISG as a function of temperature.

***Note**: **A**- Blank RXG-κ-CRG in the presence of DI water; B- Blank RXG-κ-CRG in the presence of STF; C- TAA-RXG-κ-CRG in the presence of STF; D- TAA-NC-ISG in the presence of STF and E- TAA-PLHNP-ISG in the presence of STF.

6.5 Comparison of ocular pharmacokinetic performance of various TAA nano-formulations

The comparison of PK data obtained from the time course of TAA in aqueous humor and vitreous humour following the topical ocular administration of TAA nano-formulations (TAA-NC-Susp and TAA-PLHNP-Susp) and TAA nano-formulation loaded *in situ* gels (TAA-NC-ISG and TAA-PLHNP-ISG) are given in Table 6.2. Out of the four nano-formulations, TAA-PLHNP-ISG showed the highest C_{max} as well as highest AUC_{0-t} in the vitreous humor. We can infer that TAA-PLHNP-ISG is the best formulation to achieve the highest vitreous humor exposure for TAA compared to the other nano-formulations designed in the study. In addition, TAA-PLHNP-ISG exhibited the highest $MRT_{0-\infty}$ value (16.26 h) compared to the remaining three nano-formulations. The concentrations of TAA in the vitreous humor were more

sustained from TAA-PLHNP-ISG than any of the remaining nano-formulations. Higher vitreous humor exposure and higher sustenance of TAA concentration in vitreous humor of TAA-PLHNP-ISG could be due to the combined benefit provided by the *in situ* gel as well as the polymer-lipid hybrid nanoparticles. The *in situ* gel helped in providing longer residence time in the precorneal area and also intimate contact of the formulation with the corneal epithelium. The polymer-lipid hybrid nanoparticles helped in time controlling the TAA release which resulted in sustaining the TAA concentrations in vitreous humor, the target site for the treatment of PU.

In the case of aqueous humor, TAA-NC nano-formulations showed higher C_{max} values than the TAA-PLHNP formulations. This could be due to the rapid dissolution of the TAA-NCs in the tear fluid which resulted in rapid permeation through the cornea into the aqueous humor. However, the overall exposure (expressed in terms of AUC_{0-t}) and residence time (expressed in terms of AUC_{0-t}) in aqueous humor for TAA-NC nano-formulations were lesser than compared to the TAA-PLHNP nano-formulations. This is because the concentrations of TAA are not sustained in the aqueous humor by the TAA-NC formulations as compared to the TAA-PLHNP nano-formulations.

Table 6.2 Aqueous and vitreous humour PK parameters of different TAA nano-formulations (dose equivalent to TAA of 4 mg/40 µL/eye).

Biological Matrix	PK Parameters	Units	TAA Nano-formulations			
			TAA-NC-Susp	TAA-NC-ISG	TAA-PLHNP-Susp	TAA-PLHNP-ISG
Vitreous humour	C_{max}	ng/mL	635.4	854.9	647.5	946.53
	T_{max}	h	4.0	6.0	6.0	6.0
	AUC_{0-t}	ng×h/mL	3720.2	7126.1	6094.92	10093.76
	$MRT_{0-\infty}$	h	6.0	11.2	10.77	16.26
Aqueous humour	C_{max}	ng/mL	2069.2	2202.9	1234.60	1625.32
	T_{max}	h	4.0	6.0	6.0	6.0
	AUC_{0-t}	ng×h/mL	10846.2	13355.0	10074.28	15779.39
	$MRT_{0-\infty}$	h	4.9	8.6	9.14	11.49

6.6 Conclusion

The manufacturing processes of both TAA-NCs and TAA-PLHNPs were simple, reproducible and can be scale-up easily in the pharmaceutical industries. All the TAA nano-formulations were found to be stable in their respective storage conditions for a period of 60 days. The vitreous humor PK data suggest that TAA-PLHNP nano-formulations performed better compared to the TAA-NC nano-formulations. Among the two TAA-PLHNP nano-formulations, TAA-PLHNP-ISG showed the best vitreous humor exposure and sustained TAA concentrations in the vitreous humor for longer duration.

7

CONCLUSION

The treatment of inflammatory eye diseases effecting the posterior segment of the eye is very challenging. It is very difficult to achieve therapeutic concentrations of a drug in the posterior segment of the eye by administering the drug product topically in the precorneal area of the eye. This is primarily due to the presence of various barriers, namely the static barriers, dynamic barriers and metabolic barriers, existing in the eye.

Uveitis is an inflammatory disease which can affect either the anterior segment or the posterior segment of the eye. The inflammation of the posterior uveal tract is referred to as posterior uveitis, where the retina and choroid are affected. One of the first synthetic glucocorticoids to be approved for the treatment of inflammatory eye conditions is TAA. TAA is frequently advised for the treatment of PU. Due to its poor aqueous solubility (12 mg/mL) and slow dissolving rate in the lachrymal fluids, the topical formulations of TAA (aqueous suspensions) given as ocular drops were found to be ineffective in attaining therapeutic concentrations in the vitreous humour (target tissue). As a result, TAA is marketed as a suspension formulation (Triesence) that is intended for intravitreal injection. The primary risks of intravitreal injections are postoperative infections and non-infectious illnesses, pseudoendophthalmitis and endophthalmitis, retinal detachment, cataract formation and secondary ocular hypertension.

In the current study, we explain our attempts to assess and enhance the therapeutic concentrations of TAA in the vitreous humor after topical ocular delivery of TAA using a range of formulation methodologies/strategies.

The first objective of this work was to identify the dose of TAA required for producing therapeutic concentrations of more than 100 ng/mL in the posterior segment of the eye by employing a specific and sensitive bioanalytical method. Analytical and bioanalytical methods of TAA were developed and validated as per the regulatory guidelines. The developed methods were employed for accurate and precise quantification of TAA in bulk formulations, samples

obtained from various *in vitro* experiments and *in vivo* PK studies. Aqueous suspensions of TAA with 20% HP-β-CD containing different dose strengths (1 mg/30µl, 2 mg/30µl, 4 mg/30µl) were administered in male New Zealand rabbits at a dose volume of 30 µl per eye in both the eyes to determine the time course of TAA in aqueous humor and vitreous humor. Ocular pharmacokinetic studies revealed that aqueous suspension of TAA with 20% HP-β-CD with dose strength of 4 mg/30µl/eye produced therapeutic concentrations of more than 100 ng/mL for a period of more than 3 h in the vitreous humor. Based on the results obtained in the study, a therapeutic dose of 4 mg (in a dosing volume of NMT 40 µl) was identified for TAA for precorneal delivery of the drug.

One of the key challenges with topical ocular delivery is the fast clearance of medications after dosing. A dual responsive *in situ* gel using a combination of κ-CRG and RXG was developed to prevent rapid ocular clearance and provide longer residence time on the corneal membrane. Many factors affecting the sol-to-gel transition temperature and the gel strength of the RXG-κ-CRG *in situ* gel were examined and modified using rheological experiments. The optimized TAA loaded RXG-κ-CRG *in situ* gel was investigated for its *in vitro* drug release, mucoadhesion and *ex vivo* ocular toxicity. Ocular PK studies were conducted for the optimized TAA loaded RXG-κ-CRG *in situ* gel and aqueous suspension of TAA with 20% HP-β-CD in male New Zealand rabbits. The PK parameters were determined from the time course of TAA in aqueous humor and vitreous humor. The TAA loaded RXG-κ-CRG *in situ* gel resulted in significantly higher concentrations (1.64 times increase in C_{max}), drug exposure (4.01 times increase in $AUC_{0\text{-}t}$) and sustained the concentration for longer duration (5.2 times increase in $MRT_{0-\infty}$) in the vitreous humor than the aqueous suspension of TAA with 20% HP-β-CD. TAA loaded RXG-κ-CRG *in situ* gel could significantly improve the delivery of TAA as compared to the conventional aqueous suspension of TAA.

Nanoparticulate drug delivery systems are known to provide significant benefits over conventional formulations, particularly in increasing the drug delivery/distribution to the target tissue as well as sustaining the drug concentrations at the target site for longer duration. Therefore, two different nano-formulations [Nanocrystals of TAA (TAA-NCs) and Polymer-lipid hybrid nanoparticles of TAA (TAA-PLHNs)] were designed and evaluated in the current research work.

Nanocrystals of TAA (TAA-NCs) were prepared utilizing the solvent-antisolvent precipitation method under ultrasonication followed by high-speed homogenization. The design of experiments (DoE) approach was used to optimize TAA-NCs to achieve a mean PS of 243 ± 5.7 nm and yield (%) of 88.5 ± 2.4. The optimized TAA-NCs had PDI and ZP of 0.24 ± 0.08 and -11 ± 1.3 mV, respectively. The pXRD and DSC analysis of optimized TAA-NCs revealed that crystalline nature of TAA in the TAA-NCs. The optimized TAA-NCs were loaded into the dual responsive RXG-κ-CRG *in situ* gel (ISG) to delay the precorneal ocular clearance and increase the residence time of the formulation following its topical ocular delivery. The rheological characterization of the TAA-NCs loaded RXG-κ-CRG *in situ* gel (TAA-NC-ISG) showed a quick sol-to-gel transition in the physiological conditions (STF at 34 ± 0.5°C) of the eye. The *in vitro* drug release studies indicate that TAA was completely dissolved within 15 min in case of optimized TAA-NCs while the drug release was slow and sustained for more than 12 h from TAA-NC-ISG. No significant differences were observed in the physical properties of the lyophilised TAA-NCs (stored at 25 ± 2 °C and 60 ± 5% RH) as well as TAA-NC-ISG (stored at refrigerated conditions (2-8 ºC)) over 60 days of study. Ocular PK evaluation in male New Zealand rabbits revealed significantly higher vitreous humour concentrations (C_{max}) for TAA-NC-ISG (854.9 ng/mL) compared to TAA-NC-Susp (635.4 ng/mL) compared to TAA-HP-β-CD-Susp (264.9 ng/mL). Further, the total vitreous humour exposure ($AUC_{0–t}$) for TAA-NC-ISG (7126.1 ng×h/mL) was 1.9 times and 8.8 times higher

than TAA-NC-Susp (3720.2 ng×h/mL) and TAA-HP-β-CD-Susp (810.4 ng×h/mL), respectively. The residence time of TAA ($MRT_{0-\infty}$) in the vitreous humor for TAA-NC-ISG (11.2 h) was 1.9 times higher than that of TAA-NC-Susp (6.0 h) and 3.6 times higher than TAA-HP-β-CD-Susp (3.1 h). This shows that the NCs formulation of TAA improved the drug delivery towards the vitreous humor compared to the aqueous suspension of TAA with 20% HP-β-CD (TAA-HP-β-CD-Susp).

TAA loaded polymer-lipid hybrid nanoparticles (TAA-PLHNPs) were prepared using a combination of PLGA and phosphatidylcholine by nanoprecipitation method under high-speed homogenization followed by ultrasonication. The TAA-PLHNPs were optimized using DoE. The optimized TAA-PLHNPs had a mean PS of 163 ± 2.8 nm, PDI of 0.27 ± 0.02, ZP of -23.4 ± 1.4 mV and LE (%) of 39.2 ± 1.9. To increase the residence time in the precorneal area, the optimized TAA-PLHNPs loaded into the dual responsive RXG- κ-CRG *in situ* gel (ISG). The rheological studies of TAA-PLHNPs loaded RXG- κ-CRG *in situ* gel (TAA-PLHNP-ISG) indicated a rapid sol-to-gel transition when exposed to the physiological conditions (STF at 34 ± 0.05°C) of the eye. The drug release from TAA-PLHNPs was found to follow Higuchi's square root kinetics. The polymer-lipid hybrid nanoparticles could prolong the drug release beyond 24 h with approximately 96% drug release at the end of 24 h. In the stability studies, conducted over a period of 60 days, no significant difference was observed in the physical properties of lyophilised TAA-PLHNPs (stored at 25 ± 2 °C and 60 ± 5% RH) as well as TAA-PLHNP-ISG (stored at refrigerated conditions (2-8 °C)). Ocular PK studies were conducted in male New Zealand rabbits to compare the time course of TAA in vitreous humor for the TAA-PLHNPs and TAA-PLHNP-ISG. The vitreous humour concentration (C_{max}) of TAA-PLHNP-ISG (946.53 ng/mL) was significantly higher compared to TAA-PLHNP-Susp (647.50 ng/mL) compared to TAA-HP-β-CD-Susp (264.9 ng/mL). In addition, the vitreous humour exposure (AUC_{0-t}) of TAA-PLHNP-ISG (10093.76 ng×h/mL) was significantly higher than TAA-

PLHNP-Susp (6094.92 ng×h/mL) compared to TAA-HP-β-CD-Susp (810.4 ng×h/mL). The residence time of TAA ($MRT_{0-\infty}$) in the vitreous humor for TAA-PLHNP-ISG (16.26 h) was 1.5 times higher than that of TAA-PLHNP-Susp (10.77 h) and 5.2 times higher than TAA-HP-β-CD-Susp (3.1 h). The *in vivo* performance of TAA loaded polymer-lipid hybrid nano-formulations (TAA-PLHNPs as well as TAA-PLHNP-ISG) exhibited higher vitreous humor exposure as well as maintained the concentrations of TAA in the vitreous humor for longer duration than compared to the aqueous suspension of TAA with 20% HP-β-CD (TAA-HP-β-CD-Susp).

Out of the various formulations designed in the current research work (TAA-HP-β-CD-Susp, TAA loaded RXG-κ-CRG, TAA nano-formulations [TAA-NCs, TAA-NC-ISG, TAA-PLHNPs and TAA-PLHNP-ISG]), based on the PK parameters obtained from the time course of TAA in the vitreous humor, TAA-PLHNP-ISG provided superior performance in terms of C_{max} (Maximum concentration), AUC_{0-t} (overall exposure) and $MRT_{0-\infty}$ (longer residence time).

The developed TAA nano-formulations are effective in producing therapeutic concentrations of TAA in the vitreous humor. All the developed TAA nano-formulations are suitable for administration as ophthalmic drops in the precorneal area and therefore, they are non-invasive, patient compliant, easy to administer and circumvent all the major side effects associated with the intravitreal injections of TAA which are currently being used in clinical practice. Overall, we can conclude that developed TAA nano-formulations are excellent alternatives to intravitreal injections of the TAA for the treatment of PU.

8

FUTURE SCOPE OF WORK

In this research work, we have designed and evaluated various formulations with the aim of enhancing the vitreous humour availability of TAA upon topical ocular application. Enhanced therapeutic TAA concentrations were produced by the developed nano-formulations loaded in *in situ* gelling system, which was a significant improvement. Quantitative *in vivo* PK studies on rabbits showed that TAA was extensively absorbed through the eyes, especially when administered in nano-formulations. Yet, it is still unknown precisely how NPs are absorbed by this topical route into the posterior segment of the eye. Mechanistic experiments must therefore be carried out to determine the various mechanisms involved in the absorption of drugs or formulations in the treatment of posterior segment disorders. This may make it possible to further optimize various formulations for effective drug absorption into the vitreous humour.

Recently, some devices (contact lenses, microneedles) have been developed specifically to treat ocular infections and anterior segment disorders (glaucoma). Several clinical studies also focus on drug delivery for the treatment of posterior region diseases/disorders. Given the promising outcomes of the recent research (in pre-clinical animals), it is critical to pursue more research aimed at adapting the findings for application in humans. When compared to the traditional intravitreal injections of TAA, this would be tremendously advantageous to the patients. Additionally, it is necessary to investigate the viability of scaling up the production of the aforementioned TAA-NCs and TAA-PLHNPs.

9

BIBLIOGRAPHY

[1] K. Nayak, M. Misra, A review on recent drug delivery systems for posterior segment of eye, Biomedicine & Pharmacotherapy. 107 (2018) 1564–1582. https://doi.org/10.1016/J.BIOPHA.2018.08.138.

[2] B. Tian, E. Bilsbury, S. Doherty, S. Teebagy, E. Wood, W. Su, G. Gao, H. Lin, Ocular Drug Delivery: Advancements and Innovations, Pharmaceutics. 14 (2022). https://doi.org/10.3390/PHARMACEUTICS14091931.

[3] M.F. Adrianto, F. Annuryanti, C.G. Wilson, R. Sheshala, R.R.S. Thakur, In vitro dissolution testing models of ocular implants for posterior segment drug delivery, Drug Deliv Transl Res. 12 (2022) 1355–1375. https://doi.org/10.1007/S13346-021-01043-Z.

[4] V.K. Yellepeddi, S. Palakurthi, Recent Advances in Topical Ocular Drug Delivery, J Ocul Pharmacol Ther. 32 (2016) 67–82. https://doi.org/10.1089/JOP.2015.0047.

[5] A. Santos, J. C. Altamirano-Vallejo, J. Navarro-Partida, A.G.-D. la Rosa, J. H. Hsiao, Breaking down the Barrier: Topical Liposomes as Nanocarriers for Drug Delivery into the Posterior Segment of the Eyeball, Role of Novel Drug Delivery Vehicles in Nanobiomedicine. (2020). https://doi.org/10.5772/INTECHOPEN.86601.

[6] M.R. Robinson, S.S. Lee, H. Kim, S. Kim, R.J. Lutz, C. Galban, P.M. Bungay, P. Yuan, N.S. Wang, J. Kim, K.G. Csaky, A rabbit model for assessing the ocular barriers to the transscleral delivery of triamcinolone acetonide, Exp Eye Res. 82 (2006) 479–487. https://doi.org/10.1016/J.EXER.2005.08.007.

[7] T.W. Olsen, S.Y. Aaberg, D.H. Geroski, H.F. Edelhauser, Human sclera: thickness and surface area, Am J Ophthalmol. 125 (1998) 237–241. https://doi.org/10.1016/S0002-9394(99)80096-8.

[8] E.M. del Amo, Topical ophthalmic administration: Can a drug instilled onto the ocular surface exert an effect at the back of the eye?, Frontiers in Drug Delivery. 2 (2022) 26. https://doi.org/10.3389/FDDEV.2022.954771.

[9] R. Gaudana, H.K. Ananthula, A. Parenky, A.K. Mitra, Ocular drug delivery., AAPS J. 12 (2010) 348–360. https://doi.org/10.1208/s12248-010-9183-3.

[10] V.H.L. Lee, J.R. Robinson, Topical ocular drug delivery: recent developments and future challenges, J Ocul Pharmacol. 2 (1986) 67–108. https://doi.org/10.1089/JOP.1986.2.67.

[11] D. Chang, K. Park, A. Famili, Hydrogels for sustained delivery of biologics to the back of the eye, Drug Discov Today. 24 (2019) 1470–1482. https://doi.org/10.1016/J.DRUDIS.2019.05.037.

[12] M. Mofidfar, B. Abdi, S. Ahadian, E. Mostafavi, T.A. Desai, F. Abbasi, Y. Sun, E.E. Manche, C.N. Ta, C.W. Flowers, Drug delivery to the anterior segment of the eye: A review of current and future treatment strategies, Int J Pharm. 607 (2021) 120924. https://doi.org/10.1016/J.IJPHARM.2021.120924.

[13] R. Gaudana, J. Jwala, S.H.S. Boddu, A.K. Mitra, Recent perspectives in ocular drug delivery, Pharm Res. 26 (2009) 1197–1216. https://doi.org/10.1007/S11095-008-9694-0.

[14] R.J. Barry, Q.D. Nguyen, R. Wlee, P. Imurray, A.K. Denniston, Pharmacotherapy for uveitis: Current management and emerging therapy, Clinical Ophthalmology. 8 (2014) 1891–1911. https://doi.org/10.2147/OPTH.S47778.

[15] C.S. Foster, S. Kothari, S.D. Anesi, A.T. Vitale, D. Chu, J.L. Metzinger, O. Cerón, The Ocular Immunology and Uveitis Foundation preferred practice patterns of uveitis management, Surv Ophthalmol. 61 (2016) 1–17. https://doi.org/10.1016/J.SURVOPHTHAL.2015.07.001.

[16] A.C. Gregory, J.H. Kempen, E. Daniel, R.O. Kaçmaz, C.S. Foster, D.A. Jabs, G.A. Levy-Clarke, R.B. Nussenblatt, J.T. Rosenbaum, E.B. Suhler, J.E. Thorne, Risk Factors for Loss of Visual Acuity among Patients with Uveitis Associated with Juvenile Idiopathic Arthritis: The Systemic Immunosuppressive Therapy for Eye Diseases Study, Ophthalmology. 120 (2013) 186–192. https://doi.org/10.1016/J.OPHTHA.2012.07.052.

[17] P. Lin, E.B. Suhler, J.T. Rosenbaum, The Future of Uveitis Treatment, Ophthalmology. 121 (2014) 365–376. https://doi.org/10.1016/J.OPHTHA.2013.08.029.

[18] J. Li, L. Du, J.N. He, K.O. Chu, C.L. Guo, M.O.M. Wong, C.P. Pang, W.K. Chu, Anti-inflammatory Effects of GTE in Eye Diseases, Front Nutr. 8 (2021). https://doi.org/10.3389/FNUT.2021.753955.

[19] A. Shome, O.O. Mugisho, R.L. Niederer, I.D. Rupenthal, Blocking the inflammasome: A novel approach to treat uveitis, Drug Discov Today. 26 (2021) 2839–2857. https://doi.org/10.1016/J.DRUDIS.2021.06.017.

[20] Y.H. Yücel, M.G. Johnston, T. Ly, M. Patel, B. Drake, E. Gümüş, S.A. Fraenkl, S. Moore, D. Tobbia, D. Armstrong, E. Horvath, N. Gupta, Identification of lymphatics in the ciliary body of the human eye: A novel "uveolymphatic" outflow pathway, Exp Eye Res. 89 (2009) 810–819. https://doi.org/10.1016/J.EXER.2009.08.010.

[21] J. Cunha-Vaz, R. Bernardes, C. Lobo, Blood-Retinal Barrier, 21 (2010) 3–9. https://doi.org/10.5301/EJO.2010.6049.

[22] A.K. Reddy, Y.S. Hwang, E.D. Mandelcorn, J.L. Davis, HLA-DR, DQ class II DNA typing in pediatric panuveitis and tubulointerstitial nephritis and uveitis, Am J Ophthalmol. 157 (2014). https://doi.org/10.1016/J.AJO.2013.12.006.

[23] J. v. Forrester, I.P. Klaska, T. Yu, L. Kuffova, Uveitis in Mouse and Man, 32 (2013) 76–96. https://doi.org/10.3109/08830185.2012.747524.

[24] J.D.F. de Groot-Mijnes, L. de Visser, S. Zuurveen, R.A. Martinus, R. Vlker, N.H. ten Dam-Van Loon, J.H. de Boer, G. Postma, R.J. de Groot, A.M. van Loon, A. Rothova, Identification of New Pathogens in the Intraocular Fluid of Patients With Uveitis, Am J Ophthalmol. 150 (2010) 628–636. https://doi.org/10.1016/J.AJO.2010.05.015.

[25] J. v. Forrester, G.M. Borthwick, Clinical relevance of S-antigen induced experimental uveoretinitis, Trans Ophthalmol Soc U K. 103 (1983) 497–502.

[26] R. Suri, S. Beg, K. Kohli, Target strategies for drug delivery bypassing ocular barriers, J Drug Deliv Sci Technol. 55 (2020) 101389. https://doi.org/10.1016/J.JDDST.2019.101389.

[27] J. Barar, A.R. Javadzadeh, Y. Omidi, Ocular novel drug delivery: impacts of membranes and barriers, Expert Opin Drug Deliv. 5 (2008) 567–581. https://doi.org/10.1517/17425247.5.5.567.

[28] O.A. Boubriak, J.P.G. Urban, S. Akhtar, K.M. Meek, A.J. Bron, The Effect of Hydration and Matrix Composition on Solute Diffusion in Rabbit Sclera, Exp Eye Res. 71 (2000) 503–514. https://doi.org/10.1006/EXER.2000.0909.

[29] J.C. Kao, D.H. Geroski, H.F. Edelhauser, Transscleral permeability of fluorescent-labeled antibiotics, J Ocul Pharmacol Ther. 21 (2005) 1–10. https://doi.org/10.1089/JOP.2005.21.1.

[30] L.P.J. Cruysberg, R.M.M.A. Nuijts, D.H. Geroski, L.H. Koole, F. Hendrikse, H.F. Edelhauser, In vitro human scleral permeability of fluorescein, dexamethasone-fluorescein, methotrexate-fluorescein and rhodamine 6G and the use of a coated coil as a new drug delivery system, J Ocul Pharmacol Ther. 18 (2002) 559–569. https://doi.org/10.1089/108076802321021108.

[31] N.P.S. Cheruvu, U.B. Kompella, Bovine and porcine transscleral solute transport: influence of lipophilicity and the Choroid-Bruch's layer, Invest Ophthalmol Vis Sci. 47 (2006) 4513–4522. https://doi.org/10.1167/IOVS.06-0404.

[32] M.R. Prausnitz, Permeability of cornea, sclera, and conjunctiva: A literature analysis for drug delivery to the eye, J Pharm Sci. 87 (1998) 1479–1488. https://doi.org/10.1021/JS9802594.

[33] I. Ahmed, R.D. Gokhale, M. v. Shah, T.F. Patton, Physicochemical determinants of drug diffusion across the conjunctiva, sclera, and cornea, J Pharm Sci. 76 (1987) 583–586. https://doi.org/10.1002/JPS.2600760802.

[34] L.P.J. Cruysberg, R.M.M.A. Nuijts, D.H. Geroski, J.A. Gilbert, F. Hendrikse, H.F. Edelhauser, The influence of intraocular pressure on the transscleral diffusion of high-molecular-weight compounds, Invest Ophthalmol Vis Sci. 46 (2005) 3790–3794. https://doi.org/10.1167/iovs.04-1414.

[35] T.L. Jackson, A. Hussain, A. Hodgetts, A.M.S. Morley, J. Hillenkamp, P.M. Sullivan, J. Marshall, Human scleral hydraulic conductivity: Age-related changes, topographical variation, and potential scleral outflow facility, Invest Ophthalmol Vis Sci. 47 (2006) 4942–4946. https://doi.org/10.1167/iovs.06-0362.

[36] R.D. Schoenwald, V. Tandon, D.E. Wurster, C.F. Barfknecht, Significance of melanin binding and metabolism in the activity of 5-acetoxyacetylimino-4-methyl-delta2-1,3,4,-thiadiazolin e-2-sulfonamide, Eur J Pharm Biopharm. 46 (1998) 39–50. https://doi.org/10.1016/S0939-6411(97)00166-5.

[37] B. Leblanc, S. Jezequel, T. Davies, G. Hanton, C. Taradach, Binding of drugs to eye melanin is not predictive of ocular toxicity, Regul Toxicol Pharmacol. 28 (1998) 124–132. https://doi.org/10.1006/RTPH.1998.1243.

[38] L. Salminen, G. Imre, R. Huupponen, The effect of ocular pigmentation on intraocular pressure response to timolol, Acta Ophthalmol Suppl (Oxf). 173 (1985) 15–18. https://doi.org/10.1111/J.1755-3768.1985.TB06829.X.

[39] L. Pitkänen, V.P. Ranta, H. Moilanen, A. Urtti, Binding of betaxolol, metoprolol and oligonucleotides to synthetic and bovine ocular melanin, and prediction of drug binding to melanin in human choroid-retinal pigment epithelium, Pharm Res. 24 (2007) 2063–2070. https://doi.org/10.1007/S11095-007-9342-0.

[40] I.K. Gipson, P. Argüeso, Role of mucins in the function of the corneal and conjunctival epithelia, Int Rev Cytol. 231 (2003) 1–49. https://doi.org/10.1016/S0074-7696(03)31001-0.

[41] A. Subrizi, E.M. del Amo, V. Korzhikov-Vlakh, T. Tennikova, M. Ruponen, A. Urtti, Design principles of ocular drug delivery systems: importance of drug payload, release rate, and material properties, Drug Discov Today. 24 (2019) 1446–1457. https://doi.org/10.1016/J.DRUDIS.2019.02.001.

[42] P. Ashton, S.K. Podder, V.H.L. Lee, Formulation Influence on Conjunctival Penetration of Four Beta Blockers in the Pigmented Rabbit: A Comparison with Corneal Penetration, Pharmaceutical Research: An Official Journal of the American Association of Pharmaceutical Scientists. 8 (1991) 1166–1174. https://doi.org/10.1023/A:1015810619869.

[43] A. Patel, K. Cholkar, V. Agrahari, A.K. Mitra, Ocular drug delivery systems: An overview, World J Pharmacol. 2 (2013) 47. https://doi.org/10.5497/WJP.V2.I2.47.

[44] N. Djebli, S. Khier, F. Griguer, A.L. Coutant, A. Tavernier, G. Fabre, C. Leriche, D. Fabre, Ocular Drug Distribution After Topical Administration: Population Pharmacokinetic Model in Rabbits, Eur J Drug Metab Pharmacokinet. 42 (2017) 59. https://doi.org/10.1007/S13318-016-0319-4.

[45] J.S. Ng, Ocular Anatomy and Physiology (2nd ed.), Optometry and Vision Science. 86 (2009) 1208. https://doi.org/10.1097/OPX.0B013E3181BAFCA3.

[46] V. Agrahari, A. Mandal, V. Agrahari, H.M. Trinh, M. Joseph, A. Ray, H. Hadji, R. Mitra, D. Pal, A.K. Mitra, A comprehensive insight on ocular pharmacokinetics, Drug Deliv Transl Res. 6 (2016) 735–754. https://doi.org/10.1007/S13346-016-0339-2.

[47] G. Smolin, R.A. Hyndiuk, Lymphatic drainage from vascularized rabbit cornea, Am J Ophthalmol. 72 (1971) 147–151. https://doi.org/10.1016/0002-9394(71)91605-9.

[48] A.C. Amrite, U.B. Kompella, Size-dependent disposition of nanoparticles and microparticles following subconjunctival administration, J Pharm Pharmacol. 57 (2005) 1555–1563. https://doi.org/10.1211/JPP.57.12.0005.

[49] C.B. Toris, M.E. Yablonski, Y.L. Wang, C.B. Camras, Aqueous humor dynamics in the aging human eye, Am J Ophthalmol. 127 (1999) 407–412. https://doi.org/10.1016/S0002-9394(98)00436-X.

[50] A. Bill, A method to determine osmotically effective albumin and gammaglobulin concentrations in tissue fluids, its application to the uvea and a note on the effects of capillary “leaks” on tissue fluid dynamics, Acta Physiol Scand. 73 (1968) 511–522. https://doi.org/10.1111/J.1365-201X.1968.TB10890.X.

[51] A. Bill, Blood circulation and fluid dynamics in the eye, Physiol Rev. 55 (1975) 383–417. https://doi.org/10.1152/PHYSREV.1975.55.3.383.

[52] P.A. Constable, J.G. Lawrenson, D.E.M. Dolman, G.B. Arden, N.J. Abbott, P-Glycoprotein expression in human retinal pigment epithelium cell lines, Exp Eye Res. 83 (2006) 24–30. https://doi.org/10.1016/J.EXER.2005.10.029.

[53] H. Steuer, A. Jaworski, B. Elger, M. Kaussmann, J. Keldenich, H. Schneider, D. Stoll, B. Schlosshauer, Functional characterization and comparison of the outer blood-retina barrier and the blood-brain barrier, Invest Ophthalmol Vis Sci. 46 (2005) 1047–1053. https://doi.org/10.1167/IOVS.04-0925.

[54] N. Zhang, R. Kannan, C.T. Okamoto, S.J. Ryan, V.H.L. Lee, D.R. Hinton, Characterization of Brimonidine Transport in Retinal Pigment Epithelium, Invest Ophthalmol Vis Sci. 47 (2006) 287–294. https://doi.org/10.1167/IOVS.05-0189.

[55] A. Kumari, S.K. Yadav, S.C. Yadav, Biodegradable polymeric nanoparticles based drug delivery systems, Colloids Surf B Biointerfaces. 75 (2010) 1–18. https://doi.org/10.1016/J.COLSURFB.2009.09.001.

[56] P. Dhananjay, V. Ramya Krishna, V. Aswani Dutt, A.K. Mitra, Biology of ocular transporters: efflux and influx transporters in the eye, Ocular Transporters and Receptors: Their Role in Drug Delivery. (2013) 37–84. https://doi.org/10.1533/9781908818317.37.

[57] S. Robertson, S. Penzak, Drug Interactions, Principles of Clinical Pharmacology. (2007) 229–247. https://doi.org/10.1016/B978-012369417-1/50055-9.

[58] D.R. Janagam, L. Wu, T.L. Lowe, Nanoparticles for drug delivery to the anterior segment of the eye, Adv Drug Deliv Rev. 122 (2017) 31–64. https://doi.org/10.1016/J.ADDR.2017.04.001.

[59] H.H. Sigurdsson, F. Konrádsdóttir, T. Loftsson, E. Stefánsson, Topical and systemic absorption in delivery of dexamethasone to the anterior and posterior segments of the eye, Acta Ophthalmol Scand. 85 (2007) 598–602. https://doi.org/10.1111/J.1600-0420.2007.00885.X.

[60] P.M. Hughes, O. Olejnik, J.E. Chang-Lin, C.G. Wilson, Topical and systemic drug delivery to the posterior segments, Adv Drug Deliv Rev. 57 (2005) 2010–2032. https://doi.org/10.1016/J.ADDR.2005.09.004.

[61] D.H. Geroski, H.F. Edelhauser, Drug delivery for posterior segment eye disease, Invest Ophthalmol Vis Sci. 41 (2000) 961–964.

[62] I. Ahmed, T.F. Patton, Importance of the noncorneal absorption route in topical ophthalmic drug delivery, Invest Ophthalmol Vis Sci. 26 (1985) 584–587.

[63] M. Löscher, C. Seiz, J. Hurst, S. Schnichels, Topical Drug Delivery to the Posterior Segment of the Eye, Pharmaceutics 2022, Vol. 14, Page 134. 14 (2022) 134. https://doi.org/10.3390/PHARMACEUTICS14010134.

[64] V. Sarao, D. Veritti, F. Boscia, P. Lanzetta, Intravitreal steroids for the treatment of retinal diseases, The Scientific World Journal. 2014 (2014). https://doi.org/10.1155/2014/989501.

[65] M. Inoue, K. Takeda, K. Morita, M. Yamada, Y. Tanigawara, Y. Oguchi, Vitreous concentrations of triamcinolone acetonide in human eyes after intravitreal or subtenon injection, Am J Ophthalmol. 138 (2004) 1046–1048. https://doi.org/10.1016/J.AJO.2004.05.028.

[66] T.W.P. Lee, J.R. Robinson, Drug Delivery to the Posterior Segment of the Eye: Some Insights on the Penetration Pathways after Subconjunctival Injection, Https://Home.Liebertpub.Com/Jop. 17 (2004) 565–572. https://doi.org/10.1089/10807680152729257.

[67] V.P. Ranta, E. Mannermaa, K. Lummepuro, A. Subrizi, A. Laukkanen, M. Antopolsky, L. Murtomäki, M. Hornof, A. Urtti, Barrier analysis of periocular drug delivery to the posterior segment, Journal of Controlled Release. 148 (2010) 42–48. https://doi.org/10.1016/J.JCONREL.2010.08.028.

[68] H. Kim, M.R. Robinson, M.J. Lizak, G. Tansey, R.J. Lutz, P. Yuan, N.S. Wang, K.G. Csaky, Controlled drug release from an ocular implant: An evaluation using dynamic three-dimensional magnetic resonance imaging, Invest Ophthalmol Vis Sci. 45 (2004) 2722–2731. https://doi.org/10.1167/IOVS.04-0091.

[69] A. Urtti, J.D. Pipkin, G. Rork, A.J. Repta, Controlled drug delivery devices for experimental ocular studies with timolol 1. In vitro release studies, Int J Pharm. 61 (1990) 235–240. https://doi.org/10.1016/0378-5173(90)90214-O.

[70] H.H. Shen, E.C. Chan, J.H. Lee, Y.S. Bee, T.W. Lin, G.J. Dusting, G.S. Liu, Nanocarriers for treatment of ocular neovascularization in the back of the eye: New vehicles for ophthalmic drug delivery, Nanomedicine. 10 (2015) 2093–2107. https://doi.org/10.2217/NNM.15.47/ASSET/IMAGES/LARGE/FIGURE4.JPEG.

[71] C.M. Jermak, J.T. Dellacroce, J. Heffez, G.A. Peyman, Triamcinolone acetonide in ocular therapeutics, Surv Ophthalmol. 52 (2007) 503–522. https://doi.org/10.1016/J.SURVOPHTHAL.2007.06.004.

[72] G.A. Peyman, R. Herbst, Bacterial endophthalmitis. Treatment with intraocular injection of gentamicin and dexamethasone, Arch Ophthalmol. 91 (1974) 416–418. https://doi.org/10.1001/ARCHOPHT.1974.03900060428017.

[73] D.A. Jabs, J.T. Rosenbaum, C.S. Foster, G.N. Holland, G.J. Jaffe, J.S. Louie, R.B. Nussenblatt, E.R. Stiehm, H. Tessler, R.N. van Gelder, S.M. Whitcup, D. Yocum, Guidelines for the use of immunosuppressive drugs in patients with ocular inflammatory disorders: recommendations of an expert panel, Am J Ophthalmol. 130 (2000) 492–513. https://doi.org/10.1016/S0002-9394(00)00659-0.

[74] S.R.J. Taylor, H. Isa, L. Joshi, S. Lightman, New Developments in Corticosteroid Therapy for Uveitis, Ophthalmologica. 224 (2010) 46–53. https://doi.org/10.1159/000318021.

[75] R. José-Vieira, A. Ferreira, P. Menéres, B. Sousa-Pinto, L. Figueira, Efficacy and safety of intravitreal and periocular injection of corticosteroids in noninfectious uveitis: a systematic review, Surv Ophthalmol. 67 (2022) 991–1013. https://doi.org/10.1016/J.SURVOPHTHAL.2021.12.002.

[76] T.L. Comstock, H.H. Decory, Advances in corticosteroid therapy for ocular inflammation: Loteprednol etabonate, Int J Inflam. 2012 (2012). https://doi.org/10.1155/2012/789623.

[77] K. Babu, P. Mahendradas, Medical Management of Uveitis – Current Trends, Indian J Ophthalmol. 61 (2013) 277. https://doi.org/10.4103/0301-4738.114099.

[78] G.M. Fernandes-Cunha, J.B. Saliba, R.C. Siqueira, R. Jorge, A. Silva-Cunha, Determination of triamcinolone acetonide in silicone oil and aqueous humor of vitrectomized rabbits' eyes: Application for a pharmacokinetic study with intravitreal triamcinolone acetonide injections (Kenalog® 40), J Pharm Biomed Anal. 89 (2014) 24–27. https://doi.org/10.1016/j.jpba.2013.10.025.

[79] A.T. Fung, T. Tran, L.L. Lim, C. Samarawickrama, J. Arnold, M. Gillies, C. Catt, L. Mitchell, A. Symons, R. Buttery, L. Cottee, K. Tumuluri, P. Beaumont, Local delivery of corticosteroids in clinical ophthalmology: A review, Clin Exp Ophthalmol. 48 (2020) 366–401. https://doi.org/10.1111/ceo.13702.

[80] L.F.C. Silva, E. Lemos-Senna, Development of triamcinolone acetonide-loaded nanoemulsion for ophthalmic drug delivery, Latin American Journal of Pharmacy. 35 (2016) 2159–2168.

[81] Y. Tao, J.B. Jonas, Intravitreal triamcinolone, Ophthalmologica. 225 (2011) 1–20. https://doi.org/10.1159/000317909.

[82] A.J.P. van Heugten, W. de Boer, W.S. de Vries, C.M.A. Markesteijn, H. Vromans, Development and validation of a stability-indicating HPLC-UV method for the determination of triamcinolone acetonide and its degradation products in an ointment formulation, J Pharm Biomed Anal. 149 (2018) 265–270. https://doi.org/10.1016/J.JPBA.2017.11.026.

[83] S.Q. Zhang, Quantification of triamcinolone acetonide in ocular tissues after intravitreal injection to rabbit using liquid chromatography-tandem mass spectrometry, J Chromatogr B Analyt Technol Biomed Life Sci. 879 (2011) 548–552. https://doi.org/10.1016/j.jchromb.2011.01.012.

[84] M.S. Khan, P.R. Ravi, T.V.R.K. Mullapudi, Dose identification of triamcinolone acetonide for noninvasive pre-corneal administration in the treatment of posterior uveitis using a rapid, sensitive HPLC method with photodiode-array detector, Biomed Chromatogr. 36 (2022). https://doi.org/10.1002/BMC.5264.

[85] S.D. Reichardt, A. Amouret, C. Muzzi, S. Vettorazzi, J.P. Tuckermann, F. Lühder, H.M. Reichardt, The Role of Glucocorticoids in Inflammatory Diseases, Cells 2021, Vol. 10, Page 2921. 10 (2021) 2921. https://doi.org/10.3390/CELLS10112921.

[86] A. Daruich, A. Matet, F. Behar-Cohen, Corticosteroids, Encyclopedia of Ophthalmology. (2018) 540–545. https://doi.org/10.1007/978-3-540-69000-9_1131.

[87] H. Derendorf, G. Hochhaus, S. Rohatagi, H. Möllmann, J. Barth, H. Sourgens, M. Erdmann, Pharmacokinetics of Triamcinolone Acetonide After Intravenous, Oral, and Inhaled Administration, The Journal of Clinical Pharmacology. 35 (1995) 302–305. https://doi.org/10.1002/j.1552-4604.1995.tb04064.x.

[88] D. Argenti, B.K. Jensen, R. Hensel, K. Bordeaux, R. Schleimer, C. Bickel, D. Heald, A mass balance study to evaluate the biotransformation and excretion of [14C]-triamcinolone acetonide following oral administration, J Clin Pharmacol. 40 (2000) 770–780. https://doi.org/10.1177/00912700022009413.

[89] Y.F. Ye, Y.F. Gao, H.T. Xie, H.J. Wang, Pharmacokinetics and retinal toxicity of various doses of intravitreal triamcinolone acetonide in rabbits, Mol Vis. 20 (2014) 629–636. http://www.molvis.org/molvis/v20/629 (accessed March 10, 2021).

[90] H.S. Chin, T.S. Park, Y.S. Moon, J.H. Oh, Difference in clearance of intravitreal triamcinolone acetonide between vitrectomized and nonvitrectomized eyes, Retina. 25 (2005) 556–560. https://doi.org/10.1097/00006982-200507000-00002.

[91] H. Kim, K.G. Csaky, L. Gravlin, P. Yuan, R.J. Lutz, P.M. Bungay, G. Tansey, F. De Monasterio, G.K. Potti, G. Grimes, M.R. Robinson, Safety and pharmacokinetics of a preservative-free triamcinolone acetonide formulation for intravitreal administration, Retina. 26 (2006) 523–530. https://doi.org/10.1097/00006982-200605000-00005.

[92] K. Nan, S. Sun, Y. Li, J. Qu, G. Li, L. Luo, H. Chen, L. Cheng, Characterisation of systemic and ocular drug level of triamcinolone acetonide following a single sub-Tenon

injection, Br J Ophthalmol. 94 (2010) 654–658. https://doi.org/10.1136/BJO.2009.172106.

[93] M. Abrishami, S. Zarei-Ghanavati, D. Soroush, M. Rouhbakhsh, M.R. Jaafari, B. Malaekeh-Nikouei, Preparation, characterization, and in vivo evaluation of nanoliposomes-encapsulated bevacizumab (avastin) for intravitreal administration, Retina. 29 (2009) 699–703. https://doi.org/10.1097/IAE.0B013E3181A2F42A.

[94] K. Nayak, M. Misra, A review on recent drug delivery systems for posterior segment of eye, Biomedicine & Pharmacotherapy. 107 (2018) 1564–1582. https://doi.org/10.1016/J.BIOPHA.2018.08.138.

[95] T. Loftsson, E. Stefánsson, Cyclodextrins and topical drug delivery to the anterior and posterior segments of the eye, Int J Pharm. 531 (2017) 413–423. https://doi.org/10.1016/J.IJPHARM.2017.04.010.

[96] J.K. Patel, V. Sutariya, J.R. Kanwar, Y. V. Pathak, Drug delivery for the retina and posterior segment disease, Drug Delivery for the Retina and Posterior Segment Disease. (2018) 1–494. https://doi.org/10.1007/978-3-319-95807-1/COVER.

[97] A. Thareja, H. Hughes, C. Alvarez-Lorenzo, J.J. Hakkarainen, Z. Ahmed, R. Herrero-Vanrell, pharmaceutics Penetration Enhancers for Topical Drug Delivery to the Ocular Posterior Segment-A Systematic Review, (2021). https://doi.org/10.3390/pharmaceutics13020276.

[98] S. Johannsdottir, P. Jansook, E. Stefansson, I.M. Kristinsdottir, Z. Fulop, G.M. Asgrimsdottir, M. Thorsteindsottir, F.F. Eiriksson, T. Loftsson, Topical drug delivery to the posterior segment of the eye: Dexamethasone concentrations in various eye tissues after topical administration for up to 15 days to rabbits, J Drug Deliv Sci Technol. 45 (2018) 449–454. https://doi.org/10.1016/J.JDDST.2018.04.007.

[99] T. Tajika, A. Isowaki, H. Sakaki, Ocular distribution of difluprednate ophthalmic emulsion 0.05% in rabbits, J Ocul Pharmacol Ther. 27 (2011) 43–49. https://doi.org/10.1089/JOP.2010.0093.

[100] K. Nayak, M. Misra, Triamcinolone Acetonide-Loaded PEGylated Microemulsion for the Posterior Segment of Eye, ACS Omega. 5 (2020) 7928–7939. https://doi.org/10.1021/ACSOMEGA.9B04244/SUPPL_FILE/AO9B04244_SI_001.PDF.

[101] M. Konatham, M.T. Gorle, N. Pathakala, V. Bakshi, Y.D. Mamidisetti, P. Chinthakindi, R.K. Jadi, In situ gel polymers: A review, International Journal of Applied Pharmaceutics. 13 (2021) 86–90. https://doi.org/10.22159/ijap.2021v13i1.39504.

[102] D.Y. Ko, U.P. Shinde, B. Yeon, B. Jeong, Recent progress of in situ formed gels for biomedical applications, Prog Polym Sci. 38 (2013) 672–701. https://doi.org/10.1016/j.progpolymsci.2012.08.002.

[103] R.C. Nagarwal, S. Kant, P.N. Singh, P. Maiti, J.K. Pandit, Polymeric nanoparticulate system: A potential approach for ocular drug delivery, Journal of Controlled Release. 136 (2009) 2–13. https://doi.org/10.1016/J.JCONREL.2008.12.018.

[104] E. Eljarrat-Binstock, J. Pe'er, A.J. Domb, New techniques for drug delivery to the posterior eye segment, Pharm Res. 27 (2010) 530–543. https://doi.org/10.1007/S11095-009-0042-9/TABLES/4.

[105] K. Tahara, K. Karasawa, R. Onodera, H. Takeuchi, Feasibility of drug delivery to the eye's posterior segment by topical instillation of PLGA nanoparticles, Asian J Pharm Sci. 12 (2017) 394–399. https://doi.org/10.1016/J.AJPS.2017.03.002.

[106] J. Araújo, S. Nikolic, M.A. Egea, E.B. Souto, M.L. Garcia, Nanostructured lipid carriers for triamcinolone acetonide delivery to the posterior segment of the eye, Colloids Surf B Biointerfaces. 88 (2011) 150–157. https://doi.org/10.1016/J.COLSURFB.2011.06.025.

[107] P. Nirbhavane, G. Sharma, B. Singh, G. Begum, M.C. Jones, S. Rauz, R. Vincent, A.K. Denniston, L.J. Hill, O.P. Katare, Triamcinolone acetonide loaded-cationic nano-lipoidal formulation for uveitis: Evidences of improved biopharmaceutical performance and anti-inflammatory activity, Colloids Surf B Biointerfaces. 190 (2020) 110902. https://doi.org/10.1016/J.COLSURFB.2020.110902.

[108] M.L. Formica, G. V. Ullio Gamboa, L.I. Tártara, J.D. Luna, J.P. Benoit, S.D. Palma, Triamcinolone acetonide-loaded lipid nanocapsules for ophthalmic applications, Int J Pharm. 573 (2020) 118795. https://doi.org/10.1016/J.IJPHARM.2019.118795.

[109] M. Khalil, U. Hashmi, R. Riaz, S. Rukh Abbas, Chitosan coated liposomes (CCL) containing triamcinolone acetonide for sustained delivery: A potential topical treatment for posterior segment diseases, Int J Biol Macromol. 143 (2020) 483–491. https://doi.org/10.1016/J.IJBIOMAC.2019.10.256.

[110] K. Cholkar, S. Gunda, R. Earla, D. Pal, A.K. Mitra, Nanomicellar Topical Aqueous Drop Formulation of Rapamycin for Back-of-the-Eye Delivery, AAPS PharmSciTech. 16 (2015) 610–622. https://doi.org/10.1208/S12249-014-0244-2/FIGURES/9.

[111] B.M. Davis, E.M. Normando, L. Guo, L.A. Turner, S. Nizari, P. O'Shea, S.E. Moss, S. Somavarapu, M.F. Cordeiro, Topical Delivery of Avastin to the Posterior Segment of the Eye In Vivo Using Annexin A5-associated Liposomes, Small. 10 (2014) 1575–1584. https://doi.org/10.1002/SMLL.201303433.

[112] Formulation and Evaluation of Betamethasone Sodium Phosphate Loaded Nanoparticles for Ophthalmic Delivery, (n.d.). https://www.longdom.org/open-access/betamethasone-sodium-phosphate-loaded-nanoparticles-for-ophthalmic-delivery-2155-9570.1000273.pdf (accessed March 11, 2023).

[113] R. Gonzalez-Pizarro, P. Carvajal-Vidal, L. Halbault Bellowa, A.C. Calpena, M. Espina, M.L. García, In-situ forming gels containing fluorometholone-loaded polymeric nanoparticles for ocular inflammatory conditions, Colloids Surf B Biointerfaces. 175 (2019) 365–374. https://doi.org/10.1016/J.COLSURFB.2018.11.065.

[114] G. Esteruelas, L. Halbaut, V. García-Torra, M. Espina, A. Cano, M. Ettcheto, A. Camins, E.B. Souto, M. Luisa García, E. Sánchez-López, Development and optimization of Riluzole-loaded biodegradable nanoparticles incorporated in a mucoadhesive in situ gel for the posterior eye segment, Int J Pharm. 612 (2022). https://doi.org/10.1016/J.IJPHARM.2021.121379.

[115] T.A. Ahmed, M.M. Alzahrani, A. Sirwi, N.A. Alhakamy, F. Craparo, pharmaceutics Study the Antifungal and Ocular Permeation of Ketoconazole from Ophthalmic Formulations Containing Trans-Ethosomes Nanoparticles, (2021). https://doi.org/10.3390/pharmaceutics13020151.

[116] A. Tatke, N. Dudhipala, K.Y. Janga, S.P. Balguri, B. Avula, M.M. Jablonski, S. Majumdar, In situ gel of triamcinolone acetonide-loaded solid lipid nanoparticles for

improved topical ocular delivery: Tear kinetics and ocular disposition studies, Nanomaterials. 9 (2019). https://doi.org/10.3390/nano9010033.

[117] V.M. Villegas, A.S. Gold, A. Wildner, A. Latiff, T.G. Murray, Intravitreal triamcinolone acetonide: a “real world” analysis of visual acuity, pressure and outcomes, Int J Ophthalmol. 9 (2016) 789. https://doi.org/10.18240/IJO.2016.05.26.

[118] P.H. Kalina, J.C. Erie, L. Rosenbaum, Biochemical quantification of triamcinolone in subconjunctival depots, Arch Ophthalmol. 113 (1995) 867–869. https://doi.org/10.1001/ARCHOPHT.1995.01100070041022.

[119] T. Leng, Preventing Intraocular Infections after Intravitreal Injections: Injection Technique, Clinical Microbiology: Open Access. 02 (2012). https://doi.org/10.4172/2327-5073.1000118.

[120] B.J. Holmberg, D.J. Maggs, The use of corticosteroids to treat ocular inflammation, Veterinary Clinics of North America - Small Animal Practice. 34 (2004) 693–705. https://doi.org/10.1016/j.cvsm.2003.12.007.

[121] F. Bongiovì, G. di Prima, F.S. Palumbo, M. Licciardi, G. Pitarresi, G. Giammona, Hyaluronic Acid-Based Micelles as Ocular Platform to Modulate the Loading, Release, and Corneal Permeation of Corticosteroids, Macromol Biosci. 17 (2017). https://doi.org/10.1002/MABI.201700261.

[122] S. Patel, C. Garapati, P. Chowdhury, H. Gupta, J. Nesamony, S. Nauli, S.H.S. Boddu, Development and evaluation of dexamethasone nanomicelles with potential for treating posterior uveitis after topical application, J Ocul Pharmacol Ther. 31 (2015) 215–227. https://doi.org/10.1089/JOP.2014.0152.

[123] H.H. Sigurdsson, F. Konrádsdóttir, T. Loftsson, E. Stefánsson, Topical and systemic absorption in delivery of dexamethasone to the anterior and posterior segments of the eye, Acta Ophthalmol Scand. 85 (2007) 598–602. https://doi.org/10.1111/J.1600-0420.2007.00885.X.

[124] T. Loftsson, D. Hreinsdóttir, E. Stefánsson, Cyclodextrin microparticles for drug delivery to the posterior segment of the eye: aqueous dexamethasone eye drops, J Pharm Pharmacol. 59 (2007) 629–635. https://doi.org/10.1211/JPP.59.5.0002.

[125] A.J.P. van Heugten, W. de Boer, W.S. de Vries, C.M.A. Markesteijn, H. Vromans, Development and validation of a stability-indicating HPLC-UV method for the determination of triamcinolone acetonide and its degradation products in an ointment formulation, J Pharm Biomed Anal. 149 (2018) 265–270. https://doi.org/10.1016/j.jpba.2017.11.026.

[126] O. Weijtens, R.C. Schoemaker, A.F. Cohen, F.P. h. t. m. Romijn, E.G. w. m. Lentjes, J. Van Rooij, J.C. Van Meurs, Dexamethasone concentration in vitreous and serum after oral administration, Am J Ophthalmol. 125 (1998) 673–679. https://doi.org/10.1016/S0002-9394(98)00003-8.

[127] J.B. Jonas, R. Degenring, U. Vossmerbauemer, B. Kamppeter, Frequency of cataract surgery after intravitreal injection of high-dosage triamcinolone acetonide, Eur J Ophthalmol. 15 (2005) 462–464. https://doi.org/10.1177/112067210501500407.

[128] M.C. Gillies, M. Kuzniarz, J. Craig, M. Ball, W. Luo, J.M. Simpson, Intravitreal triamcinolone-induced elevated intraocular pressure is associated with the development

of posterior subcapsular cataract, Ophthalmology. 112 (2005) 139–143. https://doi.org/10.1016/j.ophtha.2004.07.017.

[129] Y.K. Chu, E.J. Chung, O.W. Kwon, J.H. Lee, H.J. Koh, Objective evaluation of cataract progression associated with a high dose intravitreal triamcinolone injection, Eye. 22 (2008) 895–899. https://doi.org/10.1038/sj.eye.6702802.

[130] P. Nirbhavane, G. Sharma, B. Singh, G. Begum, M.C. Jones, S. Rauz, R. Vincent, A.K. Denniston, L.J. Hill, O.P. Katare, Triamcinolone acetonide loaded-cationic nano-lipoidal formulation for uveitis: Evidences of improved biopharmaceutical performance and anti-inflammatory activity, Colloids Surf B Biointerfaces. 190 (2020) 110902. https://doi.org/10.1016/j.colsurfb.2020.110902.

[131] M.L. Formica, G. V. Ullio Gamboa, L.I. Tártara, J.D. Luna, J.P. Benoit, S.D. Palma, Triamcinolone acetonide-loaded lipid nanocapsules for ophthalmic applications, Int J Pharm. 573 (2020) 118795. https://doi.org/10.1016/j.ijpharm.2019.118795.

[132] G. Di Prima, M. Licciardi, F. Carfì Pavia, A.I. Lo Monte, G. Cavallaro, G. Giammona, Microfibrillar polymeric ocular inserts for triamcinolone acetonide delivery, Int J Pharm. 567 (2019) 118459. https://doi.org/10.1016/j.ijpharm.2019.118459.

[133] R.C. Oliveira, A. Messias, R.C. Siqueira, M.A. Bonini-Filho, A. Haddad, F.M. Damico, A. Maia-Filho, P.T. Crispim, J.B. Saliba, J.A.S. Ribeiro, I.U. Scott, A.S. Cunha-Jr, R. Jorge, Vitreous pharmacokinetics and retinal safety of intravitreal preserved versus non-preserved triamcinolone acetonide in rabbit eyes, Curr Eye Res. 37 (2012) 55–61. https://doi.org/10.3109/02713683.2011.593722.

[134] O.A.E.A. Soliman, E.A.M. Mohamed, M.S. El-Dahan, N.A.A. Khatera, Potential Use of Cyclodextrin Complexes for Enhanced Stability, Anti-inflammatory Efficacy, and Ocular Bioavailability of Loteprednol Etabonate, AAPS PharmSciTech. 18 (2017) 1228–1241. https://doi.org/10.1208/s12249-016-0589-9.

[135] T. Loftsson, E. Stefánsson, Cyclodextrins in eye drop formulations: Enhanced topical delivery of corticosteroids to the eye, Acta Ophthalmol Scand. 80 (2002) 144–150. https://doi.org/10.1034/j.1600-0420.2002.800205.x.

[136] T. Loftsson, E. Stefánsson, Cyclodextrins and topical drug delivery to the anterior and posterior segments of the eye, Int J Pharm. 531 (2017) 413–423. https://doi.org/10.1016/j.ijpharm.2017.04.010.

[137] T. Loftssona, T. Järvinen, Cyclodextrins in ophthalmic drug delivery, Adv Drug Deliv Rev. 36 (1999) 59–79. https://doi.org/10.1016/S0169-409X(98)00055-6.

[138] J. Qu, Y. Qu, R.M. Straubinger, Ultra-sensitive quantification of corticosteroids in plasma samples using selective solid-phase extraction and reversed-phase capillary high-performance liquid chromatography/tandem mass spectrometry, Anal Chem. 79 (2007) 3786–3793. https://doi.org/10.1021/ac062184r.

[139] H. Liu, M. Yang, P. Wu, J. Guan, L. Men, H. Lin, X. Tang, Y. Zhao, Z. Yu, Simultaneous determination of triamcinolone acetonide palmitate and triamcinolone acetonide in beagle dog plasma by UPLC-MS/MS and its application to a long-term pharmacokinetic study of triamcinolone acetonide palmitate lipid emulsion injection, J Pharm Biomed Anal. 104 (2015) 105–111. https://doi.org/10.1016/j.jpba.2014.11.028.

[140] W. Sun, S. Ho, X.R. Fang, T. O'Shea, H. Liu, Simultaneous determination of triamcinolone hexacetonide and triamcinolone acetonide in rabbit plasma using a highly sensitive and selective UPLC–MS/MS method, J Pharm Biomed Anal. 153 (2018) 267–273. https://doi.org/10.1016/j.jpba.2018.02.052.

[141] J. Haneef, M. Shaharyar, A. Husain, M. Rashid, R. Mishra, S. Parveen, N. Ahmed, M. Pal, D. Kumar, Application of LC–MS/MS for quantitative analysis of glucocorticoids and stimulants in biological fluids, J Pharm Anal. 3 (2013) 341–348. https://doi.org/10.1016/J.JPHA.2013.03.005.

[142] T. A, S. VK, F. S, L. D, F. J, Simultaneous determination of eight corticosteroids in bovine tissues using liquid chromatography-tandem mass spectrometry, J Chromatogr B Analyt Technol Biomed Life Sci. 906 (2012) 75–84. https://doi.org/10.1016/J.JCHROMB.2012.08.033.

[143] T. A, S. VK, K. L, F. J, Quantification of corticosteroids in bovine urine using selective solid phase extraction and reversed-phase liquid chromatography/tandem mass spectrometry, J Chromatogr B Analyt Technol Biomed Life Sci. 878 (2010) 1471–1479. https://doi.org/10.1016/J.JCHROMB.2010.03.041.

[144] A. JH, H. LG, P. M, Optimization of solid phase extraction clean up and validation of quantitative determination of corticosteroids in urine by liquid chromatography-tandem mass spectrometry, Anal Chim Acta. 617 (2008) 216–224. https://doi.org/10.1016/J.ACA.2008.02.070.

[145] T. RL, G. SK, S. RJ, Quantitative, highly sensitive liquid chromatography-tandem mass spectrometry method for detection of synthetic corticosteroids, Clin Chem. 50 (2004) 2345–2352. https://doi.org/10.1373/CLINCHEM.2004.033605.

[146] H. Derendorf, P. Rohdewald, G. Hochhaus, H. Möllmann, HPLC determination of glucocorticoid alcohols, their phosphates and hydrocortisone in aqueous solutions and biological fluids, J Pharm Biomed Anal. 4 (1986) 197–206. https://doi.org/10.1016/0731-7085(86)80042-5.

[147] S.A. Döppenschmitt, B. Scheidel, F. Harrison, J.P. Surmann, Simultaneous determination of triamcinolone acetonide and hydrocortisone in human plasma by high-performance liquid chromatography, J Chromatogr B Biomed Appl. 682 (1996) 79–88. https://doi.org/10.1016/0378-4347(96)00060-6.

[148] M. de L.T. Vieira, R.P. Singh, H. Derendorf, Simultaneous HPLC analysis of triamcinolone acetonide and budesonide in microdialysate and rat plasma: Application to a pharmacokinetic study, J Chromatogr B Analyt Technol Biomed Life Sci. 878 (2010) 2967–2973. https://doi.org/10.1016/j.jchromb.2010.08.048.

[149] R. Karki, M. Meena, T. Prakash, T. Rajeswari, D. Goli, S. Kumar, Reduction in drop size of ophthalmic topical drop preparations and the impact of treatment, J Adv Pharm Technol Res. 2 (2011) 192. https://doi.org/10.4103/2231-4040.85540.

[150] Fda, Cder, Bioanalytical Method Validation Guidance for Industry Biopharmaceutics Bioanalytical Method Validation Guidance for Industry Biopharmaceutics Contains Nonbinding Recommendations, 2018.

[151] J. Stjernschantz, M. Astin, Anatomy and Physiology of the Eye. Physiological Aspects of Ocular Drug Therapy, Biopharmaceutics of Ocular Drug Delivery. (2019) 1–25. https://doi.org/10.1201/9780429284755-1.

[152] S. Rohatagi, G. Hochhaus, H. Möllmann, J. Barth, E. Galia, M. Erdmann, H. Sourgens, H. Derendorf, Pharmacokinetic and Pharmacodynamic Evaluation of Triamcinolone Acetonide After Intravenous, Oral, and Inhaled Administration, The Journal of Clinical Pharmacology. 35 (1995) 1187–1193. https://doi.org/10.1002/j.1552-4604.1995.tb04045.x.

[153] P.M. Beer, S.J. Bakri, R.J. Singh, W. Liu, G.B. Peters, M. Miller, Intraocular concentration and pharmacokinetics of triamcinolone acetonide after a single intravitreal injection, Ophthalmology. 110 (2003) 681–686. https://doi.org/10.1016/S0161-6420(02)01969-3.

[154] J. Song, H. Bi, X. Xie, J. Guo, X. Wang, D. Liu, Preparation and evaluation of sinomenine hydrochloride in situ gel for uveitis treatment, Int Immunopharmacol. 17 (2013) 99–107. https://doi.org/10.1016/j.intimp.2013.05.020.

[155] E. Pato, S. Muñoz-Fernández, F. Francisco, M.A. Abad, J. Maese, A. Ortiz, L. Carmona, Systematic Review on the Effectiveness of Immunosuppressants and Biological Therapies in the Treatment of Autoimmune Posterior Uveitis, Semin Arthritis Rheum. 40 (2011) 314–323. https://doi.org/10.1016/J.SEMARTHRIT.2010.05.008.

[156] J. Araújo, E. Gonzalez-Mira, M.A. Egea, M.L. Garcia, E.B. Souto, Optimization and physicochemical characterization of a triamcinolone acetonide-loaded NLC for ocular antiangiogenic applications, Int J Pharm. 393 (2010) 168–176. https://doi.org/10.1016/j.ijpharm.2010.03.034.

[157] J.M. Ruiz-Moreno, J.A. Montero, A. Bayon, J. Rueda, M. Vidal, Retinal toxicity of intravitreal triamcinolone acetonide at high doses in the rabbit, Exp Eye Res. 84 (2007) 342–348. https://doi.org/10.1016/j.exer.2006.10.006.

[158] R.C. Nagarwal, S. Kant, P.N. Singh, P. Maiti, J.K. Pandit, Polymeric nanoparticulate system: A potential approach for ocular drug delivery, Journal of Controlled Release. 136 (2009) 2–13. https://doi.org/10.1016/j.jconrel.2008.12.018.

[159] H. Qi, W. Chen, C. Huang, L. Li, C. Chen, W. Li, C. Wu, Development of a poloxamer analogs/carbopol-based in situ gelling and mucoadhesive ophthalmic delivery system for puerarin, Int J Pharm. 337 (2007) 178–187. https://doi.org/10.1016/j.ijpharm.2006.12.038.

[160] H. Gupta, S. Jain, R. Mathur, P. Mishra, A.K. Mishra, T. Velpandian, Sustained ocular drug delivery from a temperature and pH triggered novel in situ gel system, Drug Deliv. 14 (2007) 507–515. https://doi.org/10.1080/10717540701606426.

[161] A.A. Al-Kinani, G. Zidan, N. Elsaid, A. Seyfoddin, A.W.G. Alani, R.G. Alany, Ophthalmic gels: Past, present and future, Adv Drug Deliv Rev. 126 (2018) 113–126. https://doi.org/10.1016/j.addr.2017.12.017.

[162] S. R, H. GC, Y. WP, M. VS, T. RRS, In situ forming phase-inversion implants for sustained ocular delivery of triamcinolone acetonide, Drug Deliv Transl Res. 9 (2019) 534–542. https://doi.org/10.1007/S13346-018-0491-Y.

[163] A. Chowhan, T.K. Giri, Polysaccharide as renewable responsive biopolymer for in situ gel in the delivery of drug through ocular route, Int J Biol Macromol. 150 (2020) 559–572. https://doi.org/10.1016/j.ijbiomac.2020.02.097.

[164] V.D. Prajapati, G.K. Jani, N.G. Moradiya, N.P. Randeria, Pharmaceutical applications of various natural gums, mucilages and their modified forms, Carbohydr Polym. 92 (2013) 1685–1699. https://doi.org/10.1016/j.carbpol.2012.11.021.

[165] C. Jumelle, S. Gholizadeh, N. Annabi, R. Dana, Advances and limitations of drug delivery systems formulated as eye drops, Journal of Controlled Release. 321 (2020) 1–22. https://doi.org/10.1016/j.jconrel.2020.01.057.

[166] C. Chassenieux, C. Tsitsilianis, Recent trends in pH/thermo-responsive self-assembling hydrogels: From polyions to peptide-based polymeric gelators, Soft Matter. 12 (2016) 1344–1359. https://doi.org/10.1039/c5sm02710a.

[167] A.D. Kulkarni, A.A. Joshi, C.L. Patil, P.D. Amale, H.M. Patel, S.J. Surana, V.S. Belgamwar, K.S. Chaudhari, C. v. Pardeshi, Xyloglucan: A functional biomacromolecule for drug delivery applications, Int J Biol Macromol. 104 (2017) 799–812. https://doi.org/10.1016/j.ijbiomac.2017.06.088.

[168] Y. Yan, M. Takemasa, C. Zhao, L. Yu, K. Nishinari, Structure-gelation research on gallate analogs and xyloglucan by rheology, thermal analysis and NMR, Food Hydrocoll. 52 (2016) 447–459. https://doi.org/10.1016/j.foodhyd.2015.07.012.

[169] S. Poommarinvarakul, J. Tattiyakul, C. Muangnapoh, Isolation and rheological properties of tamarind seed polysaccharide from tamarind kernel powder using protease enzyme and high-intensity ultrasound, J Food Sci. 75 (2010). https://doi.org/10.1111/J.1750-3841.2010.01613.X.

[170] K.M. Zia, S. Tabasum, M. Nasif, N. Sultan, N. Aslam, A. Noreen, M. Zuber, A review on synthesis, properties and applications of natural polymer based carrageenan blends and composites, Int J Biol Macromol. 96 (2017) 282–301. https://doi.org/10.1016/j.ijbiomac.2016.11.095.

[171] T. Sangfai, V. Tantishaiyakul, N. Hirun, L. Li, Preparation and characterization of κ-carrageenan and xyloglucan blends for sustained release of a hydrophilic drug, Polymer Bulletin. 72 (2015) 1647–1661. https://doi.org/10.1007/s00289-015-1360-1.

[172] B. Bhowmick, G. Sarkar, D. Rana, I. Roy, N.R. Saha, S. Ghosh, M. Bhowmik, D. Chattopadhyay, Effect of carrageenan and potassium chloride on an in situ gelling ophthalmic drug delivery system based on methylcellulose, RSC Adv. 5 (2015) 60386–60391. https://doi.org/10.1039/c5ra06858d.

[173] A. v. Dalvi, P.R. Ravi, C.T. Uppuluri, R.R. Mahajan, S. v. Katke, V.S. Deshpande, Thermosensitive nasal in situ gelling systems of rufinamide formulated using modified tamarind seed xyloglucan for direct nose-to-brain delivery: design, physical characterization, and in vivo evaluation, J Pharm Investig. 51 (2021) 199–211. https://doi.org/10.1007/S40005-020-00505-9/FIGURES/6.

[174] A.K.A.S. Brun-Graeppi, C. Richard, M. Bessodes, D. Scherman, T. Narita, G. Ducouret, O.W. Merten, Study on the sol-gel transition of xyloglucan hydrogels, Carbohydr Polym. 80 (2010) 555–562. https://doi.org/10.1016/j.carbpol.2009.12.026.

[175] M. Han, Y. Liu, F. Zhang, D. Sun, J. Jiang, Effect of galactose side-chain on the self-assembly of xyloglucan macromolecule, Carbohydr Polym. 246 (2020) 116577. https://doi.org/10.1016/J.CARBPOL.2020.116577.

[176] J. Kochumalayil, H. Sehaqui, Q. Zhou, L.A. Berglund, Tamarind seed xyloglucan – a thermostable high-performance biopolymer from non-food feedstock, J Mater Chem. 20 (2010) 4321–4327. https://doi.org/10.1039/C0JM00367K.

[177] A. Zimmer, J. Kreuter, Microspheres and nanoparticles used in ocular delivery systems, Adv Drug Deliv Rev. 16 (1995) 61–73. https://doi.org/10.1016/0169-409X(95)00017-2.

[178] V. Gugleva, S. Titeva, N. Ermenlieva, S. Tsibranska, S. Tcholakova, S. Rangelov, D. Momekova, Development and evaluation of doxycycline niosomal thermoresponsive in situ gel for ophthalmic delivery, Int J Pharm. 591 (2020) 120010. https://doi.org/10.1016/J.IJPHARM.2020.120010.

[179] C. Vijaya, K. Goud, Ion-activated In Situ Gelling Ophthalmic Delivery Systems of Azithromycin, Indian J Pharm Sci. 73 (2011) 615. https://doi.org/10.4103/0250-474X.100234.

[180] W. Xiong, X. Gao, Y. Zhao, H. Xu, X. Yang, The dual temperature/pH-sensitive multiphase behavior of poly(N-isopropylacrylamide-co-acrylic acid) microgels for potential application in in situ gelling system, Colloids Surf B Biointerfaces. 84 (2011) 103–110. https://doi.org/10.1016/j.colsurfb.2010.12.017.

[181] T. Gratieri, G.M. Gelfuso, E.M. Rocha, V.H. Sarmento, O. de Freitas, R.F.V. Lopez, A poloxamer/chitosan in situ forming gel with prolonged retention time for ocular delivery, European Journal of Pharmaceutics and Biopharmaceutics. 75 (2010) 186–193. https://doi.org/10.1016/j.ejpb.2010.02.011.

[182] P.L. Destruel, N. Zeng, M. Maury, N. Mignet, V. Boudy, In vitro and in vivo evaluation of in situ gelling systems for sustained topical ophthalmic delivery: state of the art and beyond, Drug Discov Today. 22 (2017) 638–651. https://doi.org/10.1016/J.DRUDIS.2016.12.008.

[183] M. L, Q. F, B. A, A. L, L.R. MI, A novel poloxamers/hyaluronic acid in situ forming hydrogel for drug delivery: rheological, mucoadhesive and in vitro release properties, Eur J Pharm Biopharm. 70 (2008) 199–206. https://doi.org/10.1016/J.EJPB.2008.04.025.

[184] I.D. Rupenthal, C.R. Green, R.G. Alany, Comparison of ion-activated in situ gelling systems for ocular drug delivery. Part 1: Physicochemical characterisation and in vitro release, Int J Pharm. 411 (2011) 69–77. https://doi.org/10.1016/j.ijpharm.2011.03.042.

[185] P.L. Destruel, N. Zeng, J. Seguin, S. Douat, F. Rosa, F. Brignole-Baudouin, S. Dufaÿ, A. Dufaÿ-Wojcicki, M. Maury, N. Mignet, V. Boudy, Novel in situ gelling ophthalmic drug delivery system based on gellan gum and hydroxyethylcellulose: Innovative rheological characterization, in vitro and in vivo evidence of a sustained precorneal retention time, Int J Pharm. 574 (2020). https://doi.org/10.1016/J.IJPHARM.2019.118734.

[186] H. Wu, Z. Liu, J. Peng, L. Li, N. Li, J. Li, H. Pan, Design and evaluation of baicalin-containing in situ pH-triggered gelling system for sustained ophthalmic drug delivery, Int J Pharm. 410 (2011) 31–40. https://doi.org/10.1016/J.IJPHARM.2011.03.007.

[187] M. Sharma, S. Kohli, A. Dinda, In-vitro and in-vivo evaluation of repaglinide loaded floating microspheres prepared from different viscosity grades of HPMC polymer, Saudi Pharmaceutical Journal. 23 (2015) 675–682. https://doi.org/10.1016/j.jsps.2015.02.013.

[188] R.M. Moosa, Y.E. Choonara, L.C. du Toit, L.K. Tomar, C. Tyagi, P. Kumar, T.R. Carmichael, V. Pillay, In vivo evaluation and in-depth pharmaceutical characterization

of a rapidly dissolving solid ocular matrix for the topical delivery of timolol maleate in the rabbit eye model, Int J Pharm. 466 (2014) 296–306. https://doi.org/10.1016/J.IJPHARM.2014.02.032.

[189] G. Kaur, D. Singh, V. Brar, Bioadhesive okra polymer based buccal patches as platform for controlled drug delivery, Int J Biol Macromol. 70 (2014) 408–419. https://doi.org/10.1016/j.ijbiomac.2014.07.015.

[190] R.N. Wadetwar, A.R. Agrawal, P.S. Kanojiya, In situ gel containing Bimatoprost solid lipid nanoparticles for ocular delivery: In-vitro and ex-vivo evaluation, J Drug Deliv Sci Technol. 56 (2020) 101575. https://doi.org/10.1016/j.jddst.2020.101575.

[191] A.R. Madgulkar, M.R. Bhalekar, K.D. Asgaonkar, A.A. Dikpati, Synthesis and characterization of a novel mucoadhesive derivative of xyloglucan, Carbohydr Polym. 135 (2016) 356–362. https://doi.org/10.1016/J.CARBPOL.2015.08.045.

[192] N. Kawasaki, R. Ohkura, S. Miyazaki, Y. Uno, S. Sugimoto, D. Attwood, Thermally reversible xyloglucan gels as vehicles for oral drug delivery, Int J Pharm. 181 (1999) 227–234. https://doi.org/10.1016/S0378-5173(99)00026-5.

[193] A.K. Nayak, D. Pal, K. Santra, Swelling and drug release behavior of metformin HCl-loaded tamarind seed polysaccharide-alginate beads, Int J Biol Macromol. 82 (2016) 1023–1027. https://doi.org/10.1016/J.IJBIOMAC.2015.10.027.

[194] K.H.M. Jonsson, A. Weintraub, G. Widmalm, Structural studies of the O-antigenic polysaccharides from Shigella dysenteriae type 3 and Escherichia coli O124, a reinvestigation, Carbohydr Res. 341 (2006) 2986–2989. https://doi.org/10.1016/J.CARRES.2006.10.005.

[195] K. Chawananorasest, P. Saengtongdee, P. Kaemchantuek, Extraction and Characterization of Tamarind (Tamarind indica L.) Seed Polysaccharides (TSP) from Three Difference Sources, Molecules 2016, Vol. 21, Page 775. 21 (2016) 775. https://doi.org/10.3390/MOLECULES21060775.

[196] A. Tuomela, P. Liu, J. Puranen, S. Rönkkö, T. Laaksonen, G. Kalesnykas, O. Oksala, J. Ilkka, J. Laru, K. Järvinen, J. Hirvonen, L. Peltonen, Brinzolamide nanocrystal formulations for ophthalmic delivery: Reduction of elevated intraocular pressure in vivo, Int J Pharm. 467 (2014) 34–41. https://doi.org/10.1016/J.IJPHARM.2014.03.048.

[197] R. Bisht, A. Mandal, J.K. Jaiswal, I.D. Rupenthal, Nanocarrier mediated retinal drug delivery: overcoming ocular barriers to treat posterior eye diseases, Wiley Interdiscip Rev Nanomed Nanobiotechnol. 10 (2018) e1473. https://doi.org/10.1002/WNAN.1473.

[198] I.P. Kaur, S. Kakkar, Nanotherapy for posterior eye diseases, J Control Release. 193 (2014) 100–112. https://doi.org/10.1016/J.JCONREL.2014.05.031.

[199] V. Tambe, N. Raval, P. Gondaliya, P. Bhattacharya, K. Kalia, R.K. Tekade, To investigate fit-to-purpose nanocarrier for non-invasive drug delivery to posterior segment of eye, J Drug Deliv Sci Technol. 61 (2021) 102222. https://doi.org/10.1016/J.JDDST.2020.102222.

[200] S. Shah, P. Famta, R.S. Raghuvanshi, S.B. Singh, S. Srivastava, Lipid polymer hybrid nanocarriers: Insights into synthesis aspects, characterization, release mechanisms, surface functionalization and potential implications, Colloid Interface Sci Commun. 46 (2022) 100570. https://doi.org/10.1016/J.COLCOM.2021.100570.

[201] M. Malamatari, K.M.G. Taylor, S. Malamataris, D. Douroumis, K. Kachrimanis, Pharmaceutical nanocrystals: production by wet milling and applications, Drug Discov Today. 23 (2018) 534–547. https://doi.org/10.1016/J.DRUDIS.2018.01.016.

[202] P.K. Parmar, J. Wadhawan, A.K. Bansal, Pharmaceutical nanocrystals: A promising approach for improved topical drug delivery, Drug Discov Today. (2021). https://doi.org/10.1016/J.DRUDIS.2021.07.010.

[203] C.M. Keck, R.H. Müller, Drug nanocrystals of poorly soluble drugs produced by high pressure homogenisation, European Journal of Pharmaceutics and Biopharmaceutics. 62 (2006) 3–16. https://doi.org/10.1016/j.ejpb.2005.05.009.

[204] R.H. Müller, S. Gohla, C.M. Keck, State of the art of nanocrystals—Special features, production, nanotoxicology aspects and intracellular delivery, European Journal of Pharmaceutics and Biopharmaceutics. 78 (2011) 1–9. https://doi.org/10.1016/j.ejpb.2011.01.007.

[205] F. Fontana, P. Figueiredo, P. Zhang, J.T. Hirvonen, D. Liu, H.A. Santos, Production of pure drug nanocrystals and nano co-crystals by confinement methods, Adv Drug Deliv Rev. 131 (2018) 3–21. https://doi.org/10.1016/J.ADDR.2018.05.002.

[206] J. JU, M. RH, Nanocrystal technology, drug delivery and clinical applications, Int J Nanomedicine. 3 (2008) 295. https://doi.org/10.2147/IJN.S595.

[207] L. Peltonen, J. Hirvonen, Drug nanocrystals - Versatile option for formulation of poorly soluble materials, Int J Pharm. 537 (2018) 73–83. https://doi.org/10.1016/J.IJPHARM.2017.12.005.

[208] V.B. Junyaprasert, B. Morakul, Nanocrystals for enhancement of oral bioavailability of poorly water-soluble drugs, Asian J Pharm Sci. 10 (2015) 13–23. https://doi.org/10.1016/J.AJPS.2014.08.005.

[209] E. Merisko-Liversidge, G.G. Liversidge, E.R. Cooper, Nanosizing: a formulation approach for poorly-water-soluble compounds, European Journal of Pharmaceutical Sciences. 18 (2003) 113–120. https://doi.org/10.1016/S0928-0987(02)00251-8.

[210] M.A. Safwat, H.F. Mansour, A.K. Hussein, S. Abdelwahab, G.M. Soliman, Polymeric micelles for the ocular delivery of triamcinolone acetonide: preparation and in vivo evaluation in a rabbit ocular inflammatory model, Https://Doi.Org/10.1080/10717544.2020.1797241. 27 (2020) 1115–1124. https://doi.org/10.1080/10717544.2020.1797241.

[211] A. Sabzevari, K. Adibkia, H. Hashemi, A. Hedayatfar, N. Mohsenzadeh, F. Atyabi, M.H. Ghahremani, R. Dinarvand, Polymeric triamcinolone acetonide nanoparticles as a new alternative in the treatment of uveitis: In vitro and in vivo studies, European Journal of Pharmaceutics and Biopharmaceutics. 84 (2013) 63–71. https://doi.org/10.1016/J.EJPB.2012.12.010.

[212] M.S. Khan, P.R. Ravi, S.I. Mir, P.S. Rawat, Optimization and in vivo evaluation of triamcinolone acetonide loaded in situ gel prepared using reacted tamarind seed xyloglucan and kappa-carrageenan for ocular delivery, Int J Biol Macromol. (2023) 123533. https://doi.org/10.1016/J.IJBIOMAC.2023.123533.

[213] S.B. da Silva, D. Ferreira, M. Pintado, B. Sarmento, Chitosan-based nanoparticles for rosmarinic acid ocular delivery—In vitro tests, Int J Biol Macromol. 84 (2016) 112–120. https://doi.org/10.1016/J.IJBIOMAC.2015.11.070.

[214] S. Khan, M. De Matas, J. Zhang, J. Anwar, Nanocrystal preparation: Low-energy precipitation method revisited, Cryst Growth Des. 13 (2013) 2766–2777. https://doi.org/10.1021/CG4000473/ASSET/IMAGES/LARGE/CG-2013-000473_0014.JPEG.

[215] A.A. Thorat, S. V. Dalvi, Liquid antisolvent precipitation and stabilization of nanoparticles of poorly water soluble drugs in aqueous suspensions: Recent developments and future perspective, Chemical Engineering Journal. 181–182 (2012) 1–34. https://doi.org/10.1016/J.CEJ.2011.12.044.

[216] D. Prat, O. Pardigon, H.W. Flemming, S. Letestu, V. Ducandas, P. Isnard, E. Guntrum, T. Senac, S. Ruisseau, P. Cruciani, P. Hosek, Sanofi's Solvent Selection Guide: A Step Toward More Sustainable Processes, Org Process Res Dev. 17 (2013) 1517–1525. https://doi.org/10.1021/OP4002565.

[217] A. Tuomela, J. Hirvonen, L. Peltonen, Stabilizing Agents for Drug Nanocrystals: Effect on Bioavailability, Pharmaceutics. 8 (2016). https://doi.org/10.3390/PHARMACEUTICS8020016.

[218] A. Gagliardi, D. Paolino, M. Iannone, E. Palma, M. Fresta, D. Cosco, Sodium deoxycholate-decorated zein nanoparticles for a stable colloidal drug delivery system, Int J Nanomedicine. 13 (2018) 601–614. https://doi.org/10.2147/IJN.S156930.

[219] O.P. Sharma, V. Patel, T. Mehta, Design of experiment approach in development of febuxostat nanocrystal: Application of Soluplus® as stabilizer, Powder Technol. 302 (2016) 396–405. https://doi.org/10.1016/J.POWTEC.2016.09.004.

[220] A. Varela-Garcia, A. Concheiro, C. Alvarez-Lorenzo, Soluplus micelles for acyclovir ocular delivery: Formulation and cornea and sclera permeability, Int J Pharm. 552 (2018) 39–47. https://doi.org/10.1016/J.IJPHARM.2018.09.053.

[221] S.H. Park, J.O. Park, Simultaneous Optimization of Multiple Responses Using a Weighted Desirability Function, Quality Improvement Through Statistical Methods. (1998) 299–311. https://doi.org/10.1007/978-1-4612-1776-3_24.

[222] B. Silva, B. São Braz, E. Delgado, L. Gonçalves, Colloidal nanosystems with mucoadhesive properties designed for ocular topical delivery, Int J Pharm. 606 (2021) 120873. https://doi.org/10.1016/J.IJPHARM.2021.120873.

[223] P. Chetoni, S. Burgalassi, D. Monti, S. Tampucci, V. Tullio, A.M. Cuffini, E. Muntoni, R. Spagnolo, G.P. Zara, R. Cavalli, Solid lipid nanoparticles as promising tool for intraocular tobramycin delivery: Pharmacokinetic studies on rabbits, European Journal of Pharmaceutics and Biopharmaceutics. 109 (2016) 214–223. https://doi.org/10.1016/J.EJPB.2016.10.006.

[224] R.A. Alshaikh, C. Waeber, K.B. Ryan, Polymer based sustained drug delivery to the ocular posterior segment: barriers and future opportunities for the treatment of neovascular pathologies, Adv Drug Deliv Rev. 187 (2022) 114342. https://doi.org/10.1016/J.ADDR.2022.114342.

[225] T. Cheng, J. Li, Y. Cheng, X. Zhang, Y. Qu, Triamcinolone acetonide-chitosan coated liposomes efficiently treated retinal edema as eye drops, Exp Eye Res. 188 (2019). https://doi.org/10.1016/J.EXER.2019.107805.

[226] A. Shome, O.O. Mugisho, R.L. Niederer, I.D. Rupenthal, Blocking the inflammasome: A novel approach to treat uveitis, Drug Discov Today. 26 (2021) 2839–2857. https://doi.org/10.1016/J.DRUDIS.2021.06.017.

[227] Sci-Hub | Ocular drug delivery conventional ocular formulations. Advanced Drug Delivery Reviews, 16(1), 39–43 | 10.1016/0169-409x(95)00012-v, (n.d.). https://sci-hub.st/10.1016/0169-409x(95)00012-v (accessed February 3, 2023).

[228] S. Ding, Recent developments in ophthalmic drug delivery, Pharm Sci Technol Today. 1 (1998) 328–335. https://doi.org/10.1016/S1461-5347(98)00087-X.

[229] S.A.A. Rizvi, A.M. Saleh, Applications of nanoparticle systems in drug delivery technology, Saudi Pharmaceutical Journal. 26 (2018) 64–70. https://doi.org/10.1016/J.JSPS.2017.10.012.

[230] K. Hadinoto, A. Sundaresan, W.S. Cheow, Lipid-polymer hybrid nanoparticles as a new generation therapeutic delivery platform: A review, European Journal of Pharmaceutics and Biopharmaceutics. 85 (2013) 427–443. https://doi.org/10.1016/j.ejpb.2013.07.002.

[231] D. Sivadasan, M.H. Sultan, O. Madkhali, Y. Almoshari, N. Thangavel, Polymeric lipid hybrid nanoparticles (Plns) as emerging drug delivery platform—a comprehensive review of their properties, preparation methods, and therapeutic applications, Pharmaceutics. 13 (2021). https://doi.org/10.3390/PHARMACEUTICS13081291.

[232] V. Dave, K. Tak, A. Sohgaura, A. Gupta, V. Sadhu, K.R. Reddy, Lipid-polymer hybrid nanoparticles: Synthesis strategies and biomedical applications, J Microbiol Methods. 160 (2019) 130–142. https://doi.org/10.1016/J.MIMET.2019.03.017.

[233] J.M. Chan, L. Zhang, K.P. Yuet, G. Liao, J.W. Rhee, R. Langer, O.C. Farokhzad, PLGA-lecithin-PEG core-shell nanoparticles for controlled drug delivery, Biomaterials. 30 (2009) 1627–1634. https://doi.org/10.1016/j.biomaterials.2008.12.013.

[234] M. Chorny, I. Fishbein, H.D. Danenberg, G. Golomb, Lipophilic drug loaded nanospheres prepared by nanoprecipitation: effect of formulation variables on size, drug recovery and release kinetics, Journal of Controlled Release. 83 (2002) 389–400. https://doi.org/10.1016/S0168-3659(02)00211-0.

[235] G. Derringer, R. Suich, Simultaneous Optimization of Several Response Variables, 12 (2018) 214–219. https://doi.org/10.1080/00224065.1980.11980968.

APPENDICES

List of Publications (From Thesis Work)

1. **M.S. Khan**, P.R. Ravi, D.S. Dhavan. Design, optimization, in vitro and in vivo evaluation of triamcinolone acetonide nanocrystals loaded in situ gel for topical ocular delivery, Colloids Surf B Biointerfaces. 231 (2023) 113539. (doi.org/10.1016/J.COLSURFB.2023.113539)
2. **M.S. Khan**, P.R. Ravi, D.S. Dhavan. Design, optimization and pharmacokinetic evaluation of PLGA phosphatidylcholine hybrid nanoparticles of triamcinolone acetonide loaded in situ gel for topical ocular deliver, International Journal of Pharmaceutics (Accepted).
3. **M.S. Khan**, P.R. Ravi, S.I. Mir, P.S. Rawat, Optimization and *in vivo* evaluation of triamcinolone acetonide loaded *in situ* gel prepared using reacted tamarind seed xyloglucan and kappa-carrageenan for ocular delivery, *International Journal of Biological Macromolecules*. (doi.org/10.1016/J.IJBIOMAC.2023.123533)
4. **M.S. Khan**, P.R. Ravi, T.V.R.K. Mullapudi, Dose identification of triamcinolone acetonide for noninvasive pre-corneal administration in the treatment of posterior uveitis using a rapid, sensitive HPLC method with photodiode-array detector, Biomed Chromatography. (doi.10.1002/BMC.5264).

Other Publications

1. R. Mahajan, P.R. Ravi, M.S. Khan, Optimization of a HPLC-UV bioanalytical method using Box-Behnken design to determine the oral pharmacokinetics of neratinib maleate in Wistar rats, Biomed Chromatogr. (2023). (doi.org/10.1002/BMC.5731)
2. P.S. Rawat, P.R. Ravi, S.I. Mir, M.S. Khan, H. Kathuria, P. Katnapally, U. Bhatnagar, Design, Characterization and Pharmacokinetic-Pharmacodynamic Evaluation of Poloxamer and Kappa-Carrageenan-Based Dual-Responsive *in Situ* Gel of Nebivolol for Treatment of Open-Angle Glaucoma, Pharmaceutics. (doi.org/10.3390/PHARMACEUTICS15020405)

3. Diwan, S. Khan, P.R. Ravi, Comparative study of cilnidipine loaded PLGA nanoparticles: process optimization by DoE, physicochemical characterization and *in vivo* evaluation, *Drug Delivery and Translational Research*. (doi.org/10.1007/S13346-020-00732-5)

Workshops

1. A four-day workshop on "Exploring chromatography & Mass-Spectroscopy - Futuristic Technologies" was organized by Shimadzu, Spinco Biotech Pvt. Ltd., in collaboration with BITS-Pilani, Hyderabad Campus from June 16 to June 19, December 2019.
2. A one-day workshop on 'JMP Statistical Software for Pharmaceutical Sciences' that involved Data Visualization, Biostatistics, Design of Experiments (DOE) and Dissolution was organized by JMP: Statistical Discovery at BITS–Pilani, Hyderabad Campus on 8th November 2022.
3. A two-day Workshop on PBPK using PKSIM software that focused on the fundamentals required for building a PBPK model as well as developing the PBPK model itself, building PBPK models in special populations (Pediatric, neonate/preterm infants, Renal impaired disease populations) organized by bug works at BITS–Pilani, Hyderabad Campus, 24-25th December 2022.

Biography of Mr. Mohammed Shareef Khan

Mr. Mohammed Shareef Khan received his Bachelor of Pharmacy degree from Jawaharlal Nehru Technological University in Hyderabad in 2014 and he received his Master of Pharmacy degree with a specialization in pharmaceutics from Birla Institute of Technology and Science – Pilani, Hyderabad Campus in 2017 and continued working as JRF. In 2018, he started working as a senior research associate in the BBRC (Biocon Bristol-Mayers Squibb Research and Development Centre) on projects pertaining to Pre-Formulation/Pre-ECN studies, Pre-clinical formulation development, Micro-dissolution studies and Novel drug delivery systems. He started his doctoral studies in 2019 at the Birla Institute of Technology and Science - Pilani, Hyderabad Campus, under the supervision of Professor Punna Rao Ravi. He published multiple research papers in esteemed international peer-reviewed journals while pursuing his master's and doctoral degrees.

Biography of Prof. Punna Rao Ravi

Professor Punna Rao Ravi is working as a professor at the BITS Pilani, Hyderabad Campus, Department of Pharmacy. He graduated from BITS-Pilani University in Rajasthan with a B. Pharm, M. Pharm and PhD in Pharmaceutical Sciences. Since the year 2000, he has been working as a faculty member at BITS-Pilani. He has numerous publications in reputable national and international peer-reviewed journals and has delivered papers at scientific meetings both in India and overseas. He has successfully finished government-sponsored research projects and is anticipating receiving additional grants from scientific funding agencies.